

**Multimedia Source Apportionment of Semivolatile Organic Contaminants in
the Chicago Area of Influence.**

BY

KELLY J. GRANBERG
B.S., University of Wisconsin - Madison, 2003

THESIS

Submitted in partial fulfillment of the requirement
for the degree of Doctor of Philosophy in Civil Engineering
in the Graduate College of
the University of Illinois at Chicago, 2013

Chicago, Illinois

Defense Committee:

Karl J. Rockne, Chair and Advisor
Amid Khodadoust
An Li, Environmental and Occupational Health Sciences
Erik Christensen, University of Wisconsin - Milwaukee
Donna Kenski, Lake Michigan Air Directors Consortium
Jennifer Miller, U.S. Army Corps of Engineers

ACKNOWLEDGEMENTS

I wish to thank my advisor Dr. Karl Rockne for his guidance and support throughout my graduate studies. I am grateful for the opportunity he provided to perform innovative research, develop my intellectual interests, and contribute to the academic and professional environmental engineering community. I also thank my thesis committee members Professor Amid Khodadoust and Professor An Li from the University of Illinois at Chicago, Professor Erik Christensen from the University of Wisconsin – Milwaukee, Dr. Donna Kenski from the Lake Michigan Air Directors Consortium, and Dr. Jennifer Miller from the U.S. Army Corps of Engineers for their willingness to serve on my committee and provide constructive insight and feedback. I am especially grateful to Professor Erik Christensen for valuable discussions and suggestions on use of source apportionment modeling in my research. I would further like to thank Dr. Jennifer Miller, Le Thai, and Dr. John Marlin for their assistance obtaining project data and helpful reviews of my analyses.

I am eternally grateful for the deep support and friendship of my lab-mates Priscilla Viana, Solidea Bonina, Azivy Che Aziz-Schwanbeck, Asha Rani, Raja Kaliappan, Gregory Bourgon, and Itzel Godinez who taught, encouraged, and cheered me throughout my graduate years. Thanks to fellow colleagues Soheil Hosseini, Kamel Babaeiveli, Srinivasa Varadhan, Saikrishnan Ramamurthy, Karina Szymulanska-Ramamurthy, Jayashree Jayaraj, Ke Yin, Xiuhong Zhao, Shooka Karimpour, Burcu Uyusur, and Yonghong Zou who also supported numerous aspects of my work.

I would like to acknowledge Professor Mary Ashley and my colleagues in the Landscape, Ecological and Anthropogenic Processes (LEAP) Integrative Graduate Education and Research Training (IGERT) fellowship program at the University of Illinois at Chicago. I am especially grateful to my LEAP cohort Paul Gulezian and Jennifer Ison for collaborating together on inventive, interdisciplinary, student-led research.

Support for this work has been provided by the LEAP IGERT fellowship program (National Science Foundation Award 0549245) a pre-doctoral fellowship from the Institute for Environmental Policy (IESP) at the University of Illinois at Chicago, a grant from the Illinois Sustainable Technology Center (ISTC) at the University of Illinois at Urbana-Champaign, and a grant from Chicago Wilderness.

Finally, I extend a deep heart-felt thank you to my fiancé and family for their love, patience, wisdom, humor, and understanding. You mean the world to me and I would not have come this far without you.

KJG

TABLE OF CONTENTS

ACKNOWLEDGEMENTS	iii
TABLE OF CONTENTS.....	v
LIST OF TABLES	vii
LIST OF FIGURES	x
LIST OF ABBREVIATIONS.....	xv
SUMMARY	xviii
CHAPTER I. INTRODUCTION.....	1
CHAPTER II: LITERATURE REVIEW	3
2.1. Polycyclic Aromatic Hydrocarbons (PAHs).....	3
2.1.1. Sources of PAHs	7
2.1.2. PAH distribution in the Chicago metropolitan area.....	11
2.2. Polychlorinated Biphenyls (PCBs)	13
2.2.1. Sources of PCBs	17
2.2.2. PCB distribution in the Chicago metropolitan area	19
2.3. Source Apportionment.....	22
2.3.1. PAH diagnostic ratios	22
2.3.2. Receptor Modeling.....	25
2.3.3. Positive Matrix Factorization.....	27
2.3.4. Utility of source apportionment techniques	30
CHAPTER III: AIR MONITORING FOR THE INDIANA HARBOR AND CANAL CONFINED DISPOSAL FACILITY PROJECT: PRE-DREDGING TRENDS IN PAHS AND PCBs	32
3.1. Abstract.....	32
3.2. Introduction.....	33
3.3. Materials and Methods.....	34
3.4. Results and Discussion	47

CHAPTER IV. POSITIVE MATRIX FACTORIZATION SOURCE APPORTIONMENT OF PAHS AND PCBS AT INDIANA HARBOR AND CANAL CONFINED DISPOSAL FACILITY AIR-SHED PRE-DREDGING (2001-2012).....	73
4.1. Abstract.....	73
4.2. Introduction.....	74
4.3. Materials and Methods.....	76
4.4. Results and Discussion	102
4.5. Implications	140
CHAPTER V. SOURCE APPORTIONMENT OF POLYCYCLIC AROMATIC HYDROCARBONS IN ILLINOIS RIVER SEDIMENT	143
5.1. Abstract.....	143
5.2. Introduction.....	144
5.3. Materials and Methods.....	147
5.4. Results and Discussion	167
5.5. Implications	190
CHAPTER VI. CONCLUSIONS AND IMPLICATIONS	192
CITED LITERATURE	199
APPENDICES	220
Appendix A. Map of PAH and PCB sources near the Confined Disposal Facility.	221
Appendix B. Establishment of an Invasive Plant Species (<i>Conium maculatum</i>) in Contaminated Roadside Soil in Cook County, Illinois.	222
Appendix C. Permissions and licenses for reuse of copyrighted material.....	265
VITA	278

LIST OF TABLES

Table 2.1. Select physical properties ^a of priority PAHs.	6
Table 2.2. Physical properties ^a of select PCB congeners and Aroclors.....	15
Table 2.3. Sediment PCB concentrations in Great Lakes tributaries (ng/g dry wt.). ^a	20
Table 2.4. PAH diagnostic ratios of petroleum and combustion sources and samples. ^a	24
Table 3.1. Statistical analysis of atmospheric PAH concentrations (ng/m ³) near IHC.....	49
Table 3.2. Statistical analysis of atmospheric PCB concentrations (pg/m ³) near IHC.	50
Table 3.3. Reported total PAH and PCB concentrations in air near Chicago, Illinois USA.	52
Table 3.4. <i>t</i> -test ^a for significant differences ^b in PAHs and PCBs among monitoring stations (S, H, N, E, W), CDF construction activities, seasons, and wind source directions by quadrant (NE, SE, SW, NW).	54
Table 3.5. Pearson correlation coefficients between PAHs (bottom left) and PCBs (upper right).....	55
Table 3.6. Clausius-Clapeyron regression parameters for individual PAHs by station.....	58
Table 3.7. Clausius-Clapeyron regression parameters for individual PCBs by station. ^a	59
Table 3.8. Statistical analysis of 288 K-corrected ^a PAH concentrations (ng/m ³) near IHC.....	61
Table 3.9. Statistical analysis of 288 K-corrected PCB concentrations (pg/m ³) near IHC.....	62
Table 3.10. <i>t</i> -test ^a for significant differences ^b in 288 K-corrected ^c PAH and PCB levels among monitoring stations, CDF construction activities, seasons, and wind direction quadrants.	63
Table 3.11. Mean halving time (years \pm 1 SE) ^a for PAHs and PCBs at stations S and H.	65
Table 3.12. Wind direction regression parameters for PAHs and PCBs.	67
Table 3.13. Multiple linear regression parameters and individual regression parameters for select PAHs and PCBs. ^a	70
Table 4.1. Physical properties ^a of select PAHs and PCB congeners.	80
Table 4.2. PMF parameters used for all runs. ^a	83
Table 4.3. Coefficients of Variation (CVs) assigned to PAHs and PCBs for Monte Carlo simulation.....	86
Table 4.4. Mean PAH combustion source profiles (coal, petroleum, and wood) from the literature (%). ^a	92
Table 4.5. Percent particulate to total atmospheric PAHs.	93
Table 4.6. PAH area source profiles with adjustment for fraction in air (%).	93
Table 4.7. PAH profiles derived from the USEPA 2008 National Emissions Inventory v.2 (%). ^a	94

LIST OF TABLES (continued)

Table 4.8. PCB congener source profiles of Aroclors ^a with adjustments for fraction in air (%). ^b	97
Table 4.9. PCB congener profiles of IHC media ^a with adjustments for fraction in air ^b and city of Chicago air (%). ^c	98
Table 4.10. PCB congener atmospheric profiles of Chicago emission areas (%). ^a	98
Table 4.11. PCB profiles of Ralston sludge lagoon ^a with adjustments for fraction in air and municipal waste incinerator (%). ^b	98
Table 4.12. SCREEN3 inputs ^a for estimating impacts from various area PCB sources.....	101
Table 4.13. PMF model diagnostics for PAH and PCB four-source solutions.....	102
Table 4.14. Standard deviation of PAH and PCB concentrations for each factor from bootstrap runs.....	108
Table 4.15. Cosine ϕ similarity between select reference and modeled PAH and PCB sources. ^a	116
Table 4.16. Cosine ϕ similarity of PAH modeled and USEPA 2008 National Emissions Inventory profiles. ^a	117
Table 4.17. Cosine ϕ similarity of PAH modeled and combustion literature source profiles. ^a	119
Table 4.18. Cosine ϕ similarity of PAH modeled and area source profiles. ^a	120
Table 4.19. Cosine ϕ similarity of PCB modeled and Aroclor profiles. ^a	122
Table 4.20. Cosine ϕ similarity of PCB modeled and IHC and city of Chicago profiles. ^a	123
Table 4.21. Cosine ϕ similarity of PCB modeled and Ralston sludge lagoon and municipal waste incinerator profiles. ^a	123
Table 4.22. Cosine ϕ similarity of PCB model and Chicago emission area profiles. ^a	123
Table 4.23. Multiple linear regression parameters for modeled PAH sources. ^a	125
Table 4.24. Multiple linear regression parameters for modeled PAH sources of temperature-corrected (288 K) data. ^a	126
Table 4.25. Multiple linear regression parameters for modeled PCB sources. ^a	127
Table 4.26. Clausius-Clapeyron parameters ^a for modeled PAH and PCB source contributions.	129
Table 4.27. Pearson Correlation Coefficients between PMF-modeled source contributions with different temperature correction scenarios. ^a	129
Table 4.28. Linear regression parameters for PAH and PCB source contribution yearly moving averages. ^a	134

LIST OF TABLES (continued)

Table 4.29. SCREEN3 inputs and estimated PCB concentrations from area sources to the CDF. ^a	139
Table 5.1. PAH background soil concentrations for populated areas and soil remediation concentration objectives (ug/kg) from TACO. ^a	146
Table 5.2. Illinois River sediment PAH data (ug/kg) for source apportionment analysis. ^a	154
Table 5.3 PAH diagnostic ratios of petroleum and combustion sources and samples. ^a Diagnostic ranges are bold.....	158
Table 5.4. Coal PAH source profiles (%). ^a	164
Table 5.5. Combustion PAH source profiles (coal, petroleum, and wood) (%). ^a	165
Table 5.6. Oil, coal tar, traffic, and other particle-derived PAH source profiles (%). ^a	166
Table 5.7. PMF model diagnostics and sensitivity analysis with different sample numbers.....	174
Table 5.8. PMF model diagnostics for sensitivity analysis with a different non-detect substitution method and analyte number.	175
Table 5.9. Pearson correlation coefficients between PMF solution profiles of the base (14x80) and varied datasets. ^a	176
Table 5.10. Cosine ϕ similarity of PMF modeled and reference PAH source profiles. ^a	183

LIST OF FIGURES

Figure 2.1. Chemical structure of USEPA designated priority PAHs. Adapted with permission from Fahnrich et al. (2002). ⁶	4
Figure 2.2. Select PAH atmospheric source profiles. Coke oven through diesel engine from Li et al. (2003), ⁶⁴ IHC sediment from USACE (2010), ⁶⁶ biosolids from Gulezian et al. (2012), ⁶⁷ and diesel equipment and petroleum storage and transfer from 2008 National Emissions Inventory (v.2 USEPA).	9
Figure 2.3. Select PAH reference source profiles for sediment (note all axes are same except for new oil). Bituminous coal from Stout and Emsbo-Mattingly (2008), ⁶⁸ coal tar from Wise et al. (2010), ⁵⁵ new and used lubricating oil from Wang et al. (2000), ⁴⁶ biosolids from Gulezian et al. (2012), ⁶⁷ wood burning from Bzdusek et al. (2004), ⁶⁵ gas and diesel engine from Li et al. (2003), ⁶⁴ street dust from Boonyatumanond et al. (2006), ⁵⁰ and urban dust standard from NIST (2009). ⁶⁹	10
Figure 2.4. Mass percent contribution of individual PAHs to Σ_{14} PAHs in Chicago air. Adapted with permission from Odabasi et al. (1999). ⁷⁶	11
Figure 2.5. Source contributions of PAHs to Chicago coastal air. Adapted with permission from Simcik et al. (1999). ⁷⁷	12
Figure 2.6. Average flux contributions from petroleum (hatched), coal (black), and wood (cross hatched) combustion to six Lake Michigan cores dated 1936-1996. Adapted with permission from Christensen and Arora (2007). ⁸¹	13
Figure 2.7. PCB chemical structure and formula from ATSDR (2000). ⁸³	14
Figure 2.8. Estimated cumulative global production of the most common PCB congeners. Adapted with permission from Breivik et al. (2007). ⁸⁸	14
Figure 2.9. Select PCB atmospheric source profiles of (A) Aroclor mixtures from Frame et al. (1996) ⁹³ and (B) known reference sources: IHC air and sediment from Martinez et al. (2010), ¹⁰⁶ transformer storage yard and biosolids drying bed from Hsu et al. (2003), ¹⁰⁴ Ralston sludge lagoon from Gary Sanitary District (2007), ¹⁰⁷ and municipal waste incinerator from Ikonomou et al. (2002). ⁹⁴	18
Figure 2.10. PCB congener profile in Chicago air. Adapted with permission from Hu et al. (2010). ¹¹⁰	20
Figure 2.11. Mass budget average for 1994-1995 total PCBs in Lake Michigan (mass transported in kg/yr) from Rossmann (2006). ¹¹⁸	21
Figure 3.1. Location of atmospheric sampling stations. Land use map left (USGS National Land Cover Database, 2006) and aerial photo right (National Agriculture Imagery Program Orthoimagery, 2010).	35
Figure 3.2. Flowchart of Compendium Method TO-13A/SW-846 Method 1668/CARB 429 analytical scheme. Figure from USACE (2003). ¹⁶²	37
Figure 3.3. Flowchart of QA/QC elements for sampling and analysis stages of the air monitoring program. Figure from USACE (2003). ¹⁶²	38

LIST OF FIGURES (continued)

Figure 3.4. Detection frequency of (A) PAHs and (B) PCB congeners analyzed in air samples. Frequencies for the 14 congeners denoted with an asterisk (*) were based on limited data (seven and six measurements at stations S and H respectively) and these congeners are not considered in the present study.	40
Figure 3.5. Box plots of (A) PAH, (B) log-transformed PAH, (C) PCB, and (D) log-transformed PCB data.	41
Figure 3.6. Comparison of (A) Σ_{17} PAH (ng/m^3) and (B) Σ_{19} PCB (pg/m^3) concentrations in air at South (blue) and High School (red) stations for the entire ten year monitoring period.	48
Figure 3.7. Comparison of (A) PAH (ng/m^3) and (B) PCB (pg/m^3) concentrations in air at North (blue), East (red), and West (green) stations. Note that these stations operated during the first three years of the monitoring program.	53
Figure 3.8. Clausius-Clapeyron relationships for Σ_7 PAHs, Σ_5 PAHs (less Nap and Acy), and Σ_5 PCBs with linear regressions shown. Data are identified by sample site.	57
Figure 3.9. Comparison of (A) PAH (ng/m^3) and (B) PCB (pg/m^3) temperature-corrected (288 K) concentrations at stations S and H as a function of mean wind direction during the 24-hour sampling period for days with angular deviation less than 60° . Sinusoidal regressions are shown. North is $0/360^\circ$ and south is 180°	66
Figure 3.10. Select PAH (ng/m^3) and PCB (pg/m^3) concentrations as a function of time for all stations over the entire sampling period. Multiple linear regressions are shown.	69
Figure 3.11. Comparison of MLR model-predicted and measured Σ_7 PAH, Σ_5 PCB, Nap, Pha, PCB 8, and PCB 28 concentrations.	71
Figure 4.1. Location of atmospheric sampling stations. Land use map left (USGS National Land Cover Database, 2006) and aerial photo right (National Agriculture Imagery Program Orthoimagery, 2010).	77
Figure 4.2. Mass fraction of atmospheric PAHs and PCBs in gas phase based upon $\mu \pm \sigma$ of TSP at station S and the Weschler and Nazaroff (2010) ¹⁹¹ partitioning model.	79
Figure 4.3. Select PAH atmospheric reference source profiles (see also Tables 4.4 through 4.7). (A) Coke oven through diesel engine from Li et al. (2003), ⁶⁴ IHC sediment from USACE (2010), ⁶⁶ biosolids from Gulezian et al. (2012), ⁶⁷ and diesel equipment and petroleum storage and transfer from 2008 National Emissions Inventory (v.2 USEPA). (B) All PAH reference source profiles derived from 2008 National Emissions Inventory (v.2 USEPA).	90

LIST OF FIGURES (continued)

Figure 4.4. Select PCB atmospheric reference source profiles (see also Tables 4.8 through 4.11). (A) Aroclor mixtures from Frame et al. (1996). ⁹³ Letters A, S, and G specify different Aroclor lots from suppliers AccuStandard, Supelco, and GE Corporate R&D (Monsanto Corp.), resp. When more than one letter is specified the profile is an average of lots. (B) IHC air and sediment from Martinez et al. (2010), ¹⁰⁶ transformer storage yard and biosolids drying bed from Hsu et al. (2003), ¹⁰⁴ Ralston sludge lagoon from Gary Sanitary District (2007), ¹⁰⁷ and municipal waste incinerator from Ikonomou et al. (2002). ⁹⁴	91
Figure 4.5. PAH source profiles from PMF. Error bars are standard deviations of modeled profiles from MC generated datasets, assigned to original sources by highest correlation.....	103
Figure 4.6. PAH source contributions from PMF.....	104
Figure 4.7. PCB source profiles from PMF. Error bars are standard deviations of modeled profiles from Monte Carlo generated datasets, assigned to original sources by highest correlation.	105
Figure 4.8. PCB source contributions from PMF.	105
Figure 4.9. PAH source profiles from EPA receptor models (A) UNMIX and (B) E-PMF (Q(robust)=2633, Q(true)=3316).	107
Figure 4.10. PCB source profiles from EPA receptor models (A) UNMIX and (B) E-PMF (Q(robust)=851, Q(true)=880).	107
Figure 4.11. PAH source profiles from PMF at (A) North station (B) East station (C) West station (D) South station (E) High school station.	110
Figure 4.12. PCB source profiles from PMF at (A) North station (B) East station (C) West station (D) South station (E) High school station.	111
Figure 4.13. PMF four-source solution of PAHs corrected to 288 K (15 °C) pre-modeling. (A) PAH source profiles and (B) PAH source contributions.....	113
Figure 4.14. PMF four-source solution of PAHs corrected to 303 K (30 °C) pre-modeling. (A) PAH source profiles and (B) PAH source contributions.....	114
Figure 4.15. PMF source contributions corrected to 288 K (15 °C) post-modeling for (A) PAHs and (B) PCBs.....	128
Figure 4.16. Box plots of PAH S2 contributions by season (A-B) and wind direction (C-D) based on original (A and C) and temperature-corrected (B and D) concentrations. Differences between plots with and without temperature effects illustrate the relationship of temperature with season and with wind direction that may mask true impacts of seasonality or wind on concentrations.	130
Figure 4.17. Box plots of PAH temperature-corrected source contributions by day of week, season, station, and wind direction.	131

LIST OF FIGURES (continued)

Figure 4.18. Box plots of PCB temperature-corrected source contributions by day of week, season, station, and wind direction.....	132
Figure 4.19. Box plots of PCB S1 (t-c) contributions by construction activity. No significant differences were found for any sources based on construction activity at the CDF.....	133
Figure 4.20. Source contribution concentrations calculated as the subsequent 365-day moving average over time for total PAHs (A - B) and PCBs (C - D) at station S (A and C) and station H (B and D).	135
Figure 4.21. Nap (A and C) and PAH (B and D) county-level releases from major industrial sectors in Lake County, IN for 2002 - 2011 from Toxics Release Inventory data. Plots A - B have linear y-axis scales in metric tons (1000 kg) and plots C - D have logarithm y-axis scales for visibility of lesser sectors.	137
Figure 4.22. Nap (A and C) and PAH (B and D) county-level releases from major industrial sectors in Cook County, IN for 2002 - 2011 from Toxics Release Inventory data. Plots A - B have linear y-axis scales in metric tons (1000 kg) and plots C - D have logarithm y-axis scales in kg for visibility of lesser sectors.	138
Figure 5.1. Black carbon in Lake Peoria sediment. Error bars indicate standard deviations for 10 cm sections.	146
Figure 5.2. Map of Illinois River study location and sediment core sites. Study area is circled on the locator map (upper left) with the watershed and relationship to Chicago/Lake Michigan (upstream) and Mississippi River (downstream) shown. Cores are points and reaches are labeled (from upstream to downstream) Henry, Lacon, Upper Peoria, and Lower Peoria (see Figures 5.3 to 5.6). Counties and municipalities are also shown. Map from the ISWS (2008). ²⁰³	148
Figure 5.3. Henry (HN) sample site on the Illinois River (includes Senachwine, Sawmill, Billsbach, Weis, and Goose Lakes). Sediment core numbers and locations shown on ISWS (2008) ²⁰³ quadrangle map (A) alongside an aerial photograph (B). Satellite photo ©Google Inc. 2008.....	149
Figure 5.4. Lacon (LC) sample sites on the Illinois River (includes Wightman Lake, Sawyer Slough, Meadow Lake, and Babb Slough). Sediment core numbers and locations shown on ISWS (2008) ²⁰³ quadrangle map (A) alongside an aerial photograph (B). Satellite photo ©Google Inc. 2008.	150
Figure 5.5. Upper Peoria (UP) sample sites on the Illinois River (Upper Peoria Lake). Sediment core numbers and locations shown on ISWS (2008) ²⁰³ quadrangle map (A) alongside an aerial photograph (B). Satellite photo ©Google Inc. 2008.....	151
Figure 5.6. Lower Peoria (LP) sample sites on the Illinois River (Lower Peoria Lake). Sediment core numbers and locations shown on ISWS (2008) ²⁰³ quadrangle map (A) alongside an aerial photograph (B). Satellite photo ©Google Inc. 2008.....	152

LIST OF FIGURES (continued)

Figure 5.7. Select PAH reference source profiles. Bituminous coal (high-volatile C rank) from Stout and Emsbo-Mattingly (2008), ⁶⁸ coal tar from Wise et al. (2010), ⁵⁵ new and used lubricating oils from Wang et al. (2000), ⁴⁶ biosolids an average from two MWRD drying bed samples for Gulezian et al. (2012), ⁶⁷ wood burning from Bzdusek et al. (2004), ⁶⁵ gas and diesel engine from Li et al. (2003), ⁶⁴ street dust from Boonyatumanond et al. (2006), ⁵⁰ and urban dust standard from NIST (2009). ⁶⁹ Note all axes are the same except for new oil.....	163
Figure 5.8. Average PAH profile of IL River sediment cores from all sites (n=80). Error bars represent standard error.....	168
Figure 5.9. Histograms of Σ_{14} PAH with (A) original and (B) natural log-transformed data, indicating log-normal distribution of PAHs in Illinois River sediment. (n=80)	169
Figure 5.10. Total (Σ_{14}) PAHs for all samples (n=80) plotted roughly in transect from upstream to downstream.	169
Figure 5.11. Mean PAH levels and distribution at sampling reaches.	170
Figure 5.12. Mean PAH levels and distribution for top segments, bottom segments, and whole cores.	171
Figure 5.13. PAH differences between paired top and bottom segments. Points below the 1:1 line indicate higher PAH levels in top segments of cores than bottom. Points above the 1:1 line indicate higher levels in bottom segments.	172
Figure 5.14. PAH source composition profiles from three-source PMF solution. Profiles shown (A) together and individually for (B) S1, (C) S2, and (D) S3.	178
Figure 5.15. PAH source contributions from three-source PMF solution. The (A) overall source contribution plot is shown in greater detail by (B) HN, (C) LC, (D) UP, and (E) LP reach. Note different y-axis scales.	179
Figure 5.16. PAH diagnostic ratio plots of site-averaged Illinois River sediment and literature-compiled petrogenic and combustion samples from Table 5.3. Source ranges are delineated in blue from Yunker et al. (2002) ²⁷ according to Table 5.3. Shaded gray indicates coal domains of bituminous coal samples and pink lines delineate recently updated source ranges for Ind/Ind+BghiP from Yunker et al. (2012). ³²	185
Figure 5.17. PAH diagnostic ratio plots of Illinois River sediment samples and PMF modeled sources. Source ranges are delineated in blue from Yunker et al. (2002) ²⁷ according to Table 5.3. Shaded gray indicates coal domains of bituminous coal samples and pink lines delineate recently updated source ranges for Ind/Ind+BghiP from Yunker et al. (2012). ³²	187
Figure 5.18. PAH diagnostic ratio plots of select reference sources and PMF modeled sources. Source ranges are delineated in blue from Yunker et al. (2002) ²⁷ according to Table 5.3. Shaded gray indicates coal domains of bituminous coal samples and pink lines delineate recently updated source ranges for Ind/Ind+BghiP from Yunker et al. (2012). ³²	189

LIST OF ABBREVIATIONS

Ace	Acenaphthene
Acy	Acenaphthylene
Ant	Anthracene
AOC	Great Lakes Area of Concern
ATSDR	Agency for Toxic Substances and Disease Registry
BaA	Benzo(a)anthracene
BaP	Benzo(a)pyrene
BbF	Benzo(b)fluoranthene
BF	Benzo(k)fluoranthene
BghiP	Benzo(ghi)perylene
BkF	Benzo(k)fluoranthene
CAWS	Chicago Area Waterway System
CB	Chlorobiphenyl
C-C	Clausius-Clapeyron
CDF	Confined Disposal Facility
CERCLA	Comprehensive Environmental Response, Compensation, and Liability Act
Chr	Chrysene
CL	Confidence Level
CMB	Chemical Mass Balance
COD	Coefficient of Determination
CT	Coal Tar
CV	Coefficient of Variation
DahA	Dibenz(a,h)anthracene
DL	Detection Limit
E	East
EPA	United States Environmental Protection Agency
E-PMF	EPA Positive Matrix Factorization
EM	Error Model
EPI	Estimation Program Interface
Fla	Fluoranthene
Flo	Fluorene
FoI	Factor of Influence
H	High School
HMW	High Molecular Weight
HN	Henry
HV	High Volatile
IADN	Integrated Atmospheric Deposition Network
IGERT	Integrative Graduate Education Research and Training
ISTC	Illinois Sustainable Technology Center
IHC	Indiana Harbor and Canal
IL	Illinois
IN	Indiana
Ind	Indeno(1,2,3-cd)pyrene
ISWS	Illinois State Water Survey

LIST OF ABBREVIATIONS (continued)

IUPAC.....	International Union of Pure and Applied Chemistry
K.....	Kelvin
K _H	Henry's Law Constant
K _{OA}	Octanol Air Partition Coefficient
K _{OW}	Octanol Water Partition Coefficient
LC.....	Lacon
LCL.....	Lower Confidence Level
LEAP.....	Landscape, Ecological, and Anthropogenic Processes
LMW.....	Low Molecular Weight
LP.....	Lower Peoria
LV.....	Low Volatile
MC.....	Monte Carlo
MDL.....	Method Detection Limit
MLR.....	Multiple Linear Regression
MMW.....	Medium Molecular Weight
MRM.....	Multivariate Receptor Model
MV.....	Medium Volatile
MWRD-GC.....	Metropolitan Water Reclamation District of Greater Chicago
N.....	North
Nap.....	Naphthalene
NIST.....	National Institute of Standards and Technology
NE.....	Northeast
NEI.....	National Emissions Inventory
NW.....	Northwest
PAHs.....	Polycyclic Aromatic Hydrocarbons
PCA.....	Principal Component Analysis
PCBs.....	Polychlorinated Biphenyls
Pha.....	Phenanthrene
PMF.....	Positive Matrix Factorization
POPs.....	Persistent Organic Pollutants
Pyr.....	Pyrene
QA/QC.....	Quality Assurance/Quality Control
RCRA.....	Resource Conservation and Recovery Act
RE.....	Relative Error
RH.....	Relative Humidity
RL.....	Reporting Limit
S.....	South
SA.....	Source Apportionment
SE.....	Southeast
SEM.....	Standard Error of Mean
SIM.....	Selected Ion Monitoring
SRM.....	Standard Reference Material
SVOC.....	Semivolatile Organic Compound
SW.....	Southwest

LIST OF ABBREVIATIONS (continued)

T-c	Temperature-corrected
TRI	Toxics Release Inventory
TACO.....	Tiered Approach to Corrective Action Objectives
UP	Upper Peoria
USGS	United States Geologic Survey
USEPA.....	United States Environmental Protection Agency
USACE	United States Army Corps of Engineers
UCL.....	Upper Confidence Level
VP	Vapor Pressure
W.....	West
WD	Wind Direction
WS.....	Wind Speed
Wt.....	Weight

SUMMARY

Chicago, Illinois, USA is a highly urbanized area with over eight million people in and around the region. As a historical center of heavy and high-tech industry and a global transportation hub, Chicago has been impacted by past and present sources of environmental contamination. Hundreds of hazardous waste sites, as well as more widespread water, sediment, and soil contamination represent potential ongoing sources of contaminants into the environment. These in turn affect human health, as well as the ecological health of the of the region's aquatic systems (such as Lake Michigan and the Chicago Area Waterway System), land (soil, natural preserves, and agriculture), and air. The primary objective of this research is to investigate the utility of receptor-based source apportionment approaches to identifying the sources of semivolatile polycyclic aromatic hydrocarbons (PAHs) and polychlorinated biphenyls (PCBs) to multiple environmental media in the Chicago metropolitan 'area of influence'. The multimedia focus of this investigation includes an air-shed (the Indiana Harbor and Canal; IHC) and an aquatic system (the Illinois River). This comprehensive source apportionment analysis achieves practical results for enhancing Chicago metropolitan area natural resources while assessing the limitations of source apportionment in terms of methods, data, contaminants, media, and application.

The Indiana Harbor and Canal (IHC) study utilized an extensive air monitoring dataset of PAHs and PCBs to examine spatial and temporal variations in background contamination and local project impacts. PCBs and all PAHs except naphthalene and acenaphthylene exhibited statistically significant temperature variations predicted from the Clausius-Clapeyron (C-C) equation. Statistically significantly greater levels of PCBs were observed at stations downwind from the IHC, while no significant differences were observed in PAH levels with wind direction; consistent with an IHC source for PCBs and a non-local source or multiple sources for PAHs. A

multiple linear regression model was developed that utilized meteorological data to explain 67% of PCB variability over time. Analysis revealed on-site construction activity had no statistically significant effect on PAH and PCB concentrations, and that levels of PCBs and PAHs are decreasing at a statistically significant rate at the South station, with halving times ranging from 7-20 years for PCBs and 9-27 years for PAHs.

Source apportionment analyses of the IHC data were performed utilizing quantitative Positive Matrix Factorization (PMF) with meteorological, temporal, location, and reference source data. PAH and PCB sources were corrected to 15 °C using the C-C equation to examine environmental effects on source contributions and identify sources within the matrix of seasonal variation. Results indicate multiple unique sources of airborne pollutants to the monitoring sites from primary emitters, as well as secondary environmental emissions identified with the aid of C-C corrections. Although both PAHs and PCBs are legacy contaminants, source apportionment results highlight the importance of current coke oven emissions as the chief source of atmospheric PAHs at IHC, accounting for over half of the contaminant mass, while petroleum storage and transfer and gas and diesel exhaust and are the next largest sources. PCB results identify the IHC canal as a source of Aroclor 1248 to the air-shed, having seasonal variation consistent with a volatile release mechanism and wind directionality consistent with the location. The incentive for the Illinois River study comes from a desire to develop beneficial reuse applications for sediment in the Illinois River. Currently, reuse is limited by levels of benzo(a)pyrene above existing contaminant standards. It is hypothesized that the PAHs derive from black carbon forms that might be less bioavailable (such as coal), and thus may not represent as high a risk for beneficial reuse. A source apportionment analysis was undertaken to identify the sources of PAHs to the Illinois River and to determine if they come from these

potentially low bioavailable forms. Priority PAHs were analyzed in 80 sediment cores sampled from Illinois River pools and backwater lakes between Hennepin, IL and the Peoria Lock and Dam. PAH ratio analysis and Positive Matrix Factorization (PMF) multivariate receptor modeling were used to characterize the PAH dataset, identify sources of pollutants, and quantify their contributions to the river sediment. Detailed PMF analysis indicated that a mixed upland source including coal-derived sources, and a diffuse transportation-based source contributed 75% and 25% percent, respectively, of the observed sediment PAH levels. Coal dust was not uniquely resolved from the coal-derived sources and thus could not be assessed for reduced PAH bioavailability. Comparison of the PMF results with the widely used PAH diagnostic ratio method indicates that the latter does a relatively poor job of uniquely resolving PAH sources in these sediments.

CHAPTER I. INTRODUCTION

Anthropogenic contamination drives threats to clean water, ecological and human health, climate, biodiversity, and essential ecosystem services on a global basis. Chicago is a highly urbanized area with over eight million people in and around the region. As a historical center of heavy and high-tech industry and a global transportation hub (numerous highway, airways, and shipping routes), Chicago has been impacted by past and present sources of environmental contamination. Hundreds of hazardous waste sites, as well as more widespread sediment and soil contamination represent just some sources that release toxic contaminants into the environment. These in turn affect natural features of the region, including Lake Michigan, the extensive Chicago Area Waterway System (CAWS), high quality native remnants and habitats, hundreds of threatened and endangered species, and also the health of its residents.

It is an often overlooked requirement to understand and identify the sources of pollutants to any environment as a prerequisite not only for remediation, but also to prevent future releases of pollutants. This task is made difficult by the expensive and time consuming processes of sampling, monitoring and analysis. Even with such concentration data, it is often difficult to identify sources without a detailed understanding the transport processes relevant for a given site (coupled contaminant transport and monitoring). This is particularly true for sites with multiple possible contaminant sources through multiple possible transport pathways (i.e. air, land, sediment and water). A more recent innovation to coupled transport and monitoring is to utilize mathematical analysis of the receptor data to determine what source(s) caused the observed results. Receptor models consist of a spectrum of techniques that have different levels of assumptions on the knowledge of the sources. On one end, chemical mass balance approaches utilize the distribution of contaminants in known sources to determine the contributions to the

receptor. On the other end of the spectrum, multivariate factorization methods (e.g. matrix factorization, principal component, and vector analysis) make no assumption on the source profiles and seek to determine both the contribution and the source profile matrices and the number of sources. The multivariate techniques have the advantage that they do not make assumptions on source profiles that may lead to incorrect apportionment. The disadvantage is that they require a number of environmental samples as well as quantitative comparison to sources and profiles post-modeling for useful and accurate identifications.

The primary objective of this research is to investigate the utility of receptor-based source apportionment approaches to identifying the sources of polycyclic aromatic hydrocarbons (PAHs) and polychlorinated biphenyls (PCBs) to multiple environmental media in the Chicago metropolitan 'area of influence'. The multimedia focus of this investigation includes an air-shed (the Indiana Harbor and Canal; IHC) and an aquatic system (the Illinois River). By applying a receptor-based source apportionment approach to critical contaminated sites in the Chicago metropolitan area, contamination sources may be identified and quantified in terms of the overall pollution burden. Material and operational sources may be targeted with control measures to reduce emissions and lessen health risks to humans and biota based on source apportionment results. Contaminant source-bioavailability interactions may also be examined to inform beneficial use of sediment and other natural resources. Finally conceptual models of source-receptor relationships are formed that may reveal weathering of pollution and temporal, spatial, and trans-boundary environmental processes. This comprehensive source apportionment study achieves practical results for enhancing Chicago metropolitan area natural resources while assessing best-practices for a range of source apportionment analyses.

CHAPTER II: LITERATURE REVIEW

Polycyclic Aromatic Hydrocarbons (PAHs) and Polychlorinated Biphenyls (PCBs) are persistent and ubiquitous contaminants in the environment. In the Chicago region, PAHs and PCBs are found throughout the air, soil, water and sediments; and have been known to drive toxicity in a number of contaminated sites.¹ The first portion of this review of the literature summarizes the state of the science regarding the physical and chemical properties, sources, and distribution of these compounds in the environment. The second part of this review examines a variety of source apportionment models and methods, focusing on the Positive Matrix Factorization (PMF) receptor model.

2.1. Polycyclic Aromatic Hydrocarbons (PAHs)

Polycyclic Aromatic Hydrocarbons (PAHs) are organic chemicals composed of a number of fused benzene rings (Figure 2.1). PAHs make up significant fractions of coal, crude oil and distillates, and are produced from the incomplete combustion byproducts of fossil fuel, wood, and other organic substances. PAHs are some of the most widespread organic pollutants due to their persistence and high rates of production.^{2, 3} PAHs typically occur as mixtures in the environment. Although hundreds of different PAHs are known, including alkyl and other substituted forms, 16 PAHs are of common environmental concern and are regulated as priority pollutants by the United States Environmental Protection Agency (USEPA). These include: Naphthalene (Nap), Acenaphthylene (Acy), Acenaphthene (Ace), Fluorene (Flo), Phenanthrene (Pha), Anthracene (Ant), Fluoranthene (Fla), Pyrene (Pyr), Benzo(a)anthracene (BaA), Chrysene (Chr), Benzo(b)fluoranthene (BbF), Benzo(k)fluoranthene (BkF), Benzo(a)pyrene (BaP), Dibenz(a,h)anthracene (DahA), Indeno(1,2,3-cd)pyrene (Ind), and Benzo(ghi)perylene (BghiP).

Given their known chronic toxicity including cancer, mutation, and birth defects, PAHs remain important contaminants of concern.^{4, 5}

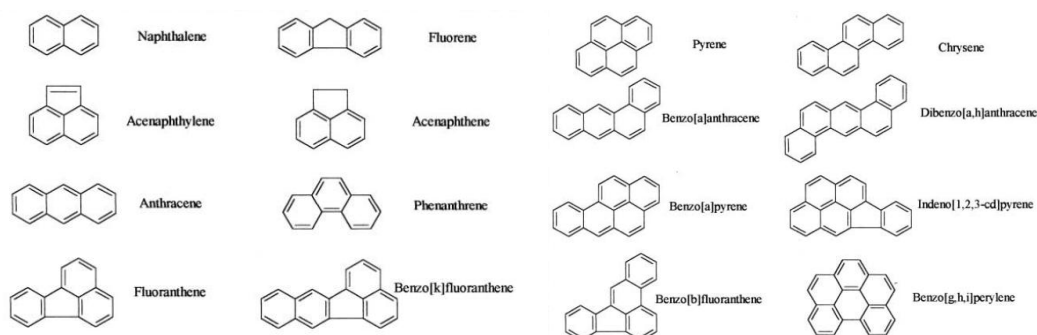


Figure 2.1. Chemical structure of USEPA designated priority PAHs. Adapted with permission from Fahnrich et al. (2002).⁶

Pyrogenic PAHs are formed during high temperature incomplete combustion of organic matter in nature and industrial processes. During pyrolysis complex organic molecules are partially broken into smaller free radicals that may reassemble during pyrosynthesis to form stable PAH compounds (and soot or ‘black carbon’).⁷ The amounts and relative ratios of different PAHs that are formed depend on the combustion conditions, primarily temperature (from 200 °C to over 2000 °C), oxygen abundance, and type of material combusted (wood, coal, etc).⁸ Petrogenic PAHs are formed from organic matter at much slower rates by diagenetic processes. Decomposition and thermal maturation of fossil fuels over geologic time scales, often under higher pressures but lower temperatures than pyrolysis (~150 °C) produce petrogenic PAHs. PAHs originating from natural biologic processes and diagenesis of shorter time scales are present at significantly lower levels than pyrogenic and petrogenic PAHs.⁷

The properties affecting fate and transport of PAHs in the environment typically vary strongly with molecular weight.⁴ In general, 2- and 3-ring PAHs (Nap, Acy, Ace, Flo, Pha, Ant) are considered low molecular weight (LMW), 4-ring PAHs (Fla, Pyr, BaA, Chr) medium molecular

weight (MMW), and 5- and 6-ring PAHs (BbF, BkF, BaP, DahA, Ind, BghiP) high molecular weight (HMW). Physical properties of the 16 priority PAHs are shown in Table 2.1 from EPI Suite (Estimation Program Interface Suite, v. 4.1, USEPA, Washington, DC, USA). PAHs are solid at standard temperature and pressure, and increase in melting and boiling point with increasing molecular weight. Aqueous solubility and vapor pressure decline rapidly with increasing molecular weight, but are within the range for semivolatile contaminants. Values of log K_{OW} (octanol-water partitioning coefficient) indicate PAHs are highly hydrophobic, generally becoming more hydrophobic with increasing with molecular weight.

PAHs disperse in the environment according to their physical and chemical characteristics. PAHs are persistent (resistant to degradation) due in part to stable bonding and relatively low vapor pressures and solubility.⁹ Vapor phase PAHs in air and dissolved phase PAHs in water and precipitation are dominated by LMW PAHs, while solid-phase PAHs in particulates, soil, and sediments are mainly HMW PAHs. Semivolatile PAHs partition between environmental surfaces and the atmosphere depending on the ambient temperature, one of the most important factors influencing their fate and behavior.¹⁰ Because warmer temperatures favor evaporation and cooler temperatures favor deposition, atmospheric concentrations are often higher in warm months than in cool months and sometimes during day than in the night; however other drivers like nearby industry or heating can increase PAH levels, particularly HMW PAHs, during cooler months.¹¹ Global long-range transport can also occur and deposit PAHs from warm latitudes to the arctic.¹² PAHs in air (gas or suspended particulate phase) may travel long distances prior to removal by dry or wet deposition, gas-terrestrial exchange, and air-water exchange.¹³ PAHs in effluents, storm water, and oil can enter surface water directly and volatilize to air or sorb to settling particles.

Table 2.1. Select physical properties^a of priority PAHs.

Compound	Mol. Formula	Mol. Weight (g/mol)	Log K _{OW}	Melting Point (°C)	Boiling Point (°C)	Vapor Pressure ^b (mm Hg)	Water Solubility ^b (mg/L)	Henry's Law Constant ^b (K _H) (atm-m ³ /mol)	Log K _{OA}
Naphthalene (Nap)	C ₁₀ H ₈	128.18	3.3	80.2	217.9	8.50E-02	31	4.40E-04	5.19
Acenaphthylene (Acy)	C ₁₂ H ₈	152.2	3.94	92.5	280	6.68E-03	16.1	1.14E-04	6.27
Acenaphthene (Ace)	C ₁₂ H ₁₀	154.21	3.92	93.4	279	2.15E-03	3.9	1.84E-04	6.31
Fluorene (Flo)	C ₁₃ H ₁₀	166.22	4.18	114.8	295	6.00E-04	1.69	9.62E-05	6.79
Phenanthrene (Pha)	C ₁₄ H ₁₀	178.24	4.46	99.24	340	1.21E-04	1.15	4.23E-05	7.57
Anthracene (Ant)	C ₁₄ H ₁₀	178.24	4.45	215	339.9	6.53E-06	0.0434	5.56E-05	7.55
Fluoranthene (Fla)	C ₁₆ C ₁₀	202.26	5.16	107.8	384	9.22E-06	0.26	8.86E-06	8.88
Pyrene (Pyr)	C ₁₆ C ₁₀	202.26	4.88	151.2	404	4.50E-06	0.135	1.19E-05	8.8
Benzo(a)anthracene (BaA)	C ₁₈ H ₁₂	228.3	5.76	84	437.6	2.10E-07	.0094	1.20E-05	9.07
Chrysene (Chr)	C ₁₈ H ₁₂	228.3	5.81	258.2	448	6.23E-09	.002	5.23E-06	9.48
Benzo(b)fluoranthene (BbF)	C ₂₀ H ₁₂	252.32	5.78	168	442.75	5.00E-07	.0015	6.57E-07	10.35
Benzo(k)fluoranthene (BkF)	C ₂₀ H ₁₂	252.32	6.11	217	480	9.65E-10	.0008	5.84E-07	10.73
Benzo(a)pyrene (BaP)	C ₂₀ H ₁₂	252.32	6.13	176.5	495	5.49E-09	.00162	4.57E-07	10.86
Dibenz(a,h)anthracene (DahA)	C ₂₂ H ₁₄	278.36	6.75	269.5	524	9.55E-10	.00249	1.41E-07	11.99
Indeno(1,2,3-cd)pyrene (Ind)	C ₂₂ H ₁₂	276.34	6.7	163.6	536	1.25E-10	.00019	3.48E-07	11.55
Benzo(ghi)perylene (BghiP)	C ₂₂ H ₁₂	276.34	6.63	278	500	1.00E-10	.00026	3.31E-07	11.50

^aValues from Estimation Programs Interface (EPI) Suite (v. 4.1, US Environmental Protection Agency, Washington, DC, USA). Experimental values are given when available. Estimated values are shown in italics.

^bAt 25 °C.

Because of their tendency to dissolve in lipoidal substances, PAHs concentrate in sediments and soils and bioaccumulate.¹⁴ PAHs can be transformed in surface waters by photooxidation, chemical oxidation, and microbial metabolism.^{15, 16} Temperature, oxygen availability, microbial populations, and other environmental conditions strongly influence these processes.¹⁷ Half-lives of PAHs dissolved in clear water with abundant oxygen and sunlight can be less than an hour, however once sorbed to particulates and sediments can be weeks to years for degradation by microbial co-metabolism.¹⁸ Bioavailability decreases drastically from the aqueous to the solid phase, where PAHs may become increasingly sequestered in organic matter by diffusion into micropores over time and high binding affinity toward condensed black carbon forms.¹⁹ Pyrogenic PAHs are distributed more widely in the environment than petrogenic PAHs, due in part to pyrolysis related black carbon making PAHs less available for degradation.⁷

PAHs accumulate in terrestrial and aquatic plants, fish, and invertebrates, though many animals can metabolize and eliminate them. PAHs in fish and crustaceans commonly bioconcentrate by factors up to 10^5 , and sub-lethal levels of PAHs can induced morphological, physiological, and development abnormalities in fish and significant reduction in egg hatchability, and larval length and weight.¹⁸ However the ability of PAHs to produce cancers in exposed organisms is the main concern.²⁰ PAHs are the largest class of suspected carcinogens and are likely potent carcinogens in humans.⁴ PAH implicated activities like tobacco smoking, eating smoked and grilled fish/meat, and exposure to air pollution are clearly linked to higher mortality.

2.1.1. Sources of PAHs

Pyrogenic PAHs generated by the incomplete combustion of organic fuels (petroleum, oil, coal, wood, biomass) are the dominant source to the environment.^{2, 8} Common anthropogenic sources include gasoline or diesel burning engines, residential wood or oil burning stoves and furnaces,

incineration, power generation, and industrial processes including coke production.² Forest fires and volcanic activity are natural sources that can produce extremely high atmospheric concentrations, but occur more rarely and contribute a relatively small fraction over time compared to anthropogenic activity.⁴ Natural hydrocarbon seeps are likely a significant source of petrogenic PAHs to the marine environment.⁷ Anthropogenic petrogenic PAH inputs include crude oil, coal, fossil fuel products or byproducts like refined oils, asphalt, coal tar, sealants, and creosote, and releases from hazardous waste processing sites such as refineries, wood treatment plants, and manufactured-gas sites. They are likely to be released through effluent discharge, runoff over land, and accidental spills during use or transport²¹ often to receiving waters. Recently coal tar based parking lot sealant has been identified as a major source of PAHs to aquatic systems.^{22, 23} Individual PAHs are not widely produced commercially; only naphthalene production is a significant source to the environment for its use in moth repellent consumer products and chemical manufacturing for polyvinyl chloride plastic.⁵

Sources of PAHs in the environment are not characterized accurately enough. Chemical inventories are generally limited and given over very large spatial and temporal scales,²⁴ and emission factors are often developed from an unrepresentative number of facilities' data that also vary within source categories.²⁵ Clearly sources to atmosphere and the aquatic environment can differ widely by space and time and due to intra-source variations related to complexity of combustion processes, different fuel mixtures etc.^{2, 4, 26} However PAHs and their relative compositions are often considered unique to various source types, and can be useful as tracers of organic matter in the environment.²⁷⁻³² PAHs have been analyzed in a number of source emissions for characteristic fingerprints or profiles in the literature. PAH profiles exist for steel and iron industry coke ovens, blast furnace, electric arc furnace, basic oxygen furnace, coal

plant, and heavy oil plant, and cement manufacturing raw materials handling and kiln feed pyroprocessing steps.^{33, 34} Profiles also are reported for coals,³⁵⁻³⁸ diesel trucks,^{39, 40} particulates,⁴¹ and biodiesel emissions,⁴² gas-powered vehicles,^{43, 44} industrial boilers and various feedstocks,⁴⁵ crude oils, fresh crankcase or lubricating oil, used crankcase oil,⁴⁶⁻⁴⁹ asphalt, tire wear,⁴⁷⁻⁴⁹ street dust,^{50, 51} roadside air, and vehicle soot.^{47, 52} In addition, PAH profiles are reported for municipal sewage sludge and medical waste incinerators,^{53, 54} coal tar,⁵⁵ coal tar sealcoat²² and parking lot dust,^{56, 57} creosote,^{58, 59} and wood and biomass burning.⁶⁰⁻⁶² In the Chicago area, Khalili et al. (1995)⁶³ reported profiles for coke ovens, gas and diesel emissions, highway tunnel, and wood burning. Li et al. (2003)⁶⁴ compiled numerous source profiles from the literature (coke oven, coal-fired power plant, residential coal burning, gas and diesel emissions, highway tunnel) and Bzdusek et al. (2004)⁶⁵ compiled wood burning literature profiles for use in source apportionment of PAHs to sediments of Lake Calumet in Chicago. Select PAH source profiles for air and sediment are shown in Figures 2.2 and 2.3, respectively.

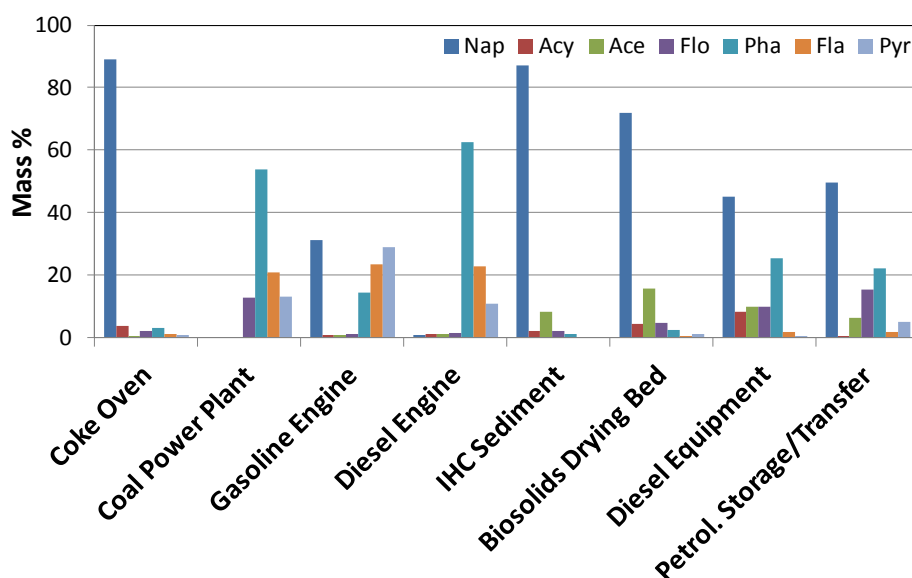


Figure 2.2. Select PAH atmospheric source profiles. Coke oven through diesel engine from Li et al. (2003),⁶⁴ IHC sediment from USACE (2010),⁶⁶ biosolids from Gulezian et al. (2012),⁶⁷ and diesel equipment and petroleum storage and transfer from 2008 National Emissions Inventory (v.2 USEPA).

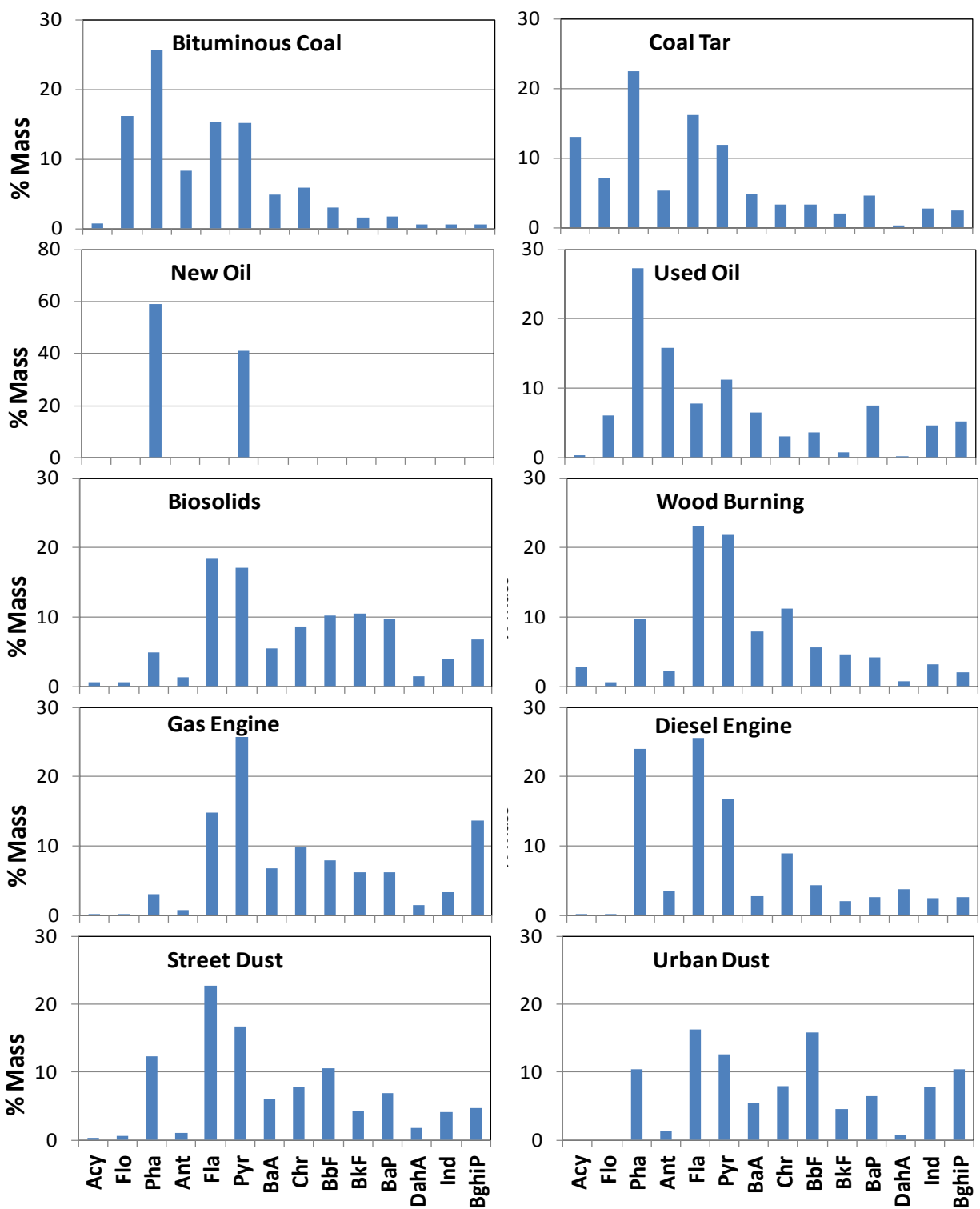


Figure 2.3. Select PAH reference source profiles for sediment (note all axes are same except for new oil). Bituminous coal from Stout and Emsbo-Mattingly (2008),⁶⁸ coal tar from Wise et al. (2010),⁵⁵ new and used lubricating oil from Wang et al. (2000),⁴⁶ biosolids from Gulezian et al. (2012),⁶⁷ wood burning from Bzdusek et al. (2004),⁶⁵ gas and diesel engine from Li et al. (2003),⁶⁴ street dust from Boonyatumanond et al. (2006),⁵⁰ and urban dust standard from NIST (2009).⁶⁹

2.1.2. PAH distribution in the Chicago metropolitan area

PAHs tend to concentrate in urban centers and decrease with increasing distance from local and regional sources.² Petrogenic PAHs typically associate with a local point source like a refinery or adjacent to roads and canals, while pyrogenic PAHs occur over broader geographic scales and typically dominate in terms of environmental abundance and distribution.⁷ Over the last half century, shifts toward non-coal fossil fuels for home heating and regulated emissions controls have reduced urban particulate pollution, improved air quality, and contributed to decreasing PAH concentrations observed in dated sediment cores.⁷⁰⁻⁷³ However traffic related pollution concurrent with rising population and density of urban metropolitan areas threatens to increase levels of PAHs in water bodies in the US,⁷⁴ and PAHs are certainly increasing in rapidly developing regions of the world.⁷⁵

Odabasi et al. (1999)⁷⁶ measured the average Σ_{14} PAHs in the Chicago atmosphere, with gas plus particulate phase concentrations as high as 428 ng/m³ and individual PAH mass contributions dominated by volatile PAHs in the gas phase (Figure 2.4). The particle/gas phase distribution varied widely among PAHs, increasing with increasing molecular weight and with decreasing temperature. Simcik et al. (1999)⁷⁷ attributed nearly half of PAHs in the Chicago urban and coastal atmosphere to coal combustion by a source apportionment analysis (Figure 2.5).

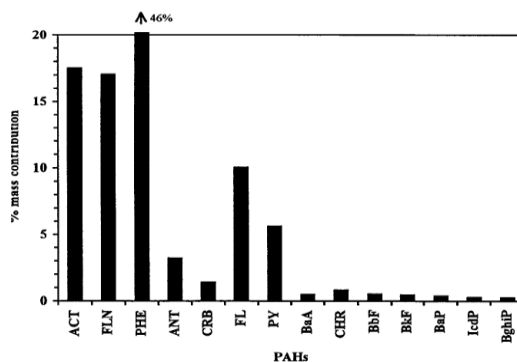


Figure 2.4. Mass percent contribution of individual PAHs to Σ_{14} PAHs in Chicago air. Adapted with permission from Odabasi et al. (1999).⁷⁶

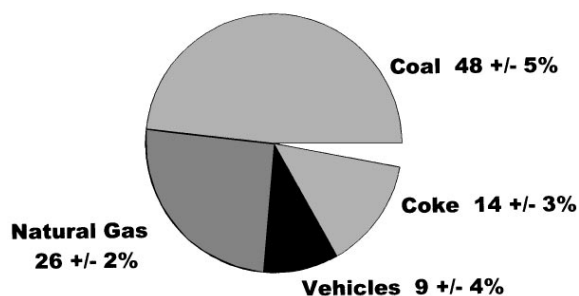


Figure 2.5. Source contributions of PAHs to Chicago coastal air. Adapted with permission from Simcik et al. (1999).⁷⁷

Sediment levels in water bodies of the Chicago metropolitan area vary widely. Surface sediment concentrations range from 0.8 mg/kg (Σ_{20} PAHs) in Lake Michigan (Rockne et al., unpublished), 4.9-20 mg/kg (Σ_{17} PAHs) in Lake Calumet,⁶⁴ and 12,000 mg/kg (Σ_{17} PAHs) in Lake of the Hills in McHenry County.⁷⁸ Small water bodies and coastal aquatic environments tend to receive PAH inputs more often from point sources and tributaries, while the majority of the PAH burden in Lake Michigan and the Great Lakes is attributed to atmospheric depositional loading.¹³ Net gas exchange dominates atmospheric loading of PAHs to the Great Lakes, while wet and dry deposition play a larger role near urban centers like Chicago.⁷⁹ PAH atmospheric loadings to the Great Lakes show no declining trend,¹³ and smaller lakes are showing an increasing trend in overall PAH loading.⁸⁰ Sediment PAHs in Lake Calumet of Chicago were apportioned by a mass balance receptor model⁶⁴ and factor analysis receptor model⁶⁵ that both identified coke ovens and vehicular traffic as the major contributors to sediment PAHs. Dated sediment cores from central Lake Michigan apportioned for PAH sources by factor analysis⁸¹ identified traffic (45%), coke oven (35%), and wood burning (20%) emission sources (Figure 2.6).

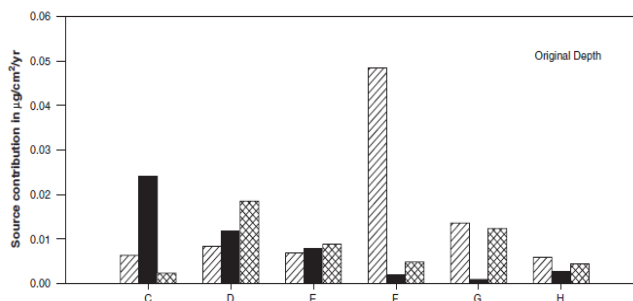


Figure 2.6. Average flux contributions from petroleum (hatched), coal (black), and wood (cross hatched) combustion to six Lake Michigan cores dated 1936-1996. Adapted with permission from Christensen and Arora (2007).⁸¹

Chicago surface soils have a median Σ_{16} PAH concentration of 10.9 mg/kg dry wt. with profiles resembling depositional particles mainly from combustion of fossil fuels.⁸² Concentrations were loosely correlated with proximity to industry but not to any other land use (including roadways) or to organic carbon content of the soil.

2.2. Polychlorinated Biphenyls (PCBs)

Polychlorinated Biphenyls (PCBs) are a class of synthetic chlorinated organic compounds used in dielectric fluids for transformers and capacitors, as plasticizers, and as additives to resins, rubber, and hydraulic and lubricating oils.^{83, 84} PCBs are classified based on the number and position of chlorine atoms on the biphenyl structure and consist of ten homolog groups and 209 possible congeners (Figure 2.7). PCB toxicity and environmental occurrence were widely reported starting in the late 1960s and early 1970s leading to voluntary production bans in the US in 1977 and federal ban on use in 1979.⁸³ Yet due to environmental persistence and bioaccumulative capacity, PCBs remain a threat for immune, nervous, reproductive, and endocrine system toxicity and carcinogenic potential. PCBs impact fish, wildlife, and human health mainly through the food web and exposure by ingestion.^{83, 85}

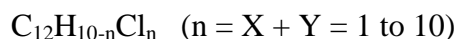
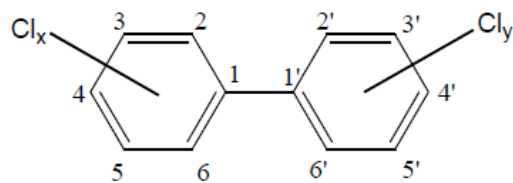


Figure 2.7. PCB chemical structure and formula from ATSDR (2000).⁸³

PCBs were formed by chlorination of biphenyl with molecular chlorine in the presence of a catalyst. Chlorine substitution increased with reaction time and conditions, producing PCB mixtures containing a range congeners of which about 130 were common.^{83, 86} Seven PCB mixtures were widely produced in the US under the trade name Aroclor with a four digit number in which the last two digits indicated the percent chlorine by mass. About 624,000 metric tons of PCBs, nearly half the worldwide production, were manufactured in the US from 1929 – 1977.^{86, 87} Historical production of the 22 most common PCB congeners are shown in Figure 2.8. Physical properties for select PCB and Aroclor mixtures are given in Table 2.2.

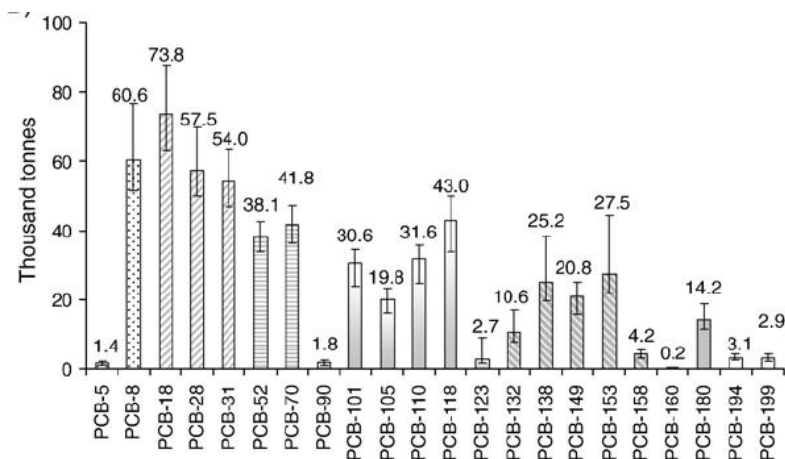


Figure 2.8. Estimated cumulative global production of the most common PCB congeners. Adapted with permission from Breivik et al. (2007).⁸⁸

Table 2.2. Physical properties^a of select PCB congeners and Aroclors.

Compound	Molecular Formula	Molecular Weight (g/mol)	Log K_{OW}	Melting Point (°C)	Boiling Point (°C)	Vapor Pressure^b (mm Hg)	Water Solubility^b (mg/L)	Henry's Law Constant^b (K_H) (atm-m³/mol)	Log K_{OA}
CB 8	C ₁₂ H ₈ CL ₂	223.1	5.09	<i>81.47</i>	<i>320.32</i>	2.09E-03	1.17	2.30E-04	7.4
CB 15	C ₁₂ H ₈ CL ₂	223.1	5.23	149.3	317	5.35E-04	0.062	1.99E-04	7.68
CB 18	C ₁₂ H ₇ CL ₃	257.55	5.55	<i>100.85</i>	<i>340.7</i>	1.05E-03	0.4	2.50E-04	7.6
CB 28	C ₁₂ H ₇ CL ₃	257.55	5.62	<i>100.85</i>	<i>340.7</i>	1.95E-04	0.27	2.00E-04	<i>7.707</i>
CB 31	C ₁₂ H ₇ CL ₃	257.55	5.69	<i>100.85</i>	<i>340.7</i>	4.00E-04	0.143	1.90E-04	7.92
CB 118	C ₁₂ H ₅ CL ₅	326.44	7.12	<i>134.6</i>	<i>378.21</i>	8.79E-06	0.0134	2.88E-04	9.82
Aroclor 1016	C ₁₂ H ₇ CL ₃	257.55	5.62	<i>100.85</i>	<i>340.7</i>	4.00E-04	0.42	2.00E-04	<i>7.707</i>
Aroclor 1242	C ₁₂ H ₆ CL ₄	291.99	7.10	<i>122.32</i>	<i>359.51</i>	8.63E-05	0.277	1.90E-04	<i>8.4</i>
Aroclor 1248	C ₁₂ H ₆ CL ₄	291.99	6.20	<i>122.32</i>	<i>359.51</i>	4.94E-04	0.1	4.40E-04	<i>7.945</i>
Aroclor 1254	C ₁₂ H ₅ CL ₅	326.44	6.50	<i>134.6</i>	<i>378.21</i>	6.53E-06	0.0034	2.83E-04	10
Aroclor 1260	C ₁₂ H ₃ CL ₇	395.33	7.55	<i>163.56</i>	<i>415.6</i>	<i>1.30E-07</i>	0.0144	3.36E-04	<i>9.412</i>

^a Values from Estimation Programs Interface (EPI) Suite (v. 4.1, US Environmental Protection Agency, Washington, DC, USA). Experimental values are given when available. Estimated values are shown in italics.

^b At 25 °C

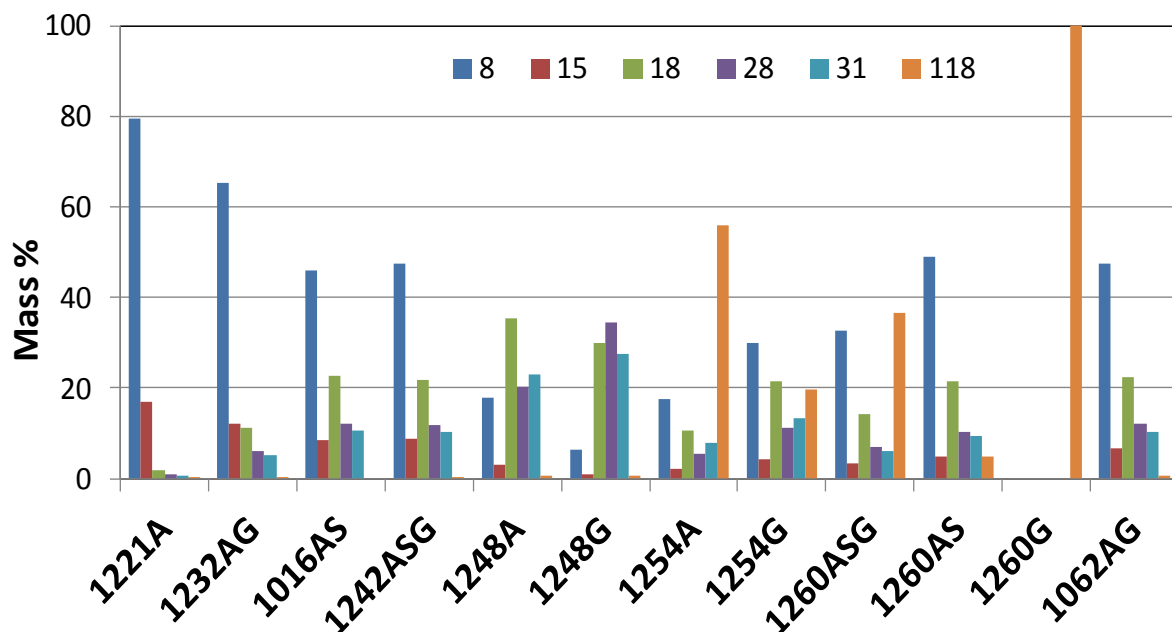
Environmental properties generally vary by degree of chlorination of the biphenyl molecule or Aroclor mixture. Solubility, vapor pressure, flammability, and reactivity tend to decrease with increasing chlorination, however properties can vary greatly within homolog groups such as vapor pressure increasing exponentially with additional *ortho* position chlorines.⁸⁵ Though most PCB congeners are solid at standard temperature and pressure, the mixtures were usually oily liquids or resins.⁸³ Characteristics like low aqueous solubility, non-flammability, resistance to oxidation, resistance to hydrolysis, and low electrical conductivity contributed to their widespread use in industrial applications as well as their persistence in the environment.

PCBs in the environment may vary from the composition of the original Aroclor mixtures through partitioning, transformation, and preferential bioaccumulation. Like PAHs, PCBs distribute among gas and particle phases and cycle between air, water, sediment, and soil.^{9, 89} Entering the atmosphere by evaporation, PCBs may deposit on land, water, and undergo long range transport to northerly latitudes and are found around the world.¹² The diurnal and seasonal effect of temperature on gas phase PCB concentrations tends to follow the Clausius-Clapeyron equation with atmospheric concentrations governed by volatilization at higher temperatures and sorption to surfaces at lower temperatures.^{85, 90} Heavier particle bound PCBs can settle into sediments and persist for years, release into the water column for uptake by aquatic organisms, and bioconcentrate to levels thousands of times higher than in water.⁸⁵ Environmental biodegradation by dioxygenase enzyme activity or anaerobic reductive dehalogenation, photolysis, and atmospheric reactions with the hydroxyl radical occur particularly with lower-chlorinated congeners. However degradation is not highly effective in decreasing total PCB concentrations in dilute systems.⁸⁵

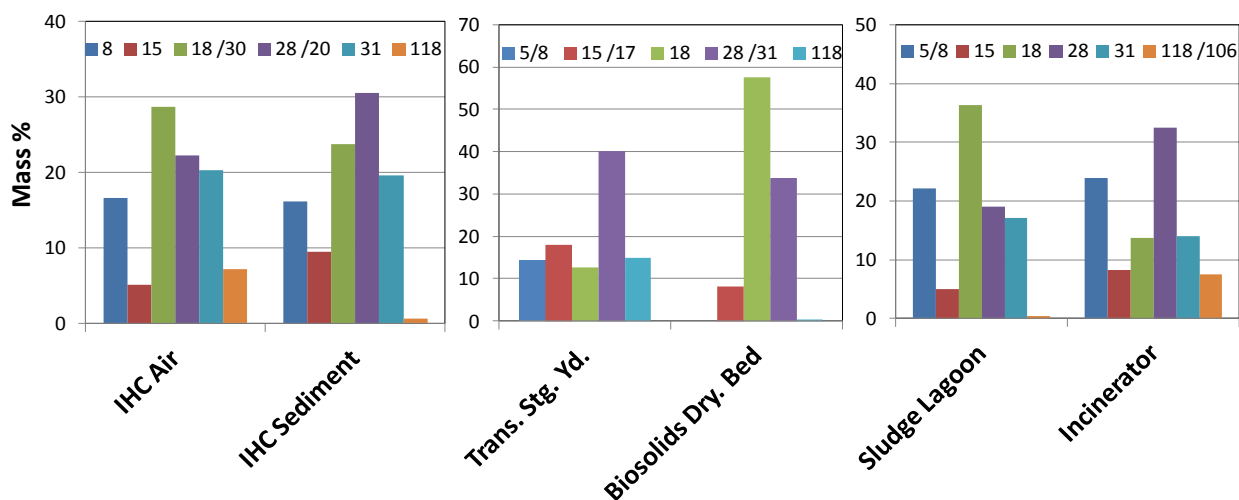
2.2.1. Sources of PCBs

Sources of current PCB releases are related to past consumption and often difficult to characterize.^{85, 91} Usage sources consist of controllable closed applications like capacitors and transformers, uncontrollable closed systems including small capacitors in fluorescent lighting, air conditioners, pumps, fans, and other electrical appliances, as well as hydraulic fluids and lubricants, and open usages such as plasticizer and fireproofing agents in paints, plastics, ink, adhesives, and copy paper.⁹¹ Disposal sources include landfills, open burning, and waste incineration. Accidental release sources include fires and spills.⁹¹

The vast majority of PCBs are unaccounted for, especially in air, and emission inventories are severely lacking.⁸⁵ Volatilization-based sources from previously deposited material, typically in urban areas, are primary sources to the atmosphere.^{85, 92} In some cases environmental contamination of PCBs still reflect the original Aroclor mixtures with known congener profiles.^{83, 93} PCB emissions and congener source profiles for a number of industries and materials have been reported in the literature, including incinerators,^{54, 94-97} metallurgical industries,⁹⁸ ships,⁹⁹ diesel engines,³⁹ biosolids drying beds,¹⁰⁰ coking plant,¹⁰¹ firewood,^{96, 102} oil furnace,¹⁰³ and power station.⁵⁴ Hsu et al. (2003)¹⁰⁴ measured atmospheric PCB profiles of landfill, transformer storage yard, and biosolids drying bed sites in Chicago, and Martinez et al. (2010)¹⁰⁵ measured atmospheric (gas-phase), water (dissolved-phase), and sediment (solid-phase) profiles for the Indiana Harbor and Canal in northwest Indiana. Atmospheric PCB profiles of Aroclor mixtures (Figure 2.9A) and Chicago area sites (Figure 2.9B) are shown.



A)



B)

Figure 2.9. Select PCB atmospheric source profiles of (A) Aroclor mixtures from Frame et al. (1996)⁹³ and (B) known reference sources: IHC air and sediment from Martinez et al. (2010),¹⁰⁶ transformer storage yard and biosolids drying bed from Hsu et al. (2003),¹⁰⁴ Ralston sludge lagoon from Gary Sanitary District (2007),¹⁰⁷ and municipal waste incinerator from Ikonomidou et al. (2002).⁹⁴

2.2.2. PCB distribution in the Chicago metropolitan area

About 400,000 tons of PCBs in the global environment is distributed approximately 60% in the hydrosphere (mainly marine), 1% in atmosphere, and the remaining in terrestrial environments.^{9, 88, 108} Dated sediment core depositional trends show PCBs decreasing the last 30 years, although their continued presence remains a threat. Lake sediment core data in North America suggest environmental PCB levels peaked around 1970 with an average decrease of about 60% in PCB fluxes since then.¹⁰⁸ Recent studies indicate revolatilization from water bodies is a principal source of PCBs to the atmosphere.⁸⁵

At the regional scale, PCB concentrations and fluxes are both significantly higher in Chicago and other urban areas than in non-urban areas.^{85, 109} Hu et al. (2010)¹¹⁰ found Σ_{169} PCBs in Chicago air ranged from 75 – 5500 pg/m³, varied as a function of temperature, were enriched in lower chlorinated congeners in the gas phase, and resembled a combination of Aroclors 1242 and 1254 in terms of PCB congener pattern (Figure 2.10). Their presence at elevated levels throughout the city suggested multiple sources rather than few locations of high emissions.¹¹⁰ The non-Aroclor PCB 11 was also discovered for the first time as a ubiquitous and sometimes major component in Chicago air,¹¹¹ perhaps associated with paint production. Martinez et al. (2010)¹⁰⁵ measured average concentrations of 4500 pg/m³ for Σ_{158} PCBs in air over Indiana Harbor and Canal and estimated a flux of 7 kg/yr from the canal to the atmosphere. Potential source contribution function modeling of PCBs in Chicago air identified three major PCB source sectors; SW of Chicago, NW of Chicago, and the south side of Chicago/Lake Calumet neighborhood.¹¹² Hsu et al. (2003)¹⁰⁴ estimated PCB fluxes from Chicago transformer storage yard, biosolids drying bed, and landfill sources (see Figure 2.9B) contributed less than 10% to overall PCB concentrations in Chicago air based on dispersion modeling and a simple box model.

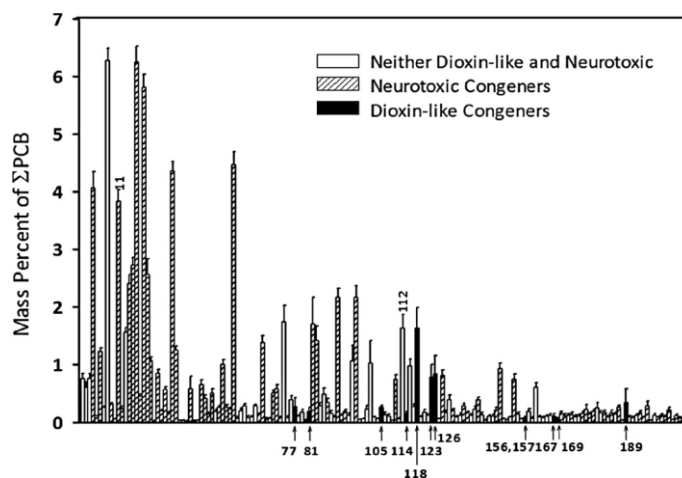


Figure 2.10. PCB congener profile in Chicago air. Adapted with permission from Hu et al. (2010).¹¹⁰

PCB concentrations in sediments are highly spatially variable and depend on a number of factors. Rivers, small lakes, and coastal areas can contain elevated amounts of PCBs due to industrial emissions. Indiana Harbor and Canal on Lake Michigan, surrounded by heavy industry and hazardous waste sites, has Σ_{163} PCB concentrations in sediments ranging from 53-35,000 ng/g dry wt. and resembling Aroclor 1248 with a small amount of weathering.¹⁰⁵ Table 2.3 lists total PCB concentrations in other Great Lakes tributary sediments from the literature.⁸⁵

Table 2.3. Sediment PCB concentrations in Great Lakes tributaries (ng/g dry wt.).^a

Location	Min	Max	Average	Date	Reference
Ashtabula, OH	500	7000	2000	1998	Imamoglu and Christensen (2002) ¹¹³
Fox, WI	132	223000	24300	1987-1994	Cacela et al. (2002) ¹¹⁴
Detroit, MI/ON	8	25000	4800	1998	Kannan et al. (2001) ¹¹⁵
Rouge, MI	470	10900	2500	1998	Kannan et al. (2001) ¹¹⁵
Manitowoc/Pine Creek, WI	< 50	1900000	44000	1993-1995	Steuer et al. (1999) ¹¹⁶
Milwaukee, WI	< 50	870000		1993-1995	Steuer et al. (1999) ¹¹⁶

^a Reproduced from Hornbuckle (2006).⁸⁵

In contrast, Lake Michigan PCB sediment concentrations average 40-70 ng/g¹¹⁷ and are dominated by atmospheric input of PCBs like other largely open or isolated water bodies.⁸⁵ A mass balance of PCBs in Lake Michigan (Figure 2.11) indicates atmospheric exchange is the most important process for PCB transport and identifies the lake as a net PCB source to the region primarily by volatilization.^{85, 118} Smaller temporal and spatial scale processes are more dynamic, for example over a number of days near Chicago net PCB gas exchange with southern Lake Michigan may change direction based on wind direction, temperature, and atmospheric PCB concentrations.¹¹⁹ PCB source apportionment analyses carried out in northern Lake Michigan canal and harbor sediments by Bzdusek et al. (2006)¹²⁰ and Rachdawong and Christensen (1997)⁸⁴ identified Aroclor mixtures in various states of weathering.

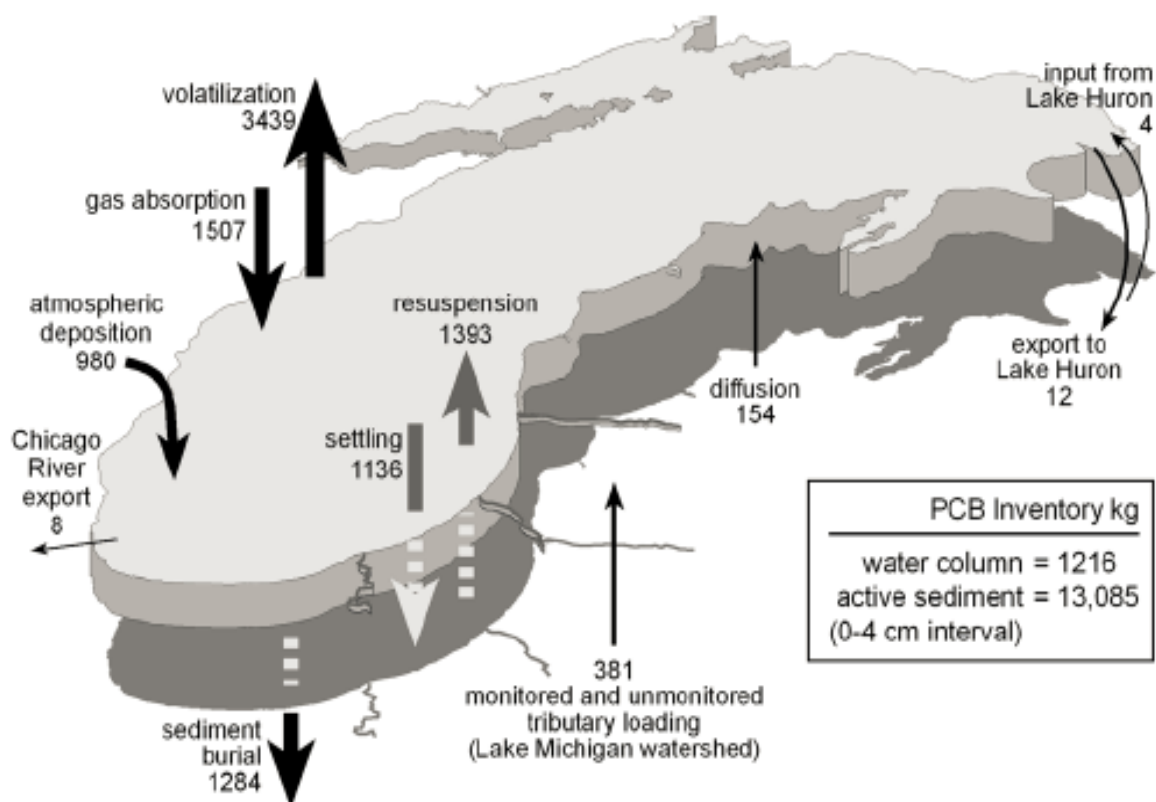


Figure 2.11. Mass budget average for 1994-1995 total PCBs in Lake Michigan (mass transported in kg/yr) from Rossmann (2006).¹¹⁸

2.3. Source Apportionment

Source apportionment aims to quantitatively apportion measured contaminant mass in the environment or ‘receptor’ to sources of contaminants. Determining which emissions sources contribute and how much each source is contributing is essential to reduce environmental contamination and ultimately health risks to humans and biota. Source apportionment methods operate on measured receptor data and exploit the fact that many sources or emitters have unique contaminant compositions that change little between source and receptor. Molecular markers, fingerprinting, and diagnostic ratios are sometimes used to qualitatively investigate sources of environmental contamination from known chemical concentrations.^{27, 121, 122} Stable isotope analysis is a relatively recent quantitative method for identifying sources of carbonaceous contaminants.¹²³ Receptor modeling is an extensive and powerful tool for source apportionment analysis, allowing for determination of multiple sources and obtaining quantitative source contributions based on conservation of mass.^{124, 125}

2.3.1. PAH diagnostic ratios

Diagnostic ratios have been developed to identify PAH sources in the environment based on relative characteristic proportions of certain PAHs in basic source types.²⁷⁻³² Relative amounts of PAHs in fossil fuels and combustion byproducts are related to thermal stability of each PAH and the temperatures at which they were formed.^{7, 27} Diagnostic ratios consist of PAHs with stability ranges that represent thermodynamic (fossil) versus kinetic (combustion) formation and distinguish between sources by an increase in proportion of one relative to the other. Ratios typically contain PAHs of a given molecular mass like 178 (which include Ant and Pha), 202 (which include Fla and Pyr), 228 (which include BaA and Chr) and 276 (which include Ind and BghiP) and are assumed to be environmentally stable based on similar properties.^{27, 28}

Yunker et al. (2002)²⁷ has reviewed four parent PAH diagnostic ratios Ant/178, Fla/Fla+Pyr, BaA/228, and Ind/Ind+BghiP for determining PAH sources to sediment and has reported ratio ranges indicating fossil versus combustion sources as well as values for a number of petroleum-derived, combustion-derived, and environmental samples (Table 2.4).^{27, 32} Some ratios further distinguish liquid (petroleum) fuel combustion from solid (biomass/coal) fuel combustion. Coal is not differentiated from petroleum fossil fuel, although ranges from samples have been reported.³² Molecular weight 178 refers to the sum of Ant+Pha, and molecular weight 228 refers to the sum of BaA+Chr+Triphenylene. The ratios are arranged in Table 2.4 as a fraction with the thermodynamically less stable PAH in the numerator and sum of the specified molecular weight PAHs in the denominator so all ratios increase with increasing combustion input and avoid division by zero or large and infinite values for ease of comparison and plotting.³² The PAH ratio method is a relatively simple tool for distinguishing sources in sediments, however there are limitations in terms of the relative discrimination ability and thermodynamic stability of different PAHs, variability of different PAH sources, relative stability of different PAHs from different sources to receptor, and ambiguity when samples are impacted from a number of sources equally.²⁷

Table 2.4. PAH diagnostic ratios of petroleum and combustion sources and samples.^a

	Ant/ 178^b	Fla/ Fla+Pyr	BaA/ 228^b	Ind/ Ind+BghiP
Petroleum	< 0.1	< 0.4	< 0.2	< 0.2 (< 0.1)^c
Kerosene	0.04	0.46	0.35	0.48
Diesel oil (n=8)	0.09	0.26	0.35	0.4
Crude oil (n=9)	0.07	0.22	0.12	0.09
Australian crude oils and fluid	0.03	0.43		
Shale oil	0.26	0.34	0.45	0.39
Lubricating oil		0.29	0.1	0.12
Coal (n=27)	0.2			
Asphalt			0.5	0.53
Coal (n=2) ^d	0.03 - 0.07	0.36 - 0.37	0.37 - 0.40	0.14 - 0.16
Combustion				
Liquid/Petroleum Fossil Fuel	> 0.1	0.4 - 0.5	> 0.35	0.2 - 0.5 (0.1 - 0.3)^c
Solid/Grass/Wood/Coal	> 0.1	> 0.5	> 0.35	> 0.5 (> 0.3)^c
Lignite and brown coal (n=3)	0.08	0.72	0.44	0.57
Bituminous coal (n=3)	0.33	0.53	0.34	0.48
Hard coal briquettes (n=9)		0.57	0.43	0.52
Coal tar (SRM 1597)	0.18	0.58	0.54	0.53
Wood soot (n=2)	0.26	0.5	0.46	0.55
Wood (n=19)	0.19	0.51	0.46	0.64
Grasses (n=6)	0.17	0.58	0.46	0.58
Gasoline (n=2)	0.11	0.44	0.355	0.155
Kerosene (n=3)	0.14	0.5	0.37	0.37
Diesel (n=25)	0.11	0.39	0.38	0.35
No. 2 fuel oil (n=2)	0.06	0.51	0.17	
Crude oil (n=4)	0.22	0.44	0.49	0.47
Environmental Samples				
Bush fire		0.61	0.23	0.7
Savanna fire particulate (n=3)		0.59		0.39
Road dust	0.18	0.42	0.13	0.51
Lubricating oil, re-refined		0.74		0.36
Used engine oil, gasoline passenger car	0.22	0.3	0.5	0.18
Used engine oil, diesel car, truck & bus		0.37		0.29
Tunnel with light duty gasoline vehicles (n=4)		0.45	0.46	0.3
Tunnel with heavy duty diesel trucks & gasoline vehicles n=5)		0.42	0.57	0.3
Roadway tunnels (n=2)	0.13	0.43	0.42	0.3
Urban air (including SRM 1648 & 649;n=3)	0.8	0.56	0.3	0.4
Creosote treated wood piling (n=4)	0.2	0.62	0.5	0.64

^a Reproduced from Yunker et al. (2002).²⁷ Petroleum and combustion ranges in bold.

^b 178 indicates Ant+Pha; 228 indicates BaA+Chr+Triphenylene.

^c Updated ranges are in parentheses, from Yunker et al. (2011, 2012).^{32, 126}

^d Coal range from Yunker et al. (2012)³² is based on samples of shipwrecked high volatile A bituminous coal.

2.3.2. Receptor Modeling

Receptor modeling is a more rigorous source apportionment method that quantifies contributions from various sources to the receptor site. Models are based on conservation of mass and operate on the premise that measured concentrations are a linear sum of independent sources.¹²⁴ Receptor models provide source information by solving the following mass balance equation (Eq. 2.1) modified from Hopke (1985)¹²⁴ for m compounds in n samples as contributions from p sources.

$$\mathbf{x}_{ij} = \sum_{k=1}^p \mathbf{g}_{ik} \mathbf{f}_{kj} + \mathbf{e}_{ij} \quad \begin{matrix} i = 1, m \\ j = 1, n \end{matrix} \quad (2.1)$$

\mathbf{x}_{ij} is the i th chemical concentration in the j th sample; \mathbf{g}_{ik} is the fractional abundance of the i th chemical (mass) in the k th source; \mathbf{f}_{kj} is the (mass) contribution of the k th source in the j th sample; \mathbf{e}_{ij} is the residual, or the difference between measured and calculated i th concentration in j th sample.

The matrix form of the equation is:

$$\mathbf{X} = \mathbf{G} \times \mathbf{F} + \mathbf{E} \quad (2.2)$$

\mathbf{X} is the measured concentration data matrix $m \times n$; \mathbf{G} is the factor-loading matrix $m \times p$ representing chemical profiles of sources; \mathbf{F} is the factor-score matrix $p \times n$ representing source contributions to sample concentrations; \mathbf{E} is the error concentration matrix $m \times n$ or the difference between measured and calculated matrices.

Receptor models have been used since the early 1970s corresponding to increased environmental awareness, regulation, and advances in analytical and computational techniques.^{124, 127} Traditionally apportionment studies focused on particulate matter and volatile organic compounds in the atmospheric field,¹²⁷⁻¹²⁹ but in the last two decades a multitude of contaminants in a variety of media including soil, sediments, and wastewater have been apportioned.^{64, 130-132} Four commonly employed receptor models include Chemical Mass Balance (CMB), Principal Component Analysis, (PCA), UNMIX, and Positive Matrix Factorization (PMF) that use different procedures to solve the basic least squares problem. CMB operates with as few as one receptor sample but requires input of known source compositions. Multivariate receptor models (MRMs) like PCA, UNMIX, and PMF require a number of samples but generate source profiles rather than requiring them as inputs, an advantage when sources are not known *a priori*. Receptor models generally assume source profiles do not change over the sampling period, remain unchanged between source and receptor site, and are not collinear to avoid misrepresentation of sources.^{64, 65, 84}

Although not needed as MRMs inputs, accurate source profiles are essential to successful modeling and should be representative of the study area and time. Source identification is often performed by comparing reference profiles with modeled profiles using a similarity metric like the cosine phi ($\cos \phi$) coefficient of proportional similarity (Eq. 2.3).^{133, 134} The cosine of the angle ϕ between model and reference profile vectors equals one if they are identical (i.e. in the same direction) and zero if they are different (i.e. perpendicular to one another).

$$\cos \varphi = \frac{\sum_{i=1}^m \mathbf{x}_i \mathbf{y}_i}{\sqrt{\sum_{i=1}^m \mathbf{x}_i^2} \sqrt{\sum_{i=1}^m \mathbf{y}_i^2}} \quad (2.3)$$

\mathbf{x}_i and \mathbf{y}_i are model and reference concentrations, respectively, for compound i .

2.3.3. Positive Matrix Factorization

Positive Matrix Factorization (PMF) is a flexible and robust multivariate receptor model^{135, 136} that has been applied to a number of contaminants in air,^{134, 137, 138} soil,¹³⁹ sediments,^{120, 133, 140} and wastewater.¹³² PAHs and PCBs have been successfully apportioned in air (gas and/or particulate phases)^{134, 141-143} and in sediments^{120, 130, 133, 144} by PMF. PMF solves the bi-linear matrix equation (Eq. 2.2) using an iterative weighted least squares fit that minimizes the objective function Q :¹³⁵

$$Q(\mathbf{E}) = \sum_{i=1}^m \sum_{j=1}^n \left(\frac{\mathbf{E}_{ij}}{\sigma_{ij}} \right)^2 \quad (2.4)$$

\mathbf{E}_{ij} is the error matrix $m \times n$; σ_{ij} is the standard deviation matrix of uncertainties weighting each measured element $m \times n$.

During minimization of Q , elements \mathbf{G} and \mathbf{F} are constrained to non-negativity to ensure realistic source profiles and contributions. By allowing weighting of measured data by their estimated uncertainties, PMF can reduce the influence of censored and outlier data on solutions and better represents signals of all strengths.^{135, 136}

This study utilizes the PMF program coded by Bzdusek (2005)¹⁴⁵ on the MATLAB platform (release 2011a, Mathworks, Inc., Natick, MA, USA) employing penalty terms for imposing constraints. This model successfully recognized source and degradation PCB patterns in lake and river sediments^{120, 130, 133} and obtained results similar to the PMF program publically available from USEPA (EPA Positive Matrix Factorization (PMF), v. 3.0, USEPA, Washington, DC, USA).^{125, 146} Major inputs to the model are the measured data matrix, the standard deviation matrix, and the number of sources to solve for. When individual uncertainties are not available for each data point, the standard deviation matrix can be estimated by environmental error model (EM) = -14^{145, 147, 148} involving detection limit (DL) and relative error (RE) information based on analytical, sampling, and environmental uncertainties (Eq. 2.5).

$$\sigma_{ij} = C_1 + C_2 \max(|X_{ij}| |X'_{ij}|) \quad (2.5)$$

σ_{ij} is the standard deviation concentration matrix; C_1 typically equals the DL; C_2 is a user defined value typically between .05 and .3 and can represent RE; X_{ij} is the original data matrix; X'_{ij} is the modeled data matrix.

The PMF solutions consist of chemical compositions of factors (**G**) (i.e. source profiles) expressed in mass percent and factor contributions to samples (**F**) (i.e. source contributions) expressed by absolute concentrations, with the overall percent of contaminant mass from each source. In addition to profiles and contributions, PMF generates a number of diagnostic tools to evaluate goodness of fit between modeled and measured data and facilitate choosing the correct solution (i.e. number of sources).¹⁴⁵ Coefficients of Determination (CODs) represent good to

excellent fit for each chemical for values ranging from 0.9 to 1.0, and the Exner function indicates excellent reproduction of the measured data for values of 0.1 to 0.0.^{133, 149} The number of degrees of freedom (ν) should also approximate the objective function Q (Eq. 2.4) in order for the error matrix \mathbf{E}_{ij} to approximate the assigned standard deviation matrix σ_{ij} .¹⁴⁹⁻¹⁵¹ The number of degrees of freedom, ν , are calculated by Equation 2.6.

$$\nu = m * n - p(m + n) \quad (2.6)$$

ν is the number of degrees of freedom; m is the number of compounds; n is the number of samples; p is the number of sources.

The possibility of multiple solutions to solve the same factorization problem may arise with PMF (i.e. rotational ambiguity), even when independent conditions or constraints like non-negativity are added to the model.^{125, 135} Rotational ambiguity is reduced when some values in the final source composition matrix \mathbf{G} and source contribution matrix \mathbf{F} are near zero, when different initial guesses of \mathbf{G} and \mathbf{F} produce the same final solution, and at times when rotational methods rather than penalty terms for non-negative constraints are used.^{145, 149}

Monte Carlo (MC) simulation provides a method to validate the PMF model and calculate uncertainties in model results by generating artificial datasets varied from known source profiles and contributions and subjecting the datasets to PMF.^{84, 120, 130} Successful reproduction of source profiles has been observed for PMF using the Monte Carlo simulation.^{84, 130} Varied datasets are generated according to Equation 2.7.

$$D_{ij} = A_{ij} + C_{ij}A_{ij}[\sqrt{2}\text{erf}^{-1}(2R_{ij} - 1)] \quad (2.7)$$

D_{ij} is the generated concentration of compound i and sample j ; A_{ij} is the original data matrix; C_{ij} is the assigned coefficient of variation (CV) of compound i from sample j ; erf^{-1} is the inverse Gaussian error function; R_{ij} is a random number between 0 and 1.

2.3.4. Utility of source apportionment techniques

Knowledge of contaminant sources and loadings to the environment is essential to pollution prevention and management. Inadequate source emission inventories are the greatest cause for uncertainty in environmental budget and mass balance calculations, particularly for persistent pollutants.⁹ Identifying sources and their contributions can verify or fill gaps of source emission inventories, direct specific emission control measures, and drive policy, institutional, and technological contaminant reduction efforts.

The benefits of source apportionment extend beyond the field of pollution prevention. For example, environmental forensics is a field developed to apply environmental analyses within the context of law to allocate liability for environmental contamination.¹²² A variety of source apportionment analyses are used in this field to determine the origin of contamination events and responsible parties.

Remediation, restoration, and reuse projects also benefit from source apportionment analysis. Source knowledge informs clean-up strategies, robust engineering and ecological design, and exposure reduction by understanding contaminant bioavailability. Bioavailability is a more important indicator of toxicity than concentration levels alone,¹⁵² and though difficult to obtain by direct measurements may be inferred by source information. For example, PAHs

preferentially partition to condensed forms of carbon that can serve to limit bioavailability,¹⁹ thus coal dust and certain pyrogenic PAHs are expected to be less bioavailable than petrogenic PAHs sourced to petroleum. Higher contributions of certain sources can suggest if bioavailability testing should be done to determine risks to ecological and human health.

Finally, source apportionment can improve our understanding of contaminant fate and transport in the environment. Contaminant transformation between source and receptor may reveal itself as a weathered or degraded profile and suggest important spatial, temporal, and environmental processes at work. For example, source apportionment has been extensively utilized to examine degradation pathways of PCBs in sediment.^{113, 120, 130, 133}

CHAPTER III: AIR MONITORING FOR THE INDIANA HARBOR AND CANAL CONFINED DISPOSAL FACILITY PROJECT: PRE-DREDGING TRENDS IN PAHS AND PCBS

3.1. Abstract

Sediments from the Indiana Harbor and Canal (IHC) are highly contaminated and the focus of a navigational dredge and disposal project. Extensive air monitoring tracking polycyclic aromatic hydrocarbons (PAHs) and polychlorinated biphenyls (PCBs), metals, and other volatile organic pollutants has taken place at the site since 2001 to assess spatial and temporal variations in background contamination and local project impacts. PAHs and PCBs were most prevalent and the focus of this investigation. All PCBs and PAHs except naphthalene and acenaphthylene exhibited statistically significant temperature variations predicted from the Clausius-Clapeyron equation. The importance of the IHC and construction of the nearby confined sediment disposal facility were investigated among myriad possible PAH and PCB sources in the highly industrialized area using the 288 K temperature-corrected data. Statistically significantly greater levels of PCBs were observed at all stations with wind from the IHC direction, while no significant differences were observed in PAH levels with wind direction; consistent with an IHC source for PCBs and dispersed or multiple sources for PAHs. A multiple linear regression model was developed that utilized meteorological data to explain 67% of PCB variability over time. Analysis revealed construction activity on-site had no statistically significant effect on PAH and PCB concentrations, and that levels of PCBs and PAHs are decreasing at a statistically significant rate at the South station, with halving times ranging from 7-20 years for PCBs and 9-25 years for PAHs. Ongoing air monitoring will provide information to determine what effect the dredging project may have on atmospheric pollution in the area.

3.2. Introduction

Polycyclic Aromatic Hydrocarbons (PAHs) and Polychlorinated Biphenyls (PCBs) are classes of persistent organic pollutants (POPs) cycling widely throughout the environment. Major sources of PAHs to the environment include incomplete combustion of fossil fuels and organic matter,^{2, 8} crude and refined fossil fuel products, and coke processing in the steel industry. PCBs were synthesized in the 20th century for a number of industrial applications and uses,⁹¹ and continue to be released from contaminated sites, incinerators, building materials,¹⁵³ fluorescent lighting and electrical equipment, and are inadvertently produced in pigments and paints.^{154, 155} Atmospheric inhalation is the greatest source of PAH exposure and the most common source of PCB exposure to the general population.^{4, 156} Urban air-sheds have elevated levels of PAHs and PCBs many times above rural concentrations, and can act as a regional source to the local environment^{4, 109, 157-159} by current production (in the case of PAHs), uncontrolled releases, and volatilization from contaminated environmental media.

The Indiana Harbor and Canal (IHC) is an active shipping harbor on the southwest shore of Lake Michigan about 27 km southeast of downtown Chicago, Illinois, USA. IHC is the most deficient United States Environmental Protection Agency (USEPA) designated Area of Concern (AOC) on the Great Lakes.¹⁶⁰ The majority of the impairment derives from so-called “legacy” pollution in the sediments; with toxicity driven by PCBs, PAHs, and heavy metals.¹ The United States Army Corps of Engineers (USACE) began a major dredging project as required to maintain navigational depth in the IHC. This project included construction of a Confined Disposal Facility (CDF) on an existing Resource Conservation and Recovery Act (RCRA) site adjacent to the Lake George branch of the canal to contain the dredged contaminated sediments. As part of the project, an ambient air monitoring program was established in 2001 at the CDF and the nearby East Chicago High School (the closest sensitive receptor) to create an ambient air quality

database, characterize background contamination levels prior to dredging activity, and document air quality impacts occur during construction of the CDF. Recently, sediment and air in this system have been studied in the literature.^{106, 161} The harbor air-shed has myriad possible air pollution sources including the canal itself,¹⁰⁶ nearby hazardous waste sites, CERCLA and Superfund sites, steel and chemical manufacturing facilities,¹⁶⁰ as well as coke plants, refineries, and other manufacturing nearby.

The goal of this study is to evaluate ambient PAH and PCB trends in a highly contaminated industrial harbor utilizing an extensive dataset spanning over ten years of atmospheric sampling, together with on-site meteorological data, at up to five monitoring stations. These data were used to investigate spatial and temporal variations through a variety of statistical analyses and combined into a regression analysis for comparison to existing studies in the Great Lakes and Chicago areas. A second goal is to identify potential PAH and PCB sources among a complex mixture of local and regional sources, as well as from nearby project and construction activity. This was achieved by the development of a receptor modeling source apportionment analysis (the subject of Chapter 4) to determine contaminant sources and their contributions to the pollution burden of the IHC air-shed. The results of these studies comprise a detailed understanding of the state of the system prior to commencement of dredging.

3.3. Materials and Methods

Atmospheric sampling and chemical analysis. Air samples were obtained approximately every six days between November 2001 and October 2008 and every twelve days between October 2008 and February 2012. Five monitoring stations were established in the study (Figure 3.1): three stations north (N), east (E), and west (W) along the perimeter of the CDF; one station south (S) across the canal from the CDF; and one station at the East Chicago High School (H) about

0.6 km further southwest of station S. The four direction-labeled stations primarily measure ambient concentrations for the CDF construction site, while station H monitors concentrations at the high school which is the nearest sensitive receptor population in the community. Petroleum storage tanks and refineries to the north, east, and west; as well as major roadways to the north and east may influence air quality conditions at the site. Station S monitors air quality nearest the canal, between the CDF and the high school. Monitoring station H may be influenced by traffic related to school parking.

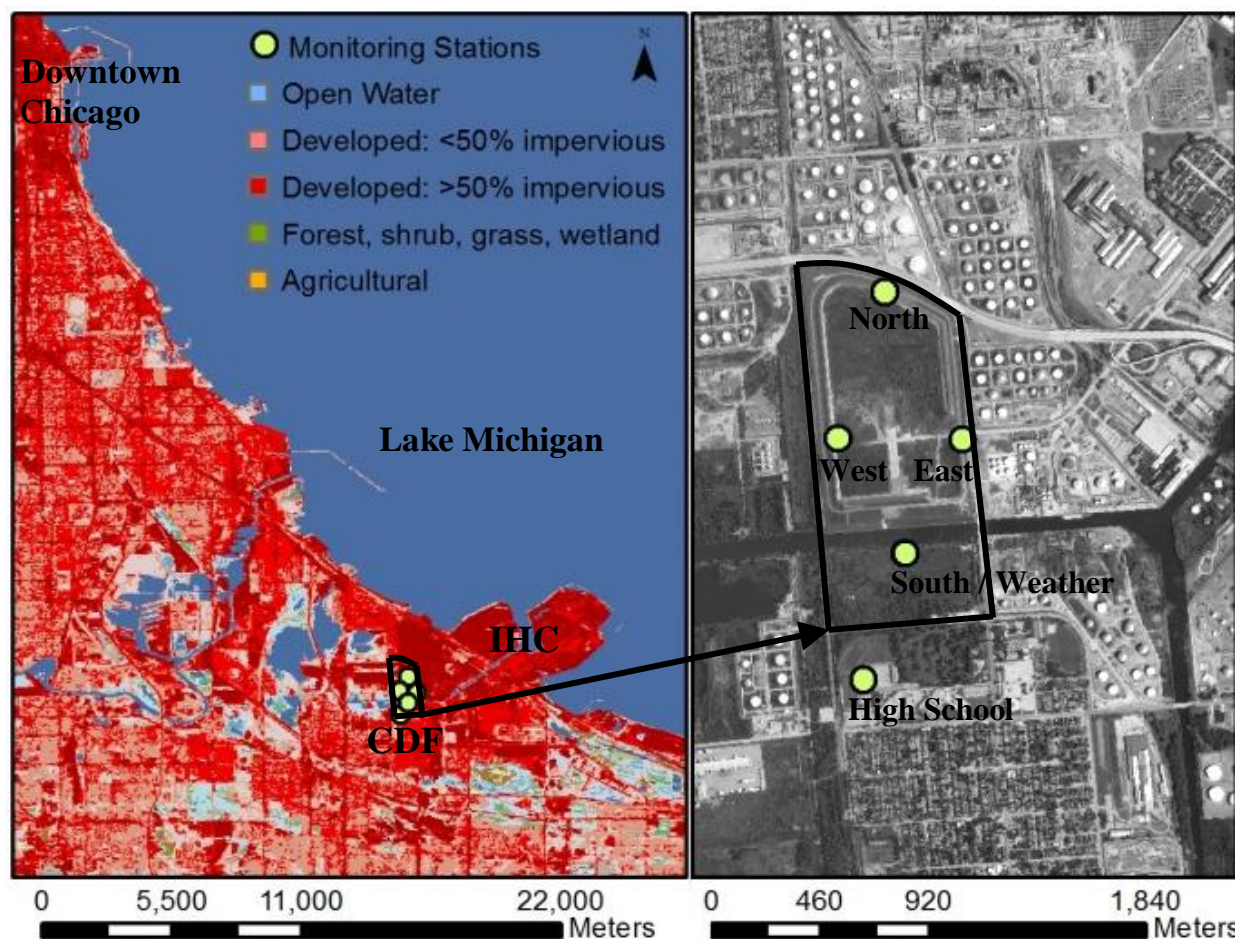


Figure 3.1. Location of atmospheric sampling stations. Land use map left (USGS National Land Cover Database, 2006) and aerial photo right (National Agriculture Imagery Program Orthoimagery, 2010).

Monitoring stations S and H were mounted on 8 ft by 8 ft pressure-treated wooden platforms; stations N, E, W, and a Quality Assurance (QA) station (not shown) were on mobile trailers. All stations were enclosed by galvanized chain-link security fence containing a locking gate and equipped with 120 V AC electrical power and appropriate weather-resistant electrical components including ground-fault circuit interrupters.

Over the ten year monitoring period from November 2001 through February 2012, over 1200 atmospheric samples were collected. Nearly three quarters of the samples were from stations S and H that operated the entire duration, with the remainder were from stations N, E, and W that ceased operation in April 2004 after findings of statistical similarities between stations.

The USEPA Compendium Method TO-13A/CARB Method 429/SW-846 Method 1668 was used for sampling and analysis of PAHs and PCB congeners in ambient air as described in Figure 3.2.¹⁶² The sampling system consisted of a vacuum pump capable of 200 to 280 L/min volumetric flow, dual sampling module, flow Venturi, elapsed time indicator, skip timer, and anodized aluminum shelter. Twenty-four hour samples were obtained about 2 m above ground surface with the high-volume sampler. A quartz fiber filter and a sandwiched polyurethane foam and adsorbent resin (PUF/XAD-2) cartridge were used for the evaluation of gas and particulate PAHs and PCBs. Samples were stored in an ice chest at 4 ± 2 °C until receipt at the analytical laboratory, at which time they were stored refrigerated at 4 ± 2 °C and prepared and analyzed within a few weeks of sample collection.

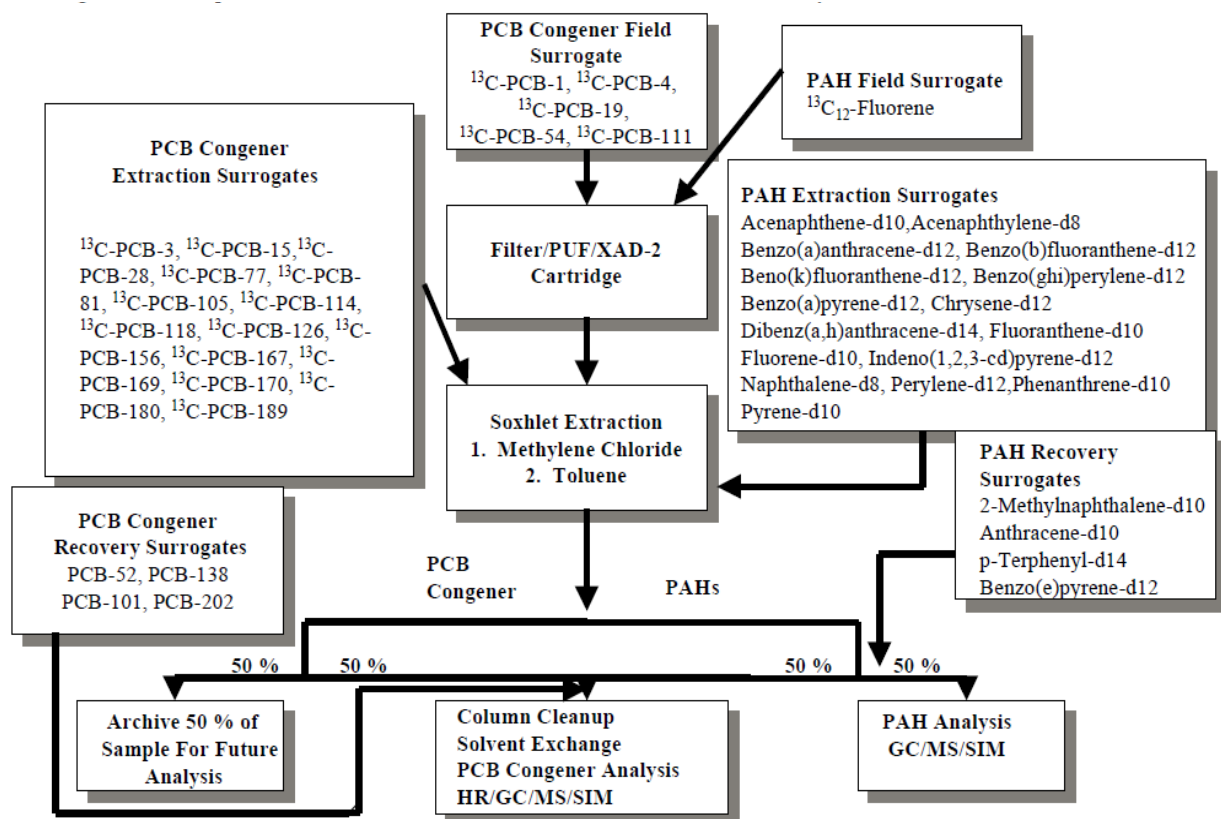


Figure 3.2. Flowchart of Compendium Method TO-13A/SW-846 Method 1668/CARB 429 analytical scheme. Figure from USACE (2003).¹⁶²

Filters and cartridges were Soxhlet extracted with methylene chloride to remove PAHs and most PCBs, and a second time with toluene to remove remaining PCBs. Half of the methylene chloride extract was used for PAH analysis by Gas Chromatography/Mass Spectrometry in selected ion monitoring (SIM) mode and the other half combined with half of the toluene extract for PCB congener analysis by High Resolution Gas Chromatography/High Resolution Mass Spectroscopy in SIM mode (the remaining half of toluene extract was archived for future analysis). In late 2011, the analytical method for PCBs was updated from 1668 to 1668A. All samples were analyzed by Test America (Sacramento and Los Angeles, CA, USA) using rigorous laboratory quality-assurance procedures. All stages of the air monitoring program include Quality Assurance/Quality Control (QA/QC) elements described in Figure 3.3. Detailed QA/QC

elements, criteria, and procedures for field sampling (Compendium Method TO-13A/4A) and laboratory analysis (Compendium Method TO-13A/CARB 429 and TO-4A/SW-846 Method 1668) of PAHs and PCB congeners are found in the Indiana Harbor and Canal Dredging and Disposal Project, Ambient Air Monitoring Plan: Volume 1.¹⁶²

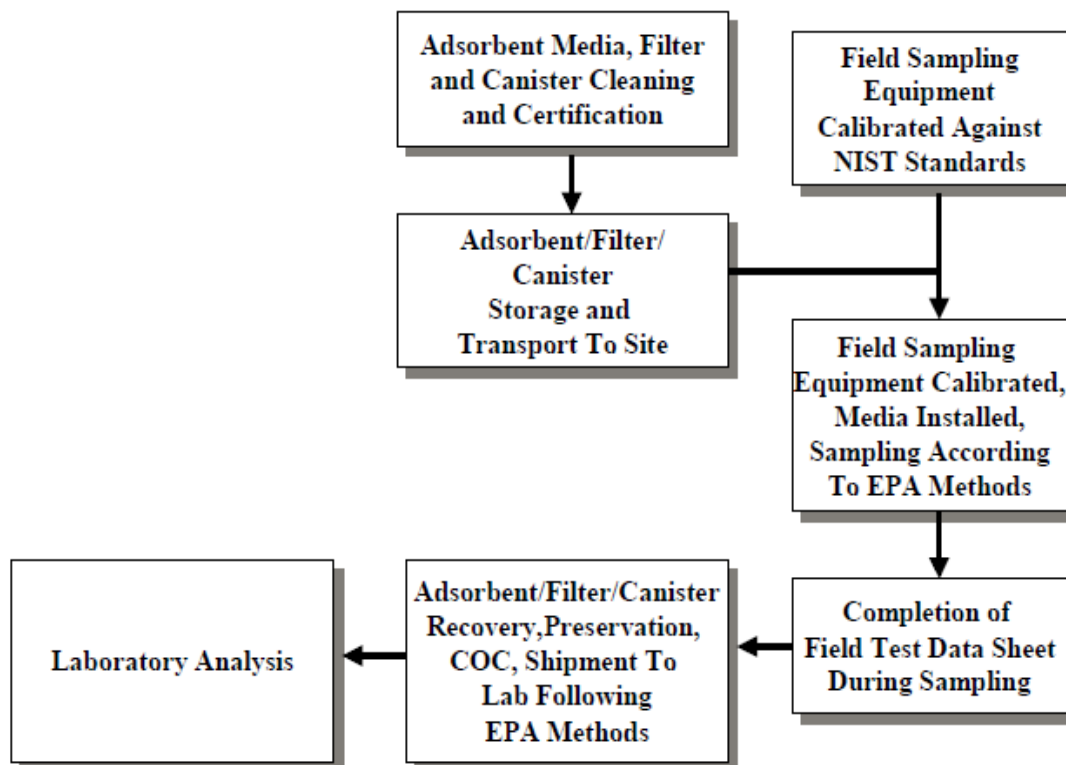


Figure 3.3. Flowchart of QA/QC elements for sampling and analysis stages of the air monitoring program. Figure from USACE (2003).¹⁶²

As part of the monitoring program, real-time on-site meteorological data were obtained to evaluate the effect of atmospheric and climatic conditions on measured pollution levels, emissions, and dispersion/transport.¹⁶² A meteorological station was established alongside station S to measure wind speed (m/s) and wind direction (degrees clockwise from true North), ambient temperature (°C), relative humidity (% moisture), barometric pressure (mbar Hg), solar radiation (W/m²), and precipitation (mm) starting in May 2002. Wind speed and direction (defining from

which way the wind is blowing) measurements were taken on a meteorological tower at a height of 10 m above ground surface. Ambient air temperature, relative humidity, barometric pressure, solar radiation, and precipitation were measured at a height of 2 m. Data were collected at 5 min intervals and then averaged over 24 hr periods consistent with the air sampling times and dates. Gaps in meteorological data occurred about 10% of the time. Meteorological monitoring guidance was provided by the EPA Quality Assurance Handbook for Air Pollution Measurement Systems, Vol. IV, Meteorological Measurements¹⁶³ and designed to be of similar quality to the pollutant monitoring program.

Further details on sample media, collection schedule, analytical methods, and QA methods are found in the Indiana Harbor and Canal Dredging and Disposal Project, Ambient Air Monitoring Plan: Volume 1.¹⁶²

Dataset preparation. Samples were analyzed for 17 PAHs and 19 PCB congeners (Figure 3.4) selected based on their significant concentrations in IHC sediment and potential to contribute to health impacts in the community. Seven of the 17 measured PAHs: naphthalene (Nap), acenaphthylene (Acy), acenaphthene (Ace), fluorene (Flo), phenanthrene (Pha), fluoranthene (Fla), and pyrene (Pyr); and five of the 19 measured PCB congeners (according to IUPAC congener number): 8, 15, 18, 28, and 31 were selected for this study based on detection frequencies over 50% (Figure 3.4). Lower molecular weight PAHs were detected over half the time except for anthracene, benzo[a]anthracene and chrysene, while high molecular weight PAHs were detected less than 10% of the time. Only dichlorinated and trichlorinated biphenyl congeners were detected over 60% of the time; all others except 105, 118, and 180 were virtually never detected.

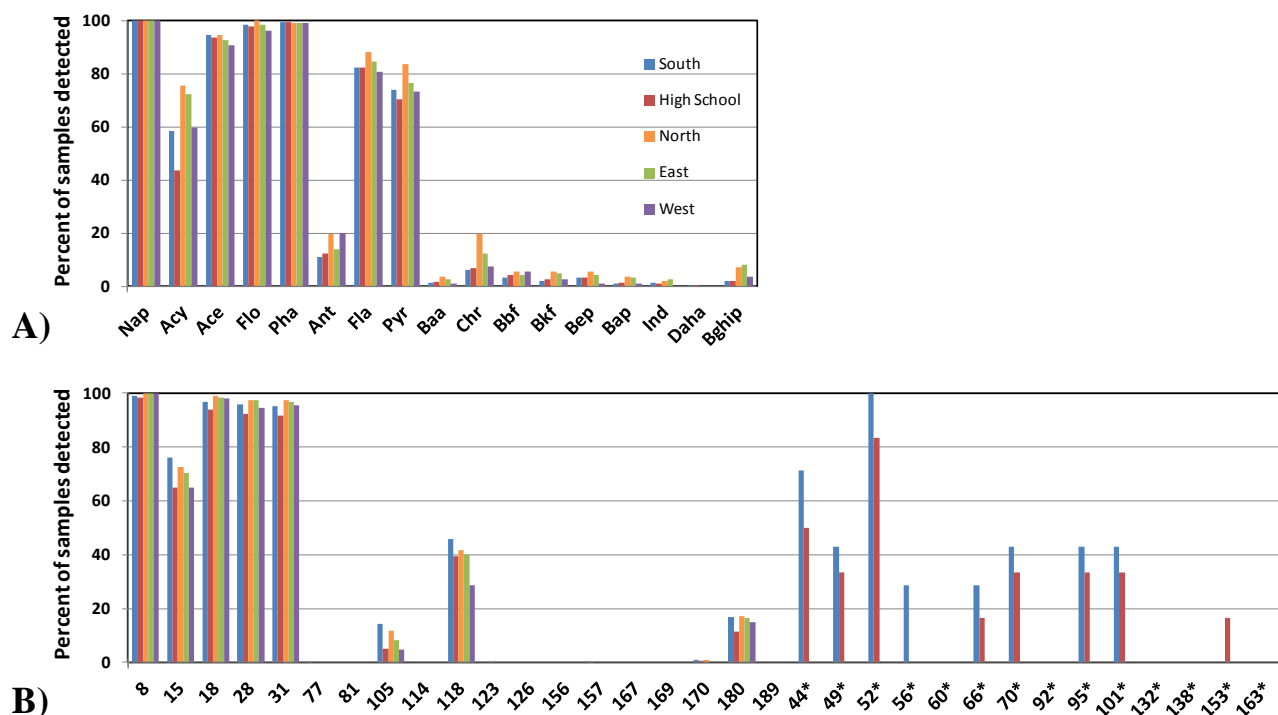


Figure 3.4. Detection frequency of (A) PAHs and (B) PCB congeners analyzed in air samples. Frequencies for the 14 congeners denoted with an asterisk (*) were based on limited data (seven and six measurements at stations S and H respectively) and these congeners are not considered in the present study.

In addition to the 19 original congeners, note that 14 more were analyzed with the updated PCB analytical method starting in late 2011 but with too few sample to include in the present study (Figure 3.4). The statistical analysis and modeling study requires a well conditioned dataset and is therefore limited to analytes present throughout the entire study period with over 50% detection frequency. Quantitation limits were 4.50-6.27 ng/m³ for Nap, 1.14-3.13 ng/m³ for other PAHs, and 2.25-3.13 pg/m³ for PCB congeners. Half the limit was substituted for non-detects remaining in the data (under 15% and 10% of the datasets for PAHs and PCBs, respectively).¹⁶⁴ Concentrations of PAHs and PCB congeners were reported in units of nanograms per standard cubic meter (ng/m³) and picograms per standard cubic meter (pg/m³), respectively, from the mass of PAHs and PCB congeners collected in the samples and the sample volumes.

Probability and box plots indicate the PAH and PCB data follow a log-normal distribution, thus data were natural log-transformed for most parametric tests and regression modeling. Original and log-transformed data distributions are illustrated in Figure 3.5. One PCB sample at station S (9/1/2005) was identified as a far outlier by PCB box plot inspection (~3 times higher than the next highest concentration) and was removed from further analysis in this study.

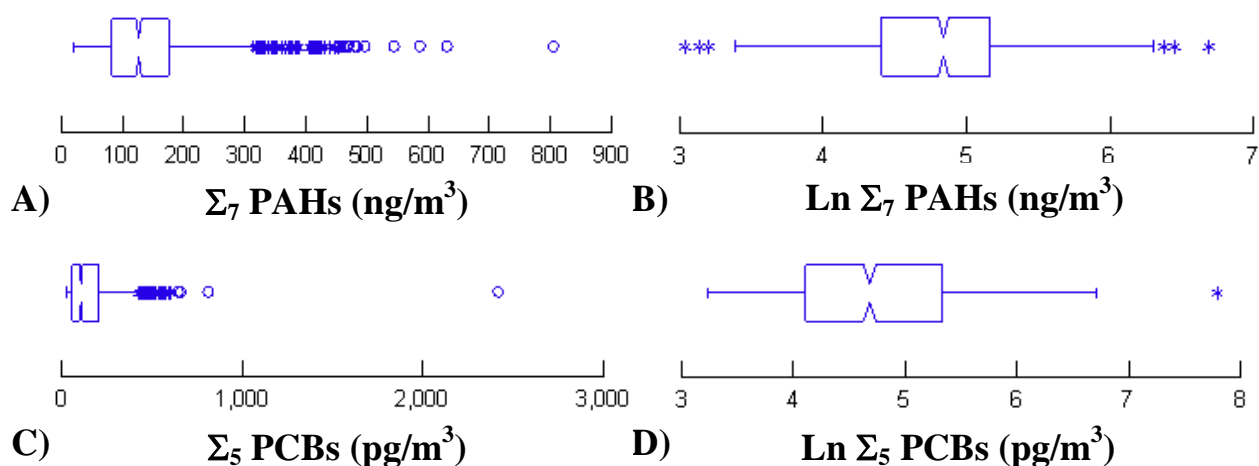


Figure 3.5. Box plots of (A) PAH, (B) log-transformed PAH, (C) PCB, and (D) log-transformed PCB data.

The final PAH dataset for analysis included seven compounds and 1233 samples and the PCB dataset included five congeners and 1229 samples. Spatial, temporal, seasonal, and presence/absence of CDF construction activity information was available for all samples. Ambient temperature, wind speed, and wind direction data were available for 1097 and 1093 of the PAH and PCB sample days, respectively. Spatial, temporal, and meteorological parameters were analyzed with contaminant data individually to identify trends and together by regression analysis to determine their overall impact on PAH and PCB levels.

Data analysis. Statistical testing, plotting, and modeling were done in Excel (v. Office 2007, Microsoft, Redmond, WA USA), SYSTAT (v. 13, Systat Software, Inc., Chicago, IL USA), and OriginPro (v. 8.6, OriginLab Corp., Northampton, MA USA). Statistical summaries of PAHs and PCBs were carried out on both temperature-corrected (288 K; described below) and unadjusted data that were grouped according to sampling station (S, H, N, E, W), astronomical season (Winter, Spring/Fall, Summer), CDF construction-related activity (Active, Idle), and wind source direction by quadrant (NE, SE, SW, NW). Group means were compared using Student's *t*-test (pairwise for stations and two-sample with separate variance for others) to determine differences at 90% and 95% confidence levels (CL). Correlations between individual PAHs and PCB congeners were calculated by the Pearson product-moment correlation coefficient.

Atmospheric concentrations of PAHs, PCBs, and other semivolatiles exhibit temperature dependency well documented and described by the Clausius-Clapeyron (C-C) relationship.¹⁶⁵⁻¹⁷⁰ This relationship is given by Equation 3.1.

$$\ln P = \frac{\Delta H_{SA}}{RT} + \text{const} = \frac{a_1}{T} + \text{constant} \quad (3.1)$$

P is the compound partial pressure (atm); ΔH_{SA} is heat of surface-air partitioning (kJ/mol); *T* is the average local atmospheric temperature over the sampling period (K); *R* is the gas constant (0.0083 kJ/K·mol). The coefficient a_1 (K), or C-C slope, is typically reported to describe the dependence of compound partial pressure on temperature.

Temperature dependency can be removed by adjusting the partial pressure to a reference temperature using Equation 3.2.

$$P_{288} = P \exp \left[a_1 \left(\frac{1}{288} - \frac{1}{T} \right) \right] \quad (3.2)$$

P_{288} is the adjusted compound partial pressure (atm) at 288 K; P is the original partial pressure (atm); T is the average local atmospheric temperature over the sampling period (K).

For this study partial pressures were calculated from atmospheric concentrations using the ideal gas law, which considers the molecular weight of each compound and the measured ambient air temperature averaged over the sampling period. Linear regressions of $\ln P$ versus $1/T$ were performed to obtain the C-C slope (a_1) and other regression parameters for each compound. Temperature-corrected partial pressures adjusted to 15°C (288 K) were calculated when statistically significant C-C slopes (95% CL) were determined. Adjusted partial pressures were converted back to atmospheric concentrations using the ideal gas law for further analysis.

With temperature-dependent seasonal effects removed, long-term temporal trends in the data were examined by the following regression (Equation 3.3).^{168, 171}

$$\ln C_{TC} = a_2 t + \text{const} \quad (3.3)$$

C_{TC} is the temperature-corrected concentration (ng/m³ for PAHs and pg/m³ for PCBs) and t is the time in Julian days starting from the first sample date of the study. Coefficient a_2 describes the relationship between the concentration and time and is a first-order rate constant with units of days⁻¹. The halving time $t_{1/2}$ (in years) can be calculated by Equation 3.4.

$$t_{1/2} = \frac{-\ln 2}{365.25 \cdot a_2} \quad (3.4)$$

The rate constant a_2 for each compound in this study was determined by regressing the natural logarithm of the 288 K temperature-corrected concentrations at stations S and H (which operated the entire 10 yr sampling period) against time. Mean halving times for all compounds were calculated using the regression-derived rate constants.

Wind direction is related to sources and transport of contaminants and can effect atmospheric concentrations particularly at shorelines though it may be highly variable.¹⁷²⁻¹⁷⁵ Resultant 24 hr wind directions for trend analyses were determined by trigonometric calculation. Compass degrees were converted to radian angles and 24 hr averages were calculated using the following equations.

$$X = \left(\frac{1}{n}\right) \sum_{i=1}^n \cos \theta_i \quad (3.5)$$

$$Y = \left(\frac{1}{n}\right) \sum_{i=1}^n \sin \theta_i \quad (3.6)$$

$$\theta = \arctan\left(\frac{Y}{X}\right) \quad (3.7)$$

θ is the wind direction angle averaged over the 24 hr sample period (in radians); n is the number of time increments measured in the 24 hr period (in our case of 5 minute intervals $n = 288$); θ_i is the measured (or average) angle for n time increments (in radians). Radian angles were converted to degree angles, and back to conventional compass degrees by a logical expression with knowledge of quadrants based on signs of X and Y .

Only resultant wind directions without high dispersion over each sampling period were used to explore trends related to larger-scale source and atmospheric transport.¹⁷⁶ Angular deviation of each average 24 hr wind direction was determined by the following equations.

$$d = \sqrt{X^2 + Y^2} \quad (3.8)$$

$$s = \frac{180}{\pi} \sqrt{-2 \ln d} \quad (3.9)$$

s is the angular deviation (in degrees) and d is a measure of angular dispersion (0 for undefined angle and 1 for completely defined angle). Sampling days with angular deviation greater than 60 degrees were removed from wind direction analyses.

Directional wind data may be expressed nonlinearly with a sinusoidal function. Equation 3.10 describes a relationship between the temperature-corrected concentration (C_{TC}) and a wind direction term used by Hafner and Hites (2005).¹⁷⁶

$$\ln C_{TC} = a_3 \sin(a_4 + \theta) + \text{const} \quad (3.10)$$

θ is the average daily wind direction angle (in radians); amplitude parameter a_3 and phase shift parameter a_4 relate the concentration increase amount to wind from a specified source direction. The Factor of Increase (FoI), or factor by which concentrations are increased when the wind is from the given source direction compared to the average concentration, is calculated by Equation 3.11. The source direction (Φ) is calculated by Equations 3.12 and 3.13.¹⁷⁶

$$\text{Factor of Increase} = \exp |a_3| \quad (3.11)$$

$$\Phi = 270 - a_4 \quad \text{for } a_3 < 0 \quad (3.12)$$

$$\Phi = 90 - a_4 \quad \text{for } a_3 \geq 0 \quad (3.13)$$

Thus model-derived wind direction parameters, Factors of Increase, and source directions were calculated for atmospheric temperature-corrected PAH and PCB concentrations at each monitoring station.

Following individual trend analysis, a multiple linear regression (MLR) analysis was used to estimate the combined importance of time and meteorological parameters on atmospheric PAH and PCB concentrations.^{177, 178} In the following regression, the natural logarithm of the original concentration is dependent on temperature (T), time (t), and wind direction (θ), in addition to wind speed (WS) and relative humidity (RH) which may also have an effect.^{92, 177, 178}

$$\ln C = \frac{a_1}{T} + a_2 t + a_3 \cos \theta + a_4 \text{WS} + a_5 \text{RH} + \text{const} \quad (3.14)$$

C is the concentration of the compound (in ng/m^3 for PAHs and pg/m^3 for PCBs); a_1 is the C-C slope (in K); a_2 is the first-order rate constant (in days^{-1}); a_3 is amplitude of the cosine term; a_4 and a_5 are parameters describing the dependence of concentration on WS and RH.

Note concentrations used in the MLR were not temperature-corrected, and the cosine function was used with wind direction as it showed a better fit in preliminary analyses than the sine function. The ability of the regression to explain variability in concentration was given by a total coefficient of determination or R^2 . The contribution of each term to the total variability was estimated by forward stepwise regression that incorporated each term based on the strength of its squared semi-partial correlation. In addition, individual regressions on the independent variables were performed for comparison to MLR as well as the analyses done with temperature correction.

3.4. Results and Discussion

The IHC air-shed is highly industrialized with high concentrations of PAHs and PCBs.

Atmospheric concentrations of Σ_{17} PAHs and Σ_{19} PCBs at the South (S) and High School (H) stations varied by well over an order of magnitude over the 10+ year monitoring period (Figure 3.6). Σ_{17} PAHs ranged from 21 to 806 ng/m³ (143 ± 88 ng/m³ $\mu \pm \sigma$), and Σ_{19} PCBs ranged from 26 to 816 pg/m³ (149 ± 118 pg/m³ $\mu \pm \sigma$; Tables 3.1-3.2) for all stations. High levels of PAHs and PCBs are not unexpected given the industrial and urban surroundings of the IHC (see Figure 3.1). Chicago has been studied extensively for its concentrations of POPs, particularly in air and sediment, and is considered a major source of PAHs and PCBs to the Great Lakes region.¹⁷⁹⁻¹⁸² The Integrated Atmospheric Deposition Network (IADN) monitoring program has measured PAHs and PCBs in the Great Lakes atmosphere since the early 1990s and found PAHs over ten times higher and PCBs over 14 times higher in Chicago than at remote monitoring sites,^{157, 158} and PCB congener 11 was over 22 times higher from 2004-2007.¹⁸³ PAHs have been reported to range from 82 to 428 ng/m³^{10, 76, 157, 174} and PCBs from 800 to 2685 pg/m³^{110, 158, 173, 184} in the Chicago atmosphere, with significant variation of PCB levels observed within the city.^{110, 159}

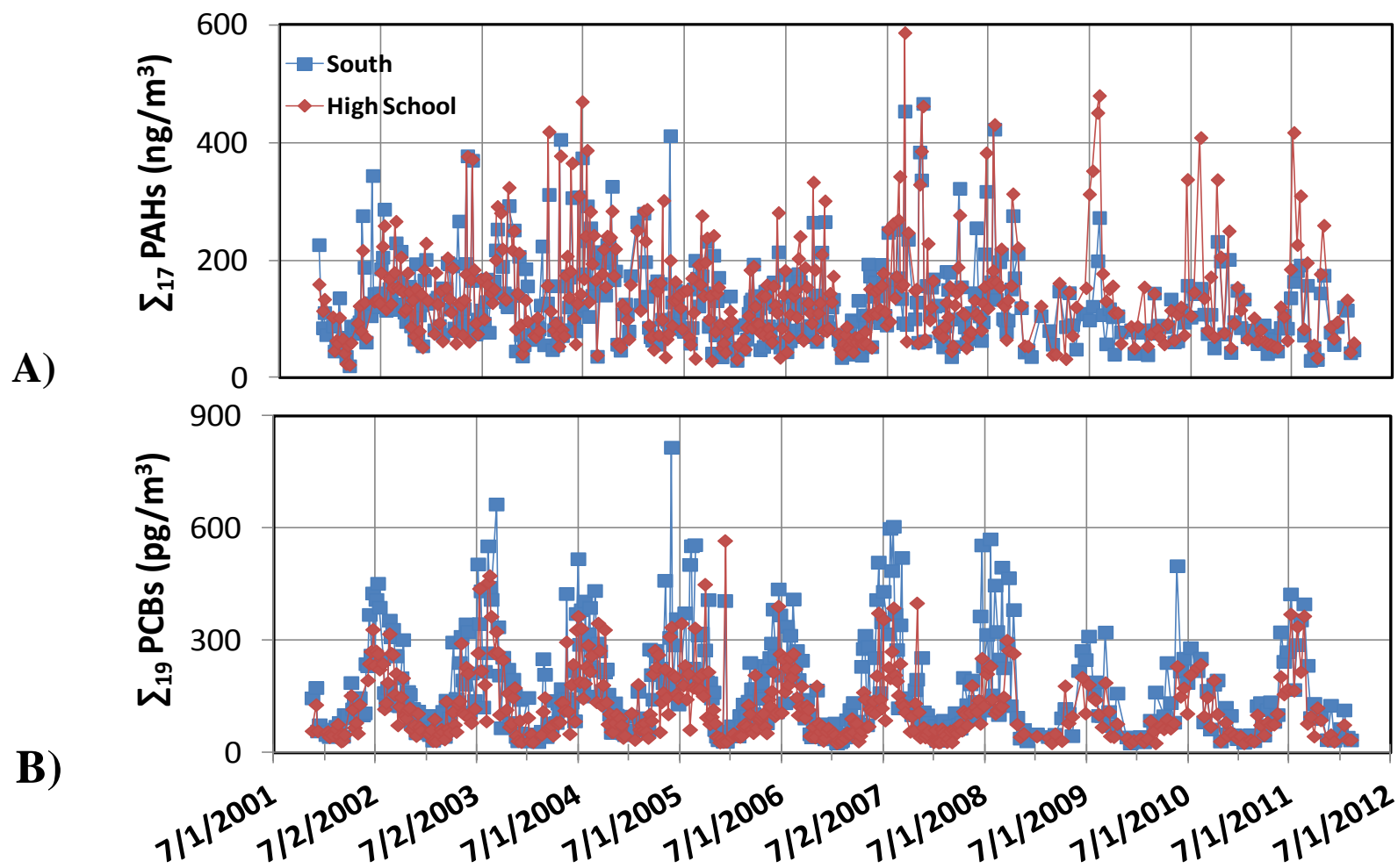


Figure 3.6. Comparison of (A) Σ_{17} PAH (ng/m^3) and (B) Σ_{19} PCB (pg/m^3) concentrations in air at South (blue) and High School (red) stations for the entire ten year monitoring period.

Table 3.1. Statistical analysis of atmospheric PAH concentrations (ng/m³) near IHC.

PAHs	No. of Cases	Minimum	Maximum	Interquartile Range	Median	Arithmetic Mean	SEM ^a	95.0% LCL ^b	95.0% UCL ^b	σ	Skewness
All samples											
Σ ₁₇ PAHs	1,233	20.81	805.80	93.10	126.28	143.31	2.50	138.40	148.22	87.94	1.83
Nap	1,233	6.40	685.99	66.12	70.36	87.68	1.91	83.93	91.43	67.19	2.61
Acy	1,233	0.72	21.58	2.68	1.71	2.54	0.08	2.39	2.69	2.65	2.53
Ace	1,233	0.72	68.67	8.52	6.90	9.41	0.26	8.90	9.92	9.06	2.52
Flo	1,233	0.72	71.65	8.73	7.82	9.93	0.22	9.49	10.37	7.81	2.17
Pha	1,233	0.72	158.23	18.41	14.77	19.40	0.45	18.51	20.29	15.92	2.52
Fla	1,233	0.72	44.79	3.68	3.20	4.03	0.10	3.84	4.22	3.47	3.00
Pyr	1,233	0.72	21.95	2.76	2.18	2.56	0.05	2.46	2.66	1.81	2.04
Σ₁₇ PAHs by group											
South	447	20.81	467.13	82.12	114.67	130.02	3.51	123.13	136.91	74.13	1.54
High School	443	23.00	587.64	94.00	122.73	139.43	4.16	131.27	147.60	87.47	1.65
North	111	33.42	805.80	124.55	158.33	188.55	11.88	165.02	212.09	125.13	2.04
East	123	43.01	496.85	104.97	145.21	156.68	7.35	142.14	171.22	81.47	1.42
West	109	30.48	440.21	103.78	134.52	152.41	8.34	135.87	168.95	87.11	1.21
Active	543	29.60	805.80	88.44	134.40	148.31	3.71	141.03	155.59	86.37	2.21
Idle	690	20.81	587.64	97.79	117.37	139.37	3.39	132.72	146.03	89.02	1.59
Winter	291	20.81	632.19	82.00	89.39	117.05	4.86	107.48	126.62	82.94	2.48
Spring/Fall	643	29.60	805.80	85.90	119.70	139.89	3.46	133.10	146.69	87.73	2.05
Summer	299	30.18	587.64	85.34	159.38	176.21	4.81	166.75	185.68	83.13	1.42
Northeast	204	29.60	417.92	100.63	135.78	148.95	5.57	137.97	159.93	79.55	0.89
Southeast	197	30.24	470.38	78.54	119.70	140.99	5.99	129.16	152.81	84.13	1.50
Southwest	435	34.94	805.80	93.32	118.07	136.10	4.20	127.85	144.36	87.64	2.32
Northwest	252	33.29	632.19	95.80	150.37	173.26	6.15	161.16	185.36	97.55	1.79

^a Standard Error of Arithmetic Mean (SEM).

^b Lower Confidence Level (LCL) and Upper Confidence Level (UCL) of the arithmetic mean.

Table 3.2. Statistical analysis of atmospheric PCB concentrations (pg/m³) near IHC.

PCBs	No. of Cases	Minimum	Maximum	Interquartile Range	Median	Arithmetic Mean	SEM ^a	95.0% LCL ^b	95.0% UCL ^b	σ	Skewness
All samples											
Σ ₁₉ PCBs	1,229	25.56	815.79	146.18	107.80	148.82	3.35	142.24	155.40	117.56	1.53
8	1,229	1.35	344.25	43.86	29.19	43.12	1.20	40.76	45.48	42.14	2.08
15	1,229	1.35	48.25	8.58	4.98	6.96	0.18	6.61	7.32	6.35	1.54
18	1,229	1.35	277.79	33.55	19.80	30.57	0.87	28.87	32.27	30.36	1.99
28	1,229	1.35	156.11	24.95	15.73	23.05	0.62	21.83	24.28	21.84	1.71
31	1,229	1.35	159.96	25.03	15.74	23.55	0.66	22.27	24.84	23.01	1.92
Σ₁₉ PCBs by group											
South	446	25.56	815.79	168.58	132.67	173.12	6.29	160.76	185.48	132.83	1.35
High School	443	25.56	566.45	121.07	98.75	125.73	4.41	117.06	134.39	92.77	1.41
North	110	31.03	497.90	137.48	100.18	140.67	10.22	120.42	160.92	107.15	1.24
East	122	29.05	651.56	158.17	122.86	167.78	12.61	142.81	192.75	139.32	1.44
West	108	28.52	540.73	112.63	92.39	130.13	9.87	110.57	149.69	102.55	1.48
Active	544	25.56	815.79	159.09	136.42	177.45	5.66	166.33	188.56	131.99	1.36
Idle	685	25.56	574.72	115.44	90.03	126.09	3.79	118.66	133.52	99.05	1.49
Winter	286	25.56	276.07	32.92	52.67	68.16	2.72	62.82	73.51	45.92	2.23
Spring/Fall	643	25.56	815.79	94.90	103.30	130.01	3.63	122.89	137.13	91.96	2.07
Summer	300	38.00	663.95	179.13	249.60	266.04	7.26	251.75	280.33	125.78	0.69
Northeast	204	25.56	554.57	166.28	133.42	175.55	8.73	158.33	192.77	124.73	1.14
Southeast	197	27.60	604.48	112.67	78.74	129.62	8.16	113.53	145.70	114.49	1.65
Southwest	436	25.56	663.95	116.66	92.90	122.89	4.71	113.64	132.15	98.34	1.86
Northwest	247	25.56	815.79	174.88	180.84	204.43	8.26	188.16	220.70	129.85	1.17

^a Standard Error of Arithmetic Mean (SEM).

^b Lower Confidence Level (LCL) and Upper Confidence Level (UCL) of the arithmetic mean.

PAHs measured in this study fall within the range of other studies from the area (Table 3.3). Studies reporting the highest levels typically occurred during warm months only, and without temperature information and/or correction an accurate basis of comparison may not be possible (see discussion of temperature correction below). The study by Sun et al. (2006a)¹⁵⁷ occurred over multiple years and all seasons, and included temperature-corrected (to 288 K) results for direct comparison. The present study shows higher mean 288 K-corrected total PAH levels (145 ng/m³) than those reported in Sun et al. (2006a) (85.4 ng/m³), but also wider variations; possibly related to local sources or effects (Table 3.3). Mean 288 K-corrected total PCB concentrations on the other hand are lower (149 pg/m³) in the present study than other studies in the area. This may be due in part to the smaller number of congeners analyzed in the present study. We utilized the congener fractions reported in Hu et al. (2010)¹¹⁰ and Martinez et al. (2010)¹⁰⁶ to extrapolate Σ_{209} PCBs from the Σ_{17} PCBs in the current study which resulted in estimated Σ_{209} PCB values of 540-570 pg/m³ (Table 3.3); within the variation of several studies in the Chicago region.^{110, 158, 173, 184}

A clearly observable oscillatory pattern in concentration indicates seasonal temperature dependence for PCB levels at the monitoring stations (Figures 3.6 and 3.7). Concentrations at stations S and H appear largely similar, although Σ_{17} PAHs were slightly higher at station H and Σ_{19} PCBs were higher at station S. Statistical summaries of the PAH dataset (see Table 3.1) and the PCB dataset (see Table 3.2) include comparisons among compounds, monitoring stations, construction activities, seasons, and wind directions. Over half of the total PAH mass is contributed by Nap (>70% on a molar basis), followed in decreasing order by Pha, Flo, Ace, Fla, Pyr, Acy. Higher PAH concentrations were observed at station N, and during active construction days, warm seasons, and northerly wind directions (see Table 3.1).

Table 3.3. Reported total PAH and PCB concentrations in air near Chicago, Illinois USA.

PAHs (ng/m ³); mean ± σ	No. PAHs or PCB congeners	No. of samples	Location	Dates measured	Reference
143 ± 88 ^a	17	1233	East Chicago, IN/CDF	Nov 2001-Mar 2012	Present study
82 ± 5.2 ^b	16 ^c	181	Chicago, IL	1996-2003	Sun et al. (2006a) ¹⁵⁷
167 ± 116	26 ^d	22	Chicago, IL	May & Jul 1994, Jan 1995	Simcik et al. (1998) ¹⁰
428 ± 240	14 ^e	12	Chicago, IL	June - Oct 1995	Odabasi et al. (1999) ⁷⁶
201 ± 100	14 ^e	21	Chicago, IL	Aug - Sept 1997	Vardar et al. (2004) ¹⁷⁴
PCBs (pg/m³); mean ± σ					
149 ± 118 ^f	19	1229	East Chicago, IN/CDF	Nov 2001-Mar 2012	Present study
840 ± 940	209 (169 peaks)	184	Chicago, IL	Nov 2006-Nov 2007	Hu et al. (2010) ¹¹⁰
4500 ± 1800 ^{g,h}	209 (158 peaks)	17	East Chicago, IN/IHC	August 2006	Martinez et al. (2010) ¹⁰⁶
1400 ± 100 ^g	84	181	Chicago, IL	1996-2003	Tasdemir et al. (2004) ¹⁷³
1900 ± 1700	50 (43 peaks)	37	Chicago, IL	Jun-Oct 1995	Sun et al. (2006b) ¹⁵⁸
1010 ± 450	113 (77 peaks)	22	Wheaton, IL	Jul-Sept 1999	Hsu et al. (2003) ¹⁰⁴
2685 ± 1901	98	18	Chicago, IL	Apr 1994-Oct 1995	Miller et al. (2001) ¹⁸⁴
540 ⁱ	209 ⁱ	1229	East Chicago, IN/CDF	Nov 2001-Mar 2012	Present study; Hu et al. (2010) ¹¹⁰
570 ^j	209 ^j	1229	East Chicago, IN/CDF	Nov 2001-Mar 2012	Present study; Martinez et al. (2010) ¹⁰⁶

^a Mean concentration (Σ₇ PAHs 1097 samples) corrected to 288 K: 145 ± 91.

^b Mean concentration corrected to 288 K: 85.4 ± 3.2 (μ ± σ).

^c Includes retene, coronene, and co-eluting triphenylene + Chr; no Nap, Ace, Acy.

^d Includes five methylated PAHs, anthanthrene, coronene, benzo[a]fluorene, benzo[b]fluorene, perylene, and retene; co-eluting BbF+BkF; no Nap.

^e Includes carbazole; no Nap, Acy, BghiP, DahA.

^f Mean concentration (Σ₅ PCBs 1093 samples) corrected to 288 K: 145 ± 114 (μ ± σ).

^g Gas phase only.

^h Non-ambient; taken above the water.

ⁱ Predicted concentration if all PCBs measured, calculated from congener mass fractions from Hu et al. (2010).¹¹⁰

^j Predicted concentration if all PCBs measured, from congener mass fractions calculated from Martinez et al. (2010).¹⁰⁵

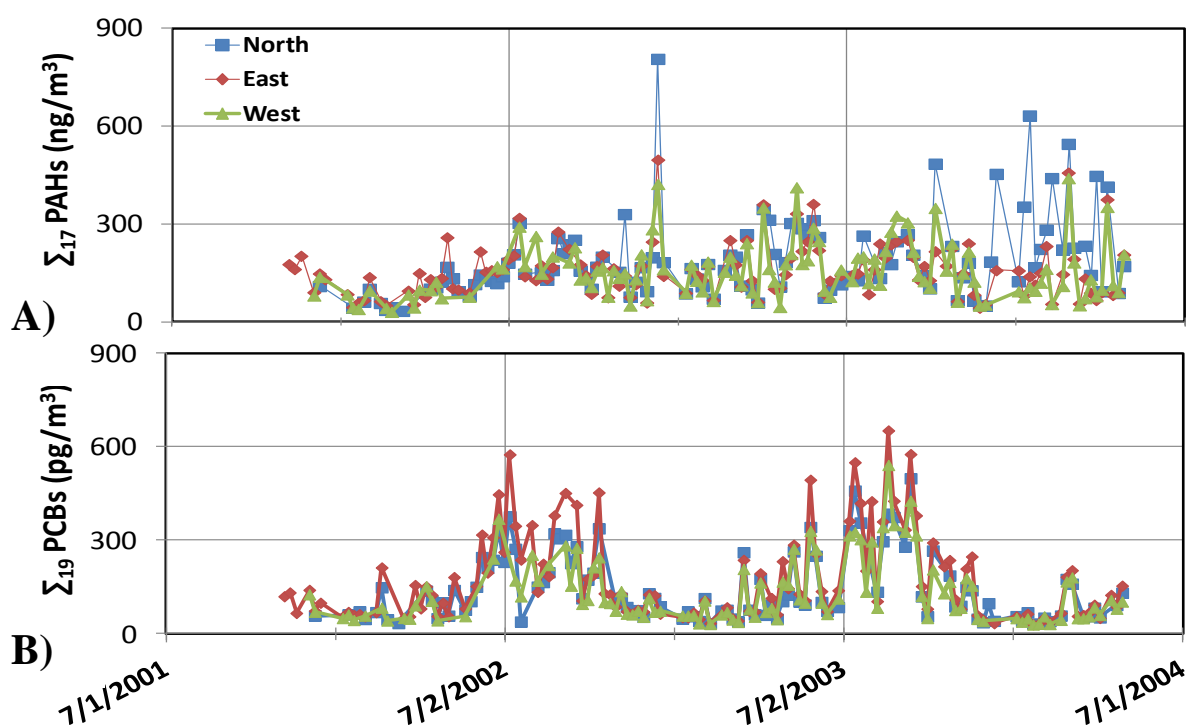


Figure 3.7. Comparison of (A) PAH (ng/m^3) and (B) PCB (pg/m^3) concentrations in air at North (blue), East (red), and West (green) stations. Note that these stations operated during the first three years of the monitoring program.

Σ_{19} PCB concentrations were primarily composed of congeners 8, 18, 31, 28, and 15 contributing 29%, 21%, 16%, 15%, and 5% of the total mass, respectively (see Table 3.2). Elevated concentrations occur at station S, as well as during warm months and northerly wind directions. Statistical significance (95% CL) is attributed to most differences between stations, construction activities, seasons, and wind directions for the PAHs and PCBs (Table 3.4). But it is important to note that these comparisons may be influenced by seasonal bias (e.g. seasonal wind patterns and construction schedules), thus temperature correction is employed in the next section. Pearson correlation coefficients show most PAHs are positively linearly related (Ace, Flo, Pha, Fla, and Pyr); however Nap and Acy do not correlate well with any PAHs (Table 3.5). Interestingly, Nap at station N is not correlated with Nap at other stations (results by station not shown). In contrast, all PCBs are highly correlated (Table 3.5). All correlations are significant at the 95% CL.

Table 3.4. *t*-test^a for significant differences^b in PAHs and PCBs among monitoring stations (S, H, N, E, W), CDF construction activities, seasons, and wind source directions by quadrant (NE, SE, SW, NW).

	S-H	S-N	S-E	S-W	H-N	H-E	H-W	N-E	N-W	E-W	Act-Idle	Wint-Sp/F	Wint-Sumr	Sp/F-Sumr	NE-SE	NE-SW	NE-NW	SE-SW	SE-NW	SW-NW
Σ_{17} PAHs	X X	X X	X X	X X	X X	X X	X X	/ -	X X	- -	/ X	X X	X X	X X	- -	/ X	X X	- -	X X	X X
Nap	X X	X X	X X	X X	X X	X X	- -	X X	X X	X X	- -	- -	- -	- -	- -	X X	X X	- X	X X	X X
Acy	X X	- -	X X	- -	X X	X X	X X	X X	- -	X X	- -	- -	X X	X X	- -	- -	- -	- X	- -	- X
Ace	/ X	- -	- -	X X	X X	X X	X X	- -	X /	X X	X X	X X	X X	X X	X X	/ X	- /	- -	X X	X X
Flo	- X	- -	- -	X -	X X	X X	X X	- -	X -	X -	X X	X X	X X	X X	- X	- -	X X	- -	X X	X X
Pha	X X	/ X	X X	X X	X X	X X	X X	/ -	X -	X -	X X	X X	X X	X X	- X	- -	X X	//	X X	X X
Fla	X X	- -	- X	- X	- -	- /	X X	X -	X -	X -	X X	X X	X X	X X	X X	- -	X X	X X	X X	X X
Pyr	- /	X X	X X	X -	X X	X X	X X	X /	- -	- X	X X	X X	X X	X X	X X	X X	- -	- /	X X	X X
Σ_{19} PCBs	X X	X X	- -	X X	X X	X X	X /	X X	/ X	X X	X X	X X	X X	X X	X X	X X	X X	- -	X X	X X
8	X X	/ -	/ -	X X	- X	X X	- -	X X	- X	X X	X X	X X	X X	X X	/ X	- X	X X	- -	X X	X X
15	X X	X X	- X	X X	X X	X X	X X	X X	X X	X X	X X	X X	X X	X X	X X	X X	X X	- -	X X	X X
18	X X	X X	- -	X X	X X	X X	X X	X X	- -	X X	X X	X X	X X	X X	X X	X X	- -	/ -	X X	X X
28	X X	X X	- -	X X	X X	X X	X X	X X	- -	X X	X X	X X	X X	X X	X X	X X	- -	- -	X X	X X
31	X X	X X	- /	X X	X X	X X	X X	X X	- X	X X	X X	X X	X X	X X	X X	X X	- -	/ -	X X	X X

^a Paired for monitoring stations, two-sample separate variance for all others.

^b Denoted by: X for Confidence Level (CL) > 95%, / for 90% < CL < 95%, and - for CL < 90% for original and log-transformed datasets, respectively.

Table 3.5. Pearson correlation coefficients between PAHs (bottom left) and PCBs (upper right).

Original (untransformed) data

			Σ_5 PCBs	8	15	18	28	31	
Σ_7 PAHs	1		1	0.901	0.97	0.9	0.95	0.942	Σ_5 PCBs
Nap	0.919	1		1	0.9	0.686	0.76	0.754	8
Acy	0.541	0.543	1		1	0.815	0.932	0.915	15
Ace	0.687	0.391	0.22	1		1	0.856	0.84	18
Flo	0.692	0.362	0.269	0.933	1		1	0.972	28
Pha	0.59	0.236	0.16	0.829	0.936	1		1	31
Fla	0.526	0.21	0.169	0.689	0.797	0.868	1		
Pyr	0.601	0.346	0.442	0.588	0.721	0.774	0.84	1	
	Σ_7 PAHs	Nap	Acy	Ace	Flo	Pha	Fla	Pyr	

Natural log-transformed data

			Σ_5 PCBs	8	15	18	28	31	
Σ_7 PAHs	1		1	0.936	0.946	0.909	0.977	0.971	Σ_5 PCBs
Nap	0.905	1		1	0.9	0.782	0.87	0.868	8
Acy	0.579	0.602	1		1	0.818	0.923	0.915	15
Ace	0.727	0.458	0.283	1		1	0.88	0.871	18
Flo	0.766	0.468	0.351	0.913	1		1	0.98	28
Pha	0.697	0.365	0.273	0.827	0.915	1		1	31
Fla	0.667	0.353	0.263	0.761	0.828	0.882	1		
Pyr	0.705	0.442	0.442	0.685	0.773	0.818	0.899	1	
	Σ_7 PAHs	Nap	Acy	Ace	Flo	Pha	Fla	Pyr	

PAHs and PCBs exhibit strong seasonal variation. The seasonal variation of atmospheric PCBs (and to a lesser extent PAHs) is clearly evident from the temporal data (see Figures 3.6 and 3.7) with significantly higher concentrations occurring in the summer than the winter (see Tables 3.1 and 3.2). To understand and account for the temperature dependence of atmospheric contaminant levels (and to facilitate comparability between other studies), a Clausius-Clapeyron (C-C) regression analysis was performed for each compound over the entire study period. Note that temperature independence was not observed at temperatures below 0 °C in our dataset, so the traditional C-C model was used rather than a ‘frozen water’ model,¹⁶⁶ resulting in a better fit. Σ_7 PAHs, Σ_5 PAHs (Nap and Acy removed), and Σ_5 PCB regressions revealed statistically significant C-C slopes for all PCBs and most PAHs (Figure 3.8; Tables 3.6 and 3.7). Σ_5 PAH (less Nap and Acy) and Σ_5 PCB exhibit strong temperature dependence based on negative slopes of -4099 and -5651 and R^2 values of 0.51 and 0.58, respectively (Figure 3.8). The Σ_5 PAH slope (-4099) and individual site-specific PAH slopes found in the present study (Table 3.6) are less steep than the range previously reported for Chicago (-7302 to -8882)¹⁶⁹ but are much steeper than the slope reported for Pha in New Jersey (-815).¹⁶⁷ Steeper slopes are consistent with atmospheric exchange as a primary source mechanism, whereas flat and/or insignificant slopes might indicate non-exchange emissions such as combustion related activities. C-C slopes for total PAHs (i.e. Σ_7 PAHs, including Nap and Acy) were not significant at all sites (Table 3.6) with an overall value of -1063 and R^2 of 0.05 (Figure 3.8). This resulted from the influence of Nap, which had non-significant negative slopes (except for a statistically significant positive slope at station N possibly from influence of a winter-emitting source nearby), and Acy, which had significant positive slopes at some stations (Table 3.6).

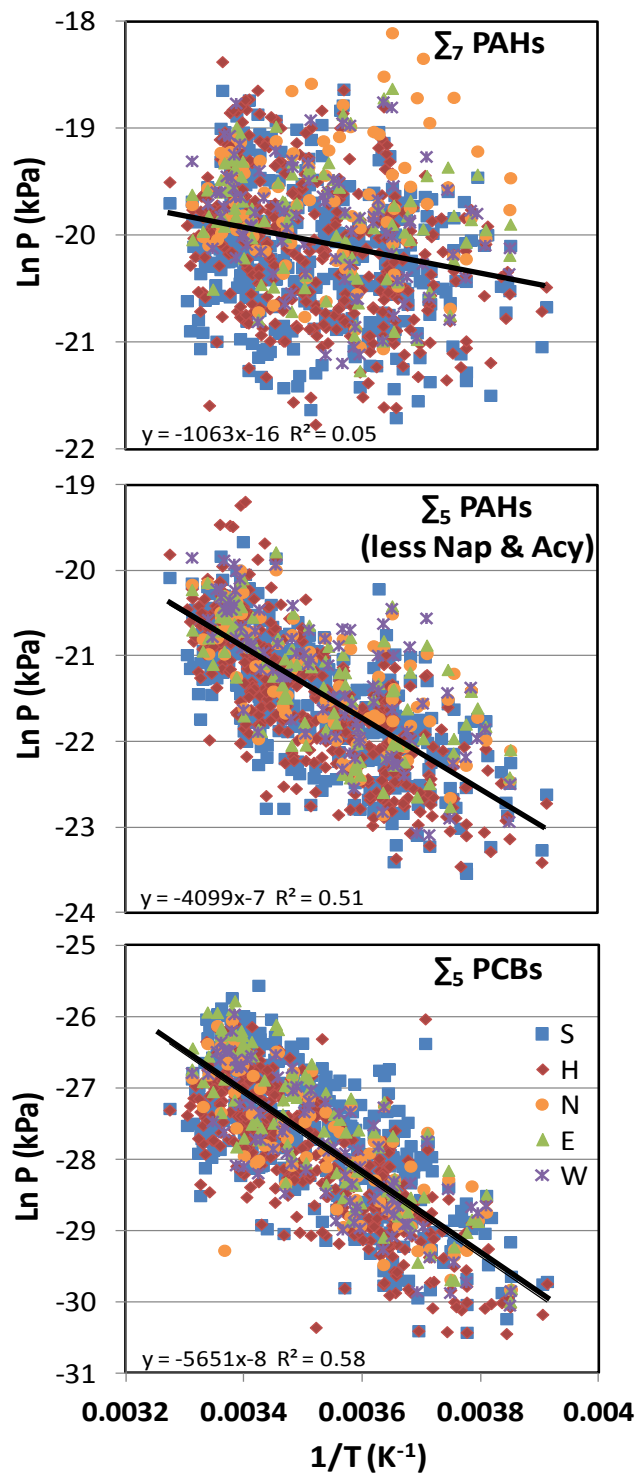


Figure 3.8. Clausius-Clapeyron relationships for Σ_7 PAHs, Σ_5 PAHs (less Nap and Acy), and Σ_5 PCBs with linear regressions shown. Data are identified by sample site.

Table 3.6. Clausius-Clapeyron regression parameters for individual PAHs by station.

Sample Site	Compound(s)	slope ^a	SE	p-value	R ²
South N = 405	Σ ₇ PAHs	-1054	212	<0.001	0.06
	Nap	221	249	0.37	0.00
	Acy	1452	300	<0.001	0.06
	Ace	-4146	243	<0.001	0.42
	Flo	-3564	210	<0.001	0.42
	Pha	-4100	198	<0.001	0.52
	Fla	-4144	217	<0.001	0.47
	Pyr	-2655	221	<0.001	0.26
High School N = 401	Σ ₇ PAHs	-1538	223	<0.001	0.11
	Nap	-249	255	0.33	0.00
	Acy	1263	294	<0.001	0.04
	Ace	-5754	230	<0.001	0.61
	Flo	-4864	206	<0.001	0.58
	Pha	-4749	212	<0.001	0.56
	Fla	-4671	225	<0.001	0.52
	Pyr	-3080	224	<0.001	0.32
North N = 97	Σ ₇ PAHs	155	442	0.73	0.00
	Nap	1181	489	0.02	0.06
	Acy	1422	599	0.02	0.06
	Ace	-3513	443	<0.001	0.40
	Flo	-2811	370	<0.001	0.38
	Pha	-3440	436	<0.001	0.40
	Fla	-3464	431	<0.001	0.41
	Pyr	-1900	453	<0.001	0.16
East N = 100	Σ ₇ PAHs	-817	376	0.03	0.05
	Nap	125	401	0.76	0.00
	Acy	1071	621	0.09	0.03
	Ace	-3990	423	<0.001	0.48
	Flo	-3096	379	<0.001	0.41
	Pha	-3478	454	<0.001	0.38
	Fla	-3328	450	<0.001	0.36
	Pyr	-1913	494	<0.001	0.13
West N = 94	Σ ₇ PAHs	-1345	422	<0.001	0.10
	Nap	-233	459	0.61	0.00
	Acy	903	724	0.22	0.02
	Ace	-5307	516	<0.001	0.54
	Flo	-3869	441	<0.001	0.46
	Pha	-3945	513	<0.001	0.39
	Fla	-4374	464	<0.001	0.49
	Pyr	-2953	483	<0.001	0.29

Table 3.7. Clausius-Clapeyron regression parameters for individual PCBs by station.^a

Sample Site	Compound(s)	slope ^a	SE	R ²
South N = 404	Σ_5 PCBs	-5416	255	0.53
	8	-5285	268	0.49
	15	-5275	251	0.52
	18	-5050	326	0.37
	28	-5922	275	0.54
	31	-5705	303	0.47
High School N = 401	Σ_5 PCBs	-5789	226	0.62
	8	-5674	272	0.52
	15	-5338	223	0.59
	18	-5597	286	0.49
	28	-6227	216	0.68
	31	-6185	230	0.65
North N = 96	Σ_5 PCBs	-5469	435	0.63
	8	-5427	460	0.60
	15	-5635	436	0.64
	18	-4861	569	0.44
	28	-5848	431	0.66
	31	-5698	454	0.63
East N = 99	Σ_5 PCBs	-6280	399	0.72
	8	-6077	455	0.65
	15	-6569	421	0.72
	18	-5770	529	0.55
	28	-6770	380	0.77
	31	-6784	418	0.73
West N = 93	Σ_5 PCBs	-5935	437	0.67
	8	-5848	487	0.61
	15	-5912	456	0.65
	18	-5527	511	0.56
	28	-6385	436	0.70
	31	-6305	456	0.68

^a Slope is statistically significant (p-value < 0.001) for all PCBs.

Temperature explained < 6% of Nap and Acy variability at all stations based on R² (Table 3.6) thus is a relatively unimportant factor for these compounds, despite the fact that temperature dependence varies with compound physical/chemical properties and lighter PAHs like Nap and Acy would presumably be affected by temperature to a greater extent. The Σ_5 PCB C-C slopes at each station range from -5416 to -6280 (Table 3.7), within the range reported for PCBs in Chicago from the IADN dataset (-5130 ± 300 , R² = 0.63).¹⁶⁶

Temperature-corrected trends. All PCB and PAH concentrations except Nap and Acy were temperature-corrected (t-c) to 288 K using the C-C relation (Eq. 3.2) and are summarized in Tables 3.8 and 3.9. Mean PAH and PCB levels did not change drastically with temperature correction to 288 K; Σ_7 PAHs changed from $143 \pm 88 \text{ ng/m}^3$ to $145 \pm 91 \text{ ng/m}^3$, and Σ_5 PCBs changed from $149 \pm 118 \text{ pg/m}^3$ to $145 \pm 114 \text{ pg/m}^3$. In addition, temperature correction did not change the rank order of PCBs or PAHs by mass. This is not unexpected, considering that the average temperature over the entire sampling period was 284 K. However, conclusions regarding the comparisons made among stations, construction activities, seasons, and wind directions do change considerably when we use temperature correction.

Σ_7 PAHs remain statistically significantly highest at station N and lowest at station S; and are significantly higher with wind from the NW and lowest when wind is from the SW (Table 3.8). However, Σ_7 PAHs are now higher in the winter and on days without construction activity, with neither comparison statistically significant at the 95% CL (Table 3.10). Thus the original relationships between elevated PAHs during summer and during active construction are no longer present. This suggests that construction activity was biased towards periods with higher temperature, in agreement with known construction activity schedules. No statistical differences are seen for most compounds between winter and summer, although spring and fall are lower in higher molecular weight PAHs than either summer or winter. This may be due to seasonal factors such as frequency of temperature inversions, higher summer traffic and/or winter heating.

Table 3.8. Statistical analysis of 288 K-corrected^a PAH concentrations (ng/m³) near IHC.

PAHs	No. of Cases ^b	Minimum	Maximum	Interquartile Range	Median	Arithmetic Mean	SEM ^c	95.0% LCL ^d	95.0% UCL ^d	σ	Skewness
All samples											
Σ ₇ PAHs ^a	1,097	16.95	869.01	96.32	122.98	145.13	2.75	139.74	150.52	90.92	1.97
Nap ^a	1,097	6.40	685.99	68.48	71.99	90.64	2.10	86.53	94.75	69.41	2.55
Acy ^a	1,097	0.72	21.58	2.86	1.80	2.64	0.08	2.48	2.80	2.71	2.49
Ace	1,097	1.13	110.00	7.74	8.59	10.98	0.27	10.46	11.50	8.83	3.65
Flo	1,097	1.39	62.10	7.54	9.81	11.35	0.21	10.93	11.76	7.01	2.16
Pha	1,097	0.51	114.22	13.64	19.77	21.91	0.37	21.18	22.64	12.32	1.97
Fla	1,097	0.39	31.72	2.83	4.01	4.66	0.09	4.48	4.84	3.08	2.42
Pyr	1,097	0.48	18.12	2.04	2.49	2.96	0.06	2.84	3.08	2.04	2.34
Σ₇ PAHs by grouping											
South	405	26.34	485.36	88.60	110.80	129.29	3.74	121.94	136.65	75.29	1.44
High School	401	16.95	517.48	93.07	115.54	136.86	4.19	128.63	145.08	83.81	1.53
North	97	48.79	869.01	131.76	170.36	202.55	13.83	175.11	230.00	136.18	2.17
East	100	43.35	574.29	97.65	150.80	165.26	8.95	147.51	183.02	89.49	1.79
West	94	45.79	525.87	111.64	149.96	167.99	9.86	148.41	187.57	95.60	1.55
Active	518	16.95	869.01	91.82	121.59	139.34	3.87	131.74	146.94	88.08	2.66
Idle	579	26.34	577.21	106.86	124.22	150.31	3.87	142.71	157.92	93.17	1.45
Winter	240	29.87	662.30	108.85	127.58	152.37	6.24	140.08	164.65	96.62	1.88
Spring/Fall	581	25.49	869.01	101.29	115.98	141.96	3.96	134.19	149.74	95.43	2.08
Summer	276	16.95	517.48	77.88	127.82	145.50	4.49	136.67	154.34	74.56	1.52
Northeast	202	25.49	384.49	111.61	130.71	145.96	5.54	135.03	156.89	78.79	0.79
Southeast	193	29.87	517.34	90.00	123.97	146.95	5.80	135.52	158.39	80.54	1.45
Southwest	435	28.69	869.01	90.87	107.13	131.87	4.39	123.23	140.50	91.63	2.63
Northwest	250	16.95	662.30	103.99	142.15	167.58	6.39	154.99	180.16	101.04	1.82

^a Except for Nap and Acy.

^b Fewer samples are shown than in Table 3.1 due to fewer days with complete meteorological data available.

^c Standard Error of Arithmetic Mean (SEM).

^d Lower Confidence Level (LCL) and Upper Confidence Level (UCL) of the arithmetic mean.

Table 3.9. Statistical analysis of 288 K-corrected PCB concentrations (pg/m³) near IHC.

PCBs	No. of Cases ^a	Minimum	Maximum	Interquartile Range	Median	Arithmetic Mean	SEM ^b	95.0% LCL ^c	95.0% UCL ^c	σ	Skewness
All samples											
Σ ₅ PCBs	1,093	9.04	2,129.33	117.14	120.11	144.71	3.45	137.94	151.47	114.00	6.63
8	1,093	0.81	634.42	39.58	39.41	48.75	1.21	46.38	51.11	39.86	4.89
15	1,093	0.62	102.81	6.62	6.65	7.87	0.18	7.52	8.23	6.01	5.78
18	1,093	0.74	546.51	31.37	27.83	34.82	0.94	32.97	36.67	31.13	5.47
28	1,093	1.69	418.58	20.97	20.99	26.25	0.68	24.93	27.58	22.33	7.25
31	1,093	0.99	427.01	22.23	21.29	27.01	0.72	25.59	28.43	23.93	6.28
Σ₅ PCBs by group											
South	404	18.62	1,374.77	137.19	147.22	166.45	5.91	154.84	178.06	118.71	3.36
High School	401	9.04	2,129.33	87.61	94.60	115.69	6.02	103.86	127.51	120.47	11.97
North	96	11.01	397.39	103.35	125.57	144.74	7.95	128.97	160.52	77.85	0.92
East	99	48.08	476.59	139.57	159.56	177.63	9.75	158.28	196.99	97.04	1.01
West	93	38.38	399.46	108.13	116.86	140.30	8.18	124.06	156.54	78.85	1.06
Active	519	18.62	610.81	121.42	127.39	142.58	3.88	134.97	150.20	88.29	1.12
Idle	574	9.04	2,129.33	111.86	116.43	146.63	5.56	135.71	157.54	133.09	7.63
Winter	240	9.04	661.48	117.22	113.45	147.36	6.54	134.48	160.23	101.27	1.68
Spring/Fall	576	18.62	2,129.33	116.98	115.95	142.16	5.52	131.33	152.99	132.37	7.71
Summer	277	11.01	443.75	109.87	142.49	147.70	4.66	138.53	156.87	77.53	0.72
Northeast	202	11.01	661.48	117.39	155.02	168.23	7.10	154.22	182.23	100.93	1.42
Southeast	193	28.90	431.58	105.33	134.06	151.04	5.79	139.62	162.46	80.41	0.97
Southwest	436	18.62	2,129.33	73.31	82.94	113.43	6.54	100.58	126.28	136.52	9.55
Northwest	245	9.04	610.81	110.98	168.70	175.71	5.60	164.68	186.75	87.66	1.27

^a Fewer samples are shown than in Table 3.2 due to fewer days with complete meteorological data available.

^b Standard Error of Arithmetic Mean (SEM).

^c Lower Confidence Level (LCL) and Upper Confidence Level (UCL) of the arithmetic mean.

Table 3.10. *t*-test^a for significant differences^b in 288 K-corrected^c PAH and PCB levels among monitoring stations, CDF construction activities, seasons, and wind direction quadrants.

	S-H	S-N	S-E	S-W	H-N	H-E	H-W	N-E	N-W	E-W	Act- Idle	Win- Sp/F	Win- Sum	Sp/F -Sum	NE- SE	NE- SW	NE- NW	SE- SW	SE- NW	SW- NW
Σ ₇ PAHs	X X	X X	X X	X X	X X	X X	X X	X X	X X	--	X /	- /	--	- X	--	X X	X X	X X	X X	X X
Nap	X X	X X	X X	X X	X X	X X	--	X X	X X	X X	X X	--	--	--	--	X X	X X	/ X	X X	X X
Acy	X X	--	X X	--	X X	X X	X X	X X	--	X X	- /	- X	X X	X X	--	--	/ -	- X	--	- X
Ace	--	--	--	X X	- X	X X	X X	--	X X	X X	- /	--	--	- X	--	X X	--	X X	--	X X
Flo	X X	--	--	X X	X X	X X	X X	--	X X	X X	--	X X	--	X X	--	- /	X X	X X	--	X X
Pha	--	--	X X	X X	X X	X X	X X	--	X X	X X	--	X X	--	X X	--	--	X X	/ X	- /	X X
Fla	X X	--	--	- X	--	--	X X	/ -	X X	X X	--	X X	X -	X X	--	--	X X	--	X X	X X
Pyr	--	--	X X	X X	- /	X X	X X	X /	--	--	--	X X	/ -	X X	_ X	X X	--	--	/ X	X X
Σ ₅ PCBs	X X	X -	--	X X	X X	X X	X X	X X	--	X X	--	--	--	- X	/ -	X X	- /	X X	X X	X X
8	X X	--	X X	X X	--	X X	--	X X	- /	X X	--	- /	--	- X	--	_ X	--	X X	X X	X X
15	X X	X X	--	X X	X X	X X	X X	X X	X X	X X	--	- /	- X	/ X	//	X X	--	X X	X X	X X
18	X X	X X	--	X X	/ -	X X	X X	X X	--	X X	--	--	--	--	X -	X X	X -	X X	/ -	X X
28	X X	X X	--	X X	X X	X X	X X	X X	--	X X	--	--	--	- X	X X	X X	/ -	X X	- X	X X
31	X X	X X	--	X X	X X	X X	X X	X X	--	X X	--	--	--	- X	X X	X X	X -	X X	- /	X X

^a Paired for monitoring stations, two-sample separate variance for all others.

^b Denoted by: X for CL > 95%, / for 90% < CL < 95%, and – for CL < 90% for original and log-transformed datasets, respectively.

^c Except for Nap and Acy.

Σ_5 PCBs remain highest at stations S and E (95% CL), whereas all PCBs are lowest at station H of all stations (Table 3.9 and Table 3.10). Similar to the case with PAHs, upon temperature correction there are no statistically significant differences in Σ_5 PCBs based on construction activity and season. Finally, Σ_5 PCB levels are statistically significantly highest when wind is from the N (either NW or NE) and significantly lowest when wind is from the SW.

Accurate determination of significant differences between the stations is important to determine if CDF activity or the canal are impacting air quality. Because Σ_7 PAHs are less at station S compared to other stations, it would appear that at least some of the PAHs at station H come from sources other than the CDF or canal. Further, Σ_5 PCBs are significantly higher at the two sites closest to the canal, and decrease with increasing distance.

PCBs and PAHs are decreasing in the IHC air-shed. Long-term trends in atmospheric concentrations of PAHs and PCBs were determined by calculating first-order rate constants from linear regressions of log-transformed 288 K-corrected concentrations versus time. The results demonstrate that concentrations of most PAHs and all PCBs are decreasing in a statistically significant manner. Mean halving times at station S range from 8.7 to 26.5 years for the seven PAHs and 7.0 to 19.6 years for five PCBs (Table 3.11). Halving times at station H were slightly longer for PAHs and slightly shorter for PCBs, though not significant at the 95% CL. These PAH halving times are somewhat longer than 6 to 10 years for Flo and Pyr¹⁵⁷ and 10.8 ± 1.5 years for Pha¹⁷¹ previously reported for Chicago air (the latter estimate from a C-C model similar to the present study). Sun et al. (2006a)¹⁵⁷ attributed the decrease in PAHs to improvements in fuels, engine performance, and pollution control technology. PCB halving times in the present study are somewhat longer than those reported by Sun et al. (2006b)¹⁵⁸ (7.7 ± 1.1 years) while the halving time for PCB 18 is similar to that reported by Venier et al. (2012)¹⁷¹ (8.84 ± 0.84 years).

Table 3.11. Mean halving time (years \pm 1 SE)^a for PAHs and PCBs at stations S and H.

Compound	South		High School	
Nap ^b	12.4	(10.1 - 15.9)	15.7	(12.1 - 22.4)
Acy ^b	8.7	(7.3 - 10.8)	13.2	(10.2 - 18.7)
Ace	24.9	(17.2 - 45.1)	NS ^c	
Flo	17.0	(13.5 - 23.0)	NS	
Pha	26.5	(19.1 - 43.3)	NS	
Fla	15.3	(12.3 - 20.2)	NS	
Pyr	12.2	(10.2 - 15.1)	18.3	(14.0 - 26.2)
PCB 8	7.0	(6.2 - 8.1)	7.3	(6.4 - 8.5)
PCB 15	11.4	(9.4 - 14.3)	10.8	(9.2 - 13.1)
PCB 18	9.5	(7.7 - 12.3)	7.8	(6.7 - 9.3)
PCB 28	19.6	(14.0 - 32.6)	12.8	(10.7 - 16.0)
PCB 31	14.0	(10.7 - 20.4)	10.0	(8.6 - 12.0)

^a Halving times obtained from the slopes (\pm 1 SE) of first-order decay model using temperature-corrected PAHs and PCBs. Standard error not symmetric about the mean halving time due to the natural log term in the equation.

^b Nap and Acy not temperature-corrected.

^c NS indicates slope is not statistically significant at the 95% CL.

Wind direction data suggests local PCB source and multiple PAH sources. A nonlinear sinusoidal model was fit to temperature-corrected PAH and PCB concentration and wind direction data using a parametric wind direction term from Hafner and Hites (2005),¹⁷⁶ which gave a better fit to our PAH and PCB data than other sinusoidal functions. As is readily apparent, PAH levels at stations S and H do not exhibit a significant correlation with wind direction (Figure 3.9A). In contrast, PCB levels exhibit a strong, statistically significant correlation with wind direction (Figure 3.9B), with Σ_5 PCBs > 1 natural log higher with wind from the NE compared to the SW. Interestingly, of all the semivolatile organic pollutants, PAHs are frequently found to have stronger relationships with wind direction.¹⁷⁶

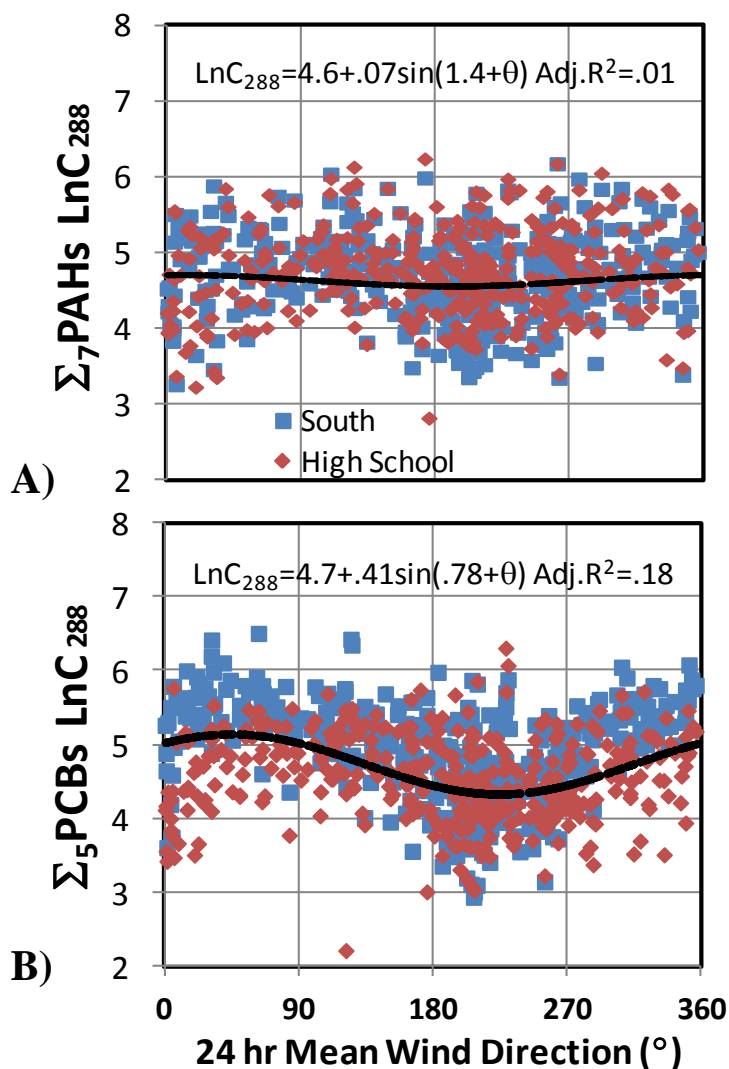


Figure 3.9. Comparison of (A) PAH (ng/m³) and (B) PCB (pg/m³) temperature-corrected (288 K) concentrations at stations S and H as a function of mean wind direction during the 24-hour sampling period for days with angular deviation less than 60°. Sinusoidal regressions are shown. North is 0/360° and south is 180°.

A clear difference in wind source direction exists for both compound classes (PAHs versus PCBs) as well as station locations (N, E, and W stations north of the canal versus S and H stations south of the canal). Σ₇ PAHs appear to have a different source direction at station H (SW wind, FoI = 1.05) compared to station S (NE wind, FoI = 1.19), although the effect is quite small at the H site shown by the low Factor of Increase (FoI) value (Table 3.12). In contrast, all

stations north of the canal have wind source directions for Σ_7 PAHs similar to that of station S (wind source direction ranging from 71°-109° with FoI values from 1.29-1.37; Table 3.12). Σ_5 PCB levels at stations S and H south of the canal both have wind source directions from the NE (FoI 1.87 and 1.29 for stations S and H, respectively; Table 3.12). Stations N, W, and E all have PCB levels correlated with wind from the SE, with FoI values from 1.49-1.54. These results are consistent with a canal source for PCBs at all sample sites. For the Chicago IADN site, Hafner and Hites (2005)¹⁷⁶ calculated a W/SW wind source direction for both PAHs and PCBs (252° with 1.44 FoI, and 270° with 1.28 FoI for PAHs and PCBs, respectively). In the present study several different source directions were found for PAHs and PCBs, indicating numerous and/or local contaminant sources at IHC. Ultimately wind direction alone is not sufficient to predict contaminant levels, as with other studies that have attributed a relatively small importance to wind direction.^{172, 178}

Table 3.12. Wind direction regression parameters for PAHs and PCBs.

Station	Σ_7 PAHs		Σ_5 PCBs	
	Source direction (°) ^a	Factor of Increase	Source direction (°)	Factor of Increase
N	99	1.19	124	1.53
E	71	1.29	128	1.54
W	109	1.37	117	1.49
S	20	1.19	33	1.87
H	217	1.05	76	1.29
S + H	11	1.08	45	1.50
All	56	1.10	62	1.39

^a 0°-90°=NE; 90°-180°=SE; 180°-270°=SW; 270°-360°=NW

Multiple linear regression models predict Σ_5 PCBs and Σ_5 PAHs. Multiple linear regressions for predicting PAH and PCB concentrations were performed with temperature, time, wind direction, wind speed, and relative humidity data. The regressions for Σ_7 PAHs, Nap, Pha, Σ_5 PCBs, PCB 8, and PCB 28 (Figure 3.10, Table 3.13) explain 37, 28, 64, 67, 66, and 67% of the variability in their respective concentrations, based on adjusted R^2 values. For all PCBs and Pha, the majority of explanatory power (45-58%) comes from the temperature term, followed by wind speed for Pha (15%) and wind speed and/or time for PCBs (2-6%) based on stepwise R^2 values (Table 3.13). In contrast, Nap and Σ_7 PAH variation is explained primarily by wind speed (12-26%) followed by time (8%). The negative relationship with wind speed is consistent with a wind dilution effect that disperses contaminants further from the source. Wind direction explains a maximum of 3% of the variability, and relative humidity (not shown in the Figure 3.10 regression; see Table 3.13) is the least important variable explaining a maximum of 1%. The wind direction term was significant for all compounds by multiple regressions, but was only significant for Pha and PCB 8 by individual regressions. Finally, a scatter plot of measured versus predicted concentrations demonstrates a high degree of agreement (within ± 1 natural log unit) between model-predicted and measured values for most compounds, except for Nap as expected (Figure 3.11).

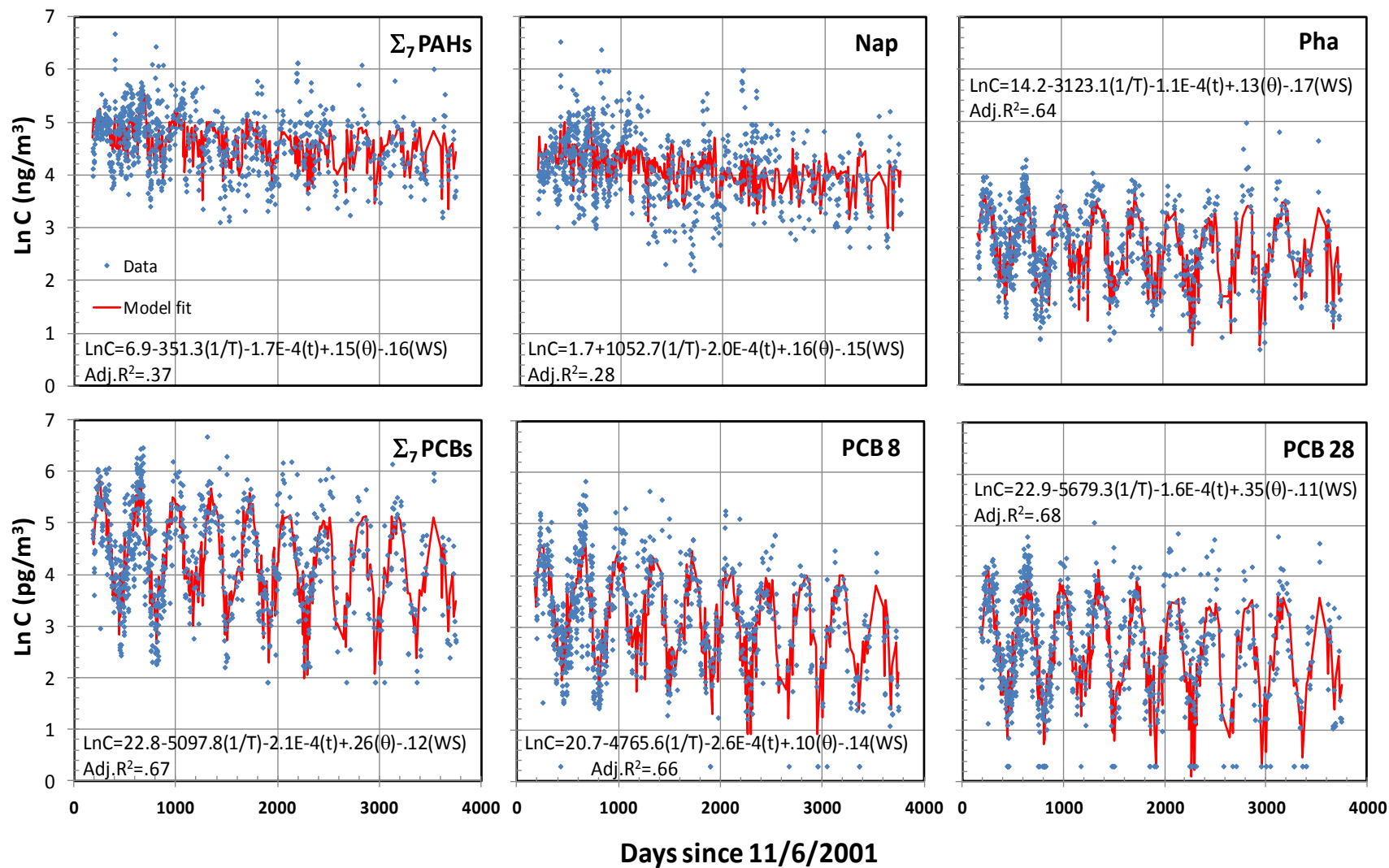


Figure 3.10. Select PAH (ng/m³) and PCB (pg/m³) concentrations as a function of time for all stations over the entire sampling period. Multiple linear regressions are shown.

Table 3.13. Multiple linear regression parameters and individual regression parameters for select PAHs and PCBs.^a

		Multiple linear regression ^b				Individual regression			
	n=852	Coefficient	SE	Adj. R ²	R ²	Coefficient	SE	p-value	R ²
Σ_7 PAH	Intercept	6.89	0.41	0.37					
	1/T	-351	117		0.01	-813	137	0.00	0.04
	Jul Day	0.00	0.00		0.08	0.00	0.00	0.00	0.07
	cosWD	0.15	0.02		0.03	-0.02	0.03	0.48	0.00
	WS	-0.16	0.01		0.26	-0.15	0.01	0.00	0.26
Σ_5 PCB	Intercept	22.8	0.53	0.67					
	1/T	-5100	146		0.57	-5310	159	0.00	0.57
	Jul Day	0.00	0.00		0.04	0.00	0.00	0.00	0.04
	cosWD	0.26	0.03		0.03	-0.10	0.05	0.05	0.00
	WS	-0.12	0.01		0.03	-0.18	0.02	0.00	0.14
	RH	0.01	0.00		0.01	0.01	0.00	0.00	0.01
Nap	Intercept	1.66	0.53	0.28					
	1/T	1050	145		0.06	624	159	0.00	0.02
	Jul Day	0.00	0.00		0.08	0.00	0.00	0.00	0.07
	cosWD	0.16	0.03		0.02	0.05	0.03	0.11	0.00
	WS	-0.15	0.01		0.12	-0.11	0.01	0.00	0.12
Pha	Intercept	14.2	0.43	0.64					
	1/T	-3120	119		0.45	-3670	139	0.00	0.45
	Jul Day	0.00	0.00		0.02	0.00	0.00	0.00	0.02
	cosWD	0.14	0.03		0.02	-0.16	0.04	0.00	0.02
	WS	-0.17	0.01		0.15	-0.21	0.01	0.00	0.31
	RH	0.01	0.00		0.01	0.01	0.00	0.00	0.01
8	Intercept	20.7	0.56	0.66					
	1/T	-4770	153		0.54	-5250	167	0.00	0.54
	Jul Day	0.00	0.00		0.06	0.00	0.00	0.00	0.06
	cosWD	0.10	0.03		0.01	-0.26	0.05	0.00	0.03
	WS	-0.14	0.01		0.06	-0.21	0.02	0.00	0.18
	RH	0.01	0.00		0.00	0.01	0.00	0.02	0.01
28	Intercept	23.0	0.57	0.68					
	1/T	-5680	155		0.58	-5740	166	0.00	0.58
	Jul Day	0.00	0.00		0.02	0.00	0.00	0.00	0.02
	cosWD	0.35	0.03		0.03	-0.02	0.05	0.70	0.00
	WS	-0.11	0.01		0.04	-0.18	0.02	0.00	0.11
	RH	0.01	0.00		0.01	0.01	0.00	0.00	0.02

^a p-value < .005.

^b Adj. R² of complete regression; R² of each term from forward stepwise regression.

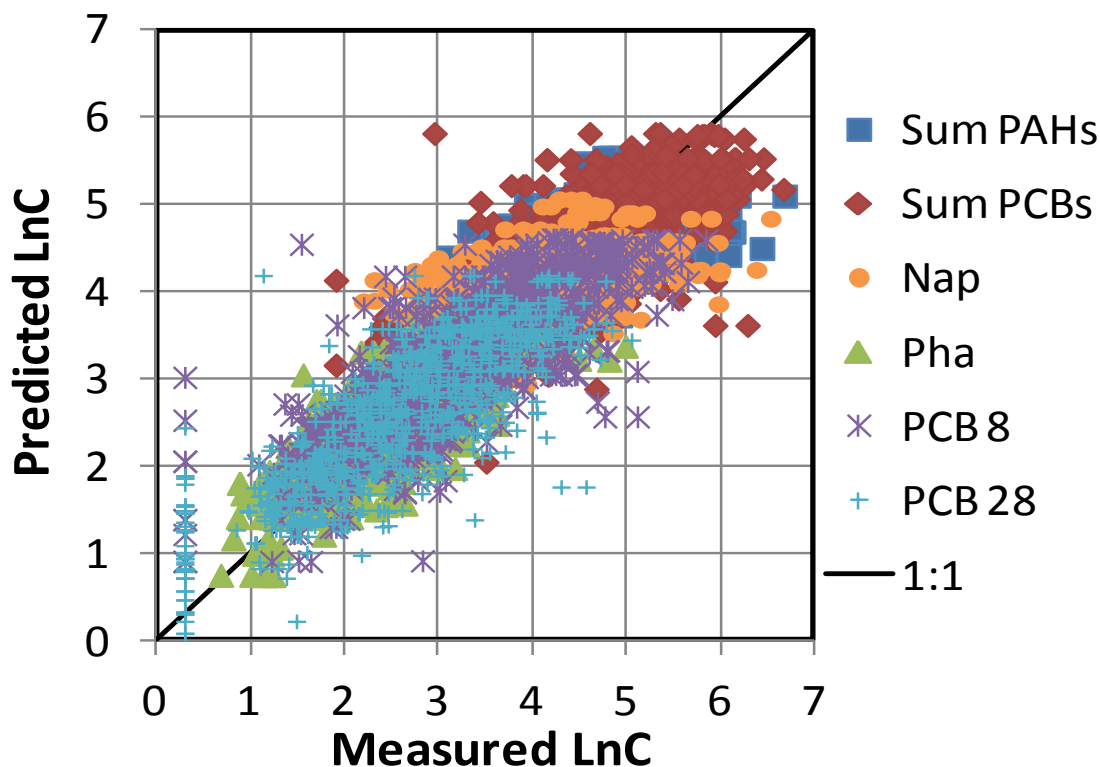


Figure 3.11. Comparison of MLR model-predicted and measured Σ_7 PAH, Σ_5 PCB, Nap, Pha, PCB 8, and PCB 28 concentrations.

Our findings can be compared with results from Venier et al. (2010)¹⁷⁷ MLR of IADN data from Chicago and other Great Lakes sites. Venier et al. (2010) found PAH and PCB concentrations were strongly related to population density (which explained 74% of PAH and 55% of PCB variability)^{177, 185} although not a valid term for the present local urban analysis. In the IADN study temperature accounted for 4.5% and 22.7% of PAH and PCB variability respectively, then wind direction for PAHs (1.3%) and time for PCBs (2.9%), with about 20% of PAH and PCB variability remaining unexplained.¹⁷⁷ In the present study, a third of the variability in Σ_5 PCBs and about two thirds of the variability in Σ_7 PAHs and Nap are unexplained (Table 3.13). Inspection of Figure 3.10 demonstrates that much of the missed variability occurs on the peaks and indicates source-related terms (particularly for Nap) are important yet lacking from the

current analysis. Fully understanding atmospheric contamination at IHC will require identification of sources through a more advanced source apportionment analysis.

In conclusion, PAHs and PCBs are elevated in the IHC air-shed and consistent with an IHC source for PCBs and dispersed and/or multiple sources for PAHs. Controlling the data for temperature was essential for accurate comparison between different construction activities, seasons, wind directions, and monitoring stations. Levels of most compounds decreased with halving times ranging from 7 to 20 years for PCBs and 9 to 25 years for PAHs. A regression model was developed that utilized meteorological and temporal data to partially explain the observations. Continued monitoring during the multi-year dredging of the IHC will provide essential information to determine what effect the navigation project may have on atmospheric pollution in the area.

CHAPTER IV. POSITIVE MATRIX FACTORIZATION SOURCE APPORTIONMENT OF PAHS AND PCBS AT INDIANA HARBOR AND CANAL CONFINED DISPOSAL FACILITY AIR-SHED PRE-DREDGING (2001-2012)

4.1. Abstract

High levels of polycyclic aromatic hydrocarbons (PAHs) and polychlorinated biphenyls (PCBs) are in sediments of the Indiana Harbor and Canal (IHC) on Lake Michigan (a federally designated Great Lakes Area of Concern). IHC is the focus of a US Army Corps of Engineers navigation project including a Confined Disposal Facility (CDF) for sediment dredged from the area. An extensive atmospheric monitoring of toxins including PAHs and PCBs has taken place at the site since 2001 to evaluate background contamination and local project impacts. A source apportionment analysis of these data was performed to identify possible sources of air pollution among current and historic industries in the area utilizing quantitative Positive Matrix Factorization (PMF) with meteorological, temporal, spatial, and reference source data. PAH and PCB sources were corrected to 15 °C using the Clausius-Clapeyron (C-C) equation to examine environmental effects on source loading and identify sources within the matrix of seasonal variation. Results indicate multiple unique sources of airborne pollutants to the monitoring stations from primary emitters as well as secondary environmental emission sites identified with the aid of C-C corrections. Although both PAHs and PCBs are legacy contaminants, source apportionment results highlight the importance of current PAH releases. Coke oven emissions are the chief source of atmospheric PAHs at IHC and account for over half of the contaminant mass burden, while petroleum storage and transfer and gas and diesel exhaust are the next largest sources. PCB results indicate the canal and other environmental sources of Aroclor 1248 may impact the local atmosphere, exhibiting seasonal variation consistent with volatile release

mechanisms from secondary sources. The use of multiple receptor models, identification approaches, and supporting data enables determination of PAH and PCB sources to the IHC airshed and understanding of local air quality in this complex, multi-source, heavily industrialized region.

4.2. Introduction

The Indiana Harbor and Canal (IHC) is an active port near the southern tip of Lake Michigan and the current focus of a US Army Corps of Engineers (USACE) navigation project that includes a Confined Disposal Facility (CDF) adjacent to the canal for dredged sediment. IHC is part of the Grand Calumet River Area of Concern (AOC), the only US Environmental Protection Agency (USEPA) Great Lakes AOC exhibiting all beneficial use impairments.¹⁸⁶ Located 27 km southeast of downtown Chicago and in one of the most heavily-industrialized regions in the nation, IHC suffers from widespread legacy contamination. The USACE therefore established an extensive atmospheric monitoring program for toxins including polycyclic aromatic hydrocarbons (PAHs) and polychlorinated biphenyls (PCBs) since 2001 to evaluate background contamination at the CDF and local project impacts. A detailed trend analysis of PAHs and PCBs using USACE monitoring data from 2001 to 2012 (prior to dredging) is given in Granberg (2013).¹⁹⁰ PAHs and PCBs drive the majority of IHC sediment toxicity¹ and have been studied in IHC air considering their impacts to Lake Michigan from the Chicago metropolitan area^{106, 109, 175, 184, 187} and possible community health effects.^{156, 188} Sources of atmospheric PCBs in Chicago are of considerable interest due to the widespread presence of congeners with dioxin-like behavior, neurotoxicity,¹¹⁰ lack of identified sources,¹¹¹ inputs to Lake Michigan,¹⁸⁹ and lacking evidence for the success of long-term reduction strategies.¹⁴¹

Major sources of PAHs to the environment include the incomplete combustion of fossil fuels and organic matter;^{2, 8} as well as crude and refined fossil fuel products, and coke processing in the steel industry. PCBs, synthesized in the twentieth century for a number of industrial applications,⁹¹ continue to be released from environmental sources, incinerators, electrical and hydraulic equipment, and building materials;¹⁵³ and are inadvertently produced in pigments and paints.^{154, 155} The myriad possible pollution sources to the IHC air-shed include evaporation from the canal itself,¹⁰⁶ over 400 Resource Conservation and Recovery Act (RCRA) hazardous waste sites within the AOC (including the CDF which was historically a refinery), and over 50 Comprehensive Environmental Response Compensation and Liability Act sites (including a heavily PCB-contaminated lagoon) five of which are Superfund sites listed on the EPA National Priorities List.¹⁸⁶ Three of the largest steel manufacturing plants in the country reside in the AOC, along with integrated and independent coking operations producing millions of tons of coke for the steel industry, and various metal finishing and product facilities. The petroleum industry within the AOC includes one of the largest refineries in the nation, a used oil refinery adjacent to the CDF, crude oil pipelines, numerous petroleum storage, transfer and distribution facilities surrounding the CDF (Figure 4.1), and petroleum products companies. While steel and petroleum dominate the industry, other manufacturing including chemical, cement, food, and auto parts are active within and outside the AOC in Chicago. The region also contains coal burning power plants, waste and wood incinerators, a transformer storage yard, residential wood burning, biosolids drying beds, and traffic from a dense network of national highways (including interstates within a few kilometers or adjacent to the CDF in every direction), three international airports (including one in the AOC), and rail and water shipping. Locations of a number of relevant PAH and PCB sources are identified in the map in Appendix A (Figure A1).

A Positive Matrix Factorization (PMF) source apportionment analysis of PAHs and PCBs in the IHC air-shed with Monte Carlo simulation for uncertainty estimation was undertaken utilizing data from the decade spanning 2001-2012. A comprehensive weight of evidence approach was taken including use of various multivariate receptor models and a dispersion model to aid in interpreting apportionment results. Site-specific meteorological data were further employed along with temperature correction, temporal and spatial features, local industrial and historical information, and known reference sources and emission inventories together with the previous trend analysis¹⁹⁰ to identify sources. These findings support PAH and PCB inventories and establish a baseline for future source apportionment analyses with ongoing monitoring. These results also inform IHC dredging, monitoring, and other remediation/site development projects as well as the industrial operations that drive emissions in the area. Pollution prevention, control, and removal solutions are suggested to reduce impacts to IHC and the surrounding AOC, Chicago, and Lake Michigan.

4.3. Materials and Methods

Atmospheric sampling and chemical analysis. All sampling and analytical methodological details are found in Granberg (2013).¹⁹⁰ In brief, air samples were obtained approximately every six days between November 2001 and October 2008 and every twelve days between October 2008 and February 2012. Five monitoring stations were established in the study (Figure 4.1): three on the CDF perimeter to the north (N), east (E), and west (W), one across the canal from the CDF to the south (S), and one at the East Chicago High School (H) about 0.6 km further SW from the S station. Station H is considered an important nearby receptor in the surrounding community. Over the ten year monitoring period from November 2001 to February 2012 more than 1200 atmospheric samples were collected. Nearly three quarters of the samples were from

stations S and H that operated the entire project duration, with the remainder from stations N, E, and W that ceased operation in April 2004. The USEPA Compendium Method TO-13A/CARB Method 429/SW-846 Method 1668 was used for sampling and analysis of gas plus particulate phase PAHs and PCB congeners in ambient air.¹⁶² Quantitation limits were 4.50-6.27 ng/m³ for Nap, 1.14-3.13 ng/m³ for other PAHs, and 2.25-3.13 pg/m³ for PCB congeners. A total of 17 PAHs (Σ_{17} PAHs) and 19 PCB congeners (Σ_{19} PCBs) were analyzed based on their potential to contribute to health impacts in the community. A meteorological station established alongside the S station sampler measured wind speed (m/s), wind direction (degrees clockwise from true N), and ambient temperature (°C) among other parameters described previously.¹⁹⁰

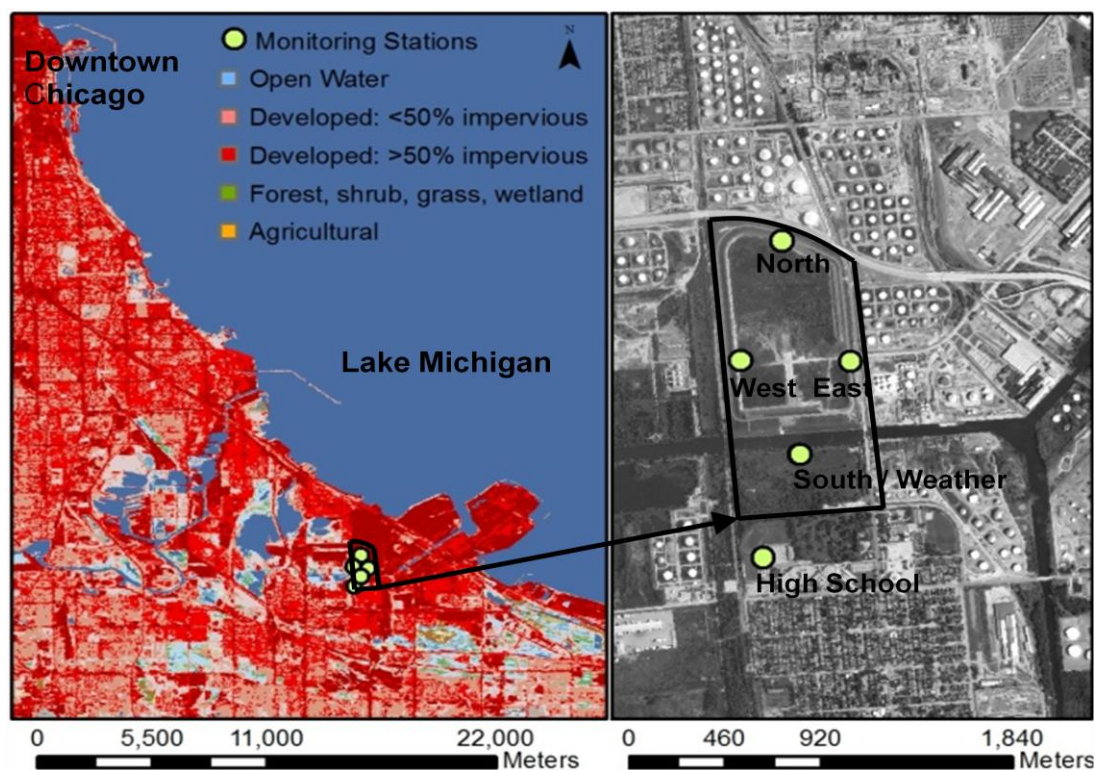


Figure 4.1. Location of atmospheric sampling stations. Land use map left (USGS National Land Cover Database, 2006) and aerial photo right (National Agriculture Imagery Program Orthoimagery, 2010).

Dataset preparation. The PAH and PCB data used for modeling are the same data described in Granberg (2013)¹⁹⁰ with the inclusion of PCB 118 here. Naphthalene (Nap), acenaphthylene (Acy), acenaphthene (Ace), fluorene (Flo), phenanthrene (Pha), fluoranthene (Fla), pyrene (Pyr), and PCB congeners 8, 15, 18, 28, 31, and 118 (by IUPAC congener number) were selected for this study based on detection frequencies over 40%. Non-detects in the data (14% and 17% of PAH and PCB datasets, respectively)¹⁶⁴ were substituted with half the detection limit for modeling purposes. One PCB sample from station S (9/1/2005) was identified as a far outlier by box plot inspection (approximately three times higher than the next highest concentration) and was thus removed from the dataset to avoid bias. The PAH dataset includes seven compounds and 1233 samples and the PCB dataset includes six congeners and 1229 samples.

Total (gas plus particulate) PAH and PCB concentrations are used in the analysis to prevent receptor modeling bias resulting from partitioning between gas and particle phases.¹³⁴ Although gas and particulate phase concentrations were not reported separately, they can be estimated using the following equilibrium partitioning model for semivolatile organic compounds (SVOCs) from Weschler and Nazaroff (2010).¹⁹¹

$$X_{gas_pred} = \frac{\rho_{part}}{\rho_{part} + TSP * f_{om_part} * K_{OA}} \quad (4.1)$$

X_{gas_pred} is the predicted mass-fraction of the SVOC in gaseous phase; ρ_{part} is the density of the airborne particles (g/m^3), assumed to be $1 \times 10^6 \text{ g}/\text{m}^3$; TSP is the mean measured mass concentration of airborne particles (g/m^3) at station S, $4.88 \pm 2.68 \times 10^{-5} \text{ g}/\text{m}^3$ ($\mu \pm \sigma$); f_{om_part} is the volume fraction of organic matter associated with airborne particles, assumed to be 0.4; K_{OA}

is the compound-specific octanol-air partition coefficient, using values in Table 4.1 from EPI Suite (Estimation Program Interface Suite, v. 4.1, USEPA, Washington, DC, USA).

Using Equation 4.1, over 98% of all PAHs and PCBs were predicted to occur in the gas phase except for PCB 118 which was estimated as 88% in gas phase (Figure 4.2).

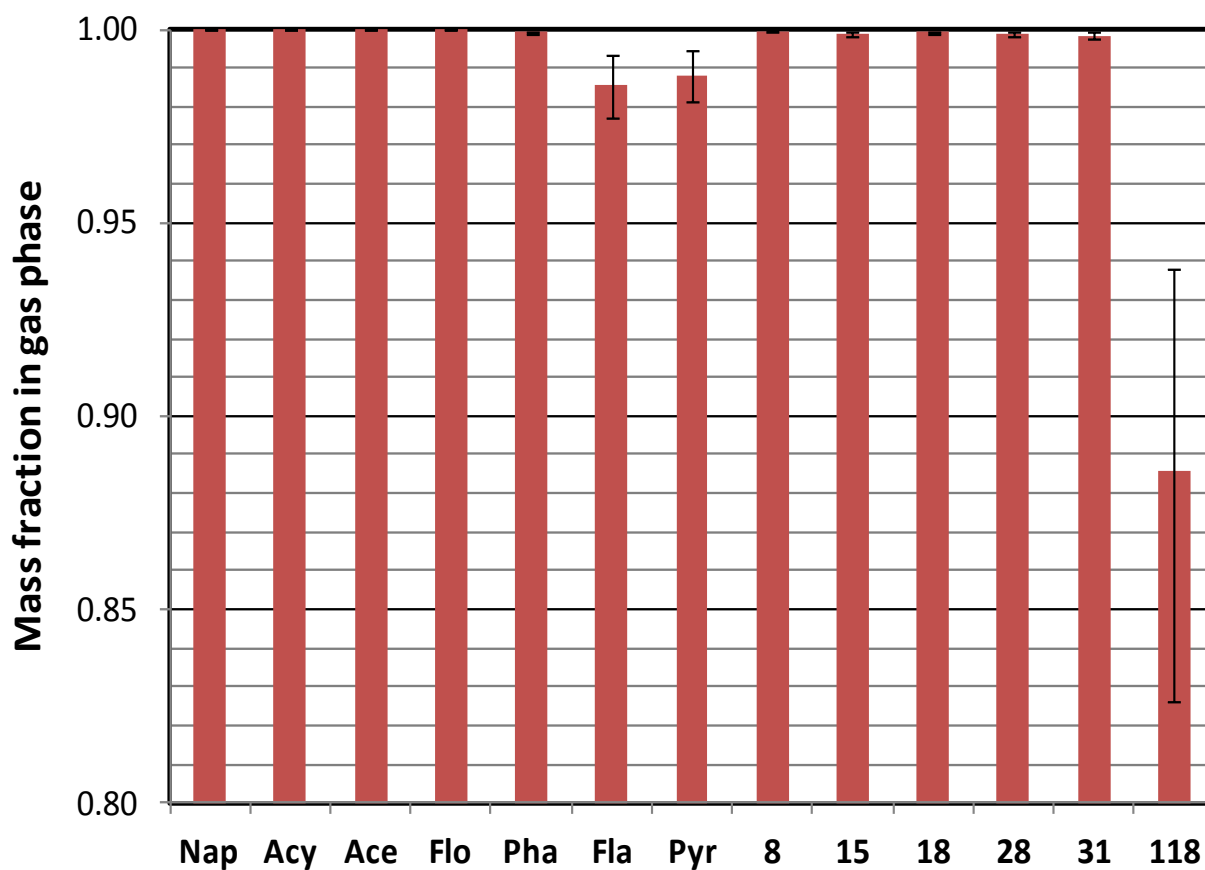


Figure 4.2. Mass fraction of atmospheric PAHs and PCBs in gas phase based upon $\mu \pm \sigma$ of TSP at station S and the Weschler and Nazaroff (2010)¹⁹¹ partitioning model.

Table 4.1. Physical properties^a of select PAHs and PCB congeners.

Compound	Mol. Formula	Mol. Weight (g/mol)	Log K _{OW}	Melting Point ^b (°C)	Boiling Point (°C)	Vapor Pressure ^b (mm Hg)	Water Solubility ^b (mg/L)	Henry's Law Constant ^b (K _H) (atm-m ³ /mol)	Log K _{OA}
Naphthalene (Nap)	C ₁₀ H ₈	128.18	3.3	80.2	217.9	8.50E-02	31	4.40E-04	5.19
Acenaphthylene (Acy)	C ₁₂ H ₈	152.2	3.94	92.5	280	6.68E-03	16.1	1.14E-04	6.272
Acenaphthene (Ace)	C ₁₂ H ₁₀	154.21	3.92	93.4	279	2.15E-03	3.9	1.84E-04	6.31
Fluorene (Flo)	C ₁₃ H ₁₀	166.22	4.18	114.8	295	6.00E-04	1.69	9.62E-05	6.79
Phenanthrene (Pha)	C ₁₄ H ₁₀	178.24	4.46	99.24	340	1.21E-04	1.15	4.23E-05	7.57
Fluoranthene (Fla)	C ₁₆ C ₁₀	202.26	5.16	107.8	384	9.22E-06	0.26	8.86E-06	8.88
Pyrene (Pyr)	C ₁₆ C ₁₀	202.26	4.88	151.2	404	4.50E-06	0.135	1.19E-05	8.8
CB 8	C ₁₂ H ₈ CL ₂	223.1	5.09	<i>81.47</i>	<i>320.32</i>	2.09E-03	1.17	2.30E-04	7.4
CB 15	C ₁₂ H ₈ CL ₂	223.1	5.23	149.3	317	5.35E-04	0.062	1.99E-04	7.68
CB 18	C ₁₂ H ₇ CL ₃	257.55	5.55	<i>100.85</i>	<i>340.7</i>	1.05E-03	0.4	2.50E-04	7.6
CB 28	C ₁₂ H ₇ CL ₃	257.55	5.62	<i>100.85</i>	<i>340.7</i>	1.95E-04	0.27	2.00E-04	<i>7.707</i>
CB 31	C ₁₂ H ₇ CL ₃	257.55	5.69	<i>100.85</i>	<i>340.7</i>	4.00E-04	0.143	1.90E-04	7.92
CB 118	C ₁₂ H ₅ CL ₅	326.44	7.12	<i>134.6</i>	<i>378.21</i>	8.79E-06	0.0134	2.88E-04	9.82

^a Values from Estimation Programs Interface (EPI) Suite (v. 4.1, US Environmental Protection Agency, Washington, DC, USA). Experimental values are given when available. Estimated values are shown in italics.

^b At 25 °C

Positive Matrix Factorization. Positive Matrix Factorization (PMF) is a multivariate receptor model used to quantitatively apportion the measured contaminant mass at a receptor in the environment to various contaminant sources.^{125, 149, 192, 193} Like most receptor models it has commonly been applied to particulate matter in air,^{137, 193-195} but PMF has also been used to apportion PAHs and PCBs (gas and/or particulate phases) in air,^{134, 141-143} as well as in soils and sediments.^{120, 130, 133, 139, 144} Multivariate receptor models assume measured concentrations are a linear sum of sources, and utilize matrix analysis to solve for m compounds in n samples as contributions from p independent sources (Eq. 4.2).^{125, 149, 192} The model assumes that many sources or emitters have unique contaminant compositions that change little between source and receptor.^{64, 196} For this study PAHs and of PCBs were considered generally stable during atmospheric transport due in part to the proximity of the receptor to likely emission sources.⁶⁵

$$\mathbf{X} = \mathbf{G} \times \mathbf{F} + \mathbf{E} \quad (4.2)$$

\mathbf{X} is the measured concentration data matrix $m \times n$; \mathbf{G} is the factor-loading matrix $m \times p$, representing chemical profiles of sources; \mathbf{F} is the factor-score matrix $p \times n$, representing source contributions to sample concentrations; \mathbf{E} is the error concentration matrix $m \times n$, or the difference between measured and calculated matrices.

PMF uses a constrained weighted least squares approach to solve the bi-linear matrix equation, iteratively computing factor profiles (\mathbf{G}) and factor contributions (\mathbf{F}) by minimizing an objective function Q , which is the weighted sum of the squares of the difference between the estimated and measured data (Eq. 4.3). During minimization of Q , elements \mathbf{G} and \mathbf{F} are constrained to non-

negativity to ensure realistic source profiles and contributions. PMF can also weight measured data by their estimated uncertainties to reduce the influence of censored and outlier data on solutions and better represents signals of all strengths.^{135, 136}

$$Q(\mathbf{E}) = \sum_{i=1}^m \sum_{j=1}^n \left(\frac{E_{ij}}{\sigma_{ij}} \right)^2 \quad (4.3)$$

\mathbf{E}_{ij} is the error concentration matrix; σ_{ij} is the standard deviation concentration matrix of uncertainties weighting each measured element.

This study utilizes the PMF program coded by Bzdusek (2005)¹⁴⁵ on the MATLAB platform (release 2011a, Mathworks, Inc., Natick, MA, USA) employing penalty terms for imposing constraints. Convergence criteria, step length control, penalty coefficients, and other variable model parameters are shown in Table 4.2. This model was used successfully in recognizing source and degradation PCB patterns in lake and river sediments^{120, 130, 133} and obtained results similar to the PMF program publically available from USEPA (EPA Positive Matrix Factorization (PMF), v. 3.0, USEPA, Washington, DC, USA).^{125, 146} Source apportionment results were also obtained from the EPA program for confirmation of this reported similarity.

Table 4.2. PMF parameters used for all runs.^a

Parameter description	Value
Number of iterations for non-negative procedures	500
Final value of the sum of squares of differences between five consecutive G matrices	0.001
Weighting matrix $\sigma_{ij} = C1 + C2 * \max(X_{ij} , X'_{ij})$; recalculated with each iteration	Yes
For C1; multiplier of the smallest value for each chemical	1
For C2; the relative error	0.25
Penalty and regularization term weights for the first second and third iteration sequence	5.0, 0.01, 0.0001
Convergence criteria for the first second and third iteration sequence	1.0, 0.1, 0.001
Lambda for step length control	0.05
Number of sub-iterations using step length for alpha and beta	50
Maximum number of iterations for main steps	200

^a Model from Bzdusek (2005).¹⁴⁵

Major inputs to the model are the measured data matrix, the uncertainty matrix, and the number of sources to solve for. The original PAH and PCB data matrices include all monitoring stations operating over the study period (7 x 1233 and 6 x 1229, respectively). Additional modeling runs were performed utilizing 15 °C and 30 °C temperature-corrected PAH datasets and individual station PAH and PCB datasets to determine whether significant differences in predicted source loadings or contributions occurred. Temperature-corrected PAH datasets each included 1092 samples based on days with corresponding temperature information and removal of five outliers (4/15/2003) with Studentized residuals less than -3 (natural log-transformed data). Nap and Acy had insignificant positive slopes and were thus not temperature-corrected. The full procedure for temperature correction using the Clausius-Clapeyron relationship is described in Granberg (2013).¹⁹⁰ PAH and PCB datasets according to station have the following sample numbers, respectively: N: 111 and 110, E: 123 and 122, W: 109 and 108, S: 447 and 446, H: 443 and 443.

The standard deviation matrix utilized in the present study is estimated by the environmental error model (EM) = -14^{145, 147, 148} and includes compound detection limits and relative errors based on analytical, sampling, and environmental uncertainties.

$$\sigma_{ij} = C_1 + C_2 \max(|X_{ij}| |X'_{ij}|) \quad (4.4)$$

σ_{ij} is the standard deviation concentration matrix; C_1 is the smallest value in data matrix for each compound (in this case the detection limit divided by two); C_2 represents the relative error due to analytic, sampling, and environmental uncertainty (assumed to be 0.25 for both PAHs and PCBs based on average analytical recoveries of 0.18); X_{ij} is the original data matrix; X'_{ij} is the modeled data matrix (thus new weights are found after each iteration).

The PMF model was run multiple times investigating different numbers of sources. Each run generates diagnostic tools with each solution, including coefficients of determination (CODs), Exner function calculation, the objective function Q, and the number of degrees of freedom to assist in evaluating goodness of fit between modeled and measured data and in choosing the correction solution (i.e. number of sources).¹⁴⁵ CODs represent good to excellent fit for values ranging from 0.9 to 1.0, and the Exner function indicates excellent reproduction of the measured data for values from 0.1 to 0.0.^{133, 149} The objective function Q (Eq. 4.3) should also approximate the number of degrees of freedom (ν) for the error matrix E_{ij} to approximate the assigned standard deviation matrix σ_{ij} .¹⁴⁹⁻¹⁵¹ The number of degrees of freedom, ν , are calculated by Equation 4.5. To help ensure stability of the solution, results should be replicated with different initial guesses of **G** and **F**, and zero values in the **G** and **F** matrices should be confirmed.¹⁴⁵

$$v = m * n - p(m + n) \quad (4.5)$$

v is the number of degrees of freedom; m is the number of compounds; n is the number of samples; p is the number of sources.

Monte Carlo (MC) simulation has previously been used to validate the PMF model by generating artificial data sets from known source profiles for successful reproduction by PMF.¹³⁰ Model uncertainty was determined in the present study by MC generation of artificial data matrices from each of the original PAH and PCB datasets based on Equation 4.6⁶⁵ and utilizing coefficients of variation (CVs) between 0.1 and 0.3 for compounds and samples (Table 4.3). Five varied datasets were then modeled by PMF and the standard deviation of the source profiles used to represent uncertainty. Only MC solutions correlating with the original solution (Pearson's $r > 0.6$) were retained and used in the standard deviation calculation.

$$D_{ij} = A_{ij} + C_{ij}A_{ij}[\sqrt{2}\text{erf}^{-1}(2R_{ij} - 1)] \quad (4.6)$$

D_{ij} is the generated concentration of compound i and sample j ; A_{ij} is the original data matrix (7 x 1233 for PAHs and the 6 x 1229 for PCBs); C_{ij} is the coefficient of variation (CV) of compound i from sample j (CVs between 0.1 and 0.3 were assigned to each compound based on volatility as shown in Table 4.3, and random CVs between 0.1 and 0.3 were assigned to each sample representing environmental variability); erf^{-1} is the inverse Gaussian error function; R_{ij} is a random number between 0 and 1.

Table 4.3. Coefficients of Variation (CVs) assigned to PAHs and PCBs for Monte Carlo simulation.

PAHs	Nap	Acy	Ace	Flo	Pha	Fla	Pyr
CVs	0.3	0.25	0.25	0.2	0.15	0.1	0.1
PCBs	8	15	18	28	31	118	
CVs	0.3	0.3	0.2	0.2	0.2	0.1	

Source profiles (i.e. chemical compositions of factors, **G**.) were normalized to total source contaminant mass (Σ_7 PAHs or Σ_6 PCBs) and converted to mass percent for ease in presentation and direct comparison to reference profiles. Source contributions (i.e. factor contributions to samples, **F**.) were given in absolute concentrations (ng/m³ or pg/m³) impacting each sample, as well as overall percent of contaminant mass from each source.

Source profile analysis. Inspection of PMF profiles and comparison with known references are essential for understanding potential sources. The cosine phi ($\cos \phi$) coefficient of proportional similarity was used to calculate similarity of PMF and reference source profiles where the cosine of the angle ϕ between the PMF and reference profile vectors equals one if they are identical (i.e. angle $\phi = 0$) and zero if dissimilar (i.e. perpendicular).¹³³

$$\cos \phi = \frac{\sum_{i=1}^m x_i y_i}{\sqrt{\sum_{i=1}^m x_i^2} \sqrt{\sum_{i=1}^m y_i^2}} \quad (4.7)$$

x_i and y_i are model and reference concentrations, respectively, for compound i .

Over 70 PAH and PCB reference source profiles were compiled from the literature, regional emission inventories, and reported samples and considered for accuracy, source-specificity, and

representation of the study area and time. Reference profiles were computed as a mass percent of Σ_7 PAHs or Σ_6 PCBs (note they may not add exactly to 100% due to rounding error). Profiles measured in phases other than air were first adjusted to their volatile fraction using physical properties of compounds from Table 4.1. Sediment, biosolids, and sludge compounds were multiplied by Henry's Law Constant (K_H) and dividing by the octanol water partition coefficient (K_{OW}) to simulate release from wet sorbed solids. Aroclor congeners were multiplied by their liquid vapor pressure (VP) to simulate volatilization from a liquid phase.^{134, 141} Similarity between measured and sediment-adjusted IHC air profiles (Table 4.9) suggests K_H/K_{OW} correction is a suitable method for estimating gaseous profiles from sediment. PAH and PCB reference profiles are plotted in Figures 4.3 and 4.4, tabulated in Tables 4.4 through 4.11, and described in the following sections.

PAH reference profiles. Li et al. (2003)⁶⁴ compiled PAH profiles for coal and traffic combustion sources collected from numerous studies, including coke oven, power plant, gas engine, and diesel engine emissions for use in apportioning PAH sources to sediment of Lake Calumet in south Chicago. Similarly Bzdusek et al. (2004)⁶⁵ compiled a PAH profile for wood burning (Table 4.4). Because these studies were concerned with particulate-associated PAHs they adjusted total (gas plus particulate) PAH profiles to particulate only. Three methods were used to estimate total profiles for the present study: 1) back-correct the reported profiles with reported gas-particulate partitioning for each compound from Li et al. (2003),⁶⁴ 2) back-correct reported profiles with predicted gas-particulate partitioning from Equation 4.1, and 3) consider only gas plus particulate profiles collected by Li et al. (2003).⁶⁴ Predicted particulate partitioning was much less than reported particulate partitioning for lower molecular weight PAHs (Table 4.5), altering traffic profiles in particular (Table 4.4) and casting doubt on the accuracy of Equation

4.1 results. Total profiles were similar to those adjusted by reported partitioning, except for gasoline engine and residential (Table 4.4).

PAH emissions from local sources like IHC sediment⁶⁶ and nearby biosolids drying beds⁶⁷ were considered from reported data (Table 4.6). The IHC sediment profile was derived from nineteen sediment core composites with detectable PAH levels reported in USACE (2010).⁶⁶ Multiple samples were first normalized to a profile, adjusted to volatile fraction, and then averaged. A grab sample from nearby Calumet drying bed analyzed for Gulezian et al. (2012)⁶⁷ was used as the biosolids profile (Table 4.6).

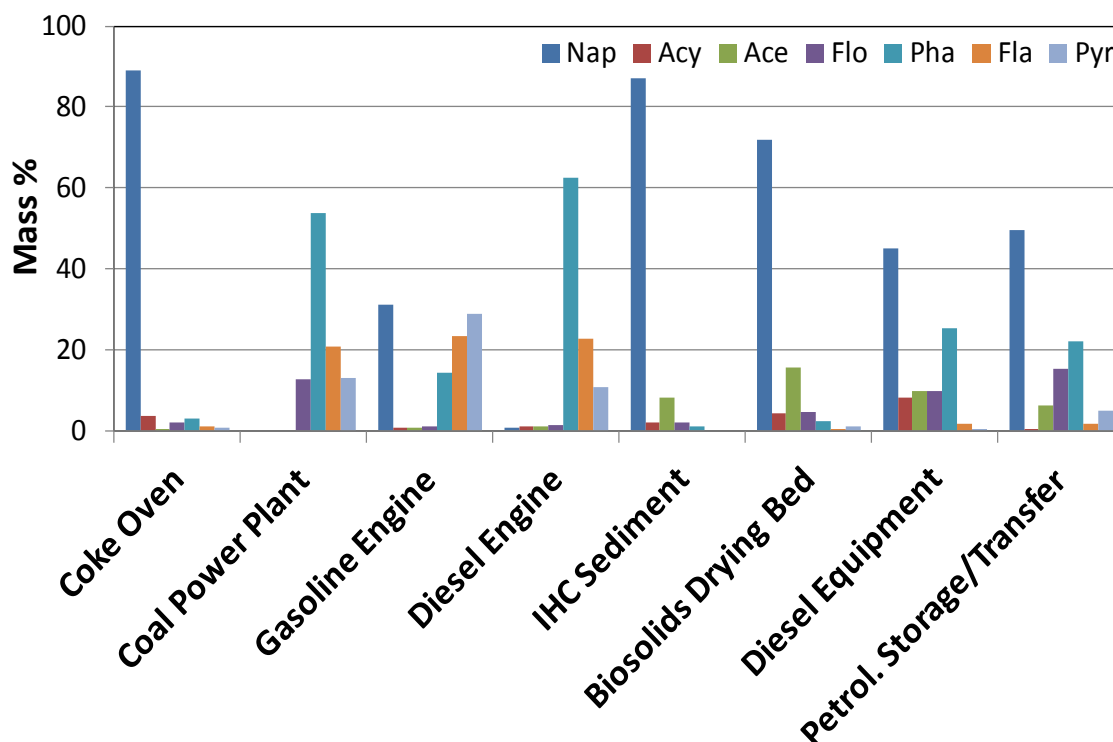
When source-specific emission or profile data were unavailable for the location or time period of interest, emission inventories were used to provide source composition information. The 2008 National Emissions Inventory (National Emissions Inventory (NEI) v. 2 USEPA, Washington, DC, USA) was queried for PAH emissions at the county (Lake County, IN and Cook County, IL) and state (IN, IL) levels (<http://www.epa.gov/ttn/chief/net/2008inventory.html> accessed on 1/18/2013) to develop PAH profiles for numerous sectors related to fuel combustion, industrial processes, and mobile sources (Table 4.7).¹⁹⁷

PCB reference profiles. PCB profiles of Aroclors 1221, 1232, 1016, 1242, 1248, 1254, 1260, and 1262, including multiple production lots, were reported by Frame et al. (1996)⁹³ (Table 4.8). Production lots of Aroclors 1248, 1254, and 1260 with unique congener profiles were shown separately, while other Aroclors were shown as an average of similar lots (Table 4.8).

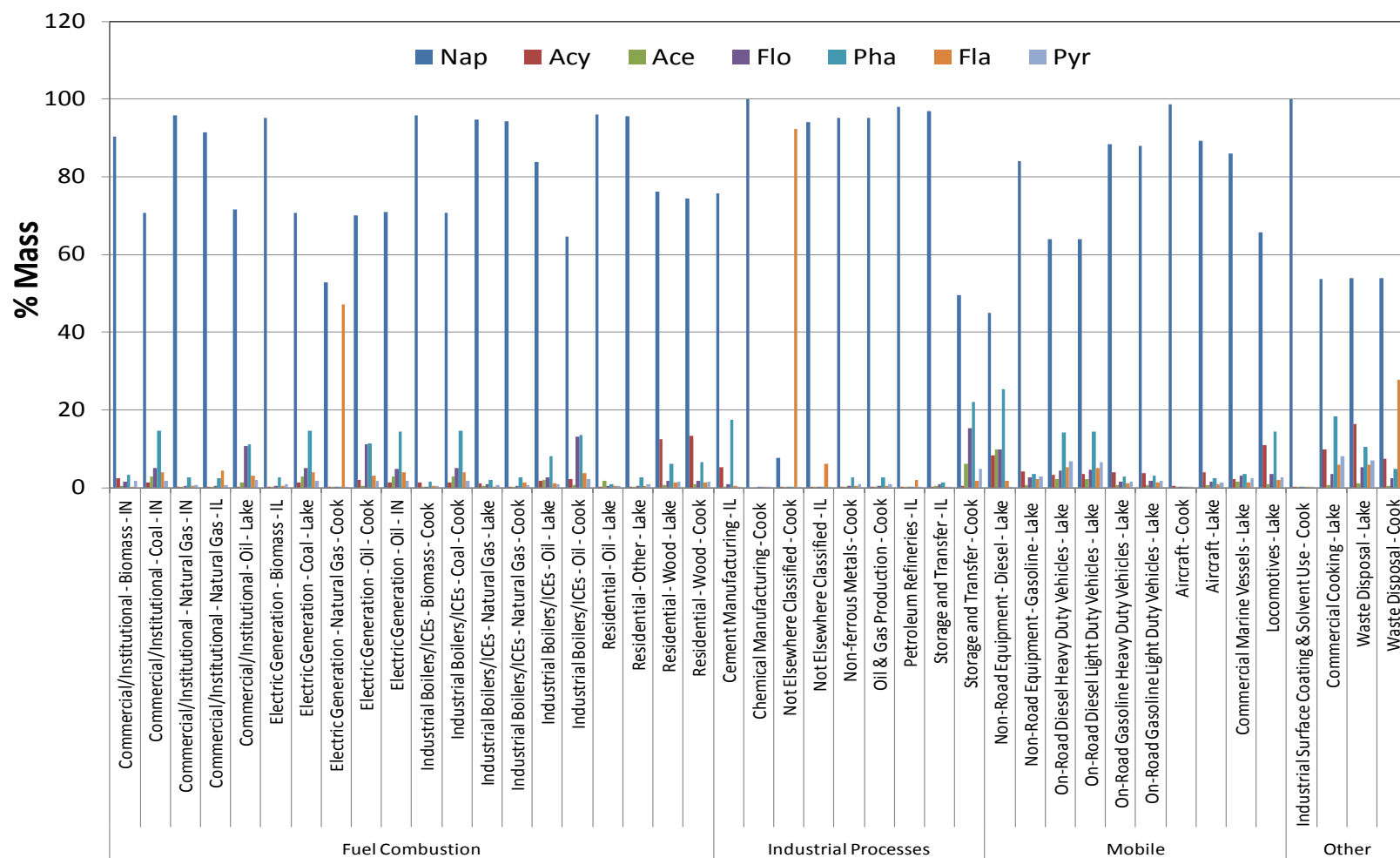
Literature PCB profiles of nearby sites included air above IHC (gas-phase), IHC water (dissolved), and IHC sediment (sorbed) from Martinez et al. (2010)¹⁰⁶ (Table 4.9), the city of Chicago from Hu et al. (2010)¹¹⁰ (Table 4.9), and Chicago landfill, transformer storage yard, and biosolids drying beds from Hsu et al. (2003)¹⁰⁴ (Table 4.10).

Profiles of nearby contaminated Ralston municipal sewage lagoon sludge were obtained from two samples reported by Gary Sanitary District (2007)¹⁰⁷ (Table 4.11). A general municipal waste incinerator profile was determined by samples reported in Ikonomou et al. (2002)⁹⁴ (Table 4.11). All congeners of interest were present in the profiles, but co-elution with more than one congener was common and reduced accuracy (Figure 4.4B, Tables 4.9 through 4.11).

While reference source profiles provide a crucial guide for PMF source identification, it is important to note that not all sources are represented because they have not all been measured, and because existing references may not represent true sources due to uncertainty in the data, sampling and analytical methods, profile computation, partitioning adjustments, temporal and spatial change, and inter- and intra- source variability.

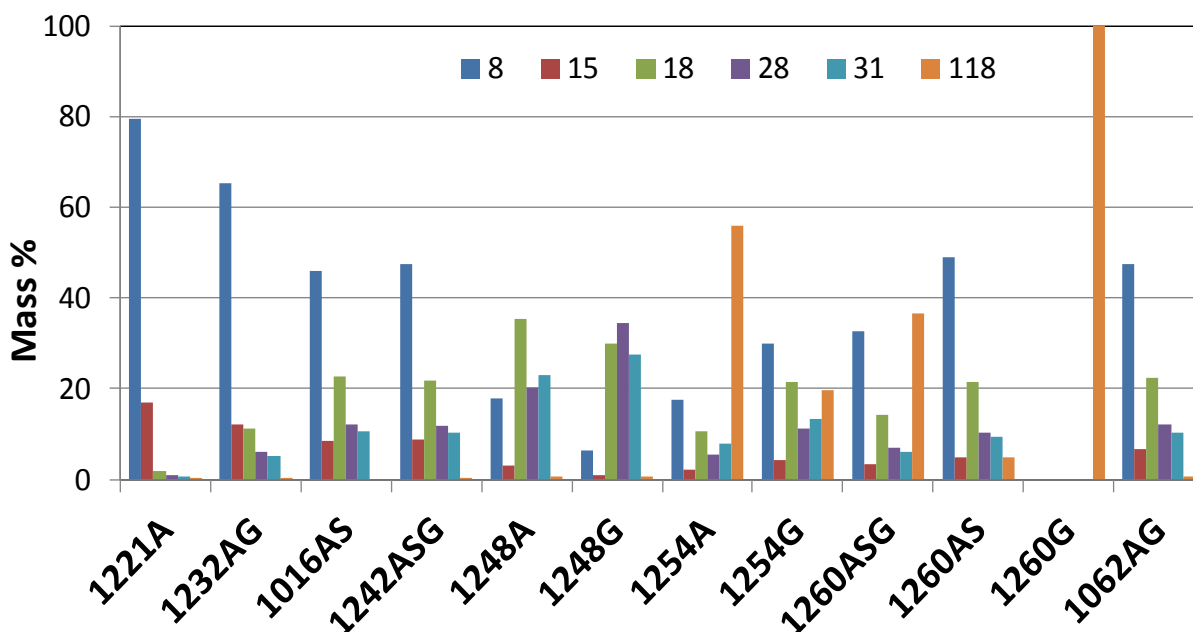


A)

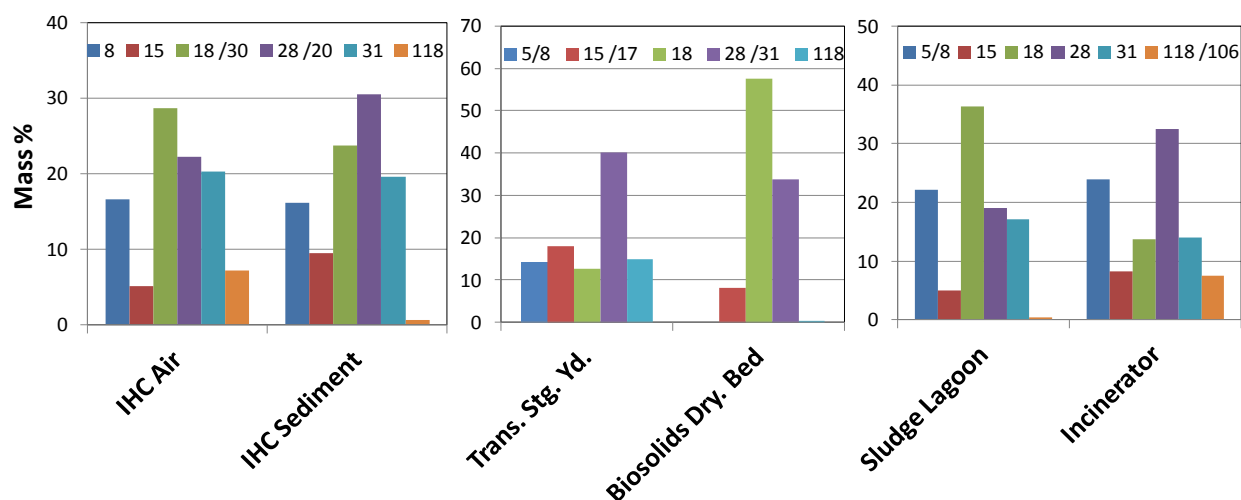


B)

Figure 4.3. Select PAH atmospheric reference source profiles (see also Tables 4.4 through 4.7). (A) Coke oven through diesel engine from Li et al. (2003),⁶⁴ IHC sediment from USACE (2010),⁶⁶ biosolids from Gulezian et al. (2012),⁶⁷ and diesel equipment and petroleum storage and transfer from 2008 National Emissions Inventory (v.2 USEPA). (B) All PAH reference source profiles derived from 2008 National Emissions Inventory (v.2 USEPA).



A)



B)

Figure 4.4. Select PCB atmospheric reference source profiles (see also Tables 4.8 through 4.11). (A) Aroclor mixtures from Frame et al. (1996).⁹³ Letters A, S, and G specify different Aroclor lots from suppliers AccuStandard, Supelco, and GE Corporate R&D (Monsanto Corp.), resp. When more than one letter is specified the profile is an average of lots. (B) IHC air and sediment from Martinez et al. (2010),¹⁰⁶ transformer storage yard and biosolids drying bed from Hsu et al. (2003),¹⁰⁴ Ralston sludge lagoon from Gary Sanitary District (2007),¹⁰⁷ and municipal waste incinerator from Ikononou et al. (2002).⁹⁴

Table 4.4. Mean PAH combustion source profiles (coal, petroleum, and wood) from the literature (%).^a

	Coke Oven	Power Plant	Residential	Gasoline	Diesel	Ave gas and diesel	Tunnel	Wood burning
Particulate profiles adjusted by reported gas-particulate partitioning ^a								
Nap	89	0	0	31	1	5	44	61
Acy	4	0	0	1	1	1	6	7
Ace	0	0	0	1	1	1	6	3
Flo	2	13	2	1	1	1	8	2
Pha	3	54	77	14	63	55	22	11
Fla	1	21	17	23	23	23	7	9
Pyr	1	13	5	29	11	13	6	6
Particulate profiles adjusted by calculated gas-particulate partitioning ^b								
Nap	100	0	0	97	27	73	92	95
Acy	0	0	0	1	7	3	3	2
Ace	0	0	0	1	11	4	3	2
Flo	0	33	4	0	2	1	1	0
Pha	0	60	92	1	49	17	1	0
Fla	0	3	3	0	3	1	0	0
Pyr	0	4	1	1	2	1	0	0
Totals only (gas + particulate phase) ^c								
Nap	89	0	0	57	1	6	51	—
Acy	4	0	0	2	1	1	7	—
Ace	1	0	0	1	1	1	7	—
Flo	2	13	56	3	2	2	9	—
Pha	3	60	0	1	73	66	19	—
Fla	1	15	0	1	15	14	3	—
Pyr	1	12	44	35	8	10	4	—

^a Reported in Li et al. (2003)⁶⁴ and Bzdusek et al. (2004).⁶⁵ See Table 4.5 for reported gas-particulate partitioning.

^b By Equation. 4.1 from Weschler and Nazaroff (2010)¹⁹¹ using TSP from station S. See Table 4.5 for calculated gas-particulate partitioning.

^c From Li et al. (2003)⁶⁴ and A. Li personal communication.

Table 4.5. Percent particulate to total atmospheric PAHs.

	Reported ^a	Calculated ^b
Nap	0.6	0.0003
Acy	1.6	0.0036
Ace	2.3	0.0040
Flo	1.3	0.012
Pha	3.4	0.072
Fla	10	1.5
Pyr	14	1.2

^a From Li et al. (2003).⁶⁴

^b By Equation 4.1 from Weschler and Nazaroff (2010)¹⁹¹ using measured TSP at station S.

Table 4.6. PAH area source profiles with adjustment for fraction in air (%).

	K _H /K _{OW} adjusted ^a			
	IHC Sediment ^b (19)	Biosolids ^c	IHC Sediment ^b (19)	Biosolids ^c
Nap	13 +/- 7	2	87 +/- 14	72
Acy	4 +/- 2	2	2 +/- 1	4
Ace	7 +/- 8	4	8 +/- 12	15
Flo	8 +/- 4	4	2 +/- 2	4
Pha	17 +/- 4	9	1 +/- 0	2
Fla	26 +/- 6	42	0 +/- 0	0
Pyr	25 +/- 5	38	0 +/- 0	1

^a K_H and K_{OW} from Table 4.1.

^b From USACE (2010).⁶⁶ Mean profiles have sample numbers in parentheses with variability given by $\pm \sigma$.

^c From sample analysis for Gulezian et al. (2012).⁶⁷

Table 4.7. PAH profiles derived from the USEPA 2008 National Emissions Inventory v.2 (%).^a

Sector	Fuel Combustion									
	Commercial/Institutional					Electric Generation				
	Biomass IN	Coal IN (IL)	Natural Gas IN	IL	Oil Lake (Cook)	Biomass IL	Coal Lake (all)	Natural Gas Cook (IL)	Oil Cook	IN
Nap	90	71	96	91	72	95	71	53	70	71
Acy	2	1	0	0	0	0	1	0	2	1
Ace	0	3	0	0	1	0	3	0	1	3
Flo	2	5	0	0	11	0	5	0	11	5
Pha	3	15	3	2	11	3	15	0	11	14
Fla	0	4	0	4	3	0	4	47	3	4
Pyr	2	2	1	1	2	1	2	0	2	2

Sector	Fuel Combustion									
	Industrial Boilers, Internal Combustion Engines						Residential			
	Biomass Cook (IN, IL)	Coal Cook (IN, IL)	Natural Gas Lake	Cook	Oil Lake	Cook	Oil Lake (all)	Other Lake (all)	Wood Lake	Cook
Nap	96	71	95	94	84	65	96	96	76	74
Acy	1	1	1	0	2	2	0	0	12	13
Ace	0	3	0	0	2	1	2	0	1	1
Flo	0	5	1	0	3	13	0	0	2	2
Pha	1	15	2	3	8	14	1	3	6	7
Fla	1	4	0	1	1	4	0	0	1	1
Pyr	0	2	1	1	1	2	0	1	2	2

Table 4.7. (continued). PAH profiles derived from the USEPA 2008 National Emissions Inventory v.2 (%).^a

Sector	Industrial Processes								
	Cement Manufacturing IL	Chemical Manufacturing Cook (IL)	Not Elsewhere Classified		Non-ferrous Metals Cook	Oil and Gas Production Cook (IL)	Petroleum Refineries IL	Storage and Transfer	
			Cook	IL				IL	Cook
Nap	76	100	8	94	95	95	98	97	50
Acy	5	0	0	0	0	0	0	0	0
Ace	0	0	0	0	0	0	0	0	6
Flo	1	0	0	0	0	0	0	1	15
Pha	17	0	0	0	3	3	0	1	22
Fla	0	0	92	6	0	0	2	0	2
Pyr	0	0	0	0	1	1	0	0	5
Sector	Solvent				Commercial Cooking		Waste Disposal		
	Industrial Surface Coating & Solvent Use								
	Cook (IL)				Lake (all)		Lake	Cook	
Nap	100				54		54	54	
Acy	0				10		16	7	
Ace	0				1		1	1	
Flo	0				3		5	2	
Pha	0				18		11	5	
Fla	0				6		6	28	
Pyr	0				8		7	3	

Table 4.7. (continued). PAH profiles derived from the USEPA 2008 National Emissions Inventory v.2 (%).^a

Sector	Mobile									
	On-Road				Non-Road Equipment		Aircraft		Locomotives	Commercial Marine Vessels
	Heavy Duty Vehicles		Light Duty Vehicles		Diesel	Gasoline	Cook	Lake	Lake (all)	Lake (all)
	Diesel	Gasoline	Diesel	Gasoline						
	Lake (all)	Lake (all)	Lake (all)	Lake (all)	Lake (all)	Lake (all)				
Nap	64	88	64	88	45	84	99	89	66	86
Acy	3	4	3	4	8	4	1	4	11	2
Ace	2	1	2	1	10	1	0	1	1	1
Flo	4	2	4	2	10	3	0	1	4	3
Pha	14	3	14	3	25	3	0	2	14	3
Fla	5	1	5	1	2	2	0	1	2	1
Pyr	7	2	7	2	0	3	0	1	3	2

^a 2008 NEI (National Emissions Inventory v.2 USEPA, Washington, DC, USA) queried for PAH emissions on 1/18/2013 from <http://www.epa.gov/ttn/chief/net/2008inventory.html>. Queried counties and states in order of relevance (i.e. proximity and specificity): Lake County, IN; Cook County, IL; state of IN; and state of IL. Similar profiles from more than one county or state are noted in parentheses; unique profiles are tabulated and labeled.

Table 4.8. PCB congener source profiles of Aroclors^a with adjustments for fraction in air (%).^b

	1221-A	1232-AG	1016-AS	1242-ASG	1248-A	1248-G	1254-A	1254-G	1260-ASG	1260-AS	1260-G	1062-AG
<i>Unadjusted</i>												
8	66	40 +/- 0	21 +/- 0	22 +/- 2	5	2	0	2	5 +/- 5	8 +/- 0	0	17 +/- 1
15	22	12 +/- 0	6 +/- 0	6 +/- 1	1	0	0	0	1 +/- 2	1 +/- 1	0	4 +/- 0
18	4	18 +/- 0	27 +/- 0	26 +/- 2	26	19	1	3	6 +/- 5	9 +/- 0	0	21 +/- 1
28	3	14 +/- 0	22 +/- 0	21 +/- 1	22	33	0	2	4 +/- 4	7 +/- 0	0	17 +/- 1
31	3	15 +/- 0	24 +/- 0	23 +/- 1	31	32	1	3	5 +/- 4	7 +/- 1	0	17 +/- 1
118	0	1 +/- 0	0 +/- 0	2 +/- 0	14	14	98	89	78 +/- 19	67 +/- 1	100	24 +/- 4
<i>VP</i>												
8	88	7 +/- 0	49 +/- 0	51 +/- 3	19	7	28	36	35 +/- 30	52 +/- 1	0	50 +/- 0
15	8	5 +/- 0	4 +/- 0	4 +/- 0	1	0	1	2	1 +/- 3	2 +/- 2	0	3 +/- 0
18	3	16 +/- 0	32 +/- 0	31 +/- 3	50	47	23	34	20 +/- 18	31 +/- 0	0	32 +/- 0
28	0	2 +/- 0	5 +/- 0	5 +/- 0	8	15	3	5	3 +/- 2	4 +/- 0	0	5 +/- 0
31	1	5 +/- 0	11 +/- 0	10 +/- 1	22	30	12	15	6 +/- 5	9 +/- 1	0	10 +/- 0
118	0	0 +/- 0	0 +/- 0	0 +/- 0	0	0	32	8	35 +/- 57	2 +/- 0	100	0 +/- 0
<i>K_H/K_{OW}</i>												
8	79	65 +/- 0	46 +/- 0	47 +/- 3	18	6	18	30	33 +/- 28	49 +/- 2	0	48 +/- 0
15	17	12 +/- 0	9 +/- 0	9 +/- 1	3	1	2	4	3 +/- 6	5 +/- 5	0	7 +/- 1
18	2	11 +/- 0	23 +/- 0	22 +/- 2	35	30	11	22	14 +/- 12	22 +/- 1	0	23 +/- 0
28	1	6 +/- 0	12 +/- 0	12 +/- 1	20	35	5	11	7 +/- 6	10 +/- 0	0	12 +/- 0
31	1	5 +/- 0	11 +/- 0	10 +/- 1	23	27	8	13	6 +/- 6	9 +/- 1	0	10 +/- 0
118	0	0 +/- 0	0 +/- 0	0 +/- 0	1	1	56	20	37 +/- 55	5 +/- 0	100	1 +/- 0

^a From Frame et al. (1996)⁹³ Letters A, S, and G specify different Aroclor lots from suppliers AccuStandard, Supelco, and GE Corporate R&D (Monsanto Corp.), resp. When more than one letter is specified the profile is the mean of lots, with variability given by $\pm \sigma$ (for three lots) or half the range (for two lots).

^b K_H, K_{OW}, and VP from Table 4.1.

Table 4.9. PCB congener profiles of IHC media^a with adjustments for fraction in air^b and city of Chicago air (%).^c

	IHC air (gas)	IHC water (dissolved)	IHC sediment (solid)	IHC water (K _H adj.)	IHC sediment (K _H /K _{OW} adj.)	Chicago air
8	17	4	5	4	16	24
15	5	5	4	5	9	6
18, 30	29	40	18	45	24	24
28, 20	22	27	33	25	31	22
31	20	21	26	18	20	17
118	7	2	14	3	1	6

^a From Martinez et al. (2010).¹⁰⁶

^b K_H and K_H/K_{OW} from Table 4.1.

^c From Hu et al. (2010).¹¹⁰

Table 4.10. PCB congener atmospheric profiles of Chicago emission areas (%).^a

	Landfill (2)	Trans. Stg. Yd. (4)	Biosolids Dry. Bed (3)
5/8	19 +/- 19	14 +/- 17	0 +/- 0
17/15	26 +/- 12	18 +/- 12	8 +/- 14
18	29 +/- 7	13 +/- 9	58 +/- 1
31/28	25 +/- 1	40 +/- 14	34 +/- 13
118	1 +/- 1	15 +/- 10	0 +/- 1

^a From Hsu et al. (2003).¹⁰⁴ Profiles are the mean of samples (sample numbers in parentheses) with variability given by $\pm \sigma$ (for three or four samples) or half the range (for two samples).

Table 4.11. PCB profiles of Ralston sludge lagoon^a with adjustments for fraction in air and municipal waste incinerator (%).^b

	K _H /K _{OW} adjusted ^c						Incinerator (11) ^d
	NW sludge	SW sludge	Average sludge (2) ^d	NW sludge	SW sludge	Average sludge (2) ^d	
8, 5	11	4	7 +/- 3	29	15	22 +/- 7	24 +/- 12
15	4	1	3 +/- 1	7	3	5 +/- 2	8 +/- 3
18	34	29	31 +/- 3	35	38	36 +/- 2	14 +/- 7
28	21	26	24 +/- 3	15	24	19 +/- 5	33 +/- 20
31	24	28	26 +/- 2	14	20	17 +/- 3	14 +/- 5
118, 106	6	12	9 +/- 3	0	0	0 +/- 1	8 +/- 7

^a From Gary Sanitary District (2007).¹⁰⁷

^b From Ikonomou et al. (2002).⁹⁴

^c K_H/K_{OW} from Table 4.1.

^d Mean profiles include sample numbers in parentheses with variability given by $\pm \sigma$ (for 11 samples) or half the range (for two samples).

Source contribution analysis. Multiple Linear Regression. Temporal and meteorological effects on PAH and PCB source contribution patterns were examined by multiple linear regressions (MLRs) similar to previous analyses.^{177, 190}

$$\ln C = \frac{a_1}{T} + a_2 t + a_3 \cos \theta + a_4 \sin \theta + a_5 WS + \text{const} \quad (4.8)$$

C is the source concentration (ng/m³ for PAHs and pg/m³ for PCBs); a_1 is the Clausius-Clapeyron (C-C) slope (K) related to T (average ambient temperature); a_2 is the first-order rate constant (days⁻¹) related to t (time); a_3 and a_4 are amplitudes of the cosine and sine terms, respectively, related to θ (wind direction); and a_5 (s/m) describes the dependence of concentration on WS (wind speed).

The ability of the regression to explain source concentration variability was described by an overall coefficient of determination (R^2) and the portion of total variability from each term was estimated by forward stepwise regression as described in Granberg (2013).¹⁹⁰

Temperature correction. PAH and PCB contributions were analyzed by removing the temperature dependency of each source post-modeling (similar to removing the temperature dependency of PAH data pre-modeling). Clausius-Clapeyron (C-C) slopes were determined from a regression of the C-C equation¹⁶⁶ (Eq. 4.9) and source contribution concentrations were corrected to 288 K (15 °C) by Equation 4.10.

$$\ln C = \frac{a_1}{T} + \text{const} \quad (4.9)$$

$$C_{288} = C \exp \left[a_1 \left(\frac{1}{288} - \frac{1}{T} \right) \right] \quad (4.10)$$

C is the source concentration (ng/m^3 for PAHs and pg/m^3 for PCBs); a_l is the Clausius-Clapeyron (C-C) slope (K); T is the average ambient temperature, and C_{288} is the source concentration corrected to a reference temperature of 288 K.

Notched box plot comparisons. PAH and PCB source contributions were grouped according to corresponding season, day of week, wind direction quadrant (for days with wind dispersion less than 60%), sampling station, and CDF construction activity as described in Granberg (2013).¹⁹⁰ Sources were summarized by group in notched box plots and analyzed for significant differences by comparing median concentrations with upper and lower 95% confidence intervals.

Yearly moving average. To investigate long-term temporal source contribution trends without seasonality or assuming exponential decay, yearly concentration averages were calculated for each source by averaging all data points from the following 365-day period. Source contribution concentrations were plotted versus time similar to Rodenburg et al. (2013).¹⁴¹

Toxics Release Inventory. Toxics Release Inventory (TRI) Release Reports (Toxics Release Inventory, 2011 National Analysis dataset updated March 2013, USEPA, Washington, DC, USA) were generated for on-site PAH and Nap releases (accessed 4/16/2013 from http://iaspub.epa.gov/triexplorer/tri_release.chemical) from the major industrial sectors in Lake County, IN and Cook County, IL including chemicals, stone/clay/glass, petroleum, petroleum bulk terminals, fabricated metals, and primary metals, for years 2002 through 2011. TRI data were plotted and compared to source contribution and yearly moving average concentrations. No analogous PCB data were available.

Dispersion modeling confirmation. A conservative screening-level air dispersion model SCREEN3 (Screen View Screening Air Dispersion Model, v. 3.5.0, Lakes Environmental

Software, Waterloo, Ontario, CA) was used to predict maximum 1-hr concentrations at the CDF downwind from potential PCB emission sources: IHC, Ralston sludge lagoon, Calumet biosolids drying beds, and a transformer storage yard. Locations of these PCB sources relative to the CDF are identified in the map in Appendix A (Figure A1). In addition to basic mechanistic model assumptions (Gaussian plume, no atmospheric transformations or removal of pollutants) a number of conservatively chosen and built-in meteorological assumptions underlie the model runs. Major source-related inputs to the model were source type (areas in this case), emission rate, area dimensions, and release height (Table 4.12). Calculated concentrations were 1-hr concentration maximums (i.e. worst case impacts) estimated at a chosen distance or array of distances from the source based on proximity to the CDF. Estimates were compared to confirm those sources having the largest potential impact at the CDF.

Table 4.12. SCREEN3 inputs^a for estimating impacts from various area PCB sources.

	Emission Rate (g/s/m ²)	Long Side (m)	Short Side (m)	Release Ht. (m)
IHC canal (near)	7.87E-11 ^b	1500	150	0
IHC harbor entrance	7.87E-11 ^b	1500	750	0
Sludge lagoon	7.87E-10 ^c	500	155	0
Biosolids drying beds	1.62E-10 ^d	422 ^d	311 ^d	1
Transformer storage yard	6.20E-10 ^d	150 ^d	91 ^d	1

^a Other inputs: receptor height: 2m, class: urban, wind direction: full range, terrain: simple flat, meteorology: full range, automated distance array: 1-50000 m, Brode 2 mixing height: no, anemometer height: 10 m.

^b From Martinez et al. (2010).¹⁰⁶

^c Assumed value ten times greater than IHC, similar to concentrations.

^d From Hsu et al. (2003).¹⁰⁴

4.4. Results and Discussion

PMF model performance. Four-source solutions yield the best fit between modeled and measured data for both PAHs and PCBs (Table 4.13). In both cases, the objective function Q approximates degrees of freedom ν near an expected relative error of 0.25. In addition, Exner functions are < 0.1 and Coefficients of Determination (CODs) are > 0.9 for most compounds (Table 4.13). The stability of the four-source PAH and PCB solutions are confirmed by obtaining the same Q values and final solutions from five independent model runs with different initial guesses of \mathbf{G} and \mathbf{F} . Because the \mathbf{G} and \mathbf{F} matrices have numerous zero values, rotational ambiguity is minimized.¹⁵⁰ Finally, Monte Carlo simulation shows mild to moderate effects on PMF solution variability, as indicated by the magnitude of the standard deviations of modeled PAH and PCB source profiles (Figure 4.5 and Figure 4.6, respectively).

Table 4.13. PMF model diagnostics for PAH and PCB four-source solutions.

	PAHs	PCBs
Objective function Q^a	5529.42	2260.62
Relative Error (RE) ^b	0.307	0.241
Degrees of Freedom (ν)	3671	2434
Exner Function	0.0016	0.0047
Coefficients of Determination (CODs)		
	1.00 (Nap)	1.00 (CB8)
	1.00 (Acy)	0.96 (CB15)
	0.98 (Ace)	1.00 (CB18)
	0.97 (Flo)	0.97 (CB28)
	0.96 (Pha)	0.99 (CB31)
	0.88 (Fla)	1.00 (CB118)
	0.89 (Pyr)	

^aBased on 0.25 RE of measurements.

^bRecalculated setting $Q = \nu$.

PMF source profiles and contributions. PAHs. Source 1 (S1) is the main source of PAHs to the air-shed, dominated by Nap and contributing over half the total contaminant mass (Figure 4.5). Source 2 (S2) and source 3 (S3) contribute about 20% each to the PAH load and are a mix of compounds. S2 comprises lower molecular weight PAHs and S3 consists primarily of Pha and four-ring PAHs. Source 4 (S4) contributes only 6% of PAH mass, and is mainly composed of Nap and Acy. Standard deviation error bars from Monte Carlo (MC) analysis show the solution is slightly variable with the bulk of uncertainty from S4 (Figure 4.5). PAH source contributions clearly vary over time (Figure 4.6). S1 impacts the air-shed heavily in 2003 and 2007, while S2 and S3 follow an oscillatory pattern that contribute more heavily in the summer than in the winter, indicating strong seasonal or temperature dependence.

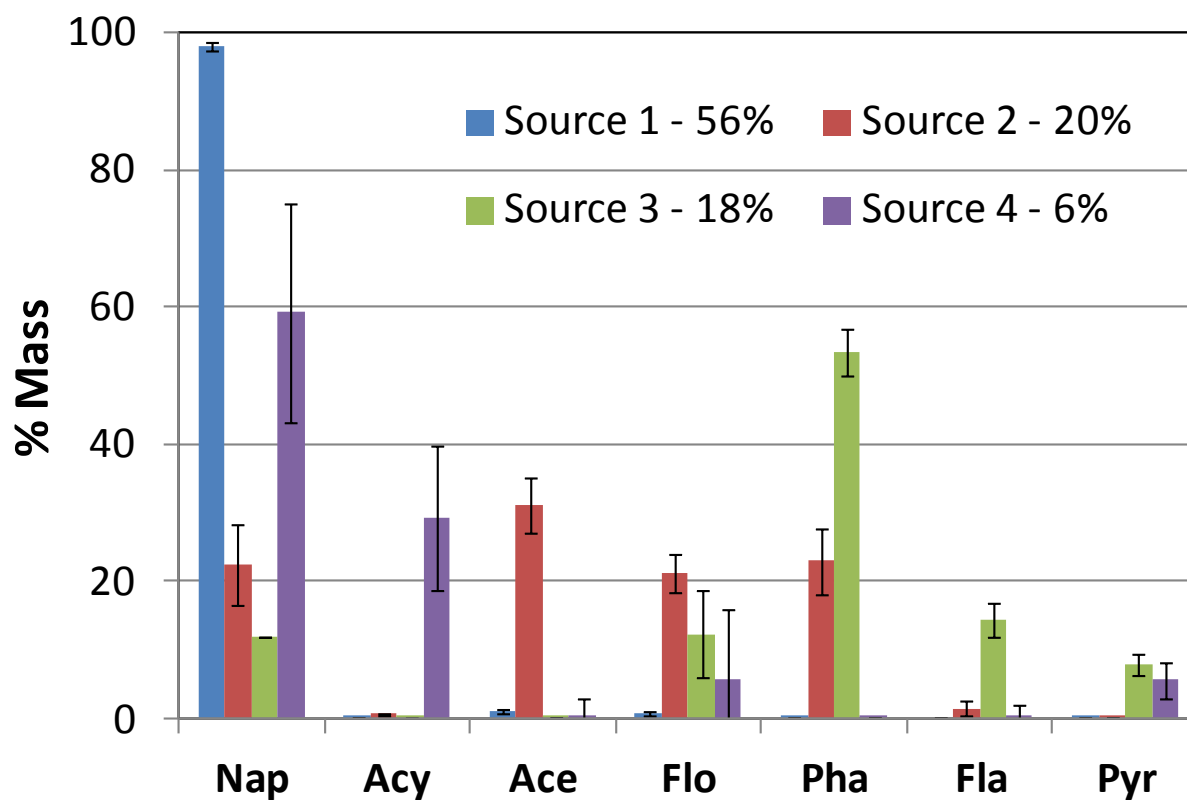


Figure 4.5. PAH source profiles from PMF. Error bars are standard deviations of modeled profiles from MC generated datasets, assigned to original sources by highest correlation.

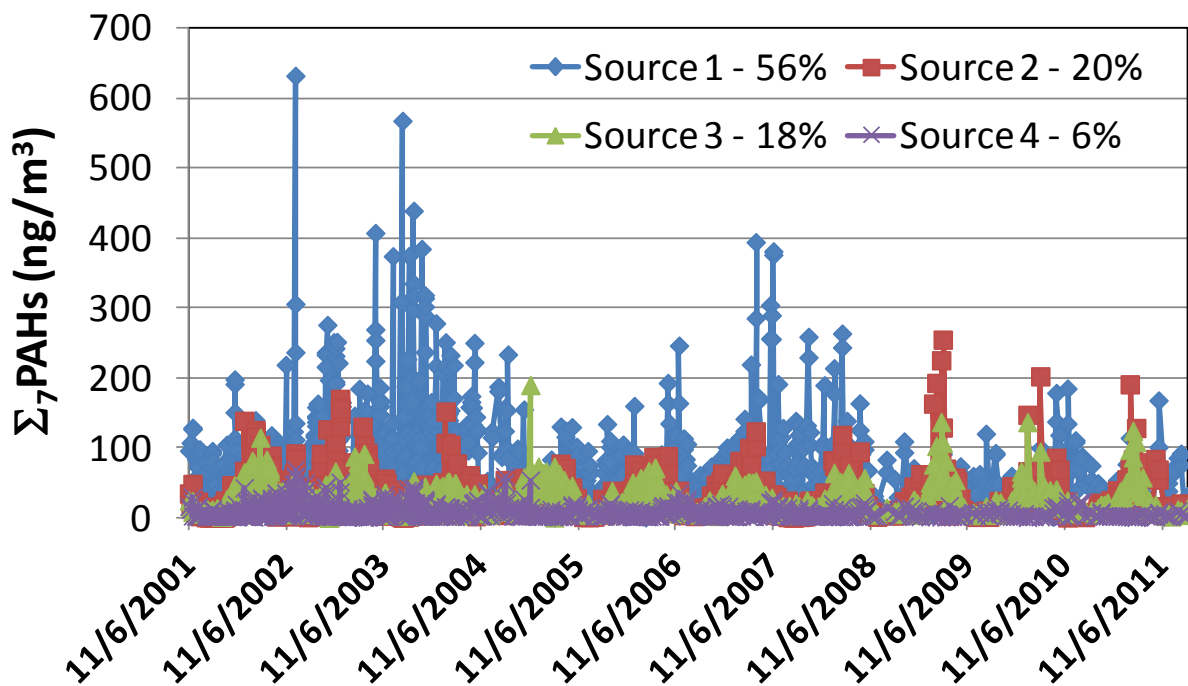


Figure 4.6. PAH source contributions from PMF.

PCBs. The three major PCB sources (S1, S2, and S3) contribute relatively evenly to the atmospheric PCB load at the CDF (Figure 4.7). These sources are composed primarily of congeners 8 (S1), 28 and 31 (S2), and 18 (S3). The minor source (S4) consists of congener 118 plus 28 and 15. Greater uncertainty is apparent for the PCB solution, especially for sources S3 and S4 (Figure 4.7). In addition, two poorly correlated Monte Carlo (MC) solutions were discarded to obtain the five included in the standard deviation. All PCB source contributions vary clearly with season, consistent with temperature-dependent volatile releases (Figure 4.8).

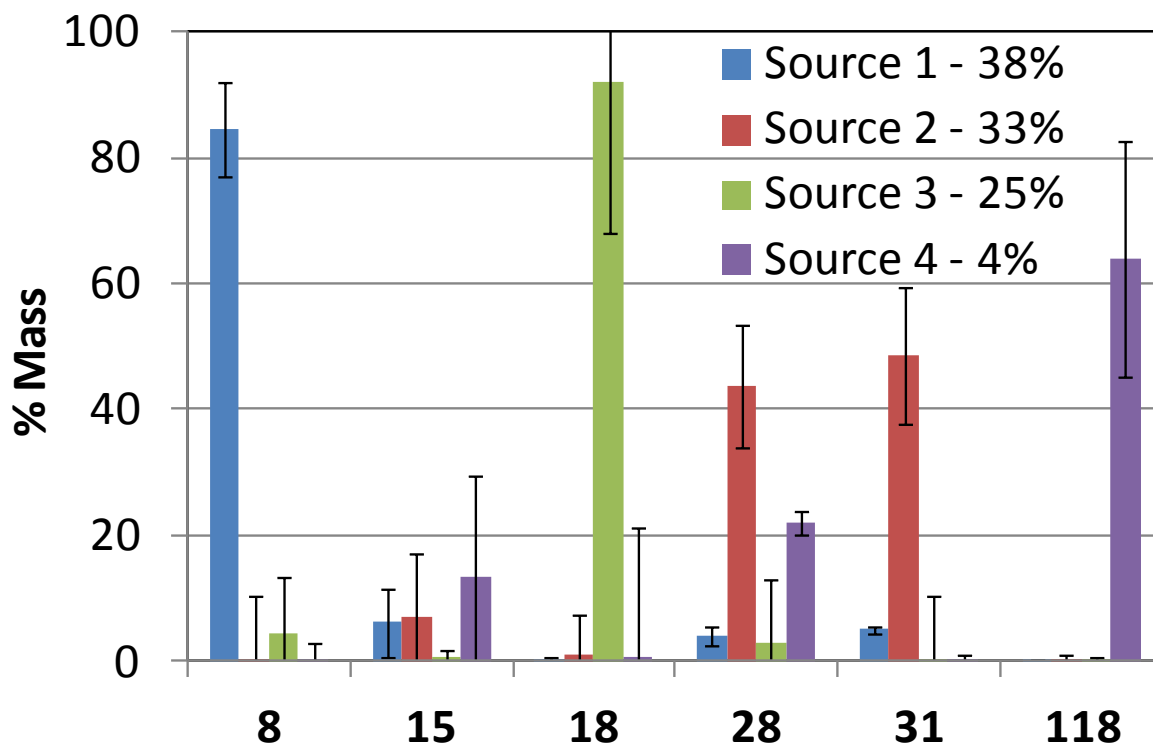


Figure 4.7. PCB source profiles from PMF. Error bars are standard deviations of modeled profiles from Monte Carlo generated datasets, assigned to original sources by highest correlation.

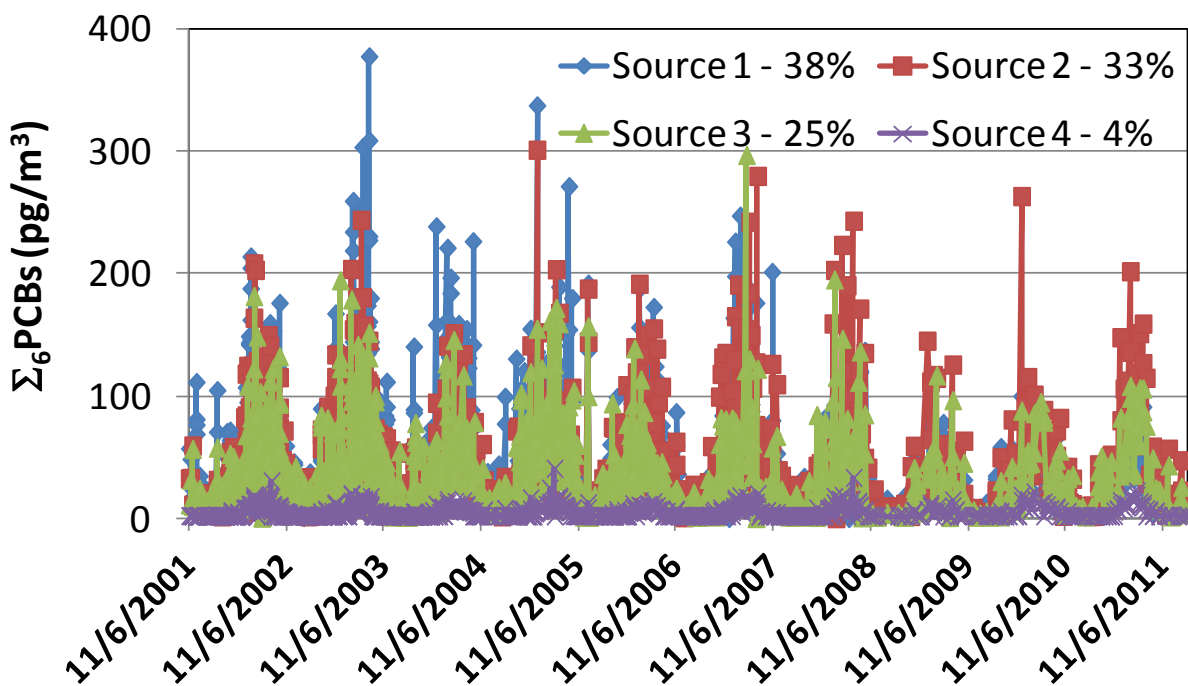


Figure 4.8. PCB source contributions from PMF.

EPA receptor model analysis. The EPA receptor model results from UNMIX and EPA PMF (E-PMF) refer to factors (F1 - F4) rather than sources to avoid confusion with the original PMF solution sets (see Figures 4.9 through 4.10), and are arranged by correlation with the original for comparison. UNMIX uses a geometric method to determine factors¹⁹⁸ and also generates a four factor solution for both PAHs and PCBs (Figures 4.9A and 4.10A), consistent with PMF results. E-PMF produces similar solutions to the original PMF as expected based on similar methodology¹⁴⁶ (Figures 4.9B and 4.10B). However these highly correlated E-PMF profiles (Pearson's r of 0.96 for PAHs and 0.86 for PCBs with the original profiles) are among a variety of other solutions not shown, particularly for PCBs, indicating rotational indeterminacy. EPA receptor model uncertainty analyses are based on block bootstrapping techniques to generate datasets, not unlike a Monte Carlo procedure. Solution variability is expressed as standard deviation of species concentration (not percent mass) in Table 4.14. For each PAH bootstrap run in E-PMF, all bootstrapped factors mapped to unique PMF base factors (random bootstrap seed, minimum Pearson's r of 0.6) indicating the chosen result is stable. In contrast, 18 of the 50 PCB bootstrap runs mapped twice to factor 3 and not to factor 4, indicating increased variability in the PCB solution and consistent with Monte Carlo uncertainty of original PCB solution. PCB factor 4 varies most among all models in terms of source composition as well as overall contribution (Figure 4.7 and 4.10).

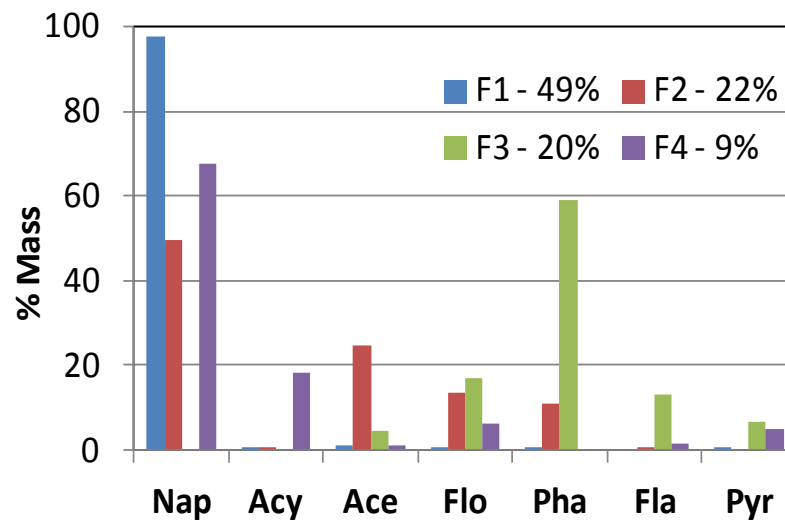
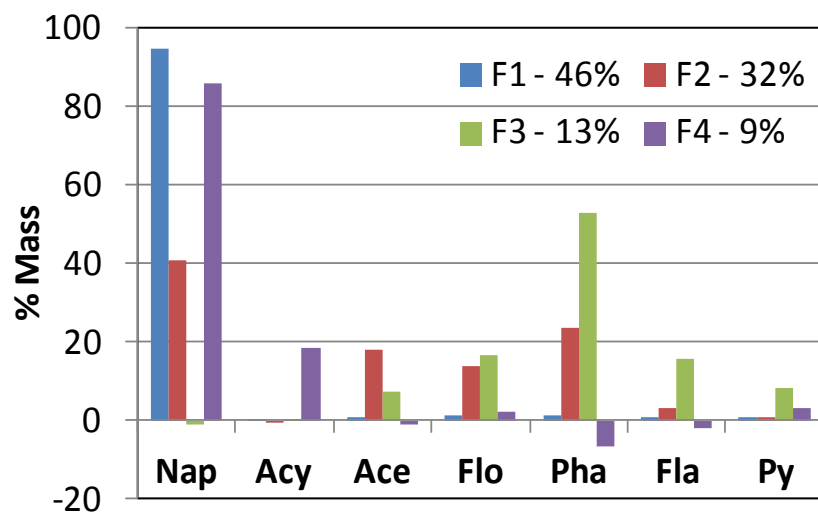


Figure 4.9. PAH source profiles from EPA receptor models (A) UNMIX and (B) E-PMF (Q(robust)=2633, Q(true)=3316).

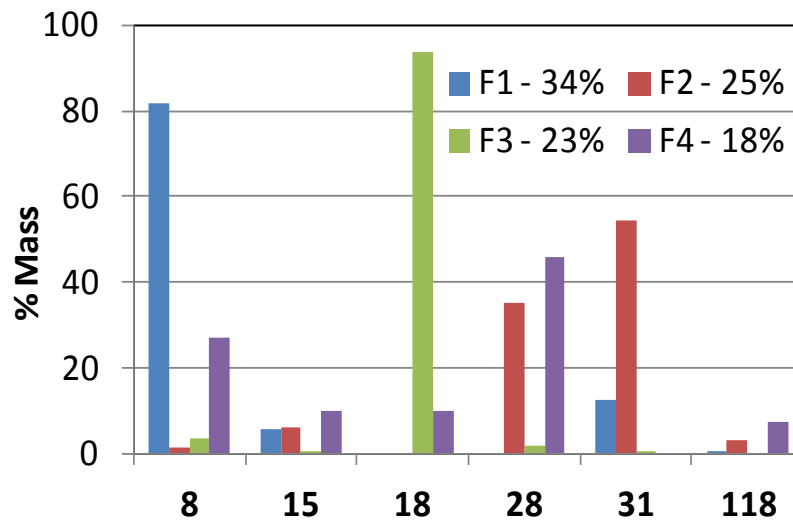
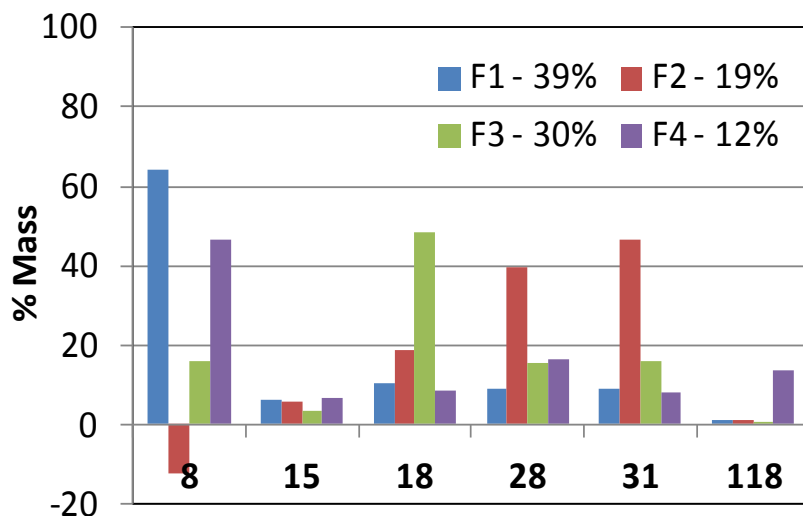


Figure 4.10. PCB source profiles from EPA receptor models (A) UNMIX and (B) E-PMF (Q(robust)=851, Q(true)=880).

Table 4.14. Standard deviation of PAH and PCB concentrations for each factor from bootstrap runs.

PAHs (ng/m ³)			PCBs (pg/m ³)		
	UNMIX ^a	E-PMF ^b		UNMIX ^a	E-PMF ^b
Factor 1			Factor 1		
Nap	5	1	8	8	3
Acy	0	0	15	1	0
Ace	0	1	18	2	1
Flo	0	0	28	1	2
Pha	1	0	31	1	2
Fla	0	0	118	0	0
Pyr	0	0			
Factor 2			Factor 2		
Nap	3	6	8	3	1
Acy	0	0	15	0	0
Ace	1	3	18	2	1
Flo	1	2	28	1	3
Pha	1	2	31	1	3
Fla	0	0	118	0	0
Pyr	0	0			
Factor 3			Factor 3		
Nap	2	3	8	3	3
Acy	0	0	15	0	1
Ace	0	1	18	1	4
Flo	1	0	28	1	4
Pha	1	2	31	1	3
Fla	0	1	118	0	1
Pyr	0	0			
Factor 4			Factor 4		
Nap	4	4	8	2	2
Acy	0	2	15	0	1
Ace	0	0	18	1	5
Flo	0	1	28	1	4
Pha	1	0	31	1	1
Fla	0	0	118	0	1
Pyr	0	1			

^a 100 bootstrap runs

^b 50 bootstrap runs (median Q(robust)=2707 for PAHs, median Q(robust)=975 for PCBs).

PMF modeling by station. Because sampling stations are within 1.5 km of each other, PMF profiles at each station are expected to be similar at least for those operating over the same time period (N, E and W from 2001-2004; S and H from 2001-2012). This is generally, but not always, the case. PAH apportionment among stations varies primarily by Nap loading, though overall the station solutions resemble the original solution (Figure 4.11A through 4.11E). In terms of profiles, stations E and S appear similar (Figures 4.11B and 4.11D), stations N and H appear similar (Figures 4.11A and 4.11E), and station W appears significantly different (Figure 4.11C). In terms of overall contributions, Source S1 is higher at station N than the others, S3 increases from northeast to southwest, and S4 increases from west to east. PCB source profiles have the same dominant congeners at all stations, but show additional congener mixing at stations N, E, and W versus stations S and H (Figures 4.12A through 4.12E). Overall source contributions differ noticeably, with S3 prevailing at stations N and E (Figures 4.12A and 4.12B), S2 leading at stations W and S (Figures 4.12C and 4.12D), and S1 only dominant at station H (Figure 4.12E). Though the original PMF yielded a stable PCB solution, variability within and among stations is consistent with higher standard deviations and poor assignment of S3 and S4 from the original uncertainty analyses (see Figure 4.7 and Table 4.14).

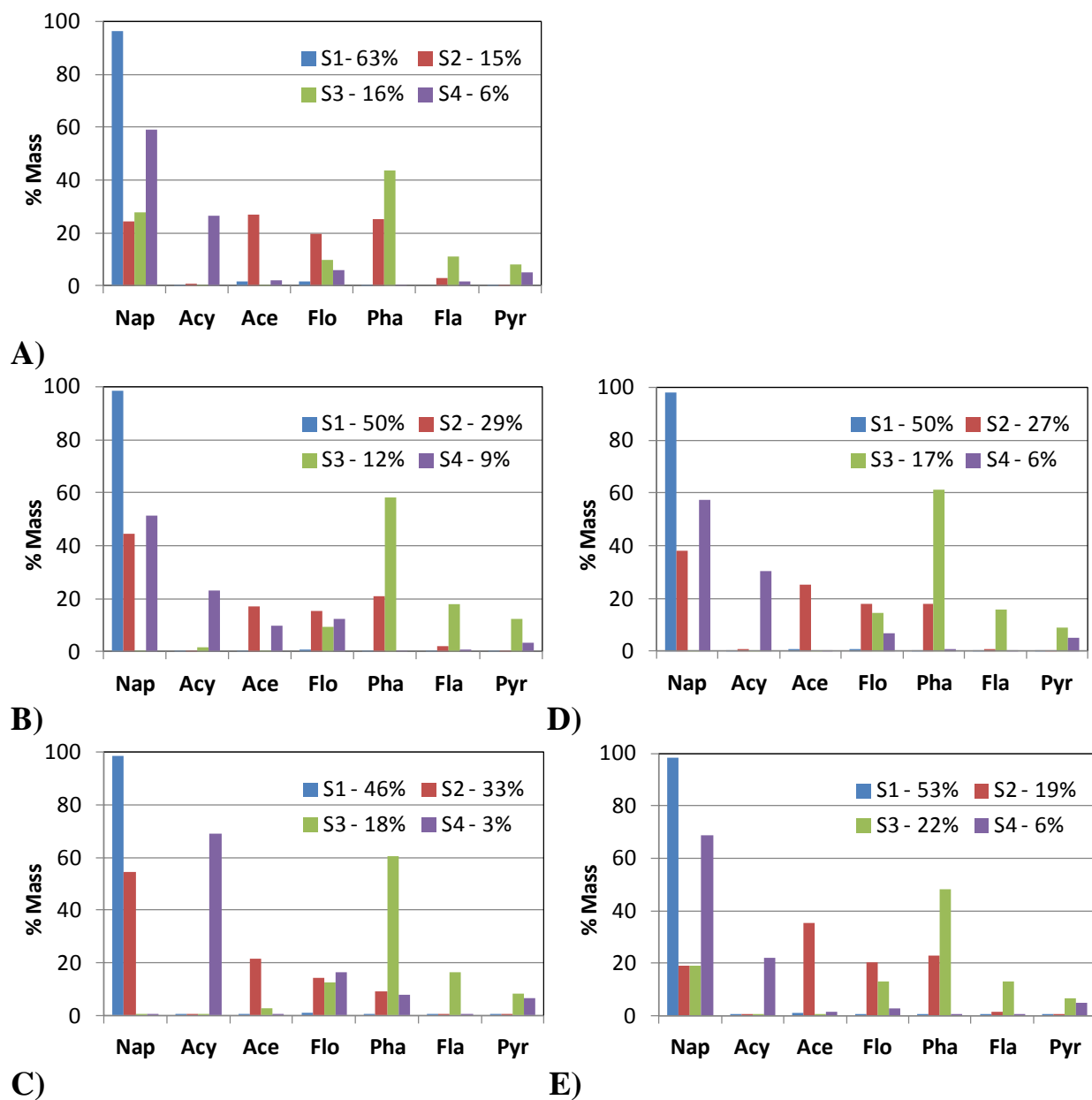


Figure 4.11. PAH source profiles from PMF at (A) North station (B) East station (C) West station (D) South station (E) High school station.

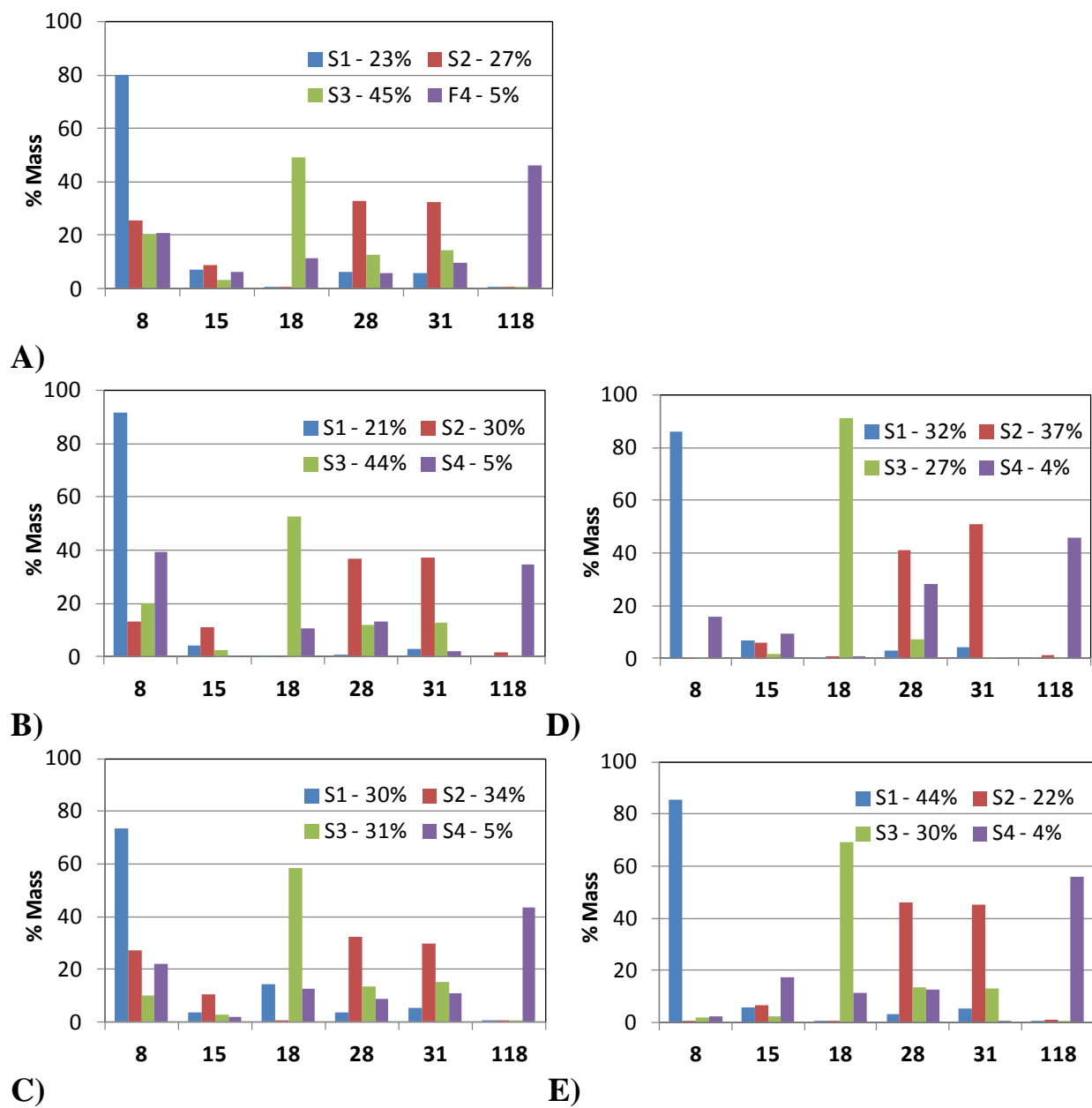
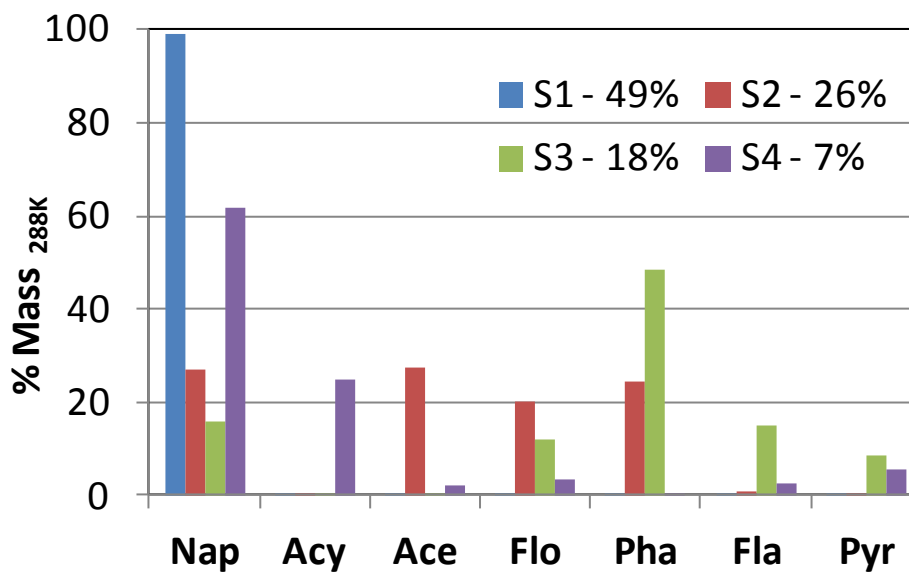
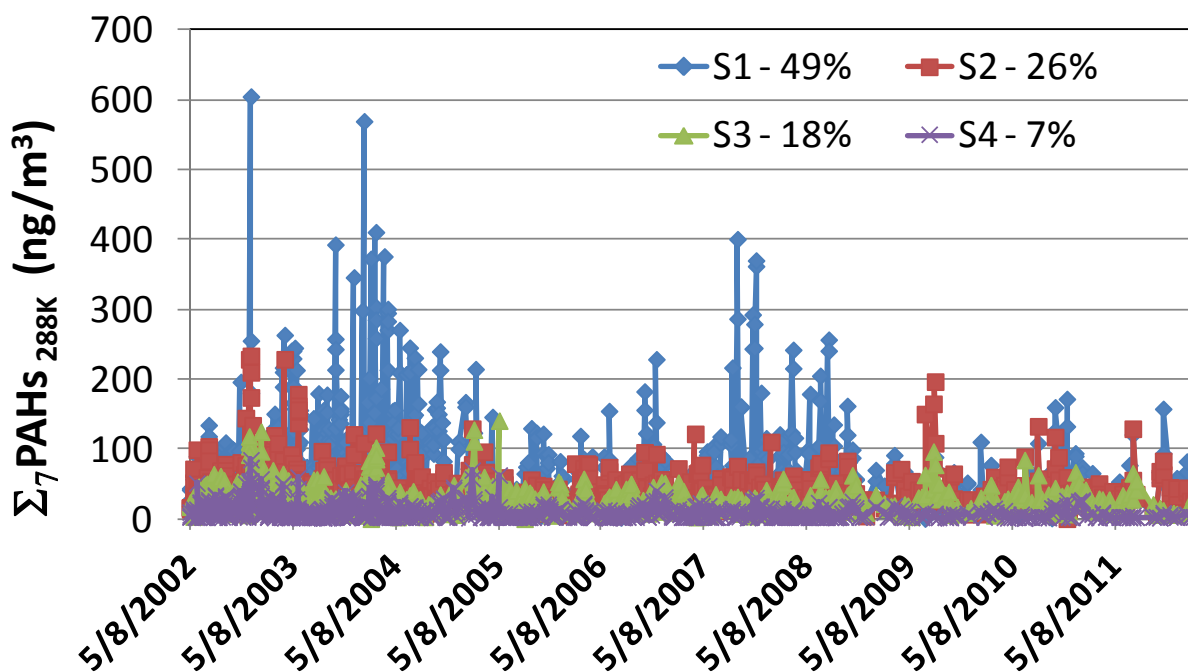


Figure 4.12. PCB source profiles from PMF at (A) North station (B) East station (C) West station (D) South station (E) High school station.

PMF of temperature-corrected (t-c) data. The majority of PAH and PCB sources appeared to be temperature-dependent (see Figures 4.6 and 4.8) as expected given the temperature-dependent levels of most PAHs and PCBs in the air-shed.¹⁹⁰ Temperature effects can be controlled at one of two stages for source apportionment: pre-modeling with original data or post-modeling with source contributions. The present study is one of the first to utilize temperature correction pre-modeling for PMF. PAH data were corrected to 288 K or 15 °C (as described previously)¹⁹⁰ and 303 K or 30 °C, then modeled by PMF (Figures 4.13 and 4.14). Solutions for 15 and 30 °C temperature-corrected (t-c) data were very similar, showing the exact reference temperature chosen may not be critical for source apportionment. T-c profile similarity was particularly interesting considering compounds' differential temperature dependencies (Figures 4.13A and 4.14A). Clear differences are observed between original and t-c solutions in terms of source contributions however (see Figure 4.6, Figures 4.13B and 4.14B). Annual S2 and S3 sinusoidal patterns are eliminated from t-c contributions and overall contributions from S2 increase and S1 decrease. S1 and S4 contribution patterns remain the same however, which is expected because S1 and S4 are composed mainly of Nap and Acy, both compounds that were not temperature-dependent. Post-modeling t-c (including PCBs) and comparison with pre-modeling t-c results are examined in the contribution analysis section below.

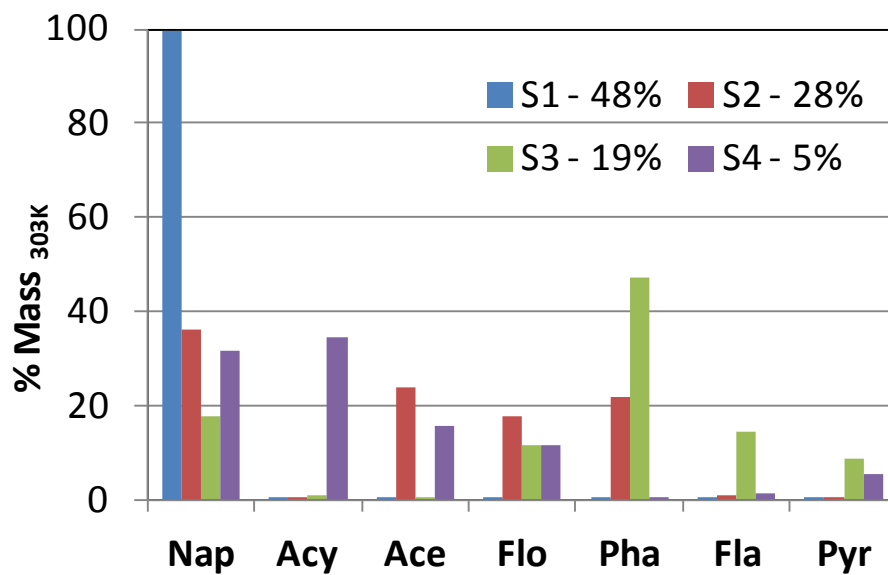


A)

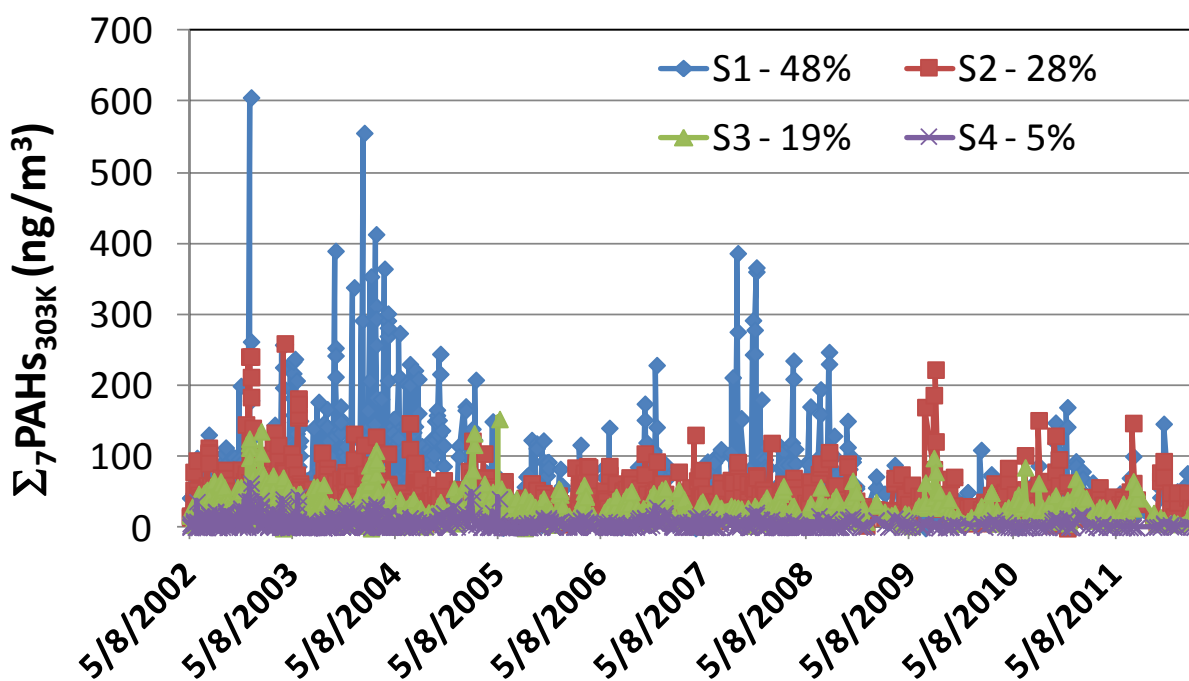


B)

Figure 4.13. PMF four-source solution of PAHs corrected to 288 K (15 °C) pre-modeling. (A) PAH source profiles and (B) PAH source contributions.



A)



B)

Figure 4.14. PMF four-source solution of PAHs corrected to 303 K (30 °C) pre-modeling. (A) PAH source profiles and (B) PAH source contributions.

Reference profile analysis. PAHs. Cos ϕ values between modeled sources (S1-S4) and select reference profiles are given in Table 4.15 (similarities over 0.7 are bolded). PAH source profiles S1 and S4 are similar to numerous industrial, traffic, and contaminated site profiles dominated by Nap, and resemble nearly all emission inventory sources (except for two) with $\cos \phi > 0.80$ (Table 4.16), coke oven and wood burning with $\cos \phi > 0.91$ (Table 4.17), and adjusted IHC and biosolids with $\cos \phi > 0.90$ (Table 4.18). PAH profile S2 is similar to two emission inventory profiles, petroleum storage and transfer (Cook County) and diesel equipment (Lake County) ($\cos \phi$ of 0.76 and 0.79, respectively) while S3 is most similar to diesel, gas-diesel mix, and power plant sources ($\cos \phi > 0.96$) (Tables 4.15 through 4.17).

Comparison with other PAH studies. PAHs in sediments of nearby Lake Calumet were apportioned a decade ago by Li et al. (2003)⁶⁴ and by Bzdusek et al. (2004)⁶⁵ utilizing chemical mass balance and factor analysis based receptor models, respectively. Both studies identified traffic and coke oven as sources of PAHs to sediment, with Bzdusek et al. (2004)⁶⁵ further identifying coke oven profile degradation and a minor wood burning source. In a source apportionment study of atmospheric PAHs in Chicago in the late 1990s by Simcik et al. (1999),⁷⁷ a modified factor analysis model was used to identify coal and gas power plant combustion as the primary PAH contributors, and coke oven and traffic as lesser PAH contributors. The current study differs from the others by a much longer and more recent sampling period including many more samples, and took place over a localized spatial scale with much higher temporal resolution as an atmospheric study rather than sediment core study. Despite these differences, it is clear that many of the same sources impact the region including coke, petroleum, electrical generation, vehicular traffic, and in this case nearby contaminated sites.

Table 4.15. Cosine ϕ similarity between select reference and modeled PAH and PCB sources.^a

PAHs	Coke Oven^b	Diesel Engine^b	Diesel Equipment	Ave. Gasoline and Diesel^b	IHC Sediment^c	Biosolids Dry. Bed^c	Petrol. Storage/Transfer
S1 - 56%	1.00	0.01	0.83	0.09	1.00	0.98	0.87
S2 - 20%	0.48	0.48	0.79	0.52	0.52	0.62	0.76
S3 - 18%	0.24	0.96	0.64	0.97	0.22	0.24	0.61
S4 - 6%	0.91	0.03	0.82	0.11	0.90	0.90	0.81
PCBs	Aroclor 1016^c	Aroclor 1242^c	Aroclor 1248a^c	Aroclor 1248b^c	Aroclor 1254a^c	Aroclor 1254b^c	Aroclor 1260^c
S1 - 38%	0.87	0.89	0.40	0.18	0.31	0.69	0.64
S2 - 33%	0.32	0.30	0.62	0.81	0.17	0.40	0.19
S3 - 25%	0.46	0.44	0.74	0.58	0.19	0.52	0.31
S4 - 4%	0.11	0.11	0.16	0.23	0.90	0.51	0.71
PCBs	IHC Air	IHC Water^c	IHC Sediment^c	Ave. Sludge Lagoon^c	Incinerator	Trans. Stg. Yd.	Biosolids Dry. Bed
S1 - 38%	0.42	0.12	0.41	0.49	0.58	0.40	0.06
S2 - 33%	0.67	0.56	0.76	0.53	0.71	0.83	0.52
S3 - 25%	0.66	0.84	0.54	0.76	0.34	0.29	0.87
S4 - 4%	0.33	0.22	0.26	0.16	0.41	0.60	0.20

^a See also Tables 4.16 through 4.22. Cos ϕ values over 0.7 are bolded.

^b Corrected to total profile by reported gas-particulate partitioning (see Table 4.5).⁶⁴

^c Adjusted to volatile fraction by K_H/K_{OW} (K_H for IHC Water).

Table 4.16. Cosine ϕ similarity of PAH modeled and USEPA 2008 National Emissions Inventory profiles.^a

Sector	Fuel Combustion									
	Commercial/Institutional					Electric Generation				
	Biomass	Coal	Natural Gas		Oil Lake	Biomass	Coal	Natural Gas	Oil	
	IN	IN (IL)	IN	IL	(Cook)	IL	Lake (all)	Cook (IL)	Cook	IN
S1 - 56%	1.00	0.98	1.00	1.00	0.98	1.00	0.98	0.75	0.97	0.98
S2 - 20%	0.48	0.59	0.47	0.47	0.59	0.47	0.59	0.36	0.59	0.59
S3 - 18%	0.24	0.41	0.23	0.24	0.38	0.23	0.41	0.32	0.39	0.41
S4 - 6%	0.90	0.88	0.89	0.89	0.88	0.89	0.88	0.67	0.89	0.88

Sector	Fuel Combustion									
	Industrial Boilers, Internal Combustion Engines							Residential		
	Biomass	Coal	Natural Gas		Oil		Oil	Other	Wood	
	Cook (IN, IL)	Cook (IN, IL)	Lake	Cook	Lake	Cook	Lake (all)	Lake (all)	Lake	Cook
S1 - 56%	1.00	0.98	1.00	1.00	0.99	0.96	1.00	1.00	0.98	0.98
S2 - 20%	0.46	0.59	0.47	0.47	0.52	0.62	0.47	0.47	0.50	0.50
S3 - 18%	0.22	0.41	0.23	0.23	0.30	0.44	0.21	0.23	0.28	0.29
S4 - 6%	0.90	0.88	0.90	0.89	0.90	0.89	0.89	0.89	0.95	0.95

Sector	Industrial Processes									
	Cement Manufacturing	Chemical Manufacturing	Not Elsewhere Classified		Non-ferrous Metals	Oil and Gas Production	Petroleum Refineries	Storage and Transfer		
	IL	Cook (IL)	Cook	IL	Cook	Cook (IL)	IL	IL	Cook	
S1 - 56%	0.97	1.00	0.08	1.00	1.00	1.00	1.00	1.00	0.87	
S2 - 20%	0.55	0.45	0.07	0.46	0.47	0.47	0.45	0.47	0.76	
S3 - 18%	0.40	0.20	0.26	0.22	0.23	0.23	0.21	0.22	0.61	
S4 - 6%	0.90	0.89	0.08	0.89	0.89	0.89	0.89	0.89	0.81	

Table 4.16. (continued). Cosine ϕ similarity of PAH modeled and USEPA 2008 National Emissions Inventory profiles.^a

Sector	Solvent						Commercial Cooking			Waste Disposal	
	Industrial Surface Coating & Solvent Use										
	Cook (IL)						Lake (all)			Lake	Cook
S1 - 56%	1.00						0.92			0.93	0.88
S2 - 20%	0.45						0.60			0.56	0.47
S3 - 18%	0.20						0.53			0.41	0.38
S4 - 6%	0.89						0.91			0.96	0.84
Sector	Mobile										
	On-Road				Non-Road Equipment		Aircraft		Locomotives	Commercial Marine Vessel	
	Heavy Duty Vehicles		Light Duty Vehicles								
	Diesel	Gas	Diesel	Gas	Diesel	Gas					
	Lake (all)	Lake (all)	Lake (all)	Lake (all)	Lake (all)	Lake (all)	Cook	Lake	Lake (all)	Lake (all)	
S1 - 56%	0.96	1.00	0.96	1.00	0.83	1.00	1.00	1.00	0.96	1.00	
S2 - 20%	0.59	0.48	0.59	0.48	0.79	0.49	0.46	0.48	0.57	0.50	
S3 - 18%	0.44	0.24	0.44	0.24	0.64	0.26	0.21	0.24	0.41	0.25	
S4 - 6%	0.89	0.91	0.89	0.91	0.82	0.91	0.89	0.91	0.93	0.90	

^a See Table 4.7 for reference profile information.

Table 4.17. Cosine ϕ similarity of PAH modeled and combustion literature source profiles.^a

	Coke Oven	Power Plant	Residential	Gasoline	Diesel	Ave gas and diesel	Tunnel	Wood burning
Particulates adjusted by reported gas-particulate partitioning ^a								
S1 - 56%	1.00	0.00	0.00	0.62	0.01	0.09	0.86	0.96
S2 - 20%	0.48	0.51	0.47	0.44	0.47	0.49	0.73	0.57
S3 - 18%	0.24	0.97	0.96	0.58	0.96	0.96	0.65	0.41
S4 - 6%	0.91	0.04	0.01	0.61	0.03	0.11	0.84	0.91
Particulates adjusted by calculated gas-particulate partitioning ^a								
S1 - 56%	1.00	0.00	0.00	1.00	0.47	0.97	1.00	1.00
S2 - 20%	0.46	0.61	0.48	0.46	0.75	0.59	0.49	0.47
S3 - 18%	0.20	0.92	0.93	0.21	0.90	0.42	0.22	0.21
S4 - 6%	0.89	0.04	0.01	0.89	0.47	0.88	0.90	0.90
Totals only (gas + particulate phase) ^a								
S1 - 56%	1.00	0.00	0.01	0.85	0.01	0.09	0.91	—
S2 - 20%	0.48	0.52	0.34	0.42	0.48	0.52	0.71	—
S3 - 18%	0.24	0.98	0.25	0.27	0.96	0.97	0.55	—
S4 - 6%	0.91	0.03	0.12	0.82	0.03	0.11	0.88	—

^a See Tables 4.4 and 4.5 for reference profile and partitioning coefficient information.

Table 4.18. Cosine ϕ similarity of PAH modeled and area source profiles.^a

	K _H /K _{OW} adjusted			
	IHC Sediment	Biosolids	IHC Sediment	Biosolids
S1 - 56%	0.29	0.03	1.00	0.98
S2 - 20%	0.51	0.18	0.52	0.62
S3 - 18%	0.67	0.44	0.22	0.24
S4 - 6%	0.37	0.11	0.90	0.90

^a See Table 4.6 for reference profile information.

PCBs. Cos ϕ values between modeled PCB sources (S1-S4) and select Aroclor and reference profiles are given in Table 4.15. PCB profile S1 is similar to Aroclors 1016 and 1242 particularly with adjustment for partitioning to air. Profiles S2 and S3 most closely match Aroclor 1248, and profile S4 is most similar to heavier Aroclors 1254A and 1260 (Table 4.19). Aroclor 1248 is known to be a source of contamination in IHC sediment^{66, 161} as well as the sludge lagoon.¹⁰⁷ However it is unclear if sources S2 and S3 represent different Aroclor 1248 production lots (Table 4.19) or weathering in the sediment from chemical, biological, and physical transformations. These include preferential loss of lower chlorinated congeners by volatilization, desorption, or microbial degradation, or the loss of more highly chlorinated congeners to lower congeners by anaerobic microbial dechlorination. Sources S2 and S3 are also similar to measured IHC profiles (Table 4.20), Ralston sludge lagoon (Table S20), transformer storage yard, and biosolids drying beds (Table S21).

Comparison with other PCB studies. Rodenburg et al. (2013)¹⁴¹ recently employed PMF to apportion gas-phase PCBs in the Chicago atmosphere using data from 1996-2007, resolving five factors that weakly resembled either unadulterated or vaporized Aroclors 1242, 1248, and 1254. Source profiles from the present study match Aroclor mixtures more closely, perhaps due to proximity to industrial equipment or environmental deposition. In other studies, Aroclors 1242 and 1254 were found to constitute Chicago air,¹¹⁰ and Aroclor 1248 was largely detected in sediments of the IHC^{66, 161} and the nearby Ralston sludge lagoon.¹⁰⁷ These Aroclors were commonly used in transformers, plastics, hydraulics, and lubricants.⁸⁴ Hsu et al. (2003a, 2003b) identified three major potential PCB source areas to Chicago from the far southwest, far northwest, and south Calumet region using a combination of hybrid receptor models¹¹² and characterized landfill, transformer yard, and drying bed PCB sources in Chicago (Table 4.10) based on upwind/downwind field sampling.¹⁰⁴ Multiple, widespread, and unknown PCB sources residing within and around Chicago require further analysis to identify.

Table 4.19. Cosine ϕ similarity of PCB modeled and Aroclor profiles.^a

	1221-A	1232-AG	1016-AS	1242-ASG	1248-A	1248-G	1254-A	1254-G	1260-ASG	1260-AS	1260-G	1062-AG
<i>Unadjusted</i>												
S1 - 38%	0.97	0.84	0.50	0.53	0.16	0.10	0.01	0.02	0.08	0.13	0.00	0.43
S2 - 33%	0.10	0.45	0.69	0.68	0.78	0.89	0.01	0.05	0.09	0.15	0.00	0.57
S3 - 25%	0.11	0.41	0.61	0.60	0.56	0.40	0.01	0.04	0.08	0.14	0.00	0.52
S4 - 4%	0.09	0.16	0.18	0.22	0.42	0.45	0.93	0.94	0.94	0.94	0.93	0.66
<i>VP</i>												
S1 - 38%	1.00	0.98	0.83	0.85	0.35	0.17	0.58	0.70	0.66	0.86	0.00	0.84
S2 - 33%	0.02	0.09	0.20	0.19	0.39	0.56	0.23	0.28	0.13	0.17	0.00	0.19
S3 - 25%	0.08	0.27	0.58	0.55	0.87	0.82	0.48	0.69	0.41	0.54	0.00	0.57
S4 - 4%	0.02	0.03	0.05	0.05	0.06	0.09	0.63	0.20	0.63	0.06	0.93	0.05
<i>K_H/K_{OW}</i>												
S1 - 38%	0.99	0.98	0.87	0.89	0.40	0.18	0.31	0.69	0.64	0.90	0.00	0.88
S2 - 33%	0.04	0.14	0.32	0.30	0.62	0.81	0.17	0.40	0.19	0.26	0.00	0.30
S3 - 25%	0.07	0.21	0.46	0.44	0.74	0.58	0.19	0.52	0.31	0.43	0.00	0.46
S4 - 4%	0.05	0.07	0.11	0.11	0.16	0.23	0.90	0.51	0.71	0.16	0.93	0.11

^a See Table 4.8 for reference profile information.

Table 4.20. Cosine ϕ similarity of PCB modeled and IHC and city of Chicago profiles.^a

	IHC air (gas)	IHC water (dissolved)	IHC sediment (solid)	IHC Water (K _H adj.)	IHC Sediment (K _H /K _{OW} adj.)	Chicago air
S1 - 38%	0.42	0.12	0.16	0.12	0.41	0.59
S2 - 33%	0.67	0.65	0.88	0.56	0.76	0.63
S3 - 25%	0.66	0.77	0.39	0.84	0.54	0.58
S4 - 4%	0.33	0.23	0.50	0.22	0.26	0.32

^a See Table 4.9 for reference profile information.**Table 4.21. Cosine ϕ similarity of PCB modeled and Ralston sludge lagoon and municipal waste incinerator profiles.^a**

	K _H /K _{OW} adjusted						Incinerator
	NW sludge	SW sludge	Ave. sludge lagoon	NW sludge	SW sludge	Ave. sludge lagoon	
S1 - 38%	0.28	0.15	0.21	0.62	0.33	0.49	0.58
S2 - 33%	0.68	0.78	0.74	0.42	0.62	0.53	0.71
S3 - 25%	0.72	0.60	0.67	0.73	0.77	0.76	0.34
S4 - 4%	0.28	0.40	0.34	0.13	0.17	0.16	0.41

^a See Table 4.11 for reference profile information.**Table 4.22. Cosine ϕ similarity of PCB model and Chicago emission area profiles.^a**

	Landfill	Transformer Storage Yard	Biosolids Drying Bed
S1 - 38%	0.47	0.40	0.06
S2 - 33%	0.53	0.83	0.52
S3 - 25%	0.62	0.29	0.87
S4 - 4%	0.28	0.60	0.20

^a See Table 4.10 for reference profile information.

Source contribution analysis. Multiple Linear Regressions. The multiple linear regression (MLR) models for PAH source contributions explain 25 and 31% of S1 and S4 variation, and 54 and 61% of S2 and S3 variation (based on R^2 , Table 4.23). Temperature drives the higher predictive capacities for S2 and S3 reflecting their strong Clausius-Clapeyron relationships; in contrast S1 and S4 decrease in concentration with increasing temperature. All PAH source contributions decrease with time and increasing wind speed. Wind direction influences source concentrations least among meteorological parameters. With PAH temperature correction prior to modeling, the regression explains < 30% of the variability of all PAH sources (Table 4.24) and temperature becomes much less important particularly for S2 and S3, decreasing with increasing concentrations. MLR models for PCB source contributions explain over half the variability of all PCB sources (Table 4.25), driven mainly by their dependency on temperature. PCB source contributions also decrease with time and wind speed, exhibiting wind dilution effects and long-term reductions.

Temperature correction. PAH post-modeling temperature-corrected (t-c) S2 and S3 contributions (Figure 4.15A) have significantly less seasonal variation than the original sources (see Figure 4.6) and are similar to the pre-modeling t-c contributions (see Figure 4.13B). All PCB sources have dramatic reductions in seasonal variation following temperature correction as well (Figure 4.15B, see Figure 4.8). Clausius-Clapeyron slopes confirm strong temperature dependence of all sources except PAH S1 and S4 (Table 4.26). Pre- and post- model t-c source contributions are strongly positively correlated (Table 4.27), thus temperature correction using either method is viable.

Table 4.23. Multiple linear regression parameters for modeled PAH sources.^a

		Coefficient	SE	Adj. R ²	Forward step-wise R ²
S1 - 56% (n=843)					
	Intercept	-2.10	0.67		
	Jul Day	-0.0002	0.00003		0.06
	WS	-0.15	0.01	0.25	0.10
	1/T	2008.58	190.53		0.06
	cosWD	0.14	0.04		0.02
	sinWD	0.13	0.04		0.01
S2 - 20% (n=838)					
	Intercept	22.09	0.71		
	Jul Day	-0.0001	0.00003		0.01
	WS	-0.17	0.02	0.54	0.05
	1/T	-5204.55	202.46		0.46
	cosWD	0.28	0.04		0.02
S3 - 18% (n=843)					
	Intercept	14.26	0.45		
	Jul Day	-0.0002	0.00002		0.04
	WS	-0.15	0.01	0.61	0.12
	1/T	-2965.38	127.92		0.44
	cosWD	0.06	0.03		0.002
	sinWD	0.07	0.03		0.005
S4 - 6% (n=843)					
	Intercept	-9.10	0.75		
	Jul Day	-0.0003	0.00003		0.08
	WS	-0.16	0.02	0.31	0.07
	1/T	3314.07	213.53		0.15
	cosWD	0.12	0.04		0.01
	sinWD	0.11	0.04		0.01

^a p-value < 0.005; p-values for independent variables ≤ 0.3.

Table 4.24. Multiple linear regression parameters for modeled PAH sources of temperature-corrected (288 K) data.^a

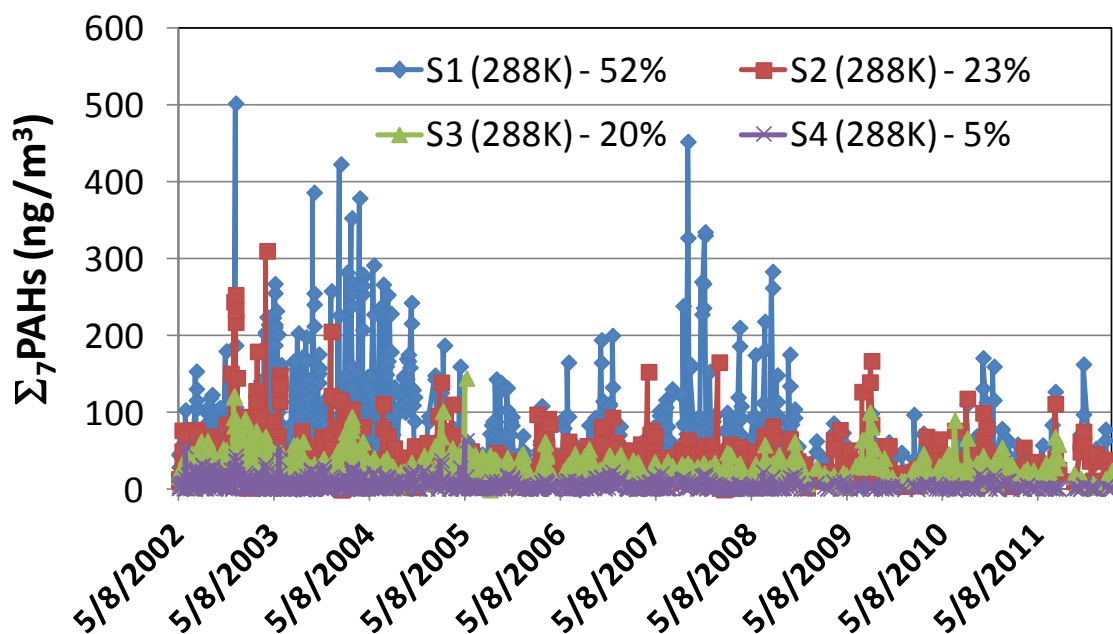
		Coefficient	SE	Adj. R ²	Forward step-wise R ²
S1 - 49% (n=838)					
	Intercept	0.33	0.68		
	Jul Day	-0.00023	0.00003		0.07
	WS	-0.16	0.01	0.21	0.08
	1/T	1298.18	193.13		0.04
	cosWD	0.13	0.04		0.02
	sinWD	0.12	0.04		0.01
S2 - 26% (n=838)					
	Intercept	0.85	0.47		
	Jul Day	-0.00010	0.00002		0.03
	WS	-0.17	0.01	0.28	0.15
	1/T	960.39	134.96		0.04
	cosWD	0.22	0.03		0.07
S3 - 18% (n=838)					
	Intercept	1.10	0.52		
	Jul Day	-0.00015	0.00002		0.05
	WS	-0.16	0.01	0.25	0.16
	1/T	811.33	148.32		0.03
	cosWD	0.07	0.03		0.01
	sinWD	0.10	0.03		0.01
S4 - 7% (n=838)					
	Intercept	-6.71	0.71		
	Jul Day	-0.00026	0.00003		0.08
	WS	-0.18	0.02	0.29	0.11
	1/T	2705.60	202.75		0.10
	cosWD	0.12	0.04		0.01
	sinWD	0.08	0.04		0.00

^a p -value < 0.005; p-value for independent variables < 0.05.

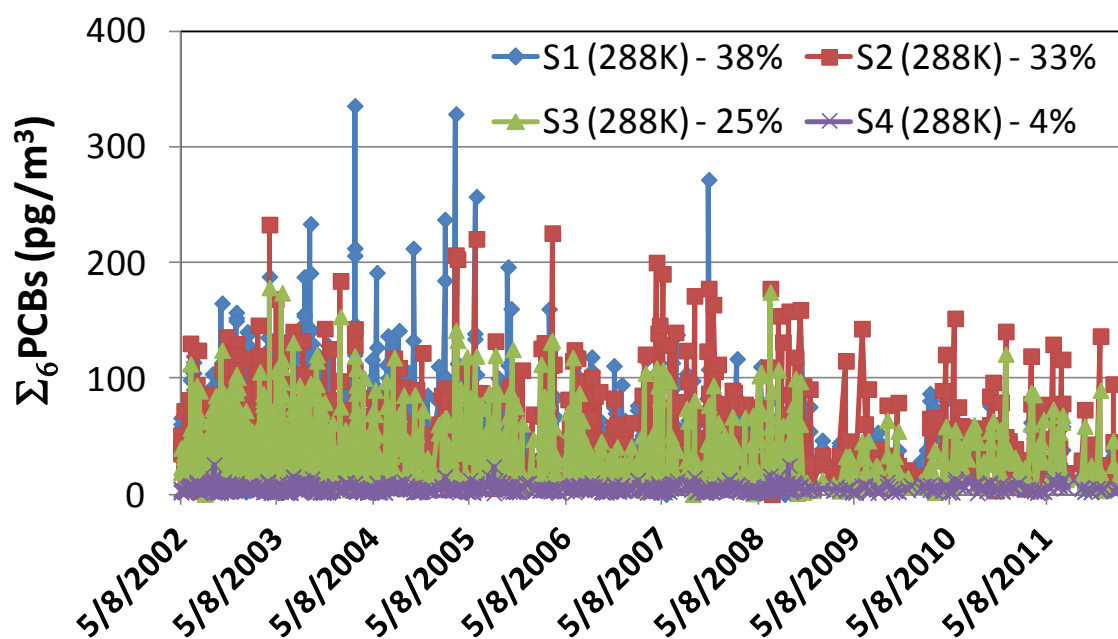
Table 4.25. Multiple linear regression parameters for modeled PCB sources.^a

		Coefficient	SE	Adj. R²	Forward step-wise R²
S1 - 38% (n=843)					
	Intercept	20.36	0.54		
	1/T	-4525.93	154.42		0.53
	Jul Day	-0.00025	0.00002	0.67	0.06
	WS	-0.15	0.01		0.064
	cosWD	0.08	0.03		0.002
	sinWD	0.21	0.03		0.021
S2 - 33% (n=843)					
	Intercept	23.32	0.65		
	1/T	-5471.37	185.23		0.51
	Jul Day	-0.00018	0.00003	0.64	0.02
	WS	-0.11	0.01		0.03
	cosWD	0.34	0.04		0.02
	sinWD	0.34	0.04		0.06
S3 - 25% (n=843)					
	Intercept	20.01	0.69		
	1/T	-4586.85	197.94		0.42
	Jul Day	-0.00023	0.00003	0.54	0.03
	WS	-0.12	0.01		0.02
	cosWD	0.27	0.04		0.02
	sinWD	0.28	0.04		0.05
S4 - 4% (n=843)					
	Intercept	13.36	0.44		
	1/T	-3296.02	126.28		0.5
	Jul Day	-0.00003	0.00002	0.56	0.002
	WS	-0.09	0.01		0.05
	cosWD	0.12	0.03		0.02
	sinWD	0.08	0.03		0.005

^a p-value < 0.005; p-value for independent variables < 0.1.



A)



B)

Figure 4.15. PMF source contributions corrected to 288 K (15 °C) post-modeling for (A) PAHs and (B) PCBs.

Table 4.26. Clausius-Clapeyron parameters^a for modeled PAH and PCB source contributions.

	PAH			PCB		
	Slope	SE	Adj. R2	Slope	SE	Adj. R2
S1	1270	193	0.04	-5200	175	0.45
S2	-5741	186	0.47	-5955	177	0.51
S3	-3642	146	0.36	-4971	195	0.37
S4	2548	212	0.12	-4011	117	0.52

^a From Equation 4.6. All are significant (p-values < 0.05). Sample numbers for PAH S1-S4 are 1097, 1096, 1092, 1097 respectively, and all PCB sources are 1093 samples.

Table 4.27. Pearson Correlation Coefficients between PMF-modeled source contributions with different temperature correction scenarios.^a

	PAHs			PCBs
	Original vs. post-model	Original vs. pre-model	Post-model vs. pre-model	Original vs. post-model
S1	0.98 (1097)	0.94 (1092)	0.95 (1092)	0.74 (1093)
S2	0.73 (1096)	0.59 (1091)	0.86 (1091)	0.7 (1093)
S3	0.8 (1092)	0.76 (1092)	0.96 (1092)	0.79 (1093)
S4	0.94 (1097)	0.97 (1092)	0.94 (1092)	0.69 (1093)

^a Concentrations were natural log-transformed prior to pairwise correlation. Original means not temperature-corrected (t-c), post-model means source contributions were t-c to 288 K after modeling, and pre-model means original data were t-c to 288 K prior to modeling. Sample pair numbers given in parentheses.

Box plot analysis. Temperature correction is beneficial to understanding atmospheric PCB sources,¹³⁴ and is used here for box plot analysis of log transformed temperature-corrected (t-c) PAH and PCB source contributions. Clearly temperature dependence can mask other potential source behavior (Figure 4.16), thus is useful to remove. Box plots show notable significant differences between seasons, stations, days of the week, and wind directions (Figures 4.17 and 4.18). PAH S1 and S2 are similar across most groups (Figure 4.17) except for elevated S1 contributions at stations N, E, and W (i.e. from 2001 to 2004) compared to stations S and H. Source S3 is higher in the summer (even t-c) and similar across other groups (Figure 4.17). Source S4 is dramatically lower on weekends (particularly Sunday), with wind from the SW, and

at station H (Figure 4.17), consistent with a local industrial emission source. PCB sources all appear elevated in summer, even t-c (Figures 4.18). PCB S1 is also significantly higher with wind from the NW (i.e. Chicago) and on most weekdays (Figure 4.18). Sources S2 and S3 are both higher at station S nearest the canal and significantly lower at station H, and are higher with wind from the N and significantly lower with wind from the SW. These results are consistent with the canal as a primary source (S2 and S3) of PCBs (Figure 4.18). Source S4 levels are higher with winds from the N/NW and in the summer (Figure 4.18). No sources are influenced by construction activity occurring on the CDF site (Figure 4.19).

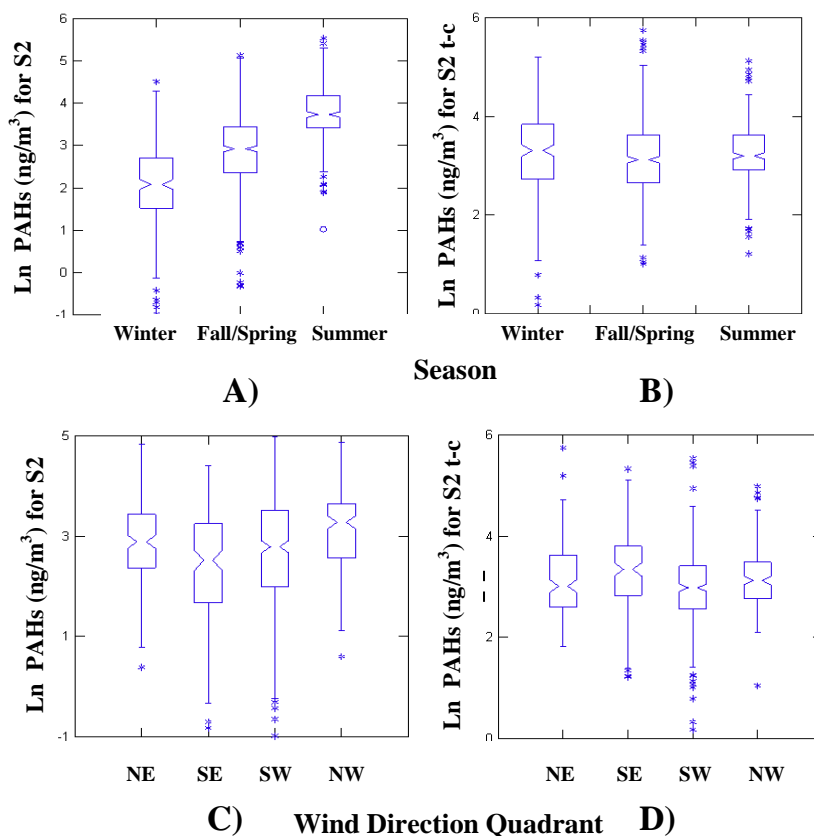


Figure 4.16. Box plots of PAH S2 contributions by season (A-B) and wind direction (C-D) based on original (A and C) and temperature-corrected (B and D) concentrations. Differences between plots with and without temperature effects illustrate the relationship of temperature with season and with wind direction that may mask true impacts of seasonality or wind on concentrations.

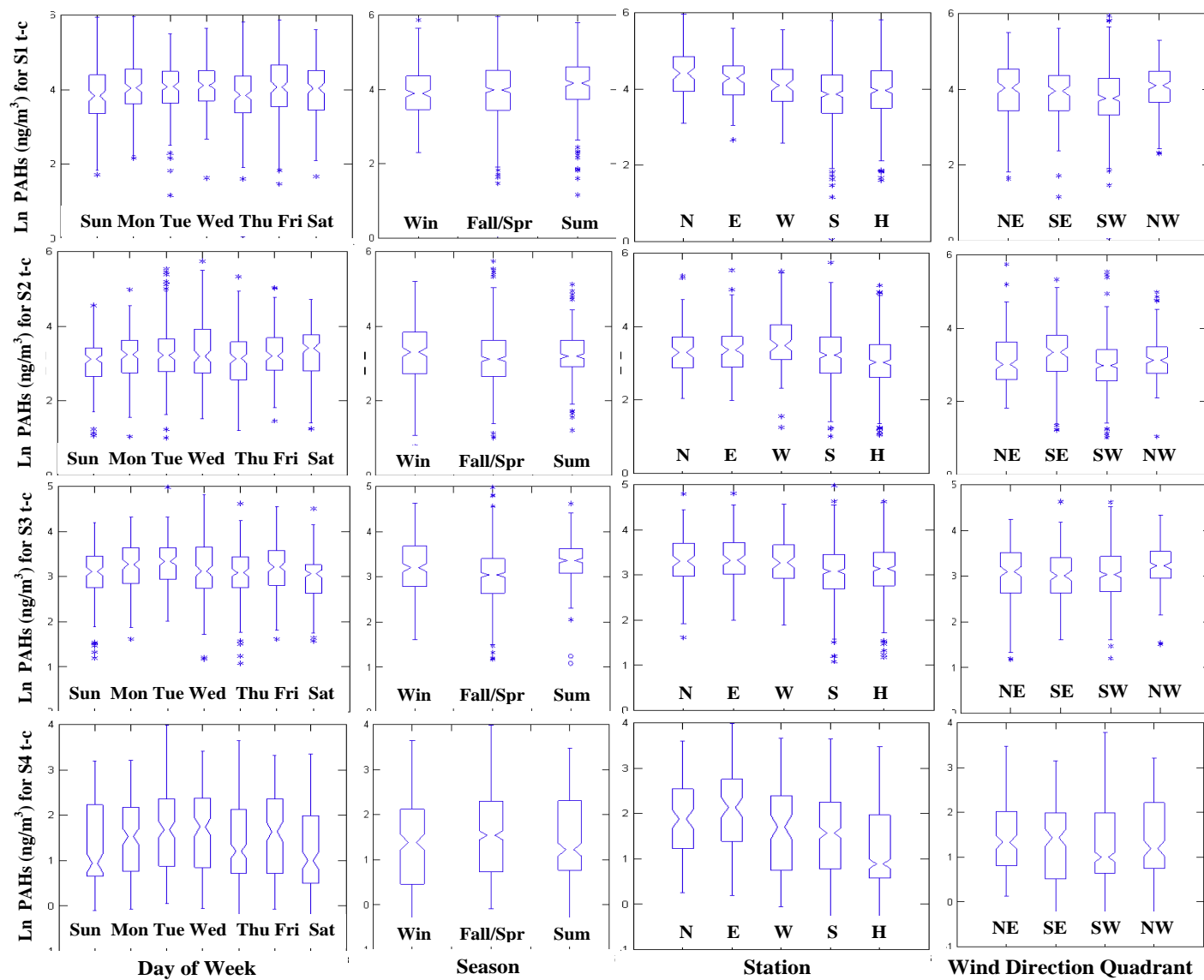


Figure 4.17. Box plots of PAH temperature-corrected source contributions by day of week, season, station, and wind direction.

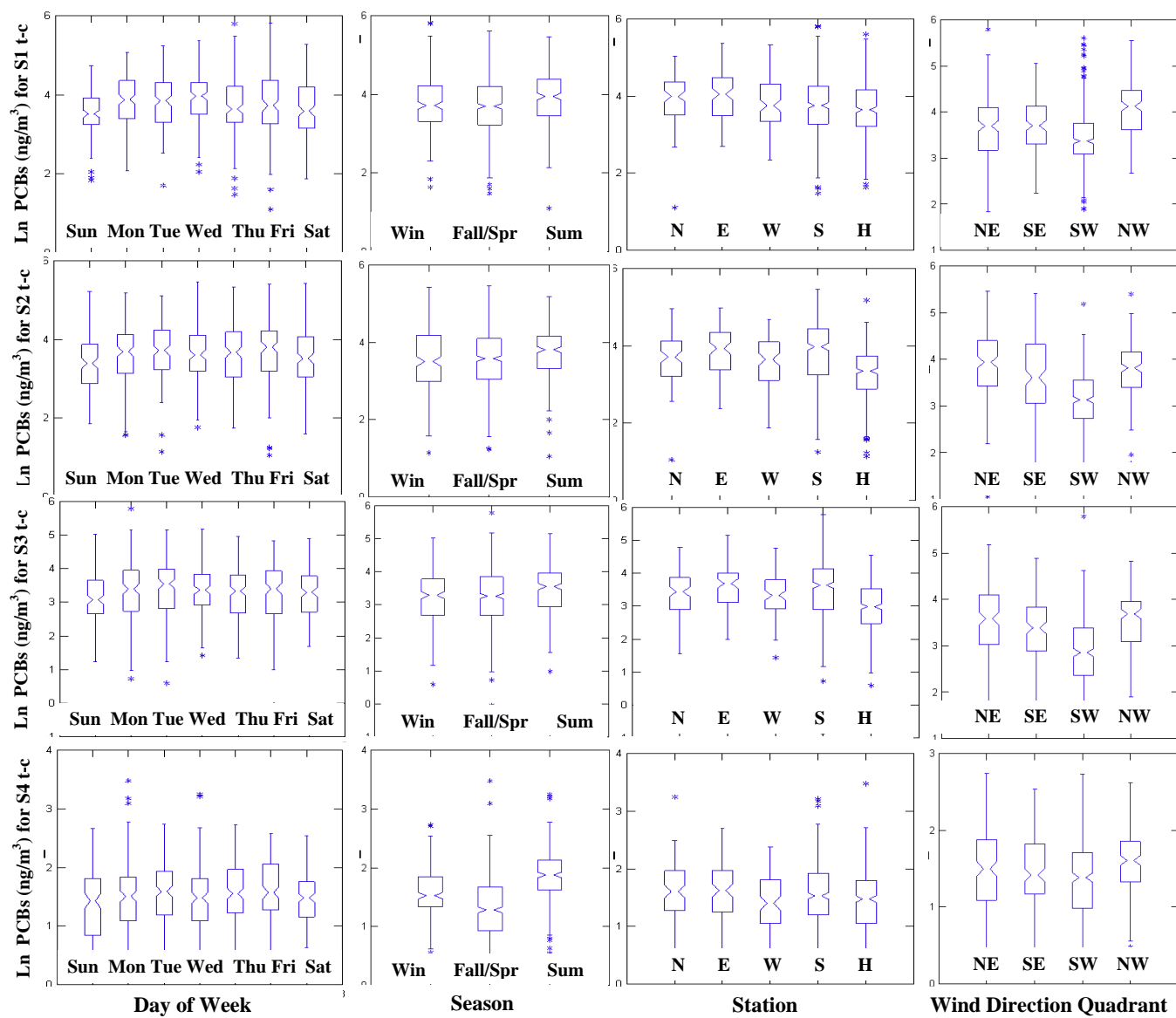


Figure 4.18. Box plots of PCB temperature-corrected source contributions by day of week, season, station, and wind direction.

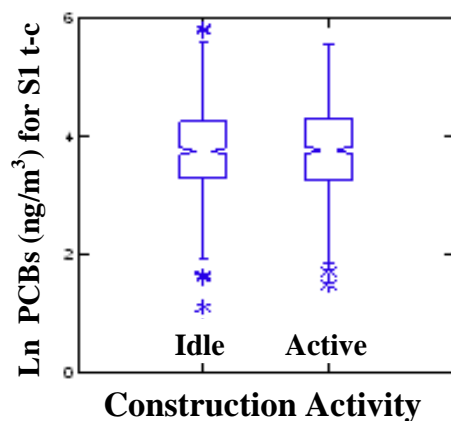


Figure 4.19. Box plots of PCB S1 (t-c) contributions by construction activity. No significant differences were found for any sources based on construction activity at the CDF.

Yearly moving averages. Yearly moving average plots of PAH and PCB source concentrations at stations S and H are shown in Figure 4.20. PAH source S1 rises dramatically in 2003 and 2007 and slightly in 2010 at both stations (Figures 4.20A and 4.20B). PAH sources S2 and S3 peak at station H alone in 2009. PCB source S1 increases from 2003 through 2005 then drops markedly through the end of the study at both stations (Figures 4.20C and 4.20D). PCB sources S2 and S3 behave similar to one another, with heightened levels and variability at station S. It is not readily apparent what causes the observed peaks in PCB sources S2 and S3 certain years (including a steady increase from 2010 till the end of the study in 2012); they may be due to heavy barge traffic or other sediment disturbances.

Simple linear regressions of yearly moving averages that include all stations over times show significant overall decreases for all sources except PAH S2 and PCB S4 (Table 4.28). Rodenburg et al. (2013)¹⁴¹ found that the majority of PCB sources in Chicago were not declining from 1997-2007. Two modeled sources that did decrease steadily with time, not unlike PCB S1, were speculated to represent air/surface exchange, natural attenuation, or the removal of Aroclor 1242-

containing equipment through normal replacement or the Great Lakes Bi-national Toxics Strategy program.¹⁴¹ Two other sources (one like Aroclor 1054) clearly increased over time, starting to peak in late 2004 through the end of the study in 2007. These sources were attributed to human activity like waste transfer, disturbance of contaminated sites, deterioration of PCB-containing equipment, or a major demolition coinciding with construction boom in 2005 in Chicago. This result is reminiscent of PCB source S4, which also appears to be increasing.

Table 4.28. Linear regression parameters for PAH and PCB source contribution yearly moving averages.^a

	PAH			PCB		
	Coefficient	SE	Adj. R2	Coefficient	SE	Adj. R2
Source 1	-0.01185	0.000209	0.28	-0.00923	0.000089	0.56
Source 2	0.00112	0.000078	0.02	-0.00134	0.000142	0.01
Source 3	-0.00033	0.000046	0.01	-0.00340	0.000103	0.12
Source 4	-0.00224	0.000019	0.62	0.00018	0.000008	0.05

^a p-values < 0.005.

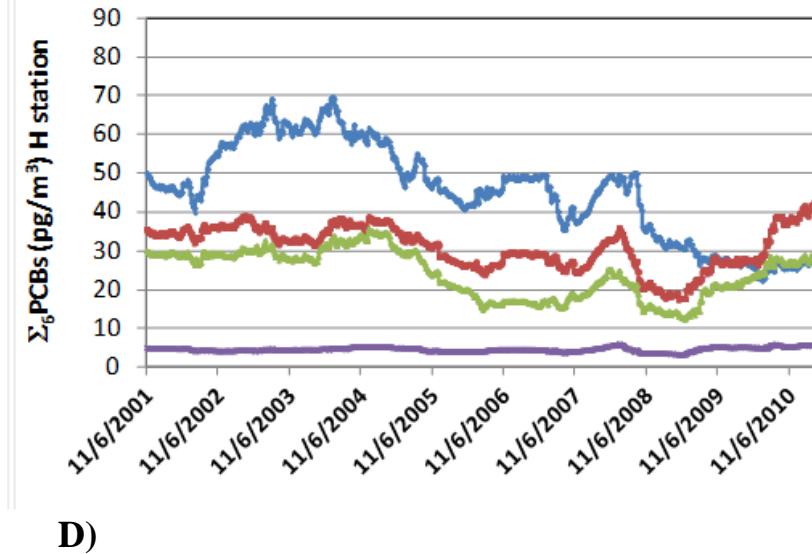
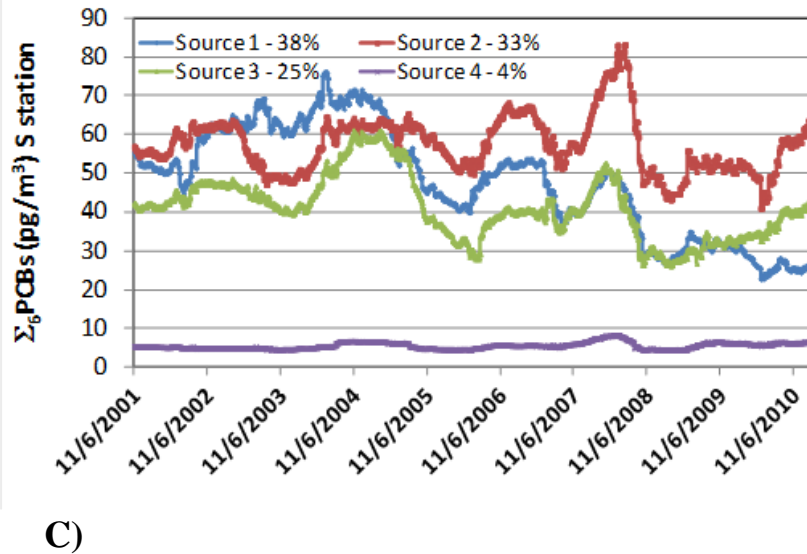
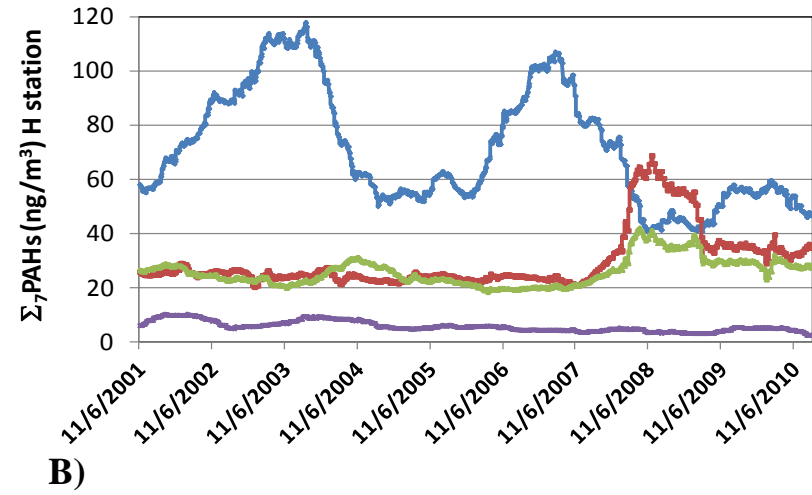
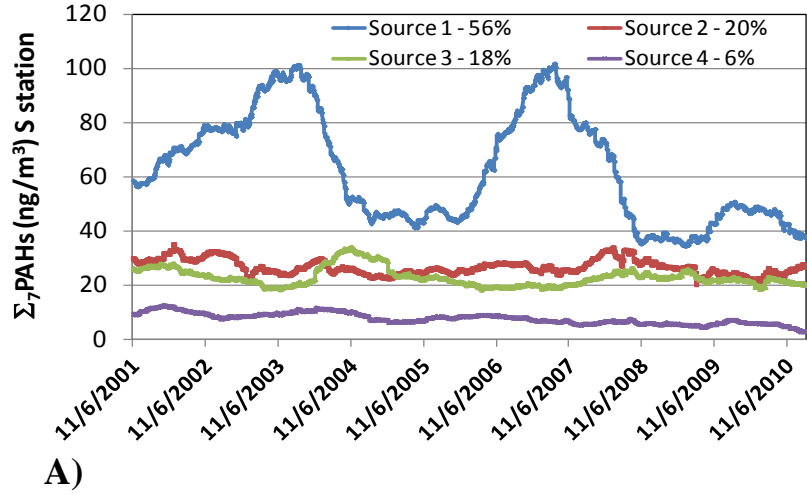
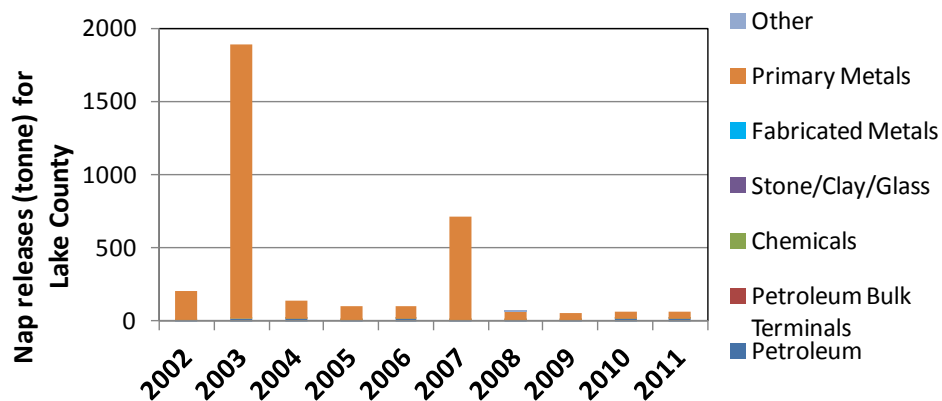
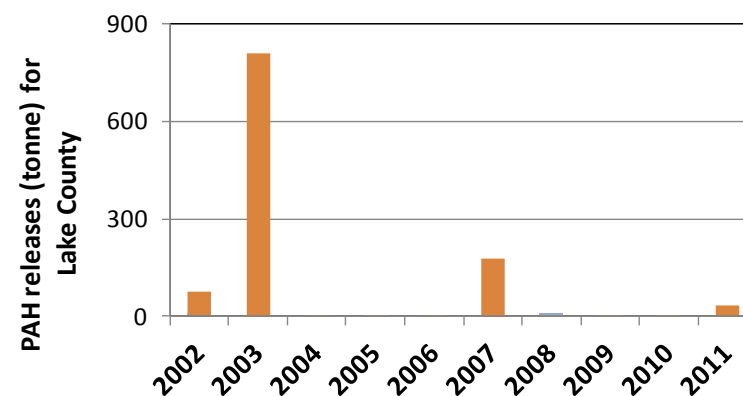


Figure 4.20. Source contribution concentrations calculated as the subsequent 365-day moving average over time for total PAHs (A - B) and PCBs (C - D) at station S (A and C) and station H (B and D).

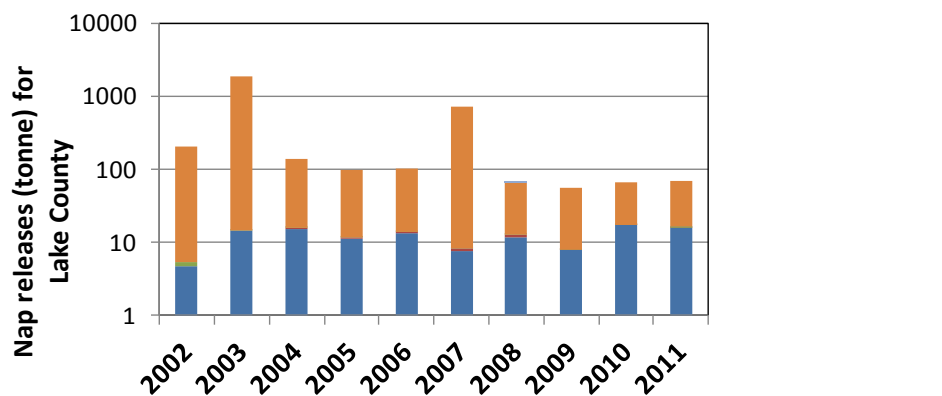
Toxics Release Inventories. Nap and PAH releases in Lake County, IN are largely from Primary Metals manufacturing, and comparatively less from Petroleum industries (Figure 4.21). Nap releases are over twice that of other PAHs, and trend closely with Primary Metals over time. In 2003 and 2007 Primary Metal releases are hundreds of times greater than other years of the study (Figure 4.21); coincident with the striking increases in source S1 contributions (see Figures 4.6 and 4.20A-B). This strongly suggests that nearby steel related coke production is responsible for the majority of atmospheric PAHs at the CDF. Cook County, IL releases are surprisingly different from Lake County in terms of mass loading and emission source (Figure 4.22). Much less Nap and PAHs are released, and contributions vary between a number of industrial sectors including Chemicals, Petroleum, Petroleum Bulk Terminals, Stone/Clay/Glass, Fabricated Metals, and Other. Chemical industry PAH releases peaked in 2008/2009 (interestingly when Nap releases were relatively low), Fabricated Metals peaked in 2004/2005 for Nap, and Other industry peaked in 2006 for Nap and in 2011 for Nap and PAHs in Cook County (Figure 4.22). The unusual increase in sources S2 and S3 at station H from 2008 to 2010 (see Figure 4.20B) may be related to the Chemical industry emission increases.



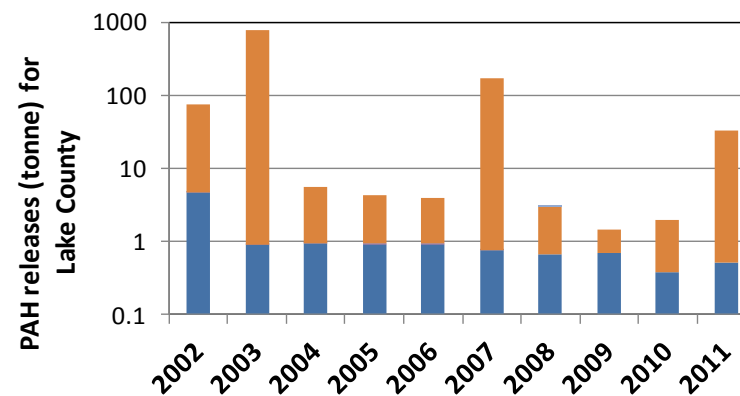
A)



B)

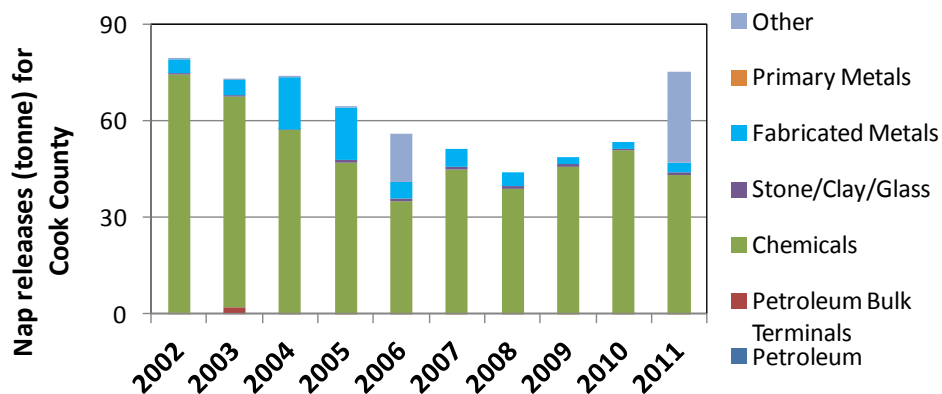


C)

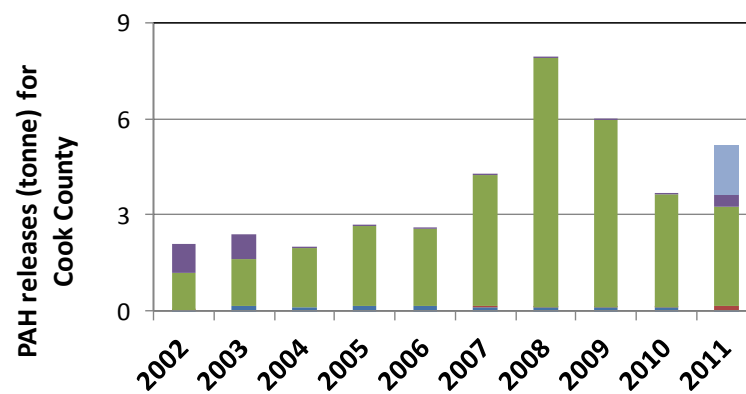


D)

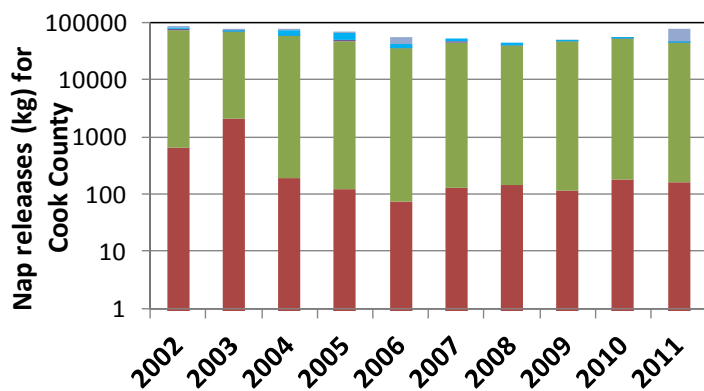
Figure 4.21. Nap (A and C) and PAH (B and D) county-level releases from major industrial sectors in Lake County, IN for 2002 - 2011 from Toxics Release Inventory data. Plots A - B have linear y-axis scales in metric tons (1000 kg) and plots C - D have logarithm y-axis scales for visibility of lesser sectors.



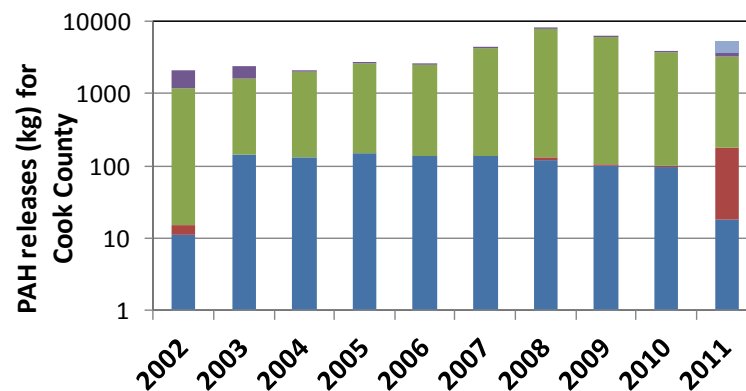
A)



B)



C)



D)

Figure 4.22. Nap (A and C) and PAH (B and D) county-level releases from major industrial sectors in Cook County, IN for 2002 - 2011 from Toxics Release Inventory data. Plots A - B have linear y-axis scales in metric tons (1000 kg) and plots C - D have logarithm y-axis scales in kg for visibility of lesser sectors.

Air dispersion model. The SCREEN3 air dispersion model was used to assess the strength of nearby PCB emission sources shown in the map in Appendix A (Figure A1): IHC,¹⁰⁶ Ralston sludge lagoon (sludge concentrations many times higher than IHC sediment located 7.5 km to the southeast),¹⁰⁷ biosolids drying beds (concentrations over two times background level located 9.5 km to the west), and a transformer storage yard (concentrations over five times background level located 30 km to the northwest).¹⁰⁴ SCREEN3 estimated maximum 1-hr concentrations at the CDF that typically varied by an order of magnitude according to the distance of each source (Table 4.29). Although IHC has lower PCB emissions than other sources, its proximity resulted in a prediction of greatest impact (PCB concentration of 3.45E-3 ug/m³) followed by the Ralston sludge lagoon, biosolids drying beds, and finally the transformer storage yard (Table 4.29). These results are consistent with predicted PCB sources from the PMF model and suggest sources S2 and S3 represent the IHC by weight of evidence.

Table 4.29. SCREEN3 inputs and estimated PCB concentrations from area sources to the CDF.^a

	Emission rate (g/s/m ²)	Long side (m)	Short side (m)	Release height (m)	Approx. distance from CDF (m)	Estimated CDF concentration (ug/m ³)
IHC canal (near)	7.87E-11	1500	150	0	756	3.45E-3
IHC harbor entrance	7.87E-11	1500	750	0	5500	4.79E-4
Sludge lagoon	7.87E-10	500	155	0	7500	2.73E-4
Biosolids drying beds	1.62E-10	422	311	1	9500	7.16E-5
Transformer stg. yard	6.20E-10	150	91	1	30000	8.30E-6

^a See Table 4.12 for input information.

4.5. Implications

PMF successfully apportioned PAHs and PCBs in the IHC air-shed from 2001 to 2012. Monte Carlo uncertainty analysis and utilization of additional receptor models lend confidence to the results while demonstrating limitations of the model particularly for PCBs. The comprehensive approach utilized in the present study to interpret PMF solutions included comparisons with numerous reference sources, temperature correction, contribution patterns across meteorological, temporal, and other source-related factors, and confirmation with local industrial and historical information to provide a weight of evidence basis for source identification. Temperature correction is important for removing temperature dependency of volatilization-driven atmospheric PAHs and PCBs, and may be performed pre-modeling with input data or post-modeling with sources.

Atmospheric PAH sources were driven by industrial and combustion-related emissions in the region. Although S1 matches both coke oven and IHC sediment adjusted to volatile fraction, the lack of seasonality in S1 is not consistent with an environmental release as would be expected for an IHC sediment source. The similarity between coke oven and IHC sediment suggests the former may be the source of the latter. Thus byproduct recovery coke ovens were identified as the main PAH source (S1 - 56%) from nearby steel manufacturing based on profile similarity, lack of temperature dependence of contributions, and agreement with Toxics Release Inventory data. The second source (S2 - 20%) is most consistent with petroleum-related storage and transfer operations based on profile similarity, proximity to storage tanks, and temperature dependency consistent with evaporative losses rather than industrial output of a refinery or power plant. Source 3 (S3 - 18%) is likely a mix of gasoline and diesel emissions based on profile similarity and proximity to traffic on nearby expressways and roadways. Source 4 (S4 - 6%) appears to be a local coke oven source from a smaller facility to the east due to profile

similarity, temperature independence, significant increases on weekdays, and high levels occurring with wind from the east where non-recovery coke ovens operate.

The importance of current production and human activities on atmospheric PAHs in the area cannot be overemphasized. Nap alone accounts for the majority of contaminant mass to the receptor (500-1000 times higher than Σ_6 PCBs). Byproduct recovery coke production releases significantly more PAHs (particularly Nap) in the area than non-recovery production due in part to coke oven operating conditions and byproduct recovery process emissions.¹⁹⁹ Emission control failures and overall releases could be reduced by improving operational and maintenance practices and use of control devices at numerous stages in the coke production and byproduct recovery plant. Fixed roof petroleum storage tanks can achieve evaporative loss reduction efficiencies of up to 98% by installing internal floating roofs equipped with proper seals and fittings, and vapor recovery systems during filling or emptying.¹⁹⁹ Improved mileage and emission standards play a role in reducing the contribution of mobile sources. Lack of power plant impacts may be due to improved operation efficiency and emission control as well.

In contrast to PAHs, atmospheric PCBs are driven by legacy Aroclor contamination of the environment. The main PCB source (S1 - 38%) is similar to several Aroclors including 1242 and 1060 that may have vaporized or have been otherwise released from sediment. Though specific sources are unknown, S1 may represent a general atmospheric background source to the AOC area inclusive of the city of Chicago, as suggested by the moderate match with Chicago atmosphere coupled with the significantly higher levels with wind from the northwest. The second and third sources (S2 - 33%, S3 - 25%) are related closely to Aroclor 1248-contaminated IHC sediment based on profile similarities, known historical contamination, and higher levels at the adjacent station S and with wind over the canal. More research is needed to determine if S2

and S3 represent two separate Aroclor 1248 production lots or differential weathering and/or environmental transport. The smallest fraction and most uncertain source (S4 - 4%) is most similar to higher molecular weight Aroclors 1254 and 1260. Source S4 increases over time and has significant seasonal variation that could be related to deterioration of PCB-containing equipment or handling of hazardous waste.

PCBs releases are generally from secondary sources, but human activities including environmental disturbances play a role. Although remediation of contaminated sites ultimately minimizes the impact of contaminants on surrounding communities and ecosystems, care must be taken during projects for the IHC, as well as nearby contaminated sites like the Ralston sludge lagoon or the Grand Calumet River to control and monitor additional releases. Removing PCB-containing equipment is another opportunity to actively reduce PCB levels and a potentially significant source. Much research is still needed to adequately address PCB reduction efforts.

These findings establish a baseline for future source apportionment analyses. Continued monitoring during the dredging phase of the IHC project will provide a unique opportunity to observe the efficacy of dredging for reductions in air emissions. Suggested pollution prevention, control, and removal solutions can reduce impacts to the IHC and surrounding AOC, Chicago, and Lake Michigan. These include eliminating release events that may have regional (such as PAHs from coke ovens) or local (such as PCBs from the canal) impacts on atmospheric concentrations. This study can support project and policy decisions for area residents and government agencies taking steps to reduce emissions and environmental health risks in the Chicago and northwest Indiana area.

CHAPTER V. SOURCE APPORTIONMENT OF POLYCYCLIC AROMATIC HYDROCARBONS IN ILLINOIS RIVER SEDIMENT

5.1. Abstract

The accumulation of over six million metric tons of sediment annually to the Illinois River Valley degrades its recreational, commercial, and ecological value. This necessitates dredging a large volume of sediment to restore water depth and makes beneficial reuses of the sediment a priority. Unfortunately, many reuse applications are limited by contamination from polycyclic aromatic hydrocarbons (PAHs), particularly benzo(a)pyrene. Existing contaminant standards do not consider whether the sources of PAHs are from current petroleum combustion-based inputs or whether they represent "legacy pollution" such as coal dust released from barges, trucks, and storage. The latter is typically found in black carbon form that might be less bioavailable, and thus may not represent as high a risk for beneficial reuse. A source apportionment (SA) analysis was undertaken to identify the sources of PAHs to the Illinois River and to determine if they come from these potentially low bioavailable forms.

Priority PAHs were analyzed in 80 sediment cores sampled from Illinois River pools and backwater lakes between Hennepin, IL and the Peoria Lock and Dam. PAH diagnostic ratio analysis and a Positive Matrix Factorization (PMF) multivariate receptor model were used to characterize the PAH dataset, identify specific sources of pollutants, and quantify source contributions to the river sediment. Predicted sources from the SA analysis were identified using a database of compiled reference PAH profiles for coal dust, coal tar sealcoat, motor oils, biosolids, as well as fossil fuel combustion residues from gasoline and diesel engines, power plants, and coke production.

Three sources (S1, S2, and S3) were required to reconstruct most of the variation in the Illinois River contaminant dataset by PMF source apportionment. PMF results suggested that a mixed upland source and coal-derived sources including coal tar sealcoat (S1 and S2, 75%) were major contributors to sediment PAHs in the Illinois River, as well as a diffuse traffic-based source (S3, 25%). Liquid petroleum was not identified as a significant source of PAHs to Illinois River sediment. Coal dust was not uniquely resolved from the coal-derived sources and thus could not be assessed for reduced PAH bioavailability. Finally, comparison of PMF results with those from the widely-used PAH diagnostic ratio method indicated that the latter does a relatively poor job of uniquely resolving PAH sources in the sediments.

5.2. Introduction

The Illinois River connects the Des Plaines River and the Kankakee River in northeast Illinois, USA to the Mississippi River, draining the largest watershed in Illinois. The drainage basin is approximately 83,000 km² and includes metropolitan areas like Chicago (metropolitan population over eight million) but is largely (80%) agricultural. Over six million metric tons of sediment are deposited in the river valley each year from tributaries, the mainline, and bluff erosion.²⁰⁰ Sedimentation has especially degraded ecological and habitat functions of river pools and backwater lakes, and severely limited recreational and commercial fishing and boating.²⁰¹ Recognizing that deposited sediments can be similar to high quality topsoil, sediment reuse advocates have called for the use of dredged material for amending restoration and reclamation sites. However, legacy sediment contaminants such as polycyclic aromatic hydrocarbons (PAHs) must be at protective levels for any beneficial use of sediment. PAHs are the most prevalent hydrophobic organic contaminant in sediments, and compose significant fractions of coal, crude

oil and distillates, and combustion residues (char, soot, and other black carbon forms) of fossil and organic fuels.²

The Illinois Sustainable Technology Center (ISTC) and other state agencies have supported the sampling and testing of Illinois River sediment for beneficial reuse projects over the past decade.²⁰¹⁻²⁰³ In some cores, PAHs were measured at levels higher than state TACO (Tiered Approach to Corrective Action Objectives, Illinois Adm. Code, 2007) cleanup standards.²⁰⁴ While Illinois does not have a standard for contaminants in topsoil, state TACO cleanup standards are sometimes used as a surrogate (Table 5.1). However from a risk standpoint, PAH bioavailability is a more important indicator of toxicity than concentration levels alone.¹⁵² While bioavailability is difficult to measure directly, an understanding of its potential effects can be inferred by PAH source information. For example, PAHs preferentially partition to condensed black carbon forms like coal dusts and large combustion particles, where they are less likely to be bioavailable than PAHs derived from direct petroleum spills and releases.¹⁹ It has been hypothesized that coal from stockpiles and transportation by barge over the past century may have heavily contributed to the sediment PAH burden. This hypothesis is supported in part by an elemental analysis of dried and combusted Upper and Lower Peoria Lake surface sediments sampled by the Illinois State Geological Survey. Our laboratory found that approximately 1.5% of the solids and nearly half of total carbon in the sediment exist as black or condensed carbon (Figure 5.1). To test this hypothesis, a source apportionment (SA) analysis was undertaken using diagnostic PAH ratios and Positive Matrix Factorization (PMF) receptor modeling to determine whether coal-based pollution was likely to have contributed to PAHs in the Illinois River. A second objective of this study was to critically compare diagnostic ratio analysis with PMF modeling for SA of priority PAHs in sediment.

Table 5.1. PAH background soil concentrations for populated areas and soil remediation concentration objectives (ug/kg) from TACO.^a

	City of Chicago	Background Other Metropolitan Area	Non-Metropolitan Areas	Remediation Objectives ^b
Nap	40	200	170	1.60E+06
Acy	30	70	40	na
Ace	90	130	40	4.70E+06
Flo	100	180	40	3.10E+06
Pha	1300	2500	990	na
Ant	250	400	140	2.30E+07
Fla	2700	4100	1800	3.10E+06
Pyr	1900	3000	1200	2.30E+06
BaA	1100	1800	720	900 ^c
Chr	1200	2700	1100	8.80E+04
BbF	1500	2100	700	900 ^c
BkF	990	1700	630	9.00E+03
BaP	1300	2100	980	90 ^c
DahA	200	420	150	90 ^c
Ind	860	1600	510	900 ^c
BghiP	680	1700	840	na

^a Tiered Approach to Corrective Action Objectives (TACO), Illinois Adm. Code, 2007.

^b Based on human health criteria and ingestion exposure route. Unavailable data labeled na.

^c For PAHs in which remediation standards are exceeded by background concentrations, background concentrations can be used instead (TACO).

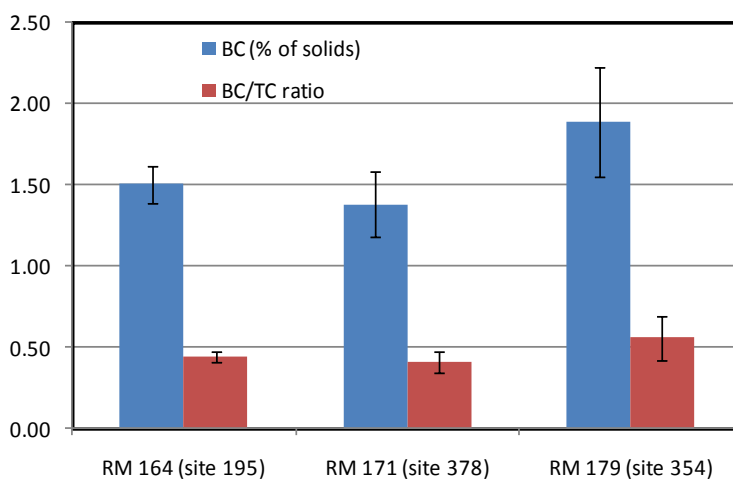


Figure 5.1. Black carbon in Lake Peoria sediment. Error bars indicate standard deviations for 10 cm sections.

5.3. Materials and Methods

Sediment sampling and PAH analysis. Over 100 segmented sediment cores were collected by the Illinois State Water Survey (ISWS) between 2004 and 2007 from the central 200 km of the Illinois River and backwaters using a vibra-coring system.²⁰³ Sediment cores were taken to an average depth of 203 cm and were segmented into evenly spaced 2 cm intervals. Composites were developed by thoroughly mixing material from the intervals for the entire length of the core, generally 2 cm of material taken every 20 cm. Cores were composited as whole cores, upper cores, or lower cores: whole cores averaged 8 cm to 203 cm (n=62), top segments averaged 8 cm to 132 cm (n=29), and bottom segments averaged 143 cm to 217 cm (n=10). Sediment cores were analyzed for a suite of contaminants by a USEPA certified laboratory utilizing USEPA standard method 8270C.²⁰³ Measured contaminants included the 16 EPA priority PAHs: naphthalene (Nap), acenaphthylene (Acy), acenaphthene (Ace), fluorene (Flo), phenanthrene (Pha), fluoranthene (Fla), pyrene (Pyr), benzo(a)anthracene (BaA), chrysene (Chr), benzo(b)fluoranthene (BbF), benzo(k)fluoranthene (BkF), benzo(a)pyrene (BaP), dibenz(a,h)anthracene (DahA), indeno(1,2,3-cd)pyrene (Ind), and benzo(ghi)perylene (BghiP). PAH concentrations were reported in ug/kg dry weight of sediment. Sample-specific reporting limits (RLs) varied from 20-330 ug/kg. Approximate concentrations were reported for measurements between the method detection limit (MDL) and the RL, and measurements below the MDL were reported as non-detect. Note dating information was not available for the cores.

The present study focused on four reaches between Hennepin, IL and the Peoria Lock and Dam (Figure 5.2) because of the high number of non-detects (40-100%) in samples downstream of the dam (n=8). Core locations are given in Figures 5.3 through 5.6 for the four study reaches named according to proximate river city and ordered from upstream to downstream: Henry (HN), Lacon (LC), Upper Peoria (UP), and Lower Peoria (LP).

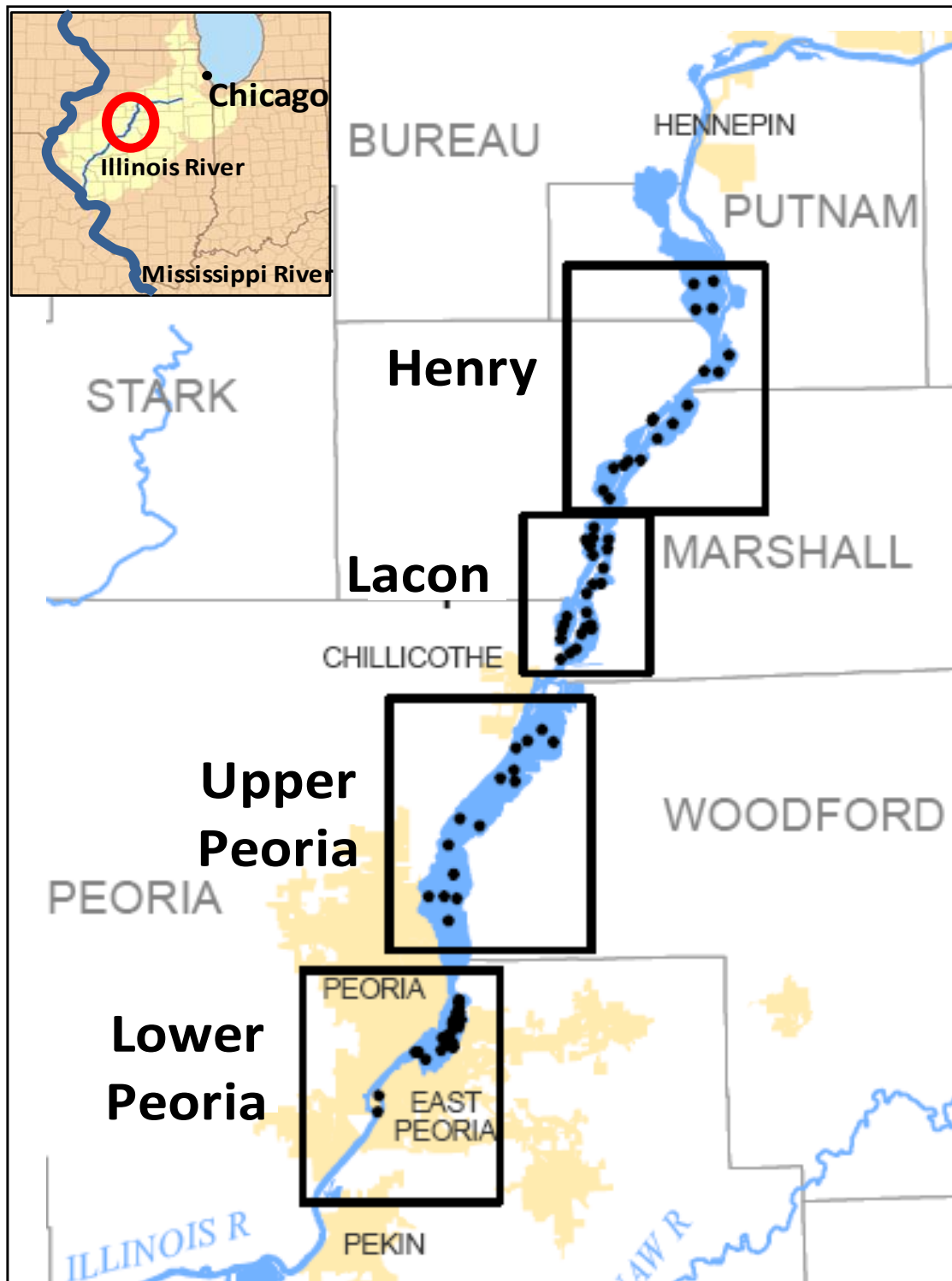
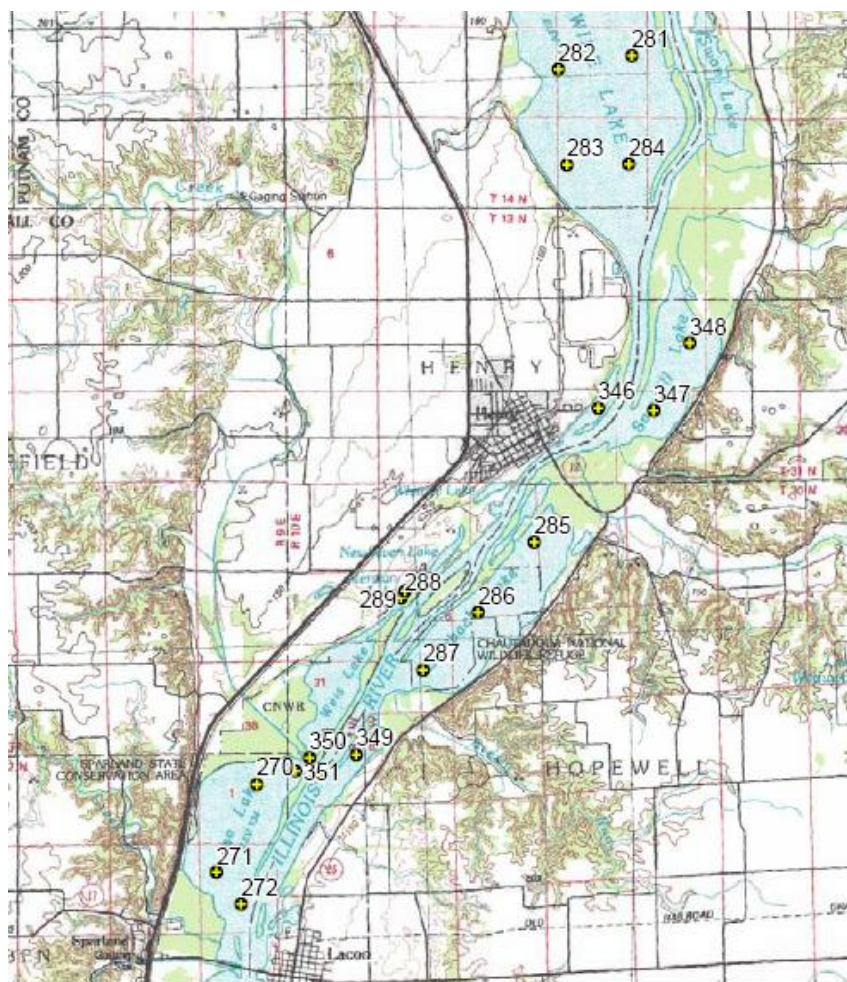
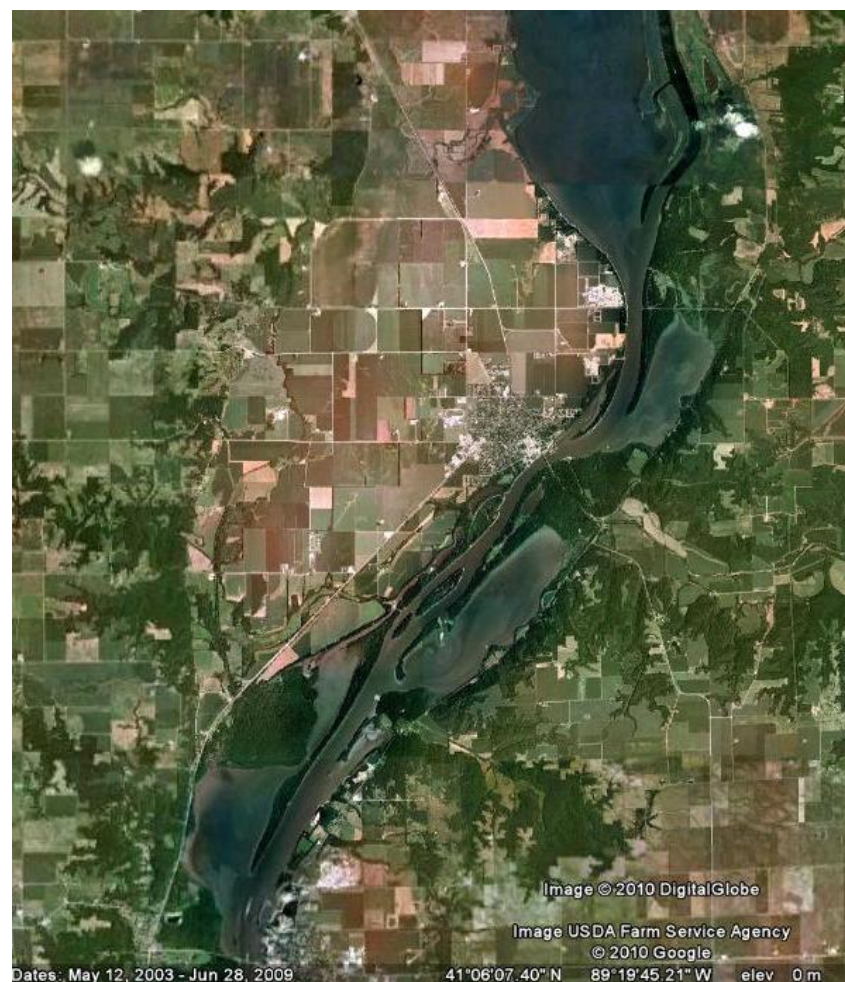


Figure 5.2. Map of Illinois River study location and sediment core sites. Study area is circled on the locator map (upper left) with the watershed and relationship to Chicago/Lake Michigan (upstream) and Mississippi River (downstream) shown. Cores are points and reaches are labeled (from upstream to downstream) Henry, Lacon, Upper Peoria, and Lower Peoria (see Figures 5.3 to 5.6). Counties and municipalities are also shown. Map from the ISWS (2008).²⁰³

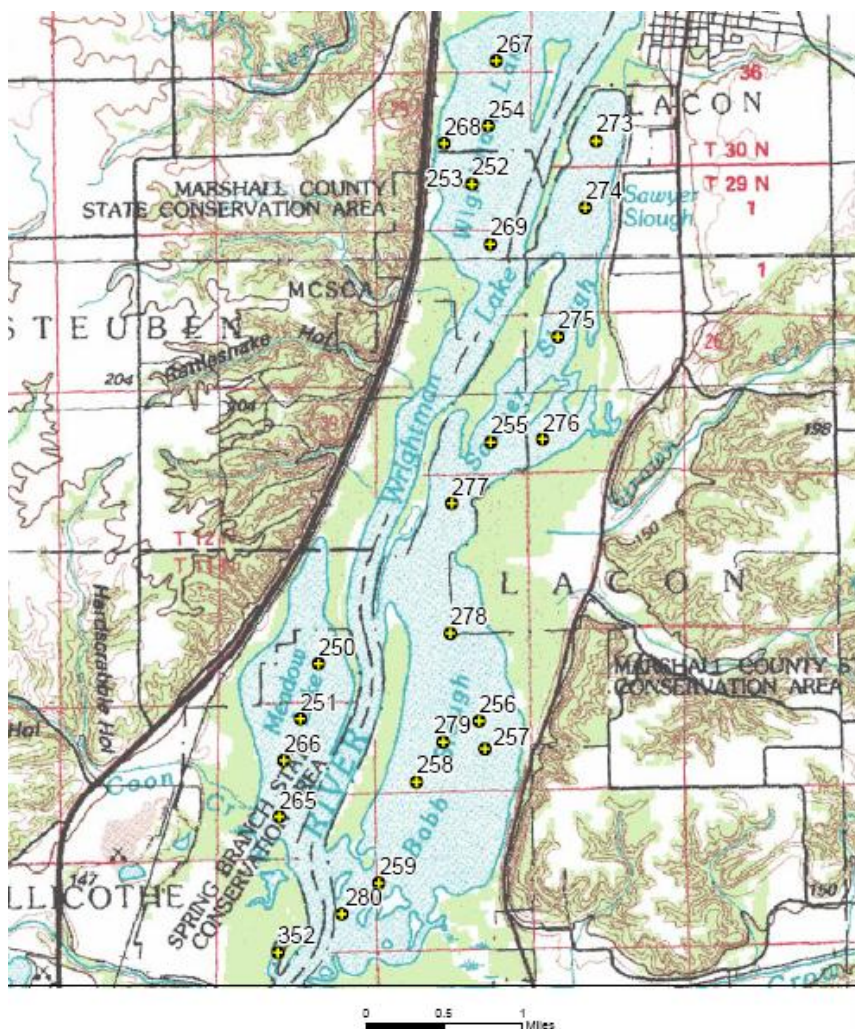


A)



B)

Figure 5.3. Henry (HN) sample site on the Illinois River (includes Senachwine, Sawmill, Billsbach, Weis, and Goose Lakes). Sediment core numbers and locations shown on ISWS (2008)²⁰³ quadrangle map (A) alongside an aerial photograph (B). Satellite photo ©Google Inc. 2008.

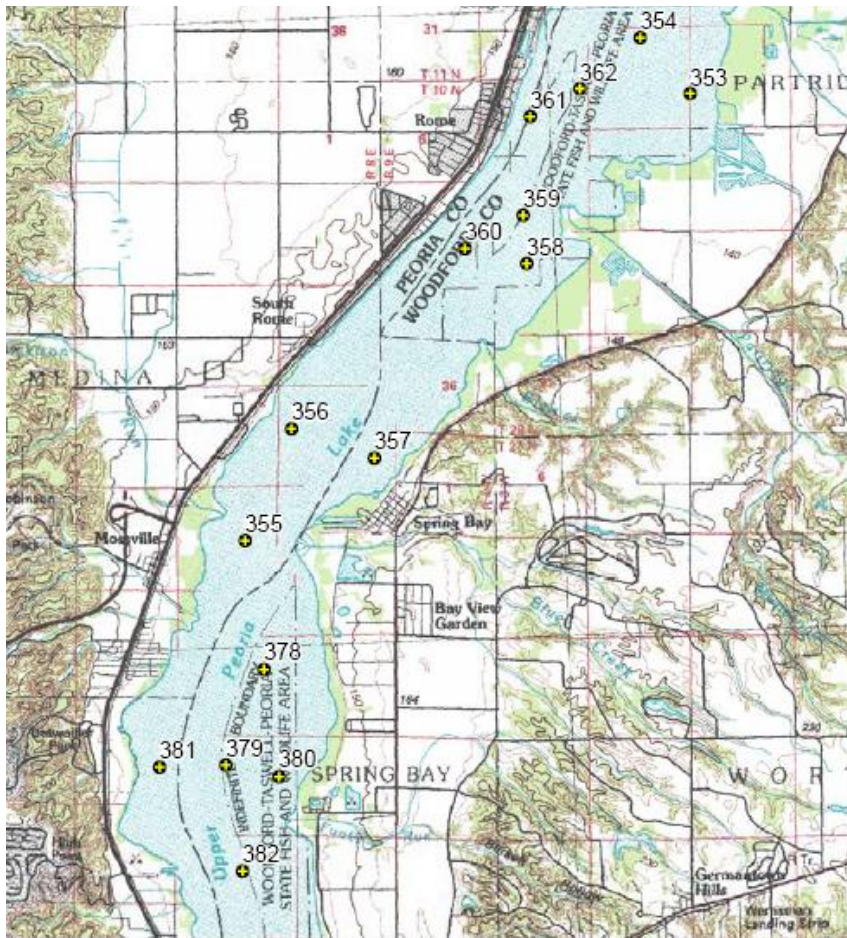


A)

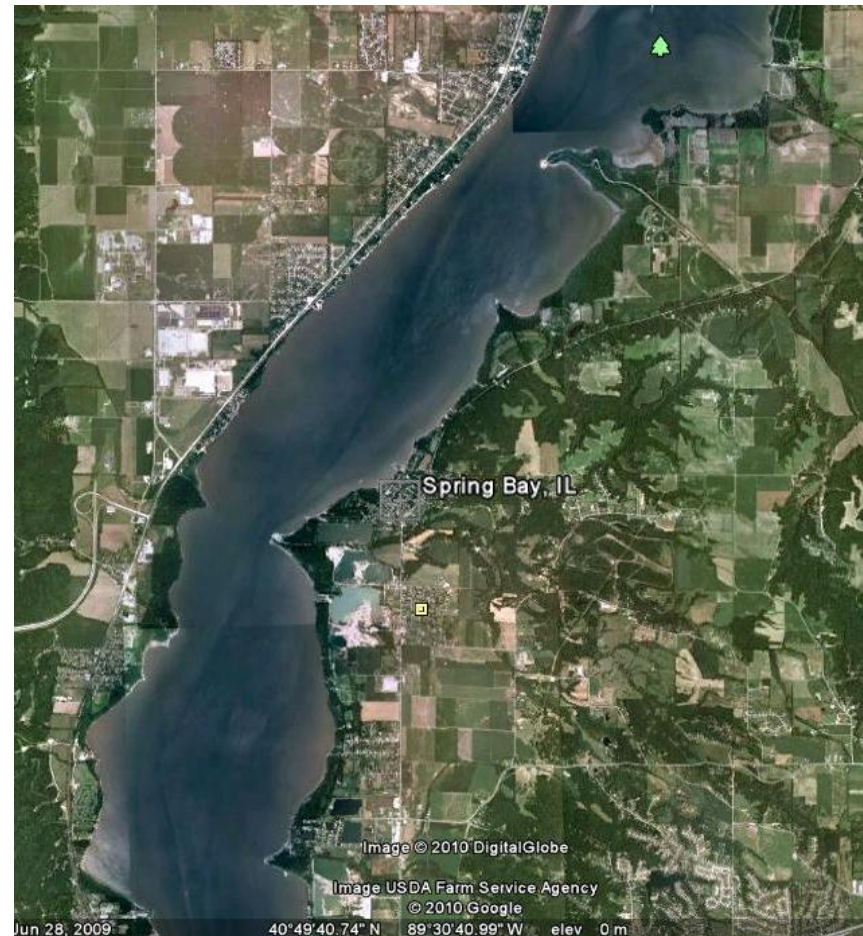


B)

Figure 5.4. Lacon (LC) sample sites on the Illinois River (includes Wightman Lake, Sawyer Slough, Meadow Lake, and Babb Slough). Sediment core numbers and locations shown on ISWS (2008)²⁰³ quadrangle map (A) alongside an aerial photograph (B). Satellite photo ©Google Inc. 2008.

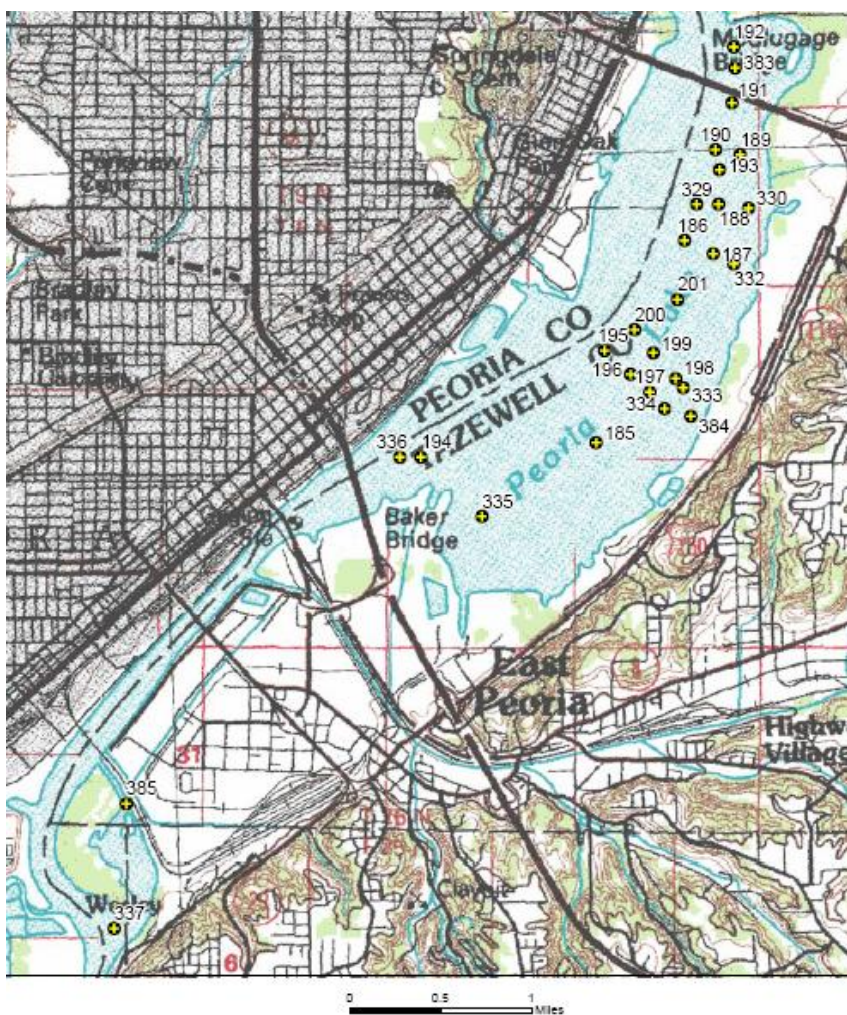


A)

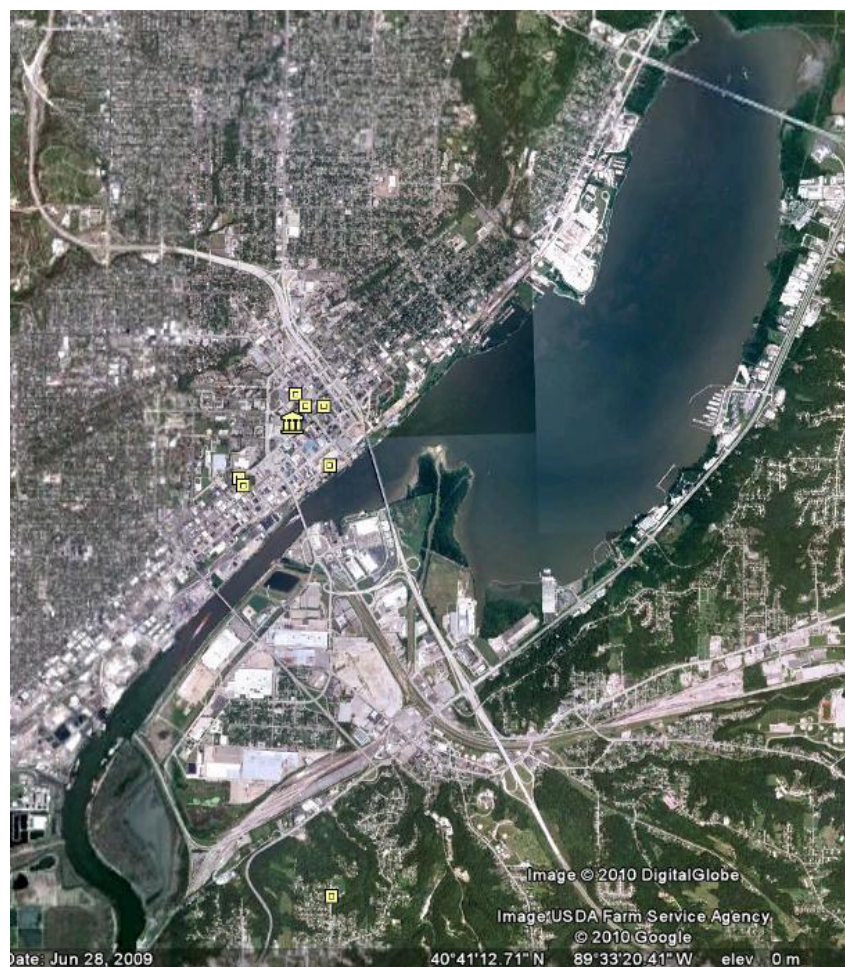


B)

Figure 5.5. Upper Peoria (UP) sample sites on the Illinois River (Upper Peoria Lake). Sediment core numbers and locations shown on ISWS (2008)²⁰³ quadrangle map (A) alongside an aerial photograph (B). Satellite photo ©Google Inc. 2008.



A)



B)

Figure 5.6. Lower Peoria (LP) sample sites on the Illinois River (Lower Peoria Lake). Sediment core numbers and locations shown on ISWS (2008)²⁰³ quadrangle map (A) alongside an aerial photograph (B). Satellite photo ©Google Inc. 2008.

Dataset preparation. A well-conditioned dataset retaining maximum informative capacity was prepared for source apportionment analysis. All samples were included except for cores over 40% non-detect (n=8, mainly bottom segments) and all priority PAHs were retained except for Nap and Ace which were detected only 16% and 52% of the time, respectively. All other PAHs had detection frequencies over 70%. Remaining non-detects (5% of the dataset) were replaced with half of the lowest measured analyte for each sample which was assumed to be near the true MDL. This process provided significantly more variation to the dataset than simply using the lowest measured sample value for each analyte. A linear regression analysis of ordered original and natural logarithm-transformed PAH data revealed two outliers with Studentized T-residuals > 3.0 for all original and many transformed PAHs, which were subsequently eliminated. The final PAH dataset is shown in Table 5.2 and comprises 14 compounds and 80 sediment cores for a total of 1120 data points.

Table 5.2. Illinois River sediment PAH data (ug/kg) for source apportionment analysis.^a

Core ^b	Depth ^c (cm)	RL ^d	Acy	Flo	Pha	Ant	Fla	Pyr	BaA	Chr	BbF	BkF	BaP	DahA	Ind	BghiP
HN281	8 - 190	29	47	24	78	63	290	360	190	320	200	220	250	73	160	200
HN282	8 - 250	37	41	39	120	70	340	400	210	320	210	200	210	27	150	190
HN283	8 - 250	37	56	18.5	100	76	410	470	260	360	240	240	260	70	140	200
HN284t	8 - 110	35	95	45	120	84	480	510	310	480	350	250	340	110	200	260
HN346	8 - 150	65	170	42	240	190	1100	1400	950	1000	1000	490	990	150	380	470
HN347	8 - 170	75	81	40	210	140	990	1100	570	670	650	290	530	68	200	250
HN348	8 - 150	70	47	28	110	70	530	560	300	390	350	210	300	51	150	190
HN285t	8 - 110	28	95	34	130	98	400	480	290	450	300	240	330	110	210	250
HN286t	8 - 110	30	59	27	100	59	280	430	180	290	180	200	210	70	65	170
HN286b	128 - 210	20	4.55	4.55	4.55	4.55	11	17	13	15	9.1	16	11	4.55	11	13
HN287t	8 - 130	30	38	22	48	32	160	220	110	190	110	130	130	42	80	130
HN287t	8 - 130	30	28	15	65	31	190	230	100	180	110	140	150	27	110	110
HN289	8 - 230	33	79	45	130	100	280	470	240	390	200	260	280	62	160	200
HN349t	8 - 130	64	49	36	130	74	460	580	250	340	340	160	290	56	140	180
HN349b	150 - 270	330	150	100	440	250	1700	1900	1000	1200	1100	510	950	170	450	560
HN270	8 - 170	27	45	18	36	38	170	220	120	160	110	120	140	38	76	98
HN271	8 - 210	33	29	17	40	37	190	190	110	150	84	110	110	30	63	82
HN272	8 - 190	28	260	97	370	280	1700	2100	1900	790	800	660	1200	230	460	550
HN272t	10 - 132	31	340	130	420	300	1900	2300	1200	1500	730	770	1000	290	480	600
HN272b	150 - 192	24	6.4	5.7	17	8.6	51	82	49	55	42	20	44	11	22	29
LC267	8 - 170	24	24	16	36	31	170	290	120	160	89	170	150	50	79	99
LC267t	10 - 112	29	47	27	65	52	360	480	260	310	190	260	240	82	130	170
LC268	8 - 246	32	31	22	60	46	270	310	160	170	110	170	160	51	88	110
LC252	8 - 250	68	140	68	230	210	1100	1100	590	660	640	430	550	76	280	350
LC254	8 - 190	63	180	64	320	250	1500	1500	980	910	770	530	750	100	320	440
LC273	8 - 210	29	5	17	63	50	240	250	140	200	120	140	180	38	81	100
LC274	8 - 230	34	110	35	180	120	700	690	390	590	300	390	510	110	230	280
LC275	8 - 90	26	50	17	49	50	230	320	170	240	170	180	220	53	110	150

Table 5.2. (continued). Illinois River sediment PAH data (ug/kg) for source apportionment analysis.^a

Core ^b	Depth ^c (cm)	RL ^d	Acy	Flo	Pha	Ant	Fla	Pyr	BaA	Chr	BbF	BkF	BaP	DahA	Ind	BghiP
LC276	8 - 250	25	5	5	11	10	38	44	28	34	26	32	35	10	19	29
LC276t	10 - 72	32	23	8.3	29	19	85	130	60	97	95	74	92	28	59	73
LC255	8 - 230	56	70	33	85	80	400	480	320	310	340	170	290	60	140	190
LC277	8 - 110	23	9.2	3.75	11	7.5	35	42	18	37	23	40	32	12	23	30
LC278	8 - 170	22	11	5.5	14	12	57	78	41	52	35	50	48	13	25	34
LC279	8 - 230	22	11	5.5	11	8.9	42	57	29	45	34	32	39	5.5	24	32
LC279t	10 - 92	27	25	9.8	32	25	110	170	77	110	83	110	100	34	68	84
LC256	8 - 230	62	34	15	39	54	200	230	110	160	170	83	120	23	73	100
LC265	8 - 170	25	28	15	53	33	150	230	160	170	130	150	160	55	95	130
LC266	8 - 190	30	63	30	100	79	400	640	310	460	300	340	420	130	210	280
LC250	8 - 170	56	96	31	140	99	500	590	420	400	450	140	390	70	190	230
LC251	8 - 230	66	120	66	170	140	710	840	550	560	530	330	460	71	220	280
LC280	8 - 130	27	71	29	300	160	710	640	410	480	330	300	430	110	210	240
LC352	8 - 90	51	8.5	8.5	40	17	98	130	65	81	97	37	93	18	49	70
UP353	8 - 90	50	4.8	4.8	21	9.6	55	85	36	52	73	35	55	11	28	37
UP354t	8 - 170	330	47	47	160	96	710	1200	490	610	650	300	520	94	250	330
UP362	8 - 170	58	120	93	350	210	1400	1900	850	1000	790	810	740	230	440	560
UP361	8 - 250	51	290	160	620	370	1900	2700	1500	1700	1600	750	1500	240	680	870
UP358	8 - 230	55	44	21	71	51	300	390	200	220	260	110	180	40	98	120
UP357	8 - 210	63	90	60	220	150	990	1300	590	660	690	320	540	96	260	340
UP356t	8 - 170	70	31	19	50	37	170	240	140	150	180	110	150	33	82	110
UP355	8 - 230	59	52	25	110	71	360	530	270	290	320	170	270	56	140	180
UP378	8 - 150	53	27	17	57	31	170	270	160	220	180	110	180	59	120	150
UP379	8 - 210	53	33	29	93	72	320	480	260	320	270	150	250	90	160	200
UP380	8 - 210	58	9	9	32	18	82	160	68	110	110	67	94	37	61	75
UP381	8 - 150	55	27	19	52	30	150	270	140	170	160	130	150	56	100	120
UP382	8 - 250	66	81	60	180	120	17	1000	450	670	490	430	500	160	290	340
LP383	8 - 250	56	39	37	92	46	370	430	230	310	200	240	210	57	130	150
LP192	8 - 230	56	34	19	74	45	300	390	130	240	180	130	150	28	77	100

Table 5.2. (continued). Illinois River sediment PAH data (ug/kg) for source apportionment analysis^a

Core ^b	Depth ^c (cm)	RL ^d	Acy	Flo	Pha	Ant	Fla	Pyr	BaA	Chr	BbF	BkF	BaP	DahA	Ind	BghiP
LP191	8 - 190	55	25	14	78	43	210	320	130	200	180	110	140	26	78	95
LP190	8 - 230	49	48	33	95	47	220	400	160	280	220	150	200	34	110	150
LP189	8 - 250	47	42	17	100	64	350	450	160	280	220	160	180	34	110	130
LP329	8 - 250	69	47	23	70	42	270	340	170	260	200	350	250	94	200	250
LP330	8 - 110	58	7	7	40	14	97	130	50	60	55	79	68	7	42	54
LP186	8 - 250	49	39	26	120	58	220	460	200	250	260	170	220	44	130	170
LP187	8 - 190	52	39	20	91	59	290	490	160	280	210	160	190	38	97	120
LP188	8 - 210	50	12	6	24	12	60	110	54	62	68	53	58	12	37	47
LP332t	8 - 90	59	8.5	8.5	24	17	130	160	61	85	92	110	76	27	59	72
LP200	8 - 250	66	78	33	160	88	410	610	250	430	460	210	340	84	190	310
LP199	8 - 250	62	47	21	110	74	380	540	220	360	380	170	250	42	140	230
LP198	8 - 150	82	21.5	21.5	21.5	21.5	100	170	63	99	120	63	62	21.5	43	92
LP197t	8 - 90	63	49	22.5	100	68	360	520	200	340	350	130	240	45	130	220
LP196	8 - 190	60	39	17.5	84	54	300	430	170	260	270	140	200	35	120	190
LP195	8 - 250	62	69	45	150	82	390	650	230	390	330	210	320	40	190	290
LP333	8 - 150	84	9.5	9.5	34	19	85	140	52	53	72	52	60	9.5	38	54
LP384	8 - 170	94	9.5	9.5	52	19	150	170	100	120	110	150	110	33	87	110
LP335t	8 - 130	69	22	11	56	42	240	280	120	170	170	180	150	45	94	130
LP335b	148 - 230	73	21	10.5	47	23	150	190	92	110	130	120	130	10.5	89	110
LP336	8 - 190	48	7	14	99	24	210	200	83	130	120	110	120	34	82	100
LP194	8 - 230	45	15	15	75	15	110	120	53	71	81	36	49	15	30	57
LP385	8 - 230	44	14	31	110	7	180	210	110	160	100	110	94	19	72	84
LP337	8 - 250	47	29	81	420	130	670	550	310	370	260	280	320	77	170	190

^a 14 PAHs and 80 samples. Bold values indicate approximate concentrations measured between the Method Detection Limit (MDL) and Reporting Limit (RL); italicized values indicate non-detect substitution with half the lowest analyte measurement (or RL in few cases where it is lower) for the sample.

^b Ordered generally from upstream to downstream. Naming convention by river reach (HN, LC, UP, LP), location number (186-385 corresponding to Figures 5.3-5.6), and whether whole core composite (no suffix) or segment composite (t denotes top, b denotes bottom).

^c Given as Upper Core Depth – Lower Core Depth.

^d Reporting Limit (RL) in ug/kg.

PAH Diagnostic Ratios. Diagnostic ratios have been developed to identify PAH sources in the environment based on relative characteristic proportions of PAHs in basic source types²⁷⁻³² and are extensively used in environmental forensics studies (e.g. Yunker et al. (2002)²⁷ has been cited in excess of 1100 times as of June, 2013). Diagnostic ratios consist of PAHs with stability ranges that represent thermodynamic (fossil) versus kinetic (combustion) formation and distinguish between sources based on relative proportions of one PAH to the other. Ratios typically contain PAHs of a given molecular mass like 178 (which includes Ant and Pha) and 202 (which includes Fla and Pyr) to minimize complications from varying PAH properties.²⁷ Yunker et al. (2002)²⁷ reviewed four parent PAH diagnostic ratios Ant/178, Fla/Fla+Pyr, BaA/228, and Ind/Ind+BghiP for determining PAH sources in sediment and has reported ratio ranges indicating fossil versus combustion sources as well as values for a number of petroleum-derived, combustion-derived, and environmental samples (Table 5.3).^{27, 32} Some ratios further distinguish liquid (petroleum) fuel combustion from solid (biomass/coal) fuel combustion. Although coal is not clearly differentiated from petroleum fossil fuel, ranges from samples have been reported.³² Molecular weight 178 refers to Ant+Pha and molecular weight 228 refers to BaA+Chr+Triphenylene (note however that the latter PAH is not considered in the present study).

Diagnostic PAH ratios were calculated for measured PAHs in Illinois River sediment and compared with diagnostic source ranges (Table 5.3) for identification in ratio scatter plots. A second diagnostic ratio analysis was performed on the Illinois River dataset following Positive Matrix Factorization (PMF) modeling (described in the next section). PAH ratios of both the PMF-modeled sources and reference sources were compared in diagnostic ratio scatter plots to provide another approach to source identification and a comparison of both methods.

Table 5.3 PAH diagnostic ratios of petroleum and combustion sources and samples.^a
Diagnostic ranges are bold.

	Ant/ 178	Fla/ Fla+Pyr	BaA/ 228	Ind/ Ind+BghiP
Petroleum	< 0.1	< 0.4	< 0.2	< 0.2 (< 0.1)^b
Kerosene	0.04	0.46	0.35	0.48
Diesel oil (n=8)	0.09	0.26	0.35	0.4
Crude oil (n=9)	0.07	0.22	0.12	0.09
Australian crude oils and fluid	0.03	0.43		
Shale oil	0.26	0.34	0.45	0.39
Lubricating oil		0.29	0.1	0.12
Coal (n=27)	0.2			
Asphalt			0.5	0.53
Coal (n=2) ^c	0.03 - 0.07	0.36 - 0.37	0.37 - 0.40	0.14 - 0.16
Combustion				
Liquid/Petroleum Fossil Fuel	> 0.1	0.4 - 0.5	> 0.35	0.2 - 0.5 (0.1 - 0.3)^b
Solid/Grass/Wood/Coal	> 0.1	> 0.5	> 0.35	> 0.5 (> 0.3)^b
Lignite and brown coal (n=3)	0.08	0.72	0.44	0.57
Bituminous coal (n=3)	0.33	0.53	0.34	0.48
Hard coal briquettes (n=9)		0.57	0.43	0.52
Coal tar (SRM 1597)	0.18	0.58	0.54	0.53
Wood soot (n=2)	0.26	0.5	0.46	0.55
Wood (n=19)	0.19	0.51	0.46	0.64
Grasses (n=6)	0.17	0.58	0.46	0.58
Gasoline (n=2)	0.11	0.44	0.355	0.155
Kerosene (n=3)	0.14	0.5	0.37	0.37
Diesel (n=25)	0.11	0.39	0.38	0.35
No. 2 fuel oil (n=2)	0.06	0.51	0.17	
Crude oil (n=4)	0.22	0.44	0.49	0.47
Environmental Samples				
Bush fire		0.61	0.23	0.7
Savanna fire particulate (n=3)		0.59		0.39
Road dust	0.18	0.42	0.13	0.51
Lubricating oil, re-refined		0.74		0.36
Used engine oil, gasoline passenger car	0.22	0.3	0.5	0.18
Used engine oil, diesel car, truck & bus		0.37		0.29
Tunnel with light duty gasoline vehicles (n=4)		0.45	0.46	0.3
Tunnel with heavy duty diesel trucks & gasoline vehicles n=5)		0.42	0.57	0.3
Roadway tunnels (n=2)	0.13	0.43	0.42	0.3
Urban air (including SRM 1648 & 649;n=3)	0.8	0.56	0.3	0.4
Creosote treated wood piling (n=4)	0.2	0.62	0.5	0.64

^a Reproduced from Yunker et al.(2003).²⁷ 178 indicates Ant+Pha and 228 indicates BaA+Chr+ Triphenylene (note only BaA and Chr are considered in the present study). Petroleum and combustion ranges used in diagnostic ratio plots are bold.

^b Updated ranges are in parentheses, from Yunker et al. (2012).³²

^c Coal range from Yunker et al. (2012)³² is based on samples of shipwrecked high volatile A bituminous coal.

Positive Matrix Factorization. A Positive Matrix Factorization (PMF) multivariate receptor model was used to quantitatively apportion measured PAH mass in Illinois River sediment to sources of contaminants. PMF has commonly been applied to particulate matter in air, but the technique has also been successfully used to apportion PAHs in sediments,¹⁴⁴ as have other multivariate^{65, 205} and mass balance^{23, 64, 206, 207} receptor models. Multivariate receptor models assume measured concentrations are a linear sum of sources and utilize factor analysis to solve Equation 5.1 for m compounds in n samples as contributions from p independent sources.^{125, 149, 192} The model assumes sources have unique contaminant compositions that change little during transport.^{64, 196} In the present study, we assume sediment receives PAHs mainly in particulate-associated form, that these PAHs are relatively stable,⁶⁴ and that they come from sources relatively nearby (such as barge coal).⁶⁵

$$\mathbf{X} = \mathbf{G} \times \mathbf{F} + \mathbf{E} \quad (5.1)$$

\mathbf{X} is the measured concentration data matrix $m \times n$; \mathbf{G} is the factor-loading matrix $m \times p$, representing chemical profiles for sources; \mathbf{F} is the factor-score matrix $p \times n$, representing source contributions for sample concentrations; \mathbf{E} is the error concentration matrix $m \times n$, difference between measured and calculated matrices.

PMF uses a constrained weighted least squares approach to solve Equation 5.1, iteratively computing \mathbf{G} and \mathbf{F} by minimizing an objective function Q (Equation 5.2). During Q minimization, \mathbf{G} and \mathbf{F} are constrained to non-negativity to ensure physically realistic source

profiles and contributions. PMF weights measured data by their estimated uncertainties to reduce the influence of censored and outlier data on solutions.^{135, 136}

$$Q(\mathbf{E}) = \sum_{i=1}^m \sum_{j=1}^n \left(\frac{E_{ij}}{\sigma_{ij}} \right)^2 \quad (5.2)$$

Q is the objective function or the weighted sum of squares difference between estimated and measured data; \mathbf{E}_{ij} is the error concentration matrix; σ_{ij} is the standard deviation concentration matrix of uncertainties weighting each measured element.

This study utilizes the PMF program coded by Bzdusek (2005)¹⁴⁵ on the MATLAB platform (release 2011a, Mathworks, Inc., Natick, MA, USA). The model employs penalty terms for imposing constraints, and has been shown to obtain results similar to the standalone PMF program available from USEPA.^{125, 146} Details of the algorithm can be found in Bzdusek (2005)¹⁴⁵ and convergence criteria, step length control, penalty coefficients, and other variable model parameters are described in Chapter 4 (see Table 4.2). Input to the model includes the measured data matrix, the weighting matrix, and the number of sources. The weighting matrix is estimated by environmental error model (EM) = -14^{147, 148} (see Chapter 4, Eq. 4.4) with a relative error of 0.25 representing analytical, sampling, and environmental uncertainties.

Sensitivity analysis. In addition to the 14x80 data matrix (referred to in the text as 14x80) three other datasets were input to assess the sensitivity of the PMF model; a 14x84 dataset including the two outliers and two cores with low rates (40-50%) of PAH detection (referred to as 14x84OUT), a 15x84 dataset including the PAH Ace (referred to as 15x84), and a 14x84 dataset with non-detects substituted with half the lowest value for each analyte rather than for each

sample (referred to as 14x84ND). The PMF model was run multiple times investigating different numbers of sources. Diagnostic tools including coefficients of determination (CODs), Exner function, the objective function Q (or chi-square), and the number of degrees of freedom were also generated with each run to assist in evaluating goodness of fit between modeled and measured data and in choosing the correct solution and number of sources.¹⁴⁵

Source profile analysis. The model output consists of source profiles (**G**) normalized to total source contaminant mass (in this case Σ_{14} PAHs for each source) in units of mass percent. Inspection of PMF profiles and comparison with known reference profiles are essential for identifying potential sources. The cosine phi ($\cos \phi$) coefficient of proportional similarity metric was used to calculate the similarity of PMF and reference source profiles where the cosine of the angle ϕ between the vectors equals one if they are identical with matching direction and zero if dissimilar and perpendicular (see Chapter 4, Eq. 4.7).¹³³ Nearly 50 coal, oil, combustion, and other urban PAH source profiles from the scientific literature were compiled, representing a variety of sources. Reference profiles were computed as a mass percent (usually of Σ_{14} PAHs) for direct comparison to model profiles. Non-detect PAHs were considered as zero or as half the detection limit (when available) for profile computation and $\cos \phi$ calculations. When individual PAHs were unavailable they were not included in the $\cos \phi$ calculations.

Select reference profiles are shown in Figure 5.7 and the complete set of reference profiles are tabulated and described in Tables 5.4 through 5.6. Note that profiles may not add to exactly 100% because of rounding. Coal profiles in Table 5.4 from Stout and Emsbo-Mattingly (2008)²⁰⁸ include coals of various levels of diagenetic alteration such as less mature lignite and sub-bituminous ‘brown’ coals commonly used for power generation, bituminous coals commonly used in industrial applications like coke production for iron and steel industry, and highly mature

less common anthracite.³⁵ Profiles of coal or coke particles recovered from marine sediments near a sunken coal carrying vessel by Victoria BC, Canada³⁶ and of coal dust used in a PAH bioavailability study³⁷ were also included. Combustion profiles (Table 5.5) include literature-compiled coal and traffic-derived profiles from Li et al. (2003)⁶⁴ and a wood burning profile from Bzdusek et al. (2004)⁶⁵ adjusted to particulate-only form using reported gas-particle partitioning in air (see Chapter 4, Table 4.5). Gasoline and diesel soot,⁴⁷ diesel particulate²⁰⁹ and modern diesel equipment (adjusted from total to particulate-only profile)³⁹ were also included. Table 5.6 includes a variety of other anthropogenic, oil, and particulate PAH sources including Metropolitan Water Reclamation District of Greater Chicago (MWRD-GC) biosolids,⁶⁷ new and used lubricating oil,⁴⁶ and a number of coal tar (CT) related sources including coal tar,⁵⁵ creosote,⁵⁹ coal tar sealcoat runoff dust,²² and coal tar sealcoat dust from Chicago suburb parking lots, driveways, and nearby streets.⁵⁶ Additional traffic related profiles include street dust⁵⁰ and tire debris, used crankcase oil, asphalt, and roadside air (adjusted from total to particulate-only profile)⁴⁷ as well as urban dust.⁶⁹

Source contribution analysis. Contributions from each source to the total PAH burden at each sample (F) are presented in concentration units (ug/kg). Source contribution plots can be examined in terms of river location (reach, lake, or main channel) and proximity to tributaries, urban runoff, and point sources to aid source identification. Though overall core depths and a few depth-resolved cores (top and bottom segments) are available, lack of sediment dating precludes the use of specific time records to inform the analysis. Physical and chemical characteristics of the sediment are not available to consider other drivers of PAH contamination.

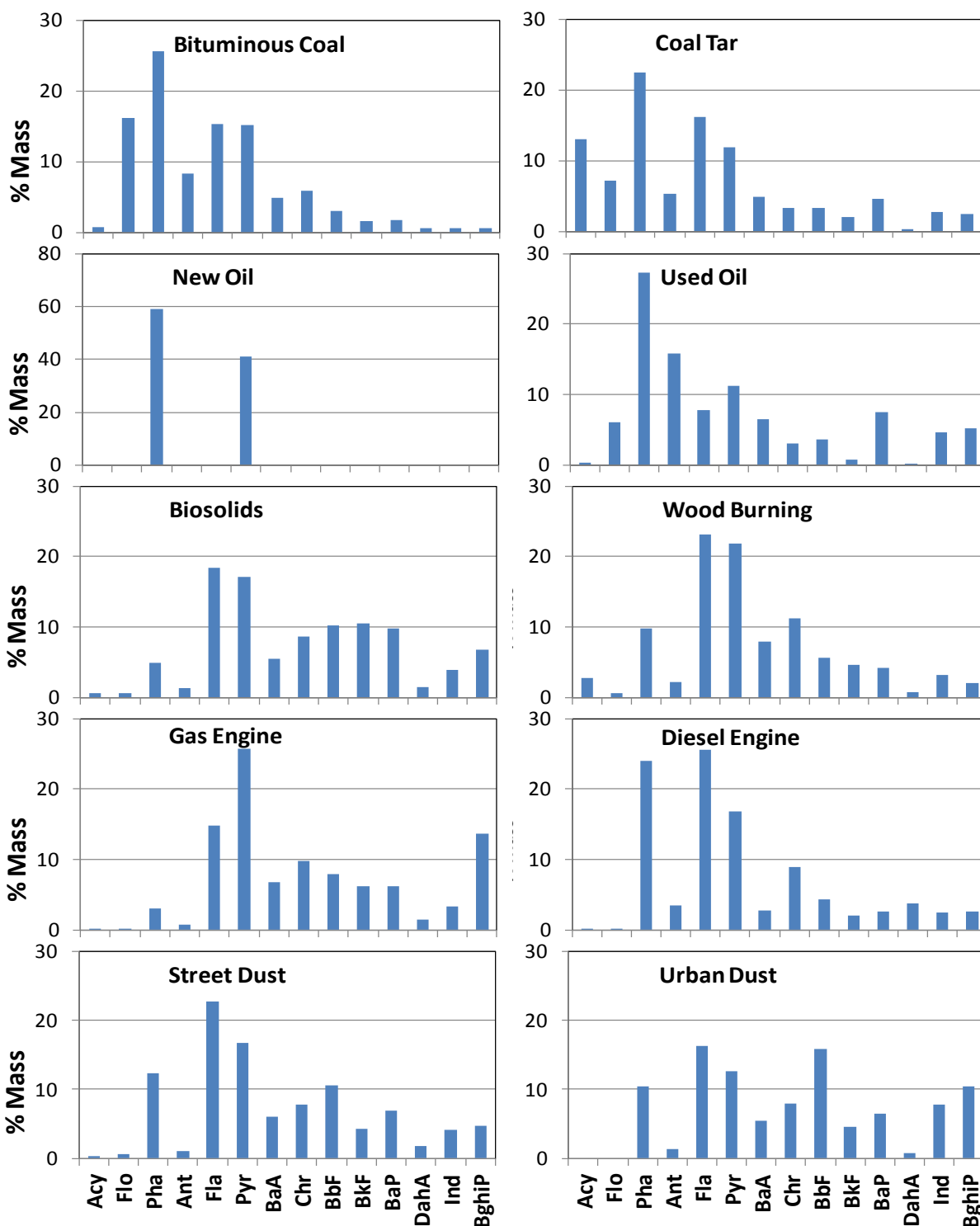


Figure 5.7. Select PAH reference source profiles. Bituminous coal (high-volatile C rank) from Stout and Emsbo-Mattingly (2008),⁶⁸ coal tar from Wise et al. (2010),⁵⁵ new and used lubricating oils from Wang et al. (2000),⁴⁶ biosolids an average from two MWRD drying bed samples for Gulezian et al. (2012),⁶⁷ wood burning from Bzdusek et al. (2004),⁶⁵ gas and diesel engine from Li et al. (2003),⁶⁴ street dust from Boonyatumanond et al. (2006),⁵⁰ and urban dust standard from NIST (2009).⁶⁹ Note all axes are the same except for new oil.

Table 5.4. Coal PAH source profiles (%).^a

	LigA1	LigA2	SubC1	SubC2	SubB1	SubB2	SubA	HVC	HVB	HVA1	HVA2	MV	LV	Semi	Anth	Coal or coke ^b	Coal dust ^c
Acy	nd	nd	nd	nd	nd	nd	0	1	1	1	3	1	0	nd	nd	2	5
Flo	2	1	3	0	8	4	0	16	15	11	10	11	23	8	28	8	9
Pha	6	8	4	10	23	15	1	26	46	23	54	60	43	30	48	26	34
Ant	1	1	1	nd	1	1	1	8	0	18	1	1	1	0	nd	7	3
Fla	31	14	24	20	23	29	17	15	5	12	4	3	1	2	nd	8	11
Pyr	17	28	41	24	23	28	18	15	10	9	7	4	3	3	24	9	9
BaA	5	10	6	5	7	6	7	5	6	7	6	3	3	1	nd	8	2
Chr	7	10	7	14	5	6	7	6	5	9	6	13	14	20	nd	8	19
BbF	16	14	6	10	3	4	21	3	3	3	2	2	6	21	nd	7	BF 6
BkF	6	7	3	5	2	2	10	2	2	2	2	0	0	1	nd	2	
BaP	2	3	2	5	2	2	7	2	4	2	3	1	1	2	nd	7	1
DahA	1	0	0	0	0	0	1	1	0	0	0	0	1	3	nd	1	na
Ind	4	4	2	5	1	1	7	1	1	1	1	0	1	3	nd	3	na
BghiP	1	1	1	3	0	1	3	1	2	1	2	1	3	5	nd	4	1

^a First fifteen profiles from concentrations in coals of various rank from Stout and Emsbo-Mattingly (2008).²⁰⁸ Lig (Lignite) A and B; Sub (Sub-bituminous) C1, C2, C3, B1, B2, and A; Bituminous HV (High Volatile) C, B, A1, and A2; Bituminous MV (Medium Volatile); Bituminous LV (Low Volatile); Semi (semi-anthracite); and Anth (anthracite). Non-detect PAHs indicated by nd.

^b From Chapman et al. (1996)³⁶ from concentrations in particles recovered from marine sediments.

^c From Bender et al. (1987)³⁷ concentrations in coal dust extract..Benzofluoranthene (BF) given in place of BbF and BkF. Unavailable PAHs indicated by na.

Table 5.5. Combustion PAH source profiles (coal, petroleum, and wood) (%).^a

	Coke Oven	Power Plant	Residential	Ave Coal	Gas Engine	Diesel Engine	Ave Gas & Diesel	Traffic Tunnel	Ave Petroleum	Wood Burning	Gas Soot	Diesel Soot	Diesel Particulate	Diesel Equip.
Acy	4	na	na	2	0	0	0	1	1	3	na	na	na	6
Flo	2	1	0	1	0	0	0	1	1	0	na	na	na	5
Pha	7	15	34	17	3	24	19	10	17	10	4	30	33	37
Ant	2	2	7	3	1	4	3	2	3	2	1	4	4	3
Fla	8	17	22	14	15	26	23	10	17	28	5	12	23	6
Pyr	8	15	9	12	26	17	19	12	17	26	9	20	21	19
BaA	11	10	5	9	7	3	4	6	5	8	5	5	3	3
Chr	12	20	7	12	10	9	9	10	10	9	5	11	6	5
BbF	13	8	7	10	8	4	5	9	6	3	BF 13	BF 7	3	4
BkF	8	2	3	5	6	2	3	6	4	3			1	1
BaP	10	4	3	6	6	3	3	7	5	3	11	5	1	3
DahA	2	1	na	1	2	4	3	4	3	0	na	na	0	0
Ind	4	3	2	3	3	3	3	9	6	2	15	3	2	3
BghiP	7	4	2	4	14	3	5	11	7	1	32	5	3	5

^a Coke oven, power plant, residential, average coal, gasoline engine, diesel engine, average gas and diesel engine, traffic tunnel, and average petroleum reported by Li et al. (2003)⁶⁴ and wood burning reported by Bzdusek et al. (2004)⁶⁵ from mean of profiles compiled from the literature and corrected to particulate- only profiles from reported gas-particulate partition coefficients. Gasoline and diesel soot from Boonyatumanond et al. (2007);⁴⁷ total benzo(a)fluoranthene (BF) given in place of BbF and BkF Diesel particulate standard from National Institute of Standards and Technology (NIST) (2008).²⁰⁹ Modern diesel equipment emission with catalytic control (steady state engine out test configuration) from Laroo et al. (2011)³⁹ was adjusted from total (gas + particulate) to particulate only profile using reported partitioning in air from Li et al. (2003).⁶⁴ Unavailable PAHs indicated by na.

Table 5.6. Oil, coal tar, traffic, and other particle-derived PAH source profiles (%).^a

	Bio- solids	New Oil	Used Oil	Coal Tar (CT)	Creosote	CT Seal Dust A	CT Seal Dust B	CT Seal Parking Lot Dust	CT Seal Drwy Dust	Street Dust by CT Lots	Street Dust	Tire Debris	Used Crankcase Oil	Asphalt	Road- side Air	Urban Dust
Acy	1 ±0	Nd	0	13	na	na	na	0 ±0	0 ±0	0 ±0	na	na	na	na	na	na
Flo	1 ±0	Nd	6	7	19	1 ±0	1 ±0	0 ±0	1 ±0	1 ±0	na	na	na	na	na	na
Pha	5 ±2	59	27	23	30	15 ±3	11 ±3	12 ±1	13 ±3	12 ±1	11	5	29	22	2	10
Ant	1 ±0	Nd	16	5	30	2 ±1	2 ±1	1 ±0	1 ±0	1 ±1	2	1	10	4	0	1
Fla	18 ±4	Nd	8	16	9	32 ±2	27 ±1	25 ±2	28 ±0	23 ±0	23	15	13	10	4	16
Pyr	17 ±4	41	11	12	5	21 ±1	21 ±1	19 ±1	20 ±1	17 ±0	25	42	21	14	7	13
BaA	6 ±1	Nd	6	5	na	6 ±2	9 ±1	5 ±1	5 ±0	6 ±1	6	2	6	3	5	6
Chr	9 ±2	Nd	3	3	5	14 ±2	16 ±1	9 ±1	8 ±1	8 ±0	11	9	5	9	12	8
BbF	10 ±1	Nd	4	3	na	na	Na	11 ±1	9 ±1	11 ±1	BF 9	BF 4	BF 4	BF 12	BF 33	16
BkF	10 ±3	Nd	1	2	na	na	Na	3 ±0	3 ±0	4 ±0						5
BaP	10 ±1	Nd	8	5	2	7 ±2	10 ±2	6 ±1	5 ±0	7 ±0	4	3	5	8	17	7
DahA	1 ±0	Nd	0	0	na	2 ±1	2 ±1	1 ±0	0 ±0	2 ±1	na	na	na	na	na	1
Ind	4 ±1	Nd	5	3	na	na	na	4 ±1	3 ±0	4 ±0	3	2	3	5	2	8
BghiP	7 ±1	Nd	5	3	na	na	na	5 ±1	4 ±0	5 ±1	7	17	4	12	17	10

^a Biosolids from two Metropolitan Water Reclamation District-Chicago District (MWRD-CD) drying bed grab samples from Gulezian et al. (2012);⁶⁷ mean profile ± range/2. New and used lubricating oil from Wang et al. (2000);⁴⁶ non-detects indicated by nd. Coal tar (CT) standard from Wise et al. (2010).⁵⁵ Creosote from Mueller et al. (1989).⁵⁹ Coal tar (CT) sealcoat dust runoff of test plots A and B from Mahler et al. (2005);²² mean profiles ± σ from n=3 sampling events for each. CT sealed parking lot, driveway, and nearby street dust of Chicago suburb from Van Metre et al. (2008);⁵⁶ mean profiles ± σ (parking lot, n=3), ± range/2 (driveway, n=2), and ± σ (street dust, n=3). Street dust from Boonyatumanond et al. (2006)⁵⁰ and tire debris, used crankcase oil, asphalt, and roadside air from Boonyatumanond et al. (2007);⁴⁷ benzo(a)fluoranthene (BF) given in place of BbF and BkF; roadside air is adjusted from total to particulate only profile using reported partitioning in air from Li et al. (2003).⁶⁴ Urban dust standard from National Institute of Standards and Technology (NIST) (2009).⁶⁹ Non-detect PAHs indicated by nd and unavailable PAHs indicated by na.

5.4. Results and Discussion

Dating information and specific sedimentation rates for these cores are unknown, however a recent study reported sedimentation rates averaged between 1 to 2 cm/yr since 1954 as determined by ^{137}Cs dating for many of the same Illinois River backwater lakes.²⁰² Previous studies referencing bathymetric surveys of Upper and Lower Peoria Lakes estimated sedimentation rates between 2 and 3 cm/yr from 1903-1985 and > 5 cm/yr between 1976 and 1985, with overall rates at Upper Peoria Lake (UP) 1.5 times higher than Lower Peoria Lake (LP).^{210, 211} Although reported sedimentation rates vary over time and space, it is likely that most/all whole cores (average depth 203 cm) span the twentieth century and witnessed major anthropogenic changes to the river. These include diversion of water from Lake Michigan, construction of navigational dams, locks, and major dredging operations, as well as changes to the drainage basin such as enlargement for the Chicago metropolitan region and dramatic increases in agricultural use and intensity.^{210, 211}

Measured levels and trends. Mean PAH concentrations (Figure 5.8) from the 80 Illinois River sediment cores ranged from 25 ug/kg (Flo) to 520 ug/kg (Pyr). The mean profile was dominated by four-ring PAHs and similar in appearance to the gas engine profile (see Figure 5.7). Sediment PAH concentrations were less than TACO²⁰⁴ background soil concentrations and cleanup standards (see Table 5.1) for all PAHs except for BaP (281 ug/kg relative to its remediation standard of 90 ug/kg).

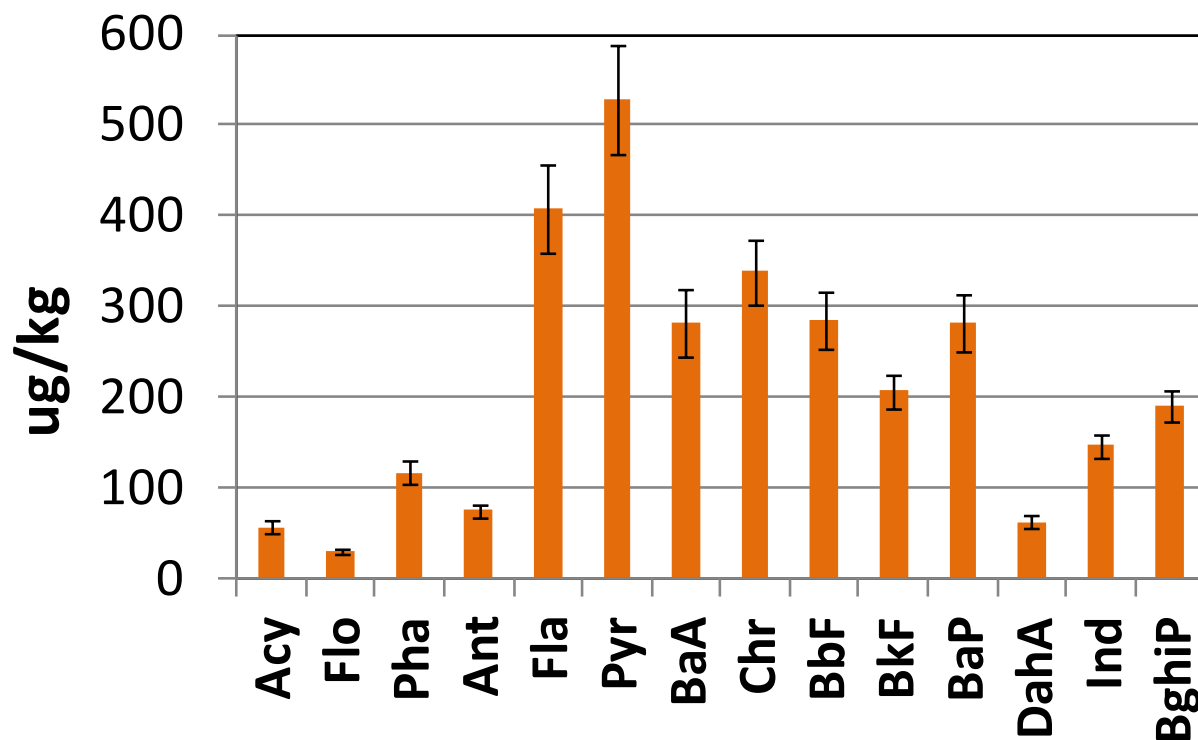


Figure 5.8. Average PAH profile of IL River sediment cores from all sites (n=80). Error bars represent standard error.

Based on Lilliefors test for normality and histogram plots (Figure 5.9), PAHs were not normally distributed and more closely approximate a log-normal distribution. Total PAHs (Σ_{14} PAHs) ranged from 139 to 14880 ug/kg (Figure 5.10). Except for site HN349, Σ_{14} PAHs in bottom segments were significantly less than in top segments and whole cores. This suggests that PAH contamination was lower in the past. While no clear trend is evident from upstream to downstream, Σ_{14} PAHs levels were typically elevated in sediments near the main channel (HN 346-347, HN 272, LC 252-254, UP 361-362). PAH levels were also lower and less variable in reach LP (Figure 5.10). UP and LP were the only reaches with significantly different ($p < 0.05$) PAH levels.

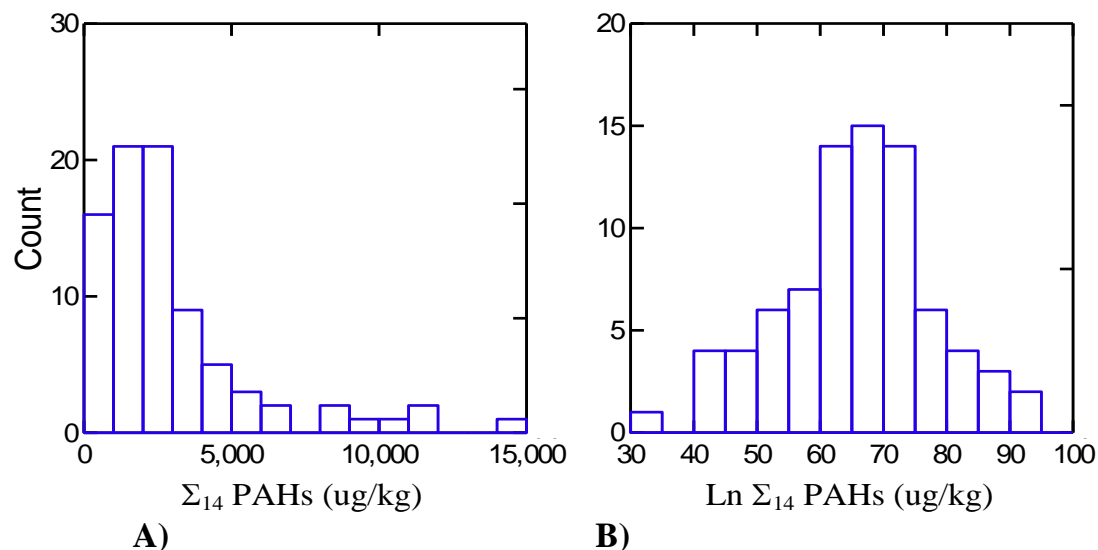


Figure 5.9. Histograms of Σ_{14} PAH with (A) original and (B) natural log-transformed data, indicating log-normal distribution of PAHs in Illinois River sediment. (n=80)

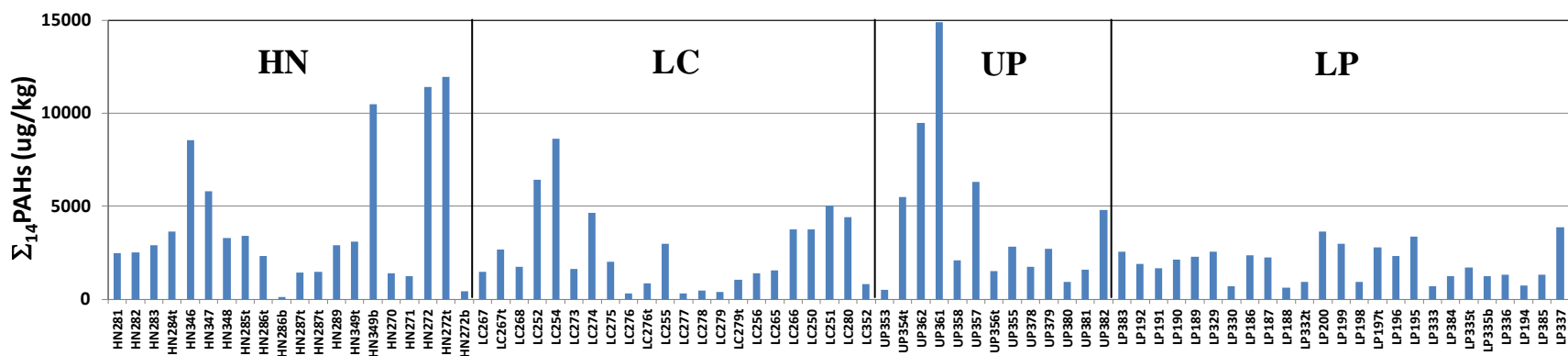


Figure 5.10. Total (Σ_{14}) PAHs for all samples (n=80) plotted roughly in transect from upstream to downstream.

Σ_{14} PAH concentrations were highest at UP (4224 ug/kg) and lowest at LP (1923 ug/kg) (Figure 5.11). The relative PAH distribution in each reach was very similar, with four-ring PAHs comprising the majority of the total. These results may suggest similar sources and differential transport of PAHs to reaches of the Illinois River.

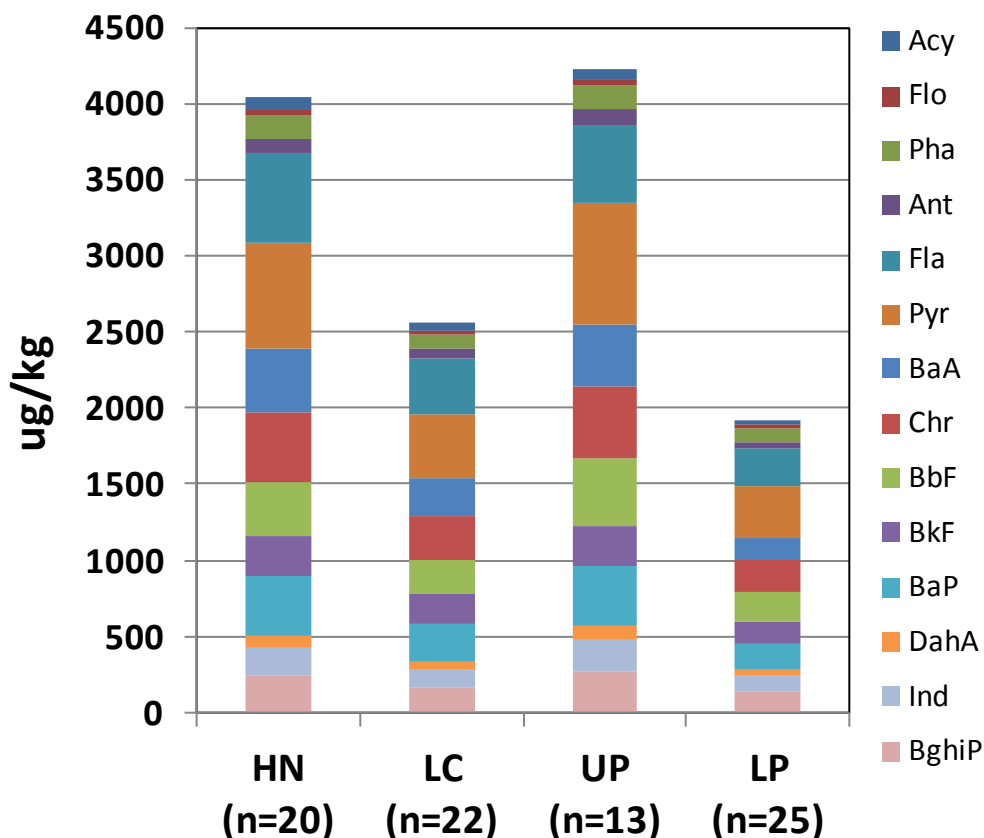


Figure 5.11. Mean PAH levels and distribution at sampling reaches.

Of the 80 core samples, only 15 top segments and four bottom segments were reported in this study (see Table 5.2). Σ_{14} PAHs in top segments were not statistically different from those in whole cores, but were significantly different at the 95% CL from Σ_{14} PAHs in all bottom cores except sample HN349b (Figure 5.12). At average depths of 144 cm to 226 cm, bottom cores that

represent older sediment had significantly less PAH input (with the exception of HN349b). Once again all cores had relatively similar PAH distributions.

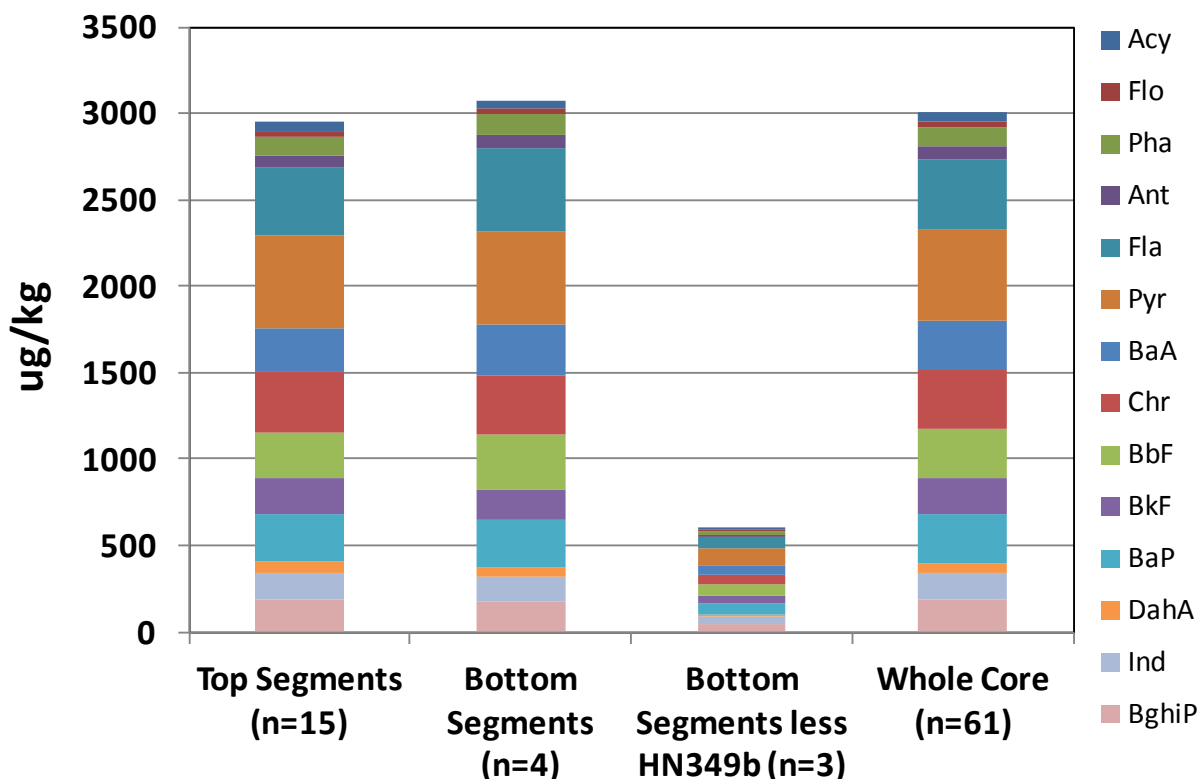


Figure 5.12. Mean PAH levels and distribution for top segments, bottom segments, and whole cores.

Comparison of individual PAHs in upper and lower core segments at each site where pairs are available further indicated that PAH deposition in the past was lower (Figure 5.13). In three out of the four cases (HN286, HN272, and LP335) PAHs were greatly enriched in upper segments (i.e. all data were well below the 1:1 line). It is unclear why HN349 contains roughly five-fold higher PAH levels in the bottom core segment than the top.

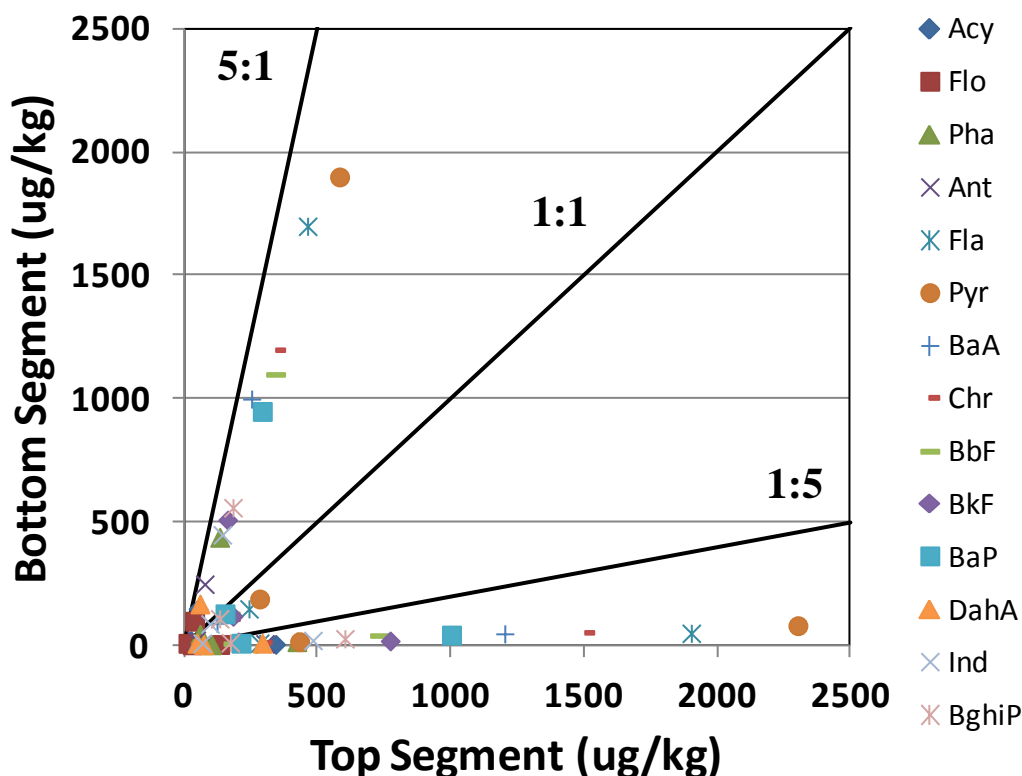


Figure 5.13. PAH differences between paired top and bottom segments. Points below the 1:1 line indicate higher PAH levels in top segments of cores than bottom. Points above the 1:1 line indicate higher levels in bottom segments.

PMF model performance and sensitivity analysis. Diagnostics for the two-, three-, and four-source PMF solutions are shown for both the 14x80 and the 14x84OUT datasets in Table 5.7. When unstable, solutions with the lowest Q value are shown. PMF solutions for the 14x80 and the 14x84OUT datasets are quite similar with only minor differences in source contributions and diagnostic values (Table 5.7), indicating that a small number of outliers and low-detect samples do not strongly influence results. In both cases the improvement in fit (CODs approaching to 1) and decrease in Q is more significant when increasing from two to three sources than when further increasing from three to four sources. The three-source solution has CODs > 0.89, the

Exner function < 0.04 , and a recalculated relative error of 0.227; indicating an adequate reconstruction of the measured data matrix.

Sensitivity of the PMF model output to different techniques for non-detect reporting were investigated using the 14x84ND dataset and the 15x84 dataset including Ace (Table 5.8). Unlike the previous sensitivity analysis, the method of non-detect replacement has a strong effect on the PMF model output, despite non-detects only comprising $< 6\%$ of the data. This is demonstrated by varied contributions and much higher Q values (Table 5.8); requiring higher source numbers to achieve reasonable relative errors compared to results in Table 5.7. The findings demonstrate that the 14x84ND dataset is not well-conditioned for PMF due to greater frequency of repeating values (i.e. all non-detects for a compound have the same value). Furthermore, this method does not make use of RL and MDL information inherent in the approximate data reported for every sample, resulting in a dataset less reflective of the true variation. The PMF output using the 15x84 dataset also yields altered contributions compared to the 14x80 dataset, particularly for the four-source solution (Table 5.8). Clearly Ace is not fit well based on the low COD value (which does not rise above 0.80 until a seven-source solution is reached) and retaining it in the analysis is not justified given its low discriminative capacity in the source profiles. PMF solution profile correlations of the base 14x80 dataset with the datasets used in sensitivity analysis (14x84OUT, 14x84ND, and 15x84) are shown in Table 5.9. As expected, 14x84OUT profiles are very similar to 14x80 profiles for all source number solutions, while 14x84ND and 15x84 profiles are much more variable. Thus the PMF model output was not significantly impacted by the inclusion of a few outliers and highly non-detect cores (14x84OUT), but was impacted by the inclusion of an infrequently-detected compound (15x84) and by using a constant non-detect replacement method (14x84ND).

Table 5.7. PMF model diagnostics and sensitivity analysis with different sample numbers.

Dataset	14x80 ^a			14x84OUT ^b		
	Two	Three ^c	Four ^c	Two	Three	Four ^c
Source number solution	Two	Three ^c	Four ^c	Two	Three	Four ^c
% Source Contributions	74, 26	48, 27, 25	42, 29, 19, 10	74, 26	47, 28, 25	43, 29, 20, 8
Objective Function Q ^d	1315.09	693.85	552.69	1418.79	765.06	607.61
Relative Error (RE) ^e	.297	0.227	0.215	.301	0.233	.220
Degrees of Freedom (ν) ^f	932	838	744	980	882	784
Exner Function ^g	.0398	0.0341	0.0256	.0426	0.0314	0.0228
Coefficients of Determination (CODs) ^h						
Acy	.87	.98	.99	.90	.97	.99
Flo	.89	.89	.90	.94	.94	.94
Pha	.87	.89	.91	.94	.93	.94
Ant	.97	.97	.97	.98	.97	.96
Fla	.97	.97	.99	.98	.96	.99
Pyr	.97	.97	.97	.99	.98	.98
BaA	.87	.89	.90	.90	.94	.94
Chr	.97	.96	.97	.93	.95	.95
BbF	.92	.96	.98	.87	.97	.98
BkF	.93	.93	.97	.93	.93	.98
BaP	.97	.97	.97	.98	.98	.98
DahA	.93	.95	.96	.93	.96	.97
Ind	.97	.98	.99	.97	.99	.99
BghiP	.95	.96	.97	.96	.98	.98

^a Dataset 14x80 from Table 5.2.

^b Dataset 14 x 18OUT with outlier and low-detect samples retained.

^c Solution instability. Chosen solution has the lowest Q value, or if Q values have < 1% difference is the most frequently generated solution.

^d Based on 0.25 RE of measurements.

^e Recalculated by setting Q = ν .

^f ν calculated by $m \cdot n + p(n+m)$.

^g Best fit at 0.

^h Best fits at 1.

Table 5.8. PMF model diagnostics for sensitivity analysis with a different non-detect substitution method and analyte number.

Dataset	14x84ND ^a				15x84 ^b		
Source number solution	Two ^c	Three ^c	Four		Two	Three	Four ^c
% Source Contributions	69, 31	39, 36, 25	37, 35, 19, 9		74, 26	42, 33, 25	57, 20, 19, 4
Objective Function Q ^d	3511.56	2695.13	1484.07		1667.33	1016.70	632.68
Relative Error (RE) ^e	.473	0.437	.344		.313	0.257	.214
Degrees of Freedom (ν) ^f	980	882	784		1062	963	864
Exner Function ^g	.0842	0.0359	0.0335		.0428	0.0345	0.0331
Coefficients of Determination (CODs) ^h							
Acy	.89	.97	.98	Acy	.90	.98	.98
Flo	.90	.90	.98	Flo	.95	.96	.98
Pha	.90	.93	.96	Pha	.94	.95	.94
Ant	.97	.98	.97	Ant	.98	.97	.96
Fla	.88	.97	.97	Fla	.95	.95	.97
Pyr	.95	.98	.98	Pyr	.99	.99	.98
BaA	.82	.91	.92	BaA	.90	.93	.92
Chr	.90	.93	.94	Chr	.93	.95	.94
BbF	.94	.96	.96	BbF	.86	.90	.95
BkF	.68	.93	.93	BkF	.93	.93	.94
BaP	.97	.97	.98	BaP	.98	.98	.98
DahA	.89	.95	.96	DahA	.93	.95	.96
Ind	.89	.99	.99	Ind	.97	.98	.99
BghiP	.87	.98	.98	BghiP	.96	.97	.98
				Ace	.72	.74	.80

^a Dataset 14x84ND has non-detects substituted with half the lowest value for each analyte.

^b Dataset 15x84 includes Ace (infrequently detected) PAH.

^c Solution instability. Chosen solution has the lowest Q value, or if Q values have < 1% difference is the most frequently generated solution.

^d Based on 0.25 RE of measurements.

^e Recalculated setting $Q = \nu$.

^f ν calculated by $m*n+p(n+m)$.

^g Best fit at 0.

^h Best fits at 1.

Table 5.9. Pearson correlation coefficients between PMF solution profiles of the base (14x80) and varied datasets.^a

		14x80										
		Two			Three				Four			
		74%	26%		48%	27%	25%		42%	29%	19%	10%
14x84OUT	74%	1.00	0.21	47%	1.00	0.73	0.31	44%	1.00	0.41	0.8	-0.11
	26%	0.23	1.00	28%	0.73	0.98	0.06	28%	0.35	1.00	0.12	0.09
				25%	0.27	0.13	1.00	19%	0.78	0.17	0.98	-0.25
								9%	-0.16	-0.07	-0.12	0.99
14x84ND	69%	0.98	0.35	39%	0.89	0.91	0.00	37%	0.90	0.71	0.63	0.02
	31%	0.39	0.85	36%	0.95	0.69	0.58	35%	0.92	0.35	0.91	-0.33
				25%	0.22	0.16	0.99	19%	0.13	0.61	0.09	0.78
								9%	0.16	0.08	0.06	0.55
15x84	74%	1.00	0.21	42%	0.88	0.96	0.16	57%	0.95	0.63	0.72	-0.05
	26%	0.23	1.00	33%	1.00	0.72	0.30	20%	0.79	0.21	0.98	-0.28
				25%	0.26	0.13	1.00	19%	0.13	0.55	0.11	0.83
								4%	-0.03	0.43	-0.51	0.03

^a. Correlation Coefficients > 0.90 bolded. See Tables 5.7 and 5.8 for dataset descriptions and two- to four-source solution diagnostics.

PMF source profiles and contributions. The three-source PMF solution from the original 14x80 dataset was chosen for further investigation, as it provided adequate reconstruction of the receptor matrix with the least number of sources and a relatively low recalculated relative error representing analytical, sampling, and environmental uncertainty (0.23) (see Table 5.7). The primary PAH source (S1) is predicted to contribute 48% of the total PAH mass to the Illinois River and is dominated by Pyr, Fla, and BbF (Figure 5.14). The second source (S2) is predicted to contribute 27% of the total PAH mass, and is high in Fla and Pyr, as well as other four-ring PAHs. The main differences between S1 and S2 are the presence of Pha in S1, the presence of Acy and DahA in S2, and higher proportions of Pyr to Fla and BbF to BkF in S1 compared to S2. The third source (S3) is predicted to contribute 25% of the PAH burden (Figure 5.14). S3 does not contain Fla, but is more uniformly loaded with four- and five-ring PAHs. S3 also has the highest relative BkF through BghiP loadings of all the sources.

PAH contributions from all sources are similar for most samples, but greater peaks and variability are evident for S1 and S2 in certain cores, particularly upstream of LP (Figure 5.15). Large relative PAH S1 contributions at sites with much higher levels of Σ_{14} PAHs may indicate local and/or point sourcing. Source S3 is least correlated with S1 and S2 at sites LC252, 254 and 256-280 (where it is lower); and sites UP382 and LP329 (where it is higher).

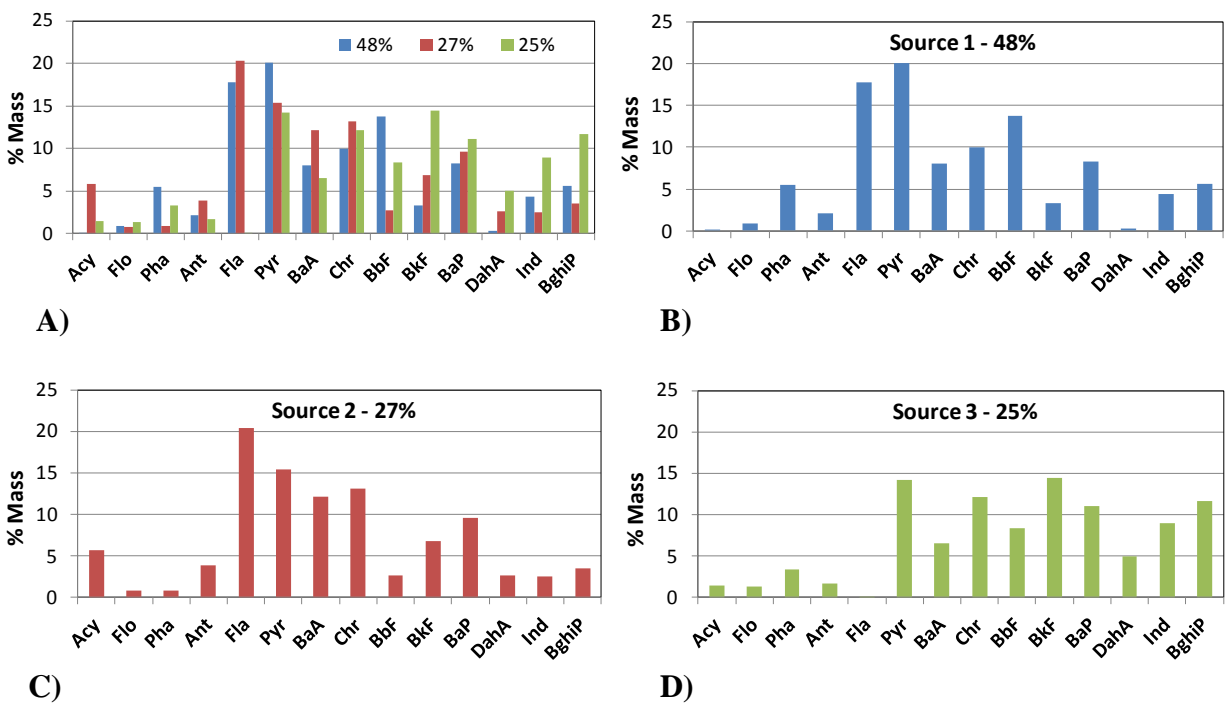


Figure 5.14. PAH source composition profiles from three-source PMF solution. Profiles shown (A) together and individually for (B) S1, (C) S2, and (D) S3.

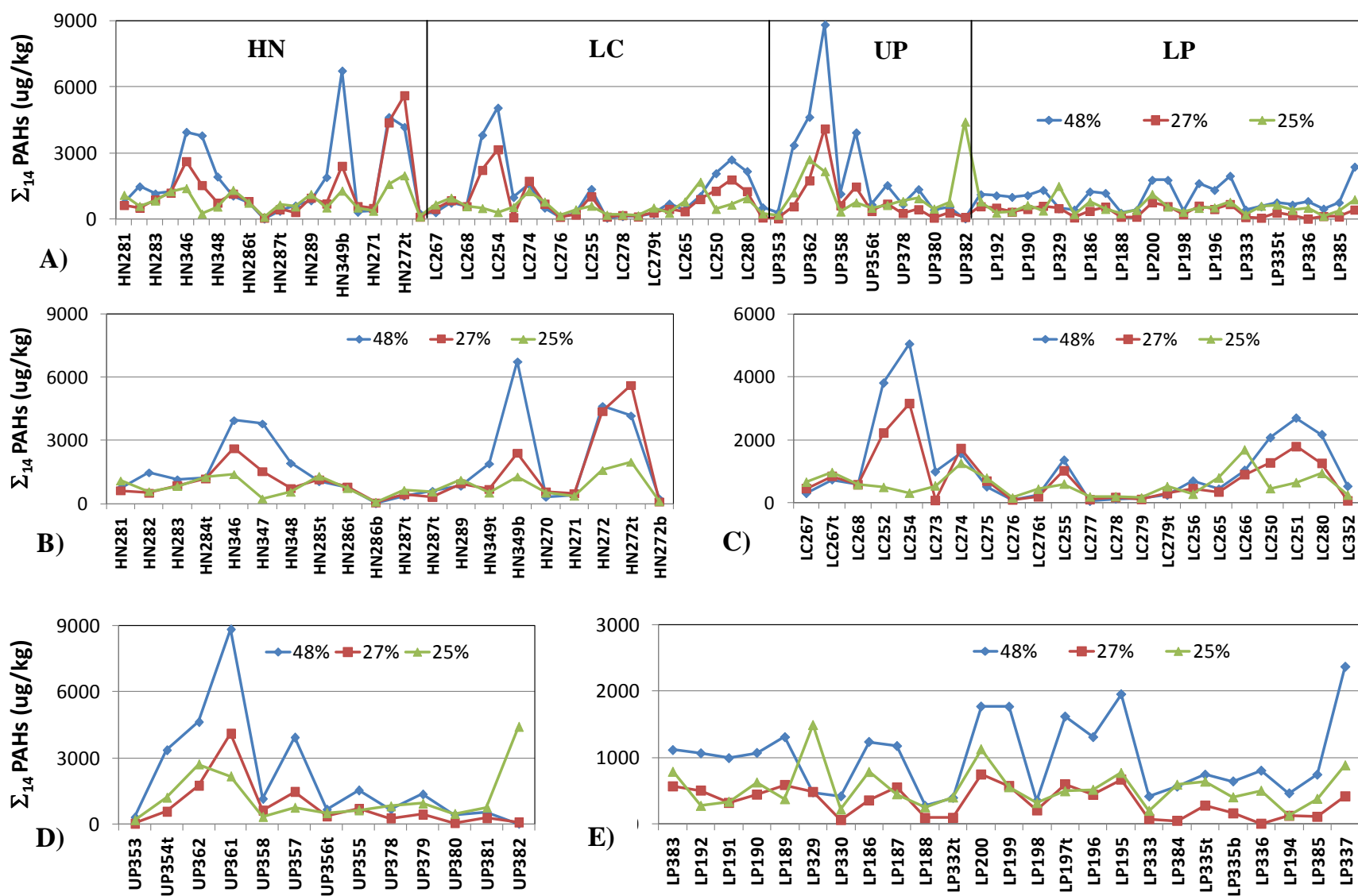


Figure 5.15. PAH source contributions from three-source PMF solution. The (A) overall source contribution plot is shown in greater detail by (B) HN, (C) LC, (D) UP, and (E) LP reaches. Note different y-axis scales.

Reference profile analysis. Cos ϕ values between modeled sources (S1-S3) and PAH reference profiles are given in Table 5.10 (values over 0.95 are in bold). Sources S1 and S2 match lignite and sub-bituminous coal profiles, but not bituminous or anthracite coal profiles. Modeled sources are similar to combustion-derived sources, with particularly strong matches between source S1 and gas engine and between sources S1 and S2 and wood burning (cos $\phi > 0.92$). Gas soot is one of the few compiled reference sources that is more similar to S3 than to S1 or S2. Most modeled sources have PAH profiles that resemble those of Illinois soils, biosolids, urban dust, roadside air, and coal tar related dust from parking lots and driveways (Table 5.10) but not new oil, used oil, coal tar, or creosote. Source S1 is very similar to background soil, coal tar sealcoat dusts, and biosolids (cos $\phi > 0.95$), S2 is most like coal tar sealcoat dust (cos $\phi > 0.95$), and S3 is most strongly related to roadside air (cos $\phi > 0.90$). Thus PMF results suggested that a mixed upland source and coal or wood-derived sources such as coal tar sealcoat (sources S1 and S2, 75%) are major contributors to sediment PAHs in the Illinois River, as well as a traffic-based roadside air source (S3, 25%). Another conclusion from these observations is that the majority of reference sources are similar to modeled sources, making definitive source assignments based solely on cos ϕ values impossible considering reference profile uncertainties. This is illustrated by the fact that more than half of S1 and S2 comparisons with compiled reference profiles have cos ϕ values > 0.7 (Table 5.10). For this reason coal dust was not uniquely resolved from the coal-derived sources and thus could not be assessed for reduced PAH bioavailability. In addition, the overall lack of naphthalene in these sediments (which is a major component of coal), is not consistent with the presence of coal in sediments.²⁰⁸

To be able to interpret the PMF results, we must first understand the nature of PAH sources to the sediment. Possible sources of PAHs to the sediment include direct discharges (wastewater, transport spills), as well as sedimentation from the upper watershed and tributaries, and erosion of agricultural soils. The soil may have acquired PAHs via atmospheric deposition, open/biomass burning, equipment use, or biosolids application. While exposed to air and sunlight, soils undergo particle aging that may alter the original source profile. Furthermore, PAH accumulation in sediments is determined by sediment composition, black carbon content, and organic content or grain size.²⁸ The agricultural nature of the Illinois River watershed, mixture of different sediment types, and various transport pathways (including PAH incorporation into soil subsequently eroded and deposited in sediments) may inhibit clear resolution of sources.

Comparison of PAH source apportionment in other sediment studies. A number of studies have analyzed sources of PAHs to different lacustrine, marine, and riverine sediment environments using various source apportionment and receptor modeling techniques. The majority of PAHs in sediments in Lake Calumet in Chicago, IL, USA have been sourced to traffic and coke oven emissions utilizing both Chemical Mass Balance⁶⁴ and factor analysis based receptor models.⁶⁵ A recent source apportionment analysis of PAHs in suburban lake sediment throughout the USA concluded that the majority of PAHs are now derived from use of the coal tar sealant, with vehicle sources as the second most important source.⁵⁷ This study did not identify coke ovens as a significant source. PAHs in Lake Michigan sediment were found to be impacted by traffic, coal (coke), and wood burning sources in an analysis of dated sediment cores.⁸¹ Marine sediments near Victoria, BC, Canada were reported to contain PAHs related to wood combustion, coal, coke, petroleum combustion, and traffic related sources from atmospheric deposition, stormwater runoff, and wastewater discharges.³² The Fraser River basin

was found to be impacted by a variety of sources dominated by petroleum combustion sources near urban areas, and biomass combustion in remote areas.²⁷ A source apportionment study of PAHs in sediment cores of the Kinnickinnic River, WI concluded coke oven, coal tar/coal wood gasification, and highway dust were the most important contributors of PAHs over time.²⁰⁷ Primary PAH sources to Black River sediments and Ashtabula River sediments in Ohio were found to be traffic, next coke oven, and finally wood burning/coal tar related.²⁰⁵ Most of the above-referenced studies utilized significant amounts of external information to make these conclusions, such as sediment characteristics, sediment dating, source sampling, and detailed watershed knowledge. Resolution of sources in riverine systems can be particularly difficult or even impossible due to differential deposition, mixing, scouring, and resuspension of sediment. In the present study, unique identification of sources in the Illinois River appears to be limited by collinearity of reference sources, lack of local and historical information, lack of core temporal resolution (i.e. modeling of core composites), and complexities in the source-receptor pathway.

Table 5.10. Cosine ϕ similarity of PMF modeled and reference PAH source profiles.^a

Coal																	
	LigA1	LigA2	SubC1	SubC2	SubB1	SubB2	SubA	HVC	HVB	HVA1	HVA2	MV	LV	Semi	Anth	Coal or coke	Coal dust
S1	0.92	0.95	0.87	0.96	0.81	0.87	0.95	0.67	0.42	0.61	0.35	0.31	0.34	0.54	0.36	0.74	0.58
S2	0.83	0.82	0.80	0.87	0.73	0.82	0.81	0.59	0.30	0.58	0.24	0.19	0.22	0.34	0.21	0.64	0.53
S3	0.52	0.72	0.54	0.69	0.46	0.47	0.74	0.41	0.34	0.43	0.28	0.24	0.31	0.51	0.27	0.61	0.45

Combustion														
	Coke Oven	Power Plant	Residential	Ave Coal	Gas Engine	Diesel Engine	Ave Gas & Diesel	Traffic Tunnel	Ave Petroleum	Wood Burning	Gas Soot	Diesel Soot	Diesel Particulate	Diesel Equip.
S1	0.86	0.89	0.66	0.90	0.94	0.81	0.88	0.90	0.91	0.94	0.63	0.75	0.72	0.58
S2	0.82	0.86	0.58	0.82	0.86	0.74	0.80	0.81	0.82	0.92	0.54	0.65	0.62	0.44
S3	0.87	0.66	0.38	0.70	0.80	0.47	0.57	0.88	0.70	0.62	0.79	0.58	0.41	0.46

Oil, coal tar (CT), traffic, and other																	
	Bio-solids	New Oil	Used Oil	Coal Tar (CT)	Creosote (CT)	CT Seal Dust A	CT Seal Dust B	CT Seal Parking Lot Dust	CT Seal Drv-way Dust	Street Dust by CT Lots	Street Dust	Tire Debris	Used Crank case Oil	Asphalt	Road-side Air	Urban Dust	Back-ground Soil ^b
S1	0.96	0.45	0.61	0.69	0.39	0.95	0.98	0.96	0.93	0.96	0.94	0.81	0.72	0.82	0.75	0.94	0.95 +/-0.01
S2	0.91	0.27	0.51	0.67	0.34	0.90	0.96	0.87	0.86	0.87	0.91	0.73	0.64	0.70	0.63	0.80	0.90+/-0.01
S3	0.80	0.33	0.49	0.45	0.31	0.61	0.73	0.61	0.55	0.64	0.65	0.62	0.50	0.76	0.93	0.76	0.77+/-0.02

^a Cos ϕ values above 0.95 or best fits > 0.90 for each source are bold. See Tables 5.4 through 5.6 for reference profile information and Figure 5.14 for modeled profiles S1 (48%), S2 (27%), and S3 (25%).

^b Soil background profile average +/- standard deviation from Chicago, other metropolitan, and non-metropolitan area (Table 5.1).

Ratio analysis. PAH ratios were calculated from sediment measurements and compared to diagnostic ratio domains to estimate the predominant PAH sources to Illinois River sediment. Site-averaged Illinois River sediment PAH data generally cluster in ratio domains consistent with combustion (Figure 5.16). The main exception is the Fla/Fla+Pyr ratio which places UP in the petroleum source domain. River reaches are likely to represent areas with similar hydrologic and watershed characteristics and thus have similar non-local PAH sources, and diagnostic ratio results indicating combustion-derived sources support this expectation. Ratios distinguishing between petroleum and coal/biomass combustion (Fla/Fla+Pyr and Ind/Ind+BghiP) indicate petroleum combustion, although ‘updated’ Ind/Ind+BghiP ranges signify coal or biomass combustion.

The observed variability among ratios (particularly for Fla/Fla+Pyr and Ind/Ind+BghiP) for reported samples casts some doubt on the ability of the ratio method to accurately and uniquely identify sources (Figure 5.16). In fact for all ratios, a number of petroleum samples appear in the petroleum combustion domain and even in the coal/biomass combustion domains. Conversely, combustion samples can also be found in conflicting petroleum domains. However, contradictory results utilizing different diagnostic ratios does not necessarily mean the results are incorrect; they may reflect a distribution of overlapping contributions of PAHs from particular sources to the total PAH mass, as shown by the PMF results discussed above. Illinois River PAH ratios are similar to those for a number of petrogenic and combustion sample types, except for the Ant/Ant+Pha ratio that computes higher values in sediments (toward the combustion range) than in reference samples (Figure 5.16).

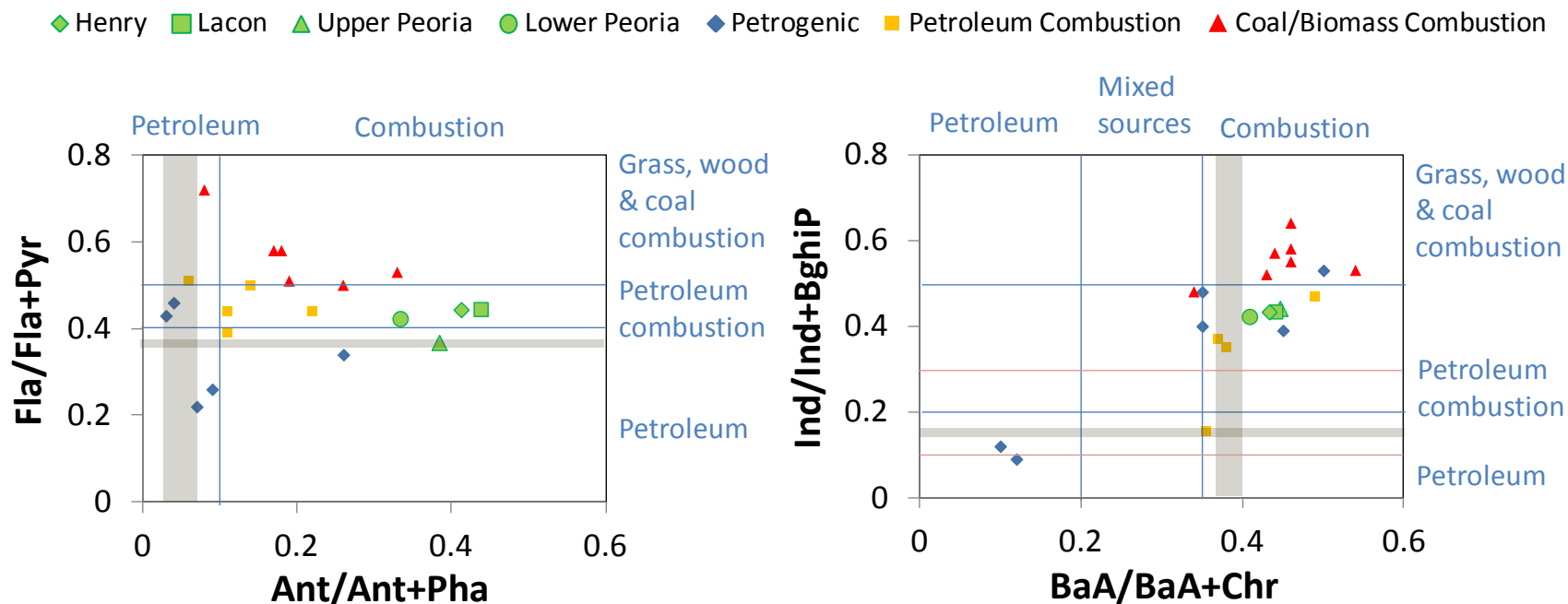


Figure 5.16. PAH diagnostic ratio plots of site-averaged Illinois River sediment and literature-compiled petrogenic and combustion samples from Table 5.3. Source ranges are delineated in blue from Yunker et al. (2002)²⁷ according to Table 5.3. Shaded gray indicates coal domains of bituminous coal samples and pink lines delineate recently updated source ranges for Ind/Ind+BghiP from Yunker et al. (2012).³²

PAH ratios in sediments from all cores as well as modeled profiles from the PMF three-source solution (S1, S2, and S3) are shown together in Figure 5.17. PAH ratios in cores are generally similar within, as well as between sites. S1 clusters with samples in the petroleum combustion region, while S2 and S3 deviate from the sample cluster for lower molecular weight ratios $\text{Ant}/\text{Ant}+\text{Pha}$ and $\text{Fla}/\text{Fla}+\text{Pyr}$, respectively. The $\text{Ind}/\text{Ind}+\text{BghiP}$, $\text{BaA}/\text{BaA}+\text{Chr}$, and $\text{Ant}/\text{Ant}+\text{Pha}$ ratios indicate all modeled sources are combustion-derived. In contrast, the $\text{Fla}/\text{Fla}+\text{Pyr}$ ratio places sources S1, S2, and S3 in petroleum combustion, coal/biomass combustion, and petroleum domains, respectively (Figure 5.17). The ratios $\text{Ant}/\text{Ant}+\text{Pha}$ and $\text{BaA}/\text{BaA}+\text{Chr}$ suggest contributions from bituminous coal sources to the Illinois River sediments, however PMF modeled sources do not fall within any coal ratio ranges. Ratio analysis suggests modeled sources are combustion-derived with possible petroleum influence on S3. However variability between and ambiguity within ratios prevents clear or detailed source assignment.

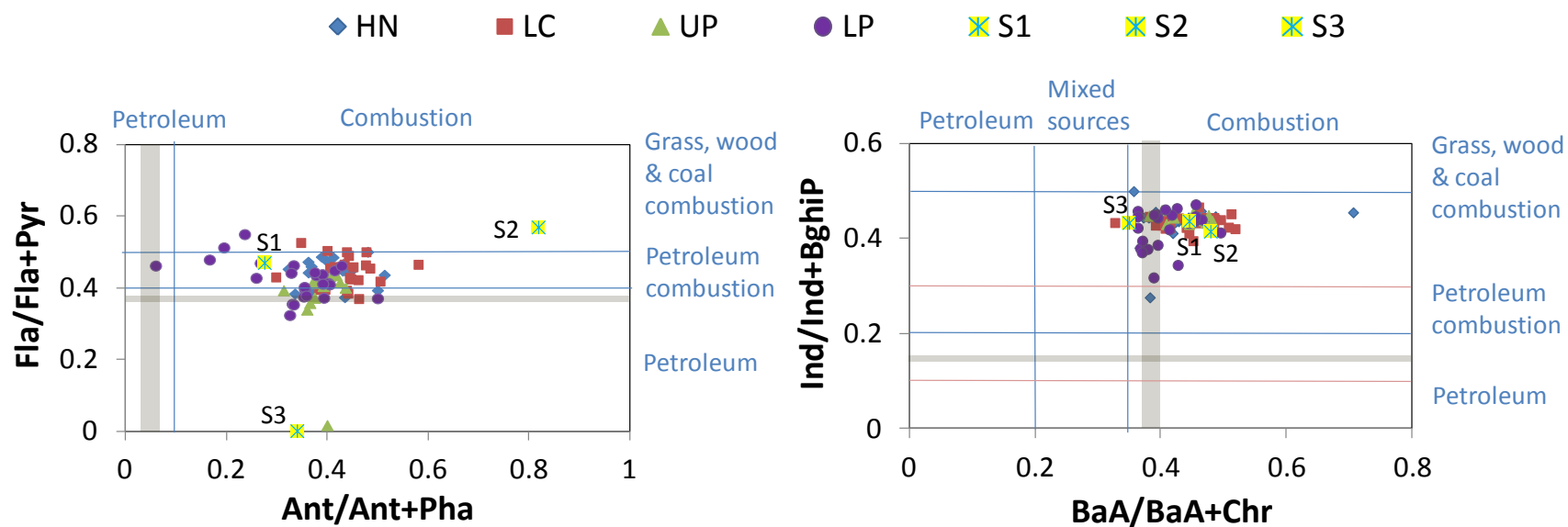


Figure 5.17. PAH diagnostic ratio plots of Illinois River sediment samples and PMF modeled sources. Source ranges are delineated in blue from Yunker et al. (2002)²⁷ according to Table 5.3. Shaded gray indicates coal domains of bituminous coal samples and pink lines delineate recently updated source ranges for Ind/Ind+BghiP from Yunker et al. (2012).³²

PAHs ratios of reference sources obtained from the literature (Figure 5.18) are not always consistent with the source identified by the diagnostic ratio domains. For instance Fla/Fla+Pyr indicates a petroleum non-combustion source for gas engine emissions and a coal/biomass combustion source for diesel engine emissions. All ratios indicate a combustion source for used lubricating oil. Many samples such as processed or weathered materials do not fit uniformly in a given ratio space. For example, the PAH ratios in parking lot dust, tire debris, and biosolids appear in conflicting diagnostic domains and clearly lack specificity. This represents a limitation of the ratio method for detailed source apportionment analysis. PAH ratios in coals generally distribute across the ratio domains, with semi-anthracite appearing in petroleum regions and lignite appearing in the combustion regions (Figure 5.18). Bituminous coal overlaps with the semi-anthracite, sub-bituminous, and lignite for Ant/Ant+Pha, Fla/Fla+Pyr, and BaA/BaA+Chr ratios, respectively. Based on varying PAH distributions with coal rank, the ratio plots as well as other diagnostic parameters²⁰⁸ cannot uniquely represent fossil coal for determination of coal particles in sediment. Modeled sources have higher Ant/Ant+Pha diagnostic ratios than most reference sources, appearing well within the combustion range (note S2 is not visible in Figure 5.18 as described in caption, but can be seen in Figure 5.17). Overestimation of Pha loading in environmental samples by mass balance receptor models using similar source profiles has been observed previously.^{23, 206} The observed lack of measured Pha in the present study, and thus lower Ant/Ant+Pha ratios, might be due to the increased mobility and/or degradation of Pha relative to Ant in the sediment. In fact, faster desorption and microbial degradation of Pha relative to Ant in soil has been reported to change the original profile or ratio.²⁸ The lability of LMW PAHs in soil or sediments may render this ratio less reliable as a diagnostic tool.

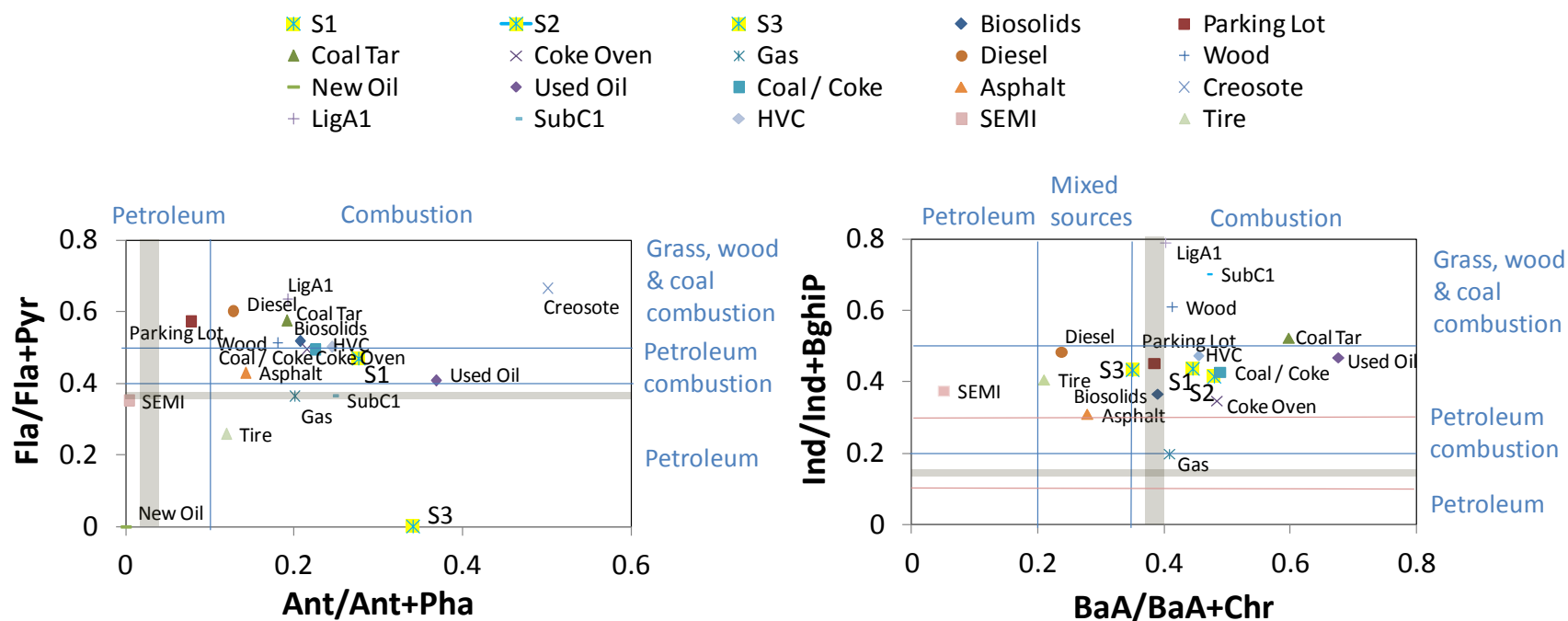


Figure 5.18. PAH diagnostic ratio plots of select reference sources and PMF modeled sources. Source ranges are delineated in blue from Yunker et al. (2002)²⁷ according to Table 5.3. Shaded gray indicates coal domains of bituminous coal samples and pink lines delineate recently updated source ranges for Ind/Ind+BghiP from Yunker et al. (2012).³² S2 has an Ant/Ant+Pha ratio of 0.82 (combustion) and a Fla/Fla+Pyr ratio of 0.57 (coal/biomass combustion) and is not shown on the left plot in order to better observe reference sources (see instead Figure 5.17).

5.5. Implications

PMF results suggested that a mixed upland source and coal-derived sources like coal tar sealcoat (sources S1 and S2, 75%) are major contributors to sediment PAHs in the Illinois River, as well as a diffuse traffic-based source (S3, 25%). The best fit predictions for PMF profiles identified lignite or sub-bituminous coal sources, biosolids, coal-tar sealcoat dust, and/or background soil sources for S1, the predominant PAH source to the Illinois River sediments. Coal dust was not uniquely resolved from the coal-derived sources, however, and thus could not be assessed for reduced PAH bioavailability. The second most important source was most closely associated with coal tar sealcoat dust. The third source did not match with any source with $\cos \phi > 0.95$, but matched traffic-related roadside air with $\cos \phi > 0.90$. None of the source profiles indicated significant petroleum inputs to sediments. Due to reference source similarity, these predicted sources of PAHs to the Illinois River must be confirmed using additional site-specific source information.

The existing dataset was prepared for PMF by removing samples and analytes over 40% non-detect and identified outliers and replacing non-detects with half the lowest analyte value (approximating the MDL) for each sample. The sensitivity analysis demonstrated that PMF was robust to minor additions of outlier and low-detect samples, mildly robust to the addition of an infrequently detected analyte, and least robust to other methods of non-detect replacement. This has important implications for use of PMF in subsequent source apportionment studies. The results indicate that non-detect estimation decreases certainty of the output in spite of the increasing degrees of freedom obtained by adding more data. Estimating non-detects with many constant values is particularly problematic for PMF and less desirable than a method that retains variation in the data.

The use of PAH diagnostic ratios predicted petroleum combustion input to Illinois River sediment, but significant limitations of the method decrease confidence in the results. Contradictory results from the four diagnostic ratios and literature-compiled environmental samples and reference profiles indicate all ratios are not accurate or reliable for all sources. Diagnostic ratio accuracy was notably poor for sources with different degrees of aging (used versus new oil, coal tar parking lot dust versus coal tar) and for fossil coal sources whose ratios were commonly distributed in combustion domains and not uniquely represented. Ratios can also be misleading if samples are impacted from more than one source. For example, ratios may indicate petroleum combustion impacts to Illinois River sediment even though they represent a combination of coal tar sealcoat, traffic, and other possible sources. The results of this study demonstrate that PMF is a more accurate method than diagnostic ratio analysis for performing a detailed, quantitative, multiple-source apportionment study. The diagnostic ratio approach alone is not sufficient to uniquely identify PAH sources, although we show a unique method of visualizing PMF sources and reference sources by combining PMF and ratio analysis.

Source apportionment results may be confirmed with additional site information. For example, the proximity of core locations to anthropogenic sources and activities could be examined (e.g. distances from towns, shorelines, main channel, harbors, docks, and coal stockpiles) and compared to PMF contribution results to aid source identification. A more definitive source apportionment analysis is also possible by increasing the number of PAHs in the dataset beyond the typical PAH priority pollutant list to better represent coal and other sources not clearly defined by priority PAHs alone, and by dating of sediment cores to improve source resolution and discern source evolution over time.

CHAPTER VI. CONCLUSIONS AND IMPLICATIONS

The Chicago region suffers from a legacy of historic contamination and continuous release of industrial and traffic related pollution. Persistent PAH and PCB semivolatile organic contaminants impact the Chicago area of influence throughout multiple environmental media including the atmosphere and sediments of the Chicago Waterway System including Indiana Harbor and Canal (IHC), the Illinois River, and Lake Michigan. This collection of Positive Matrix Factorization (PMF) source apportionment case studies examines the sources of one of the most commonly analyzed contaminant groupings, 16 priority PAHs, in a contaminated air-shed near Chicago and also in a relatively less contaminated riverbed in the Illinois River, as well as PCBs in the contaminated air-shed utilizing existing datasets. PMF is a powerful and incisive tool for quantitative source determination of contaminants, however not all analyses result in confident source assignment due to various limitations of the model, data, contaminants, media, and application. The following conclusions and recommendations are drawn from the present study to support successful source apportionment for management and reduction of pollution.

Implicated contaminant sources. The atmosphere at the IHC over the last decade has been dominated by PAHs from nearby byproduct recovery coke and steel production, followed by petroleum storage activities and then vehicular emissions. Nearby source locations, reported emissions, and meteorological data confirm this apportionment and the results demonstrate a primary need for industrial control of emissions.

Illinois River PAH source profiles resemble background soils, coal-derived sources including coal tar sealcoat, and a diffuse transportation-based source that suggest mixed upland sources rather than direct inputs may drive PAH contamination. Low rank coal dust profiles were similar

to the main PAH source profile, but were not uniquely resolved and thus not assessed for reduced PAH bioavailability.

Atmospheric PCBs are driven by legacy contamination of the environment, generally resembling the Aroclor mixtures they were used in for industry. Sediments contaminated with Aroclor 1248 are a main contributor to atmospheric PCBs at the IHC. However other sources are undefined, as most PCB sources in the Chicago region are not known or poorly characterized. While PCBs, especially dioxin-like congener 118, are often more toxic than the priority LMW PAHs, the overall health impact from PAHs may be greater considering PAH atmospheric concentrations (primarily Nap) were on average 1000 times greater.

Existing datasets for source apportionment. PMF and other source apportionment methods operate on contaminant data measured at a receptor site. In these analyses, PMF was performed on pre-existing datasets collected by agencies for monitoring and beneficial reuse programs. Use of existing data saves time and resources otherwise spent on sampling and analysis, and in many cases allows for studies that would otherwise be unfeasible such as the collection of an equivalent IHC air quality dataset spanning over ten years. However existing data may be of low or unknown quality, contain an undesirable choice of compounds or number of samples, and lack useful supplementary data.

Existing data requires thorough cleaning and validation and should undergo detailed analysis prior to source apportionment to understand overall levels, trends, and identify possible source-receptor relationships. Statistical analyses of atmospheric PAHs and PCBs revealed significant spatial, temporal, and meteorological patterns such as the reduction of most contaminants with time and dependency of most contaminants on temperature explained by the Clausius-Clapeyron relationship.

More accurate IHC and Illinois River source apportionment analyses would be possible if the full suite of PCB congeners in air and compounds outside of the typical PAH priority pollutant list in sediment were measured. In fact the priority PAHs do not clearly define sources such as coal, thus alkyl and other PAH compounds must be considered for a more confident source apportionment. Markers outside of the contaminant class may also be measured, however to be useful the compounds must be well-determined and also measured in reference profiles.

The Illinois River analysis in particular would have also benefited from resolution of PAHs by depth, core dating, sediment composition/characterization data, and additional analytical uncertainty information for increased accuracy, comparability, and confirmation. The air sampling and analysis regime on the other hand provided sufficient data and quality for source apportionment analysis with corresponding local meteorological data that were utilized extensively for confirmation of results. The lower uncertainties involved in an air quality versus a retrospective sediment study may make existing air quality data more useful for source apportionment analyses. Furthermore, sediment is a more complicated matrix for source apportionment. Sediment is the ultimate sink for most PAHs that may disperse and incorporate by numerous pathways over wide time scales with additional opportunity for partitioning, transformation, and weathering of profiles. PAHs in riverine systems in particular may differentially deposit in sediments based on particle sizes, mixing, resuspension, varying sedimentation rates, and scouring. Homogenization of the sediment ex-situ for composite cores as in Illinois River may also alter source apportionment results by removing explicit source variation of samples. Thus greater care must be taken to ensure a satisfactory sediment contamination dataset for PMF analysis.

When direct source-receptor relationships can be established, source apportionment results are clearer and more accurate. For example, PAHs in the IHC air-shed are closely linked with nearby industrial emitters and were successfully resolved by PMF. However the relationship between Illinois River PAHs and their sources is convoluted and source apportionment results less clear. Yet even without definitive source identification, multivariate receptor models provide information regarding pathways and possible sources.

PMF sensitivity and uncertainty analysis. Sensitivity analyses can be performed with different source numbers and data selection criteria to assess robustness of PMF results and prepare a well-conditioned data matrix for maximum source resolution and informative capability. PMF diagnostics and apportionment of Illinois River PAHs hardly varied with inclusion of a few outlier and low-detect samples, but results varied more so with the inclusion of an infrequently detected analyte and quite significantly using another method of non-detect replacement. While analytes detection below 60% of the time added little useful information to the Illinois River analysis, the addition of a HMW congener detected just over 40% of the time resolved an additional source for the IHC atmospheric PCB analysis. The uncertainty matrix and/or model parameters can be adjusted during sensitivity analysis as well.

PMF model uncertainty is explicitly quantified based on output variability with Monte Carlo generated datasets varied from the original. Further confidence in PMF modeling and results can be achieved by applying additional source apportionment methods. In the present study UNMIX and EPA-PMF models generated results consistent with PMF apportionment of PAHs and PCBs in the atmosphere of IHC, however diagnostic PAH ratios could not independently support source apportionment results in the Illinois River due to limitations in the method (see below).

Reference source profiles. Though not required input to PMF, reference source profiles are key for modeled profile comparison and interpretation. A major effort was made to represent as many sources as possible with the potential to impact the receptors. Over 50 atmospheric PAH profiles, nearly 20 atmospheric PCB profiles, and nearly 50 sediment PAHs profiles were obtained from the literature, emission inventories, and sampling reports; however non-definitive, uncertain, and weathered profiles proved limiting for source identification. In many cases different reference source profiles were collinear and too similar to provide definitive source identification, matching equally well to model sources. Further, source profile uncertainty is not well or consistently defined and depends on profile computation, methods of sampling and analysis, and intra-source as well as inter-source variability. Also, profiles representing agricultural sources were few. Due to these limitations reference source comparison was not exclusively relied on to interpret source apportionment results. As mentioned previously, sources may be better characterized and discerned from one another by expanding the number of compounds measured. Complications from partitioning and degradation of PAHs and PCBs between source and receptor in the environment can also be minimized by considering weathered source profiles and those nearest to the receptor. Handling the differential partitioning of compounds in the environment is also key. The present study considered total (gas plus particulate phase) atmospheric source concentrations. Differential partitioning between sources and receptors of various media was addressed by calculating profiles in the receptor phase using reported partitioning coefficients for each compound. Examining profiles of potential or suspected sources specific to the receptor site, such as the industrial emitters and contaminated sites near IHC, greatly informed source identification as well. Finally, when source profile information was limited, comparison of source contribution results with emission histories and

locations, atmospheric (and hydrologic) parameters, and other source, transport, and receptor information was critical to confirming the identify of sources.

Diagnostic PAH ratios. PAH diagnostic ratios are applied widely for source apportionment and environmental forensics despite serious limitations beyond those of PMF receptor modeling. The Illinois River analysis considered the common parent PAH ratios while the IHC study did not include ratios because of the lack of diagnostic PAHs detected (although there were a sufficient number for a successful PMF analysis). Diagnostic ratios consider a small number of PAHs analyzed individually for comparison, whereas quantitative receptor models can operate simultaneously on a full range of PAHs. Inconsistent results from the four different diagnostic ratios and Illinois River data indicated that not all ratios are accurate or reliable for all sources. Environmental samples and reference profiles from the literature were also identified incorrectly by various ratios, thus the applicability of each ratio must be examined for the source and the medium under investigation, significantly reducing method simplicity and ease of use. Ratio accuracy was particularly poor for sources with different degrees of aging (used versus new oil, coal tar parking lot dust versus coal tar). The method assumes stability of PAH ratios over time, which is not necessarily valid due to uncertainties in thermodynamic stability/relative discrimination as well as in environmental stability of different PAHs despite similar physiochemical properties. Lack of source specificity is another drawback, as diagnostic ratio ranges correspond only to general petrogenic and combustion (sometimes distinguishing between petroleum and coal/biomass combustion) sources, and fossil coal cannot be uniquely represented by parent ratios for identification in sediment. Finally, diagnostic ratios can be ambiguous or misleading if samples are impacted from more than one source, indicating only a dominant source or a mixture of sources inaccurately. For example while diagnostic PAH ratios indicate

petroleum combustion impacts to Illinois River sediment, a mix of coal/biomass combustion and petroleum sources may yield the same result as shown by PMF analysis. Thus the ratios are not sufficiently specific or accurate when applied independently. In the Illinois River study these two drawbacks were mitigated by applying diagnostic PAH ratios in tandem with PMF as a tool to visualize and compare modeled profiles and reference source profiles. However ratio comparison should not replace the more rigorous cosine ϕ similarity comparison, nor should ratios be relied on for source assignment due to previously mentioned uncertainties.

CITED LITERATURE

- (1) Ingersoll, C.; MacDonald, D.; Brumbaugh, W.; Johnson, B.; Kemble, N.; Kunz, J.; May, T.; Wang, N.; Smith, J.; Sparks, D. Toxicity assessment of sediments from the Grand Calumet River and Indiana Harbor Canal in northwestern Indiana, USA. *Archives of environmental contamination and toxicology* **2002**, 43 (2), 156-167.
- (2) Baek, S. O.; Field, R. A.; Goldstone, M. E.; Kirk, P. W.; Lester, J. N.; Perry, R. A Review of Atmospheric Polycyclic Aromatic-Hydrocarbons - Sources, Fate and Behavior. *Water Air and Soil Pollution* **1991**, 60 (3-4), 279-300.
- (3) Edwards, N. T. Polycyclic Aromatic-Hydrocarbons (Pahs) in the Terrestrial Environment - a Review. *Journal of environmental quality* **1983**, 12 (4), 427-441.
- (4) ATSDR Toxicological Profile for Polycyclic Aromatic Hydrocarbons. In US Department of Health and Human Services, P. H. S., Agency for Toxic Substances and Disease Registry, Atlanta, GA, Ed. 1995.
- (5) ATSDR Toxicological Profile for Naphthalene, 1-Methylnaphthalene, and 2-Methylnaphthalene. In US Department of Health and Human Services, P. H. S., Agency for Toxic Substances and Disease Registry, Atlanta, GA, Ed. 2005.
- (6) Fahnrich, K. A.; Pravda, M.; Guilbault, G. G. Immunochemical detection of polycyclic aromatic hydrocarbons (PAHs). *Analytical Letters* **2002**, 35 (8), 1269-1300.
- (7) Burgess, R. M.; Ahrens, M. J.; Hickey, C. W. Geochemistry of PAHs in Aquatic Environments: Source, Persistence and Distribution. In *PAHs: An Ecotoxicological Perspective*, Douben, P. E. T., Ed. Wiley: 2003; p 35.
- (8) Mastral, A. M.; Callen, M. S. A review an polycyclic aromatic hydrocarbon (PAH) emissions from energy generation. *Environmental science & technology* **2000**, 34 (15), 3051-3057.
- (9) Eduljee, G. H. Budget and Source Inventories. In *Persistent Organic Pollutants: Environmental Behavior and Pathways for Human Exposure*, Harrad, S., Ed. Kluwer Academic Publishers: 2001; pp 1-28.

- (10) Simcik, M. F.; Franz, T. P.; Zhang, H.; Eisenreich, S. J. Gas-Particle Partitioning of PCBs and PAHs in the Chicago Urban and Adjacent Coastal Atmosphere: States of Equilibrium. *Environmental Science & Technology* **1998**, *32* 251-257.
- (11) Li, A.; Schoonover, T. M.; Zou, Q.; Norlock, F.; Conroy, L. M.; Scheff, P. a.; Wadden, R. a. Polycyclic aromatic hydrocarbons in residential air of ten Chicago area homes: Concentrations and influencing factors. *Atmospheric Environment* **2005**, *39* 3491-3501.
- (12) Halsall, C. J.; Sweetman, A.; Barrie, L.; Jones, K. C. Modelling the behaviour of PAHs during atmospheric transport from the UK to the Arctic. *Atmospheric Environment* **2001**, *35* (2), 255-267.
- (13) Simcik, M. F. Polycyclic Aromatic Hydrocarbons in the Great Lakes. In *Atmospheric Deposition of Contaminants to the Great Lakes and Coastal Waters*, Baker, J. E., Ed. SETAC Press: Pensacola, FL 2006; Vol. 5, pp 307-353.
- (14) Burgess, R. M.; Ahrens, M. J.; Hickey, C. W.; den Besten, P. J.; ten Hulscher, D.; van Hattum, B.; Meador, J. P.; Douben, P. E. An Overview of Partitioning and Bioavailability of PAHs in Sediments and Soils. In *PAHs: An Ecotoxicological Perspective*, Douben, P. E. T., Ed. Wiley: 2003; p 99.
- (15) Arey, J.; Atkinson, R. Photochemical reactions of PAHs in the atmosphere. In *PAHs: An Ecotoxicological Perspective*, Douben, P. E. T., Ed. Wiley: 2003; pp 47-63.
- (16) Volkering, F.; Breure, A. M. Biodegradation and General Aspects of Bioavailability. In *PAHs: An Ecotoxicological Perspective*, Douben, P. E. T., Ed. Wiley: 2003; p 81.
- (17) Rockne, K. J.; Strand, S. E. Anaerobic biodegradation of naphthalene, phenanthrene, and biphenyl by a denitrifying enrichment culture. *Water research* **2001**, *35* (1), 291-299.
- (18) Connell, D. W. *Basic concepts of environmental chemistry*, CRC Press: 2005.
- (19) Rockne, K. J.; Shor, L. M.; Young, L. Y.; Taghon, G. L.; Kosson, D. S. Distributed sequestration and release of PAHs in weathered sediment: The role of sediment structure and organic carbon properties. *Environmental science & technology* **2002**, *36* (12), 2636-2644.
- (20) Akcha, F.; Vincent Hubert, F.; Pfhof-Leskowicz, A. Potential value of the comet assay and DNA adduct measurement in dab (*Limanda limanda*) for assessment of in situ exposure to

genotoxic compounds. *Mutation Research/Genetic Toxicology and Environmental Mutagenesis* **2003**, 534 (1-2), 21-32.

- (21) Latimer, J. S.; Zheng, J. The Sources, Transport and Fate of PAHs in the Marine Environment. In *PAHs: An Ecotoxicological Perspective*, Douben, P. E. T., Ed. Wiley: 2003; p 9.
- (22) Mahler, B. J.; Van Metre, P. C.; Bashara, T. J.; Wilson, J. T.; Johns, D. A. Parking lot sealcoat: an unrecognized source of urban polycyclic aromatic hydrocarbons. *Environmental science & technology* **2005**, 39 (15), 5560-5566.
- (23) Van Metre, P. C.; Mahler, B. J. Contribution of PAHs from coal–tar pavement sealcoat and other sources to 40 US lakes. *Science of the Total Environment* **2010**, 409 (2), 334-344.
- (24) Galarneau, E.; Makar, P. A.; Sassi, M.; Diamond, M. L. Estimation of atmospheric emissions of six semivolatile polycyclic aromatic hydrocarbons in southern Canada and the United States by use of an emissions processing system. *Environmental science & technology* **2007**, 41 (12), 4205-4213.
- (25) USEPA. Locating and Estimating Air Emissions from Sources of Polycyclic Organic Matter. US Environmental Protection Agency, Research Triangle Park, NC. 1998.
- (26) Wild, S. R.; Jones, K. C. Polynuclear aromatic hydrocarbons in the United Kingdom environment: a preliminary source inventory and budget. *Environmental Pollution* **1995**, 88 (1), 91-108.
- (27) Yunker, M. B.; Macdonald, R. W.; Vingarzan, R.; Mitchell, R. H.; Goyette, D.; Sylvestre, S. PAHs in the Fraser River basin: a critical appraisal of PAH ratios as indicators of PAH source and composition. *Organic Geochemistry* **2002**, 33 (4), 489-515.
- (28) Tobiszewski, M.; Namieśnik, J. PAH diagnostic ratios for the identification of pollution emission sources. *Environmental Pollution* **2012**, 162 110-119.
- (29) Ravindra, K.; Sokhi, R.; Van Grieken, R. Atmospheric polycyclic aromatic hydrocarbons: Source attribution, emission factors and regulation. *Atmospheric Environment* **2008**, 42 (13), 2895-2921.

- (30) Kim, D.; Kumfer, B. M.; Anastasio, C.; Kennedy, I. M.; Young, T. M. Environmental aging of polycyclic aromatic hydrocarbons on soot and its effect on source identification. *Chemosphere* **2009**, *76* (8), 1075-1081.
- (31) Steinhauer, M. S.; Boehm, P. D. The Composition and Distribution of Saturated and Aromatic-Hydrocarbons in Nearshore Sediments, River Sediments, and Coastal Peat of the Alaskan Beaufort Sea - Implications for Detecting Anthropogenic Hydrocarbon Inputs. *Marine environmental research* **1992**, *33* (4), 223-253.
- (32) Yunker, M. B.; Perreault, A.; Lowe, C. J. Source apportionment of elevated PAH concentrations in sediments near deep marine outfalls in Esquimalt and Victoria, BC, Canada: Is coal from an 1891 shipwreck the source? *Organic Geochemistry* **2012**, *46* 12-37.
- (33) Yang, H. H.; Lee, W. J.; Chen, S. J.; Lai, S. O. PAH emission from various industrial stacks. *Journal of hazardous materials* **1998**, *60* (2), 159-174.
- (34) Yang, H. H.; Lai, S. O.; Hsieh, L. T.; Hsueh, H. J.; Chi, T. W. Profiles of PAH emission from steel and iron industries. *Chemosphere* **2002**, *48* (10), 1061-1074.
- (35) Achten, C.; Hofmann, T. Native polycyclic aromatic hydrocarbons (PAH) in coals-A hardly recognized source of environmental contamination. *Science of the Total Environment* **2009**, *407* (8), 2461-2473.
- (36) Chapman, P. M.; Downie, J.; Maynard, A.; Taylor, L. A. Coal and deodorizer residues in marine sediments—contaminants or pollutants? *Environmental toxicology and chemistry* **1996**, *15* (5), 638-642.
- (37) Bender, M. E.; Roberts, M. H.; deFur, P. O. Unavailability of polynuclear aromatic hydrocarbons from coal particles to the eastern oyster. *Environmental pollution (Barking, Essex : 1987)* **1987**, *44* 243-60.
- (38) Dong, J.; Li, F.; Xie, K. Study on the source of Polycyclic aromatic hydrocarbons (PAHs) during coal pyrolysis by PY-GC-MS. *Journal of hazardous materials* **2012**.
- (39) Laroo, C. A.; Schenk, C. R.; Sanchez, L. J.; McDonald, J. Emissions of PCDD/Fs, PCBs, and PAHs from a Modern Diesel Engine Equipped with Catalyzed Emission Control Systems. *Environmental science & technology* **2011**, *45* (15), 6420-6428.

- (40) Schauer, J. J.; Kleeman, M. J.; Cass, G. R.; Simoneit, B. R. T. Measurement of emissions from air pollution sources. 2. C1 through C30 organic compounds from medium duty diesel trucks. *Environmental science & technology* **1999**, *33* (10), 1578-1587.
- (41) NIST. Certificate of analysis. Standard Reference Material 1650b. Diesel Particulate Matter. National Institute of Standards and Technology, 2006; pp 1-12.
- (42) Karavalakis, G.; Boutsika, V.; Stournas, S.; Bakeas, E. Biodiesel emissions profile in modern diesel vehicles. Part 2: Effect of biodiesel origin on carbonyl, PAH, nitro-PAH and oxy-PAH emissions. *The Science of the total environment* **2011**, *409* 738-47.
- (43) Miguel, A. H.; Kirchstetter, T. W.; Harley, R. A.; Hering, S. V. On-road emissions of particulate polycyclic aromatic hydrocarbons and black carbon from gasoline and diesel vehicles. *Environmental science & technology* **1998**, *32* (4), 450-455.
- (44) Schauer, J. J.; Kleeman, M. J.; Cass, G. R.; Simoneit, B. R. T. Measurement of emissions from air pollution sources. 5. C1-C32 organic compounds from gasoline-powered motor vehicles. *Environmental science & technology* **2002**, *36* (6), 1169-1180.
- (45) Li, C. T.; Mi, H. H.; Lee, W. J.; You, W. C.; Wang, Y. F. PAH emission from the industrial boilers. *Journal of hazardous materials* **1999**, *69* (1), 1-11.
- (46) Wang, J.; Jia, C. R.; Wong, C. K.; Wong, P. K. Characterization of polycyclic aromatic hydrocarbons created in lubricating oils. *Water, Air, & Soil Pollution* **2000**, *120* (3), 381-396.
- (47) Boonyatumanond, R.; Murakami, M.; Wattayakorn, G.; Togo, A.; Takada, H. Sources of polycyclic aromatic hydrocarbons (PAHs) in street dust in a tropical Asian mega-city, Bangkok, Thailand. *Science of the Total Environment* **2007**, *384* (1-3), 420-432.
- (48) Zakaria, M. P.; Horinouchi, A.; Tsutsumi, S.; Takada, H.; Tanabe, S.; Ismail, A. Oil Pollution in the Straits of Malacca, Malaysia: Application of molecular markers for source identification. *Environmental science & technology* **2000**, *34* (7), 1189-1196.
- (49) Zakaria, M. P.; Takada, H.; Tsutsumi, S.; Ohno, K.; Yamada, J.; Kouno, E.; Kumata, H. Distribution of polycyclic aromatic hydrocarbons (PAHs) in rivers and estuaries in Malaysia: a widespread input of petrogenic PAHs. *Environmental science & technology* **2002**, *36* (9), 1907-1918.

- (50) Boonyatumanond, R.; Wattayakorn, G.; Togo, A.; Takada, H. Distribution and origins of polycyclic aromatic hydrocarbons (PAHs) in riverine, estuarine, and marine sediments in Thailand. *Marine pollution bulletin* **2006**, 52 942-56.
- (51) Singh, A. K.; Gin, M.; Ni, F.; Christensen, E. A source-receptor method for determining non-point sources of PAHs to the Milwaukee Harbor Estuary. *Water Science & Technology* **1993**, 28 (8-9), 91-102.
- (52) Li, C. K.; Kamens, R. M. The use of polycyclic aromatic hydrocarbons as source signatures in receptor modeling. *Atmospheric Environment. Part A. General Topics* **1993**, 27 (4), 523-532.
- (53) Davies, I. W.; Harrison, R. M.; Perry, R.; Ratnayaka, D.; Wellings, R. A. Municipal incinerator as source of polynuclear aromatic hydrocarbons in environment. *Environmental science & technology* **1976**, 10 (5), 451-453.
- (54) Dyke, P. H.; Foan, C.; Fiedler, H. PCB and PAH releases from power stations and waste incineration processes in the UK. *Chemosphere* **2003**, 50 (4), 469-480.
- (55) Wise, S. A.; Poster, D. L.; Leigh, S. D.; Rimmer, C. A.; Mössner, S.; Schubert, P.; Sander, L. C.; Schantz, M. M. Polycyclic aromatic hydrocarbons (PAHs) in a coal tar standard reference material—SRM 1597a updated. *Analytical and Bioanalytical Chemistry* **2010**, 398 717-728.
- (56) Van Metre, P.; Mahler, B. J.; Burbank, T. L.; Wilson, J. T. *Collection and Analysis of Samples for Polycyclic Aromatic Hydrocarbons in Dust and Other Solids Related to Sealed and Unsealed Pavement from 10 Cities Across the United States, 2005-07*, US Department of the Interior, US Geological Survey: 2008.
- (57) Van Metre, P. C.; Mahler, B. J. Contribution of PAHs from coal-tar pavement sealcoat and other sources to 40 U.S. lakes. *The Science of the total environment* **2010**, 409 334-44.
- (58) Kohler, M.; Ku, T.; Schmid, P.; Gujer, E.; Crockett, R. Inventory and Emission Factors of Creosote , Polycyclic Aromatic Hydrocarbons (PAH), and Phenols from Railroad Ties Treated with Creosote. **2000**, 34 4766-4772.
- (59) Mueller, J. G.; Chapman, P. J.; Pritchard, P. H. Creosote-contaminated sites. Their potential for bioremediation. *Environmental science & technology* **1989**, 23 (10), 1197-1201.

- (60) Hays, M. D.; Geron, C. D.; Linna, K. J.; Smith, N. D.; Schauer, J. J. Speciation of gas-phase and fine particle emissions from burning of foliar fuels. *Environmental science & technology* **2002**, *36* (11), 2281-2295.
- (61) Jenkins, B. M.; Jones, A. D.; Turn, S. Q.; Williams, R. B. Particle concentrations, gas-particle partitioning, and species intercorrelations for polycyclic aromatic hydrocarbons (PAH) emitted during biomass burning. *Atmospheric Environment* **1996**, *30* (22), 3825-3835.
- (62) Schauer, J. J.; Kleeman, M. J.; Cass, G. R.; Simoneit, B. R. T. Measurement of emissions from air pollution sources. 3. C1-C29 organic compounds from fireplace combustion of wood. *Environmental science & technology* **2001**, *35* (9), 1716-1728.
- (63) Khalili, N. R.; Scheff, P. A.; Holsen, T. M. PAH source fingerprints for coke ovens, diesel and, gasoline engines, highway tunnels, and wood combustion emissions. *Atmospheric Environment* **1995**, *29* (4), 533-542.
- (64) Li, A.; Jang, J. K.; Scheff, P. A. Application of EPA CMB8.2 model for source apportionment of sediment PAHs in Lake Calumet, Chicago RID A-3395-2008. *Environmental science & technology* **2003**, *37* (13), 2958-2965.
- (65) Bzdusek, P. A.; Christensen, E. R.; Li, A.; Zou, Q. M. Source apportionment of sediment PAHs in Lake Calumet, Chicago: Application of factor analysis with nonnegative constraints RID A-3395-2008. *Environmental science & technology* **2004**, *38* (1), 97-103.
- (66) USACE. Draft Sediment Sampling and Analysis Report, Indiana Harbor and Canal, Indiana. US Army Corps of Engineers-Chicago District, 2010.
- (67) Gulezian, P. Z.; Ison, J. L.; Granberg, K. J. Establishment of an Invasive Plant Species (*Conium maculatum*) in Contaminated Roadside Soil in Cook County, Illinois. *The American Midland Naturalist* **2012**, *168* (2), 375-395.
- (68) Stout, S. A.; Emsbo-Mattingly, S. D. Concentration and character of PAHs and other hydrocarbons in coals of varying rank—Implications for environmental studies of soils and sediments containing particulate coal. *Organic Geochemistry* **2008**, *39* (7), 801-819.
- (69) NIST. Certificate of Analysis, Standard Reference Material 1649b. Urban Dust. National Institute of Standards and Technology, N. I. o. S. a., Ed. Gaithersburg, MD, 2009; pp 1-14.

- (70) Christensen, E. R.; Zhang, X. Sources of polycyclic aromatic hydrocarbons to Lake Michigan determined from sedimentary records. *Environmental science & technology* **1993**, 27 (1), 139-146.
- (71) National Research Council. Polycyclic aromatic hydrocarbons: evaluation of sources and effects. In National Academy Press: Washington, D.C., 1983.
- (72) Srogi, K. Monitoring of environmental exposure to polycyclic aromatic hydrocarbons: a review. *Environmental Chemistry Letters* **2007**, 5 (4), 169-195.
- (73) Charles, M. J.; Hites, R. A. Sediments as Archives of Environmental-Pollution Trends. *Advances in Chemistry Series* **1987**, (216), 365-389.
- (74) Van Metre, P. C.; Mahler, B. J.; Furlong, E. T. Urban sprawl leaves its PAH signature RID C-3999-2011. *Environmental science & technology* **2000**, 34 (19), 4064-4070.
- (75) Gao, S.; Sun, C.; Zhang, A. Chapter 5 Pollution of Polycyclic Aromatic Hydrocarbons in China. **2007**, 7.
- (76) Odabasi, M.; Vardar, N.; Sofuoglu, A.; Tasdemir, Y.; Holsen, T. M. Polycyclic aromatic hydrocarbons (PAHs) in Chicago air. *The Science of the total environment* **1999**, 227 (1), 57-67.
- (77) Simcik, M. F.; Eisenreich, S. J.; Lioy, P. J. Source apportionment and source/sink relationships of PAHs in the coastal atmosphere of Chicago and Lake Michigan. *Atmospheric Environment* **1999**, 33 (30), 5071-5079.
- (78) Van Metre, P. C.; Mahler, B. J.; Wilson, J. T. PAHs Underfoot: Contaminated Dust from Coal-Tar Sealcoated Pavement is Widespread in the United States. *Environmental science & technology* **2009**, 43 (1), 20-25.
- (79) Hillery, B. R.; Simcik, M. F.; Basu, I.; Hoff, R. M.; Strachan, W. M. J.; Burniston, D.; Chan, C. H.; Brice, K. A.; Sweet, C. W.; Hites, R. A. Atmospheric deposition of toxic pollutants to the Great Lakes as measured by the integrated atmospheric deposition network. *Environmental science & technology* **1998**, 32 (15), 2216-2221.
- (80) Van Metre, P. C.; Mahler, B. J. Trends in hydrophobic organic contaminants in urban and reference lake sediments across the United States, 1970-2001. *Environmental science & technology* **2005**, 39 (15), 5567-5574.

- (81) Christensen, E. R.; Arora, S. Source apportionment of PAHs in sediments using factor analysis by time records: Application to Lake Michigan, USA. *Water research* **2007**, *41* (1), 168-176.
- (82) Kay, R. T.; Arnold, T. L.; Cannon, W. F.; Graham, D. Concentrations of Polycyclic Aromatic Hydrocarbons and Inorganic Constituents in Ambient Surface Soils, Chicago, Illinois: 2001-2002. *Soil and Sediment Contamination* **2008**, *17* 221-236.
- (83) ASTDR Toxicological Profile for Polychlorinated Biphenyls (PCBs). In US Department of Health and Human Services, P. H. S., Agency for Toxic Substances and Disease Registry, Atlanta, GA, Ed. 2000.
- (84) Rachdawong, P.; Christensen, E. R. Determination of PCB sources by a principal component method with nonnegative constraints. *Environmental science & technology* **1997**, *31* (9), 2686-2691.
- (85) Hornbuckle, K. C.; Deborah, L. C.; Baker, J. E.; Eisenreich, S. J. Polychlorinated Biphenyls in the Great Lakes. In *Atmospheric Deposition of Contaminants to the Great Lakes and Coastal Waters*, Baker, J. E., Ed. SETAC Press: Pensacola, FL 2006; Vol. 5, pp 13-70.
- (86) Breivik, K.; Sweetman, A.; Pacyna, J. M.; Jones, K. C. Towards a global historical emission inventory for selected PCB congeners--a mass balance approach. 1. Global production and consumption. *The Science of the total environment* **2002**, *290* 181-98.
- (87) Voogt, P.; Brinkman, U. T. Production, properties and usage of polychlorinated biphenyls. *Halogenated biphenyls, terphenyls, naphtalenes, dibenzodioxins and related products. Elsevier Science Publishers BV (Biomedical Division)* **1989**, 3-45.
- (88) Breivik, K.; Sweetman, A.; Pacyna, J. M.; Jones, K. C. Towards a global historical emission inventory for selected PCB congeners - A mass balance approach-3. An update RID D-2311-2011. *Science of the Total Environment* **2007**, *377* (2-3), 296-307.
- (89) Simcik, M. F. Atmospheric fate and behaviour. In *Persistent Organic Pollutants*, Harrad, S., Ed. Kluwer Academic Publishers: 2001; pp 29-52.
- (90) Hoff, R. M.; Muir, D.; Grift, N. Annual cycle of polychlorinated biphenyls and organohalogen pesticides in air in southern Ontario. 1. Air concentration data. *Environmental science & technology* **1992**, *26* (2), 266-275.

- (91) Breivik, K.; Sweetman, A.; Pacyna, J. M.; Jones, K. C. Towards a global historical emission inventory for selected PCB congeners - a mass balance approach 2. Emissions RID D-2311-2011. *Science of the Total Environment* **2002**, 290 (1-3), 199-224.
- (92) Hornbuckle, K. C.; Eisenreich, S. J. Dynamics of gaseous semivolatile organic compounds in a terrestrial ecosystem - Effects of diurnal and seasonal climate variations. *Atmospheric Environment* **1996**, 30 (23), 3935-3945.
- (93) Frame, G. M.; Cochran, J. W.; Bøwadt, S. S. Complete PCB congener distributions for 17 aroclor mixtures determined by 3 HRGC systems optimized for comprehensive, quantitative, congener-specific analysis. *Journal of High Resolution Chromatography* **1996**, 19 (12), 657-668.
- (94) Ikonomou, M. G.; Sather, P.; Oh, J. E.; Choi, W. Y.; Chang, Y. S. PCB levels and congener patterns from Korean municipal waste incinerator stack emissions RID F-8206-2010. *Chemosphere* **2002**, 49 (2), 205-216.
- (95) Choi, K.-I.; Lee, S.-H.; Lee, D.-H. Emissions of PCDDs/DFs and dioxin-like PCBs from small waste incinerators in Korea. *Atmospheric Environment* **2008**, 42 (5), 940-948.
- (96) Pandelova, M.; Stanev, I.; Henkelmann, B.; Lenoir, D.; Schramm, K.-W. Correlation of PCDD/F and PCB at combustion experiments using wood and hospital waste. Influence of (NH₄)₂SO₄ as additive on PCDD/F and PCB emissions RID A-2996-2011. *Chemosphere* **2009**, 75 (5), 685-691.
- (97) Abad, E.; Martinez, K.; Caixach, J.; Rivera, J. Polychlorinated dibenzo-p-dioxins, dibenzofurans and 'dioxin-like' PCBs in flue gas emissions from municipal waste management plants. *Chemosphere* **2006**, 63 570-580.
- (98) Grochowalski, A.; Lassen, C.; Holtzer, M.; Sadowski, M.; Hudyma, T. Determination of PCDDs, PCDFs, PCBs and HCB emissions from the metallurgical sector in Poland. *Environmental Science and Pollution Research* **2007**, 14 (5), 326-332.
- (99) Cooper, D. A. HCB, PCB, PCDD and PCDF emissions from ships. *Atmospheric Environment* **2005**, 39 (27), 4901-4912.
- (100) Yi, S.-M.; Pagilla, S. R.; Seo, Y.-C.; Mills, W. J.; Holsen, T. M. Emissions of polychlorinated biphenyls (PCBs) from sludge drying beds to the atmosphere in Chicago. *Chemosphere* **2008**, 71 (6), 1028-1034.

- (101) Liu, G.; Zheng, M.; Liu, W.; Wang, C.; Zhang, B.; Gao, L.; Su, G.; Xiao, K.; Lv, P. Atmospheric Emission of PCDD/Fs, PCBs, Hexachlorobenzene, and Pentachlorobenzene from the Coking Industry. *Environmental science & technology* **2009**, *43* (24), 9196-9201.
- (102) Hedman, B.; Naslund, M.; Marklund, S. Emission of PCDD/F, PCB, and HCB from combustion of firewood and pellets in residential stoves and boilers. *Environmental science & technology* **2006**, *40* (16), 4968-4975.
- (103) Taucher, J. A.; Hannah, D. J.; Green, N. J. L.; Porter, L. J.; Czochanska, Z.; Cluniesross, C. M. Pcd, Pcdf and Pcb Emissions Under Variable Operating-Conditions from a Waste Oil Furnace. *Chemosphere* **1992**, *25* (7-10), 1429-1433.
- (104) Hsu, Y. K.; Holsen, T. M.; Hopke, P. K. Locating and quantifying PCB sources in Chicago: Receptor modeling and field sampling. *Environmental science & technology* **2003**, *37* (4), 681-690.
- (105) Martinez, A.; Wang, K.; Hornbuckle, K. C. Fate of PCB Congeners in an Industrial Harbor of Lake Michigan. *Environmental science & technology* **2010**, *44* 2803-2808.
- (106) Martinez, A.; Wang, K.; Hornbuckle, K. C. Fate of PCB Congeners in an Industrial Harbor of Lake Michigan†. *Environmental science & technology* **2010**, *44* (8), 2803-2808.
- (107) Gary Sanitary District. *Ralston Street Lagoon Technical and Cost Assessment*. Gary Sanitary District; Gary, IN, 2007
- (108) Sanders, G. Temporal trends in environmental contamination. In *Persistent Organic Pollutants: Environmental Behavior and Pathways for Human Exposure*, Harrad, S., Ed. Kluwer Academic Publishers: **2001**; pp 167-210.
- (109) Simcik, M. F.; Zhang, H.; Eisenreich, S. J.; Franz, T. P. Urban Contamination of the Chicago/Coastal Lake Michigan Atmosphere by PCBs and PAHs during AEOLUS. *Environmental Science & Technology* **1997**, *31* 2141-2147.
- (110) Hu, D. F.; Lehmler, H. J.; Martinez, A.; Wang, K.; Hornbuckle, K. C. Atmospheric PCB congeners across Chicago. *Atmospheric Environment* **2010**, *44* (12), 1550-1557.
- (111) Hu, D.; Martinez, A.; Hornbuckle, K. C. Discovery of non-Aroclor PCB (3, 3'-dichlorobiphenyl) in Chicago air. *Environmental science & technology* **2008**, *42* (21), 7873-7877.

- (112) Hsu, Y. K.; Holsen, T. M.; Hopke, P. K. Comparison of hybrid receptor models to locate PCB sources in Chicago. *Atmospheric Environment* **2003**, *37* (4), 545-562.
- (113) Imamoglu, I.; Li, K.; Christensen, E. R.; McMullin, J. K. Sources and dechlorination of polychlorinated biphenyl congeners in the sediments of Fox River, Wisconsin. *Environmental science & technology* **2004**, *38* (9), 2574-2583.
- (114) Cacela, D.; Beltman, D. J.; Lipton, J. Polychlorinated biphenyl source attribution in Green Bay, Wisconsin, USA, using multivariate similarity among congener profiles in sediment samples. *Environmental toxicology and chemistry* **2002**, *21* (8), 1591-1599.
- (115) Kannan, K.; Lee Kober, J.; Kang, Y. S.; Masunaga, S.; Nakanishi, J.; Ostaszewski, A.; Giesy, J. P. Polychlorinated naphthalenes, biphenyls, dibenzo-p-dioxins, and dibenzofurans as well as polycyclic aromatic hydrocarbons and alkylphenols in sediment from the Detroit and Rouge Rivers, Michigan, USA. *Environmental toxicology and chemistry* **2001**, *20* (9), 1878-1889.
- (116) Steuer, J. S.; Fitzgerald, S. A.; Hall, D. W.; District, M. M. S. *Distribution and transport of polychlorinated biphenyls and associated particulates in the Milwaukee River System, Wisconsin, 1993-95*, US Department of the Interior, US Geological Survey: **1999**.
- (117) McCarty, H.; Schofield, J.; Miller, K.; Brent, R.; Van Hoof, P.; Eadie, B. Results of the Lake Michigan mass balance study: polychlorinated biphenyls and trans-nonachlor data report. US Environmental Protection Agency **2004**.
- (118) Rossmann, R. *Results of the Lake Michigan Mass Balance Project: Polychlorinated Biphenyls Modeling Report*; U.S. Environmental Protection Agency, Office of Research and Development; 2006.
- (119) Hornbuckle, K. C.; Green, M. L. The impact of an urban-industrial region on the magnitude and variability of persistent organic pollutant deposition to Lake Michigan. *AMBIO: A Journal of the Human Environment* **2003**, *32* (6), 406-411.
- (120) Bzdusek, P. A.; Lu, J. H.; Christensen, E. R. PCB congeners and dechlorination in sediments of Sheboygan River, Wisconsin, determined by matrix factorization. *Environmental science & technology* **2006**, *40* (1), 120-129.
- (121) Saber, D. L.; Mauro, D.; Sirivedhin, T. Applications of forensic chemistry to environmental work. *Journal of Industrial Microbiology and Biotechnology* **2005**, *32* (11), 665-668.

- (122) Morrison, R. D. Application of forensic techniques for age dating and source identification in environmental litigation. *Environmental Forensics* **2000**, *1* (3), 131-153.
- (123) Schmidt, T. C.; Zwank, L.; Elsner, M.; Berg, M.; Meckenstock, R. U.; Haderlein, S. B. Compound-specific stable isotope analysis of organic contaminants in natural environments: a critical review of the state of the art, prospects, and future challenges RID A-1143-2011. *Analytical and Bioanalytical Chemistry* **2004**, *378* (2), 283-300.
- (124) Hopke, P. K. *Receptor modeling in environmental chemistry*, John Wiley & Sons: New York, NY, **1985**.
- (125) Henry, R. C.; Christensen, E. R. Selecting an Appropriate Multivariate Source Apportionment Model Result. *Environmental science & technology* **2010**, *44* (7), 2474-2481.
- (126) Yunker, M. B.; Macdonald, R. W.; Snowdon, L. R.; Fowler, B. R. Alkane and PAH biomarkers as tracers of terrigenous organic carbon in Arctic Ocean sediments. *Organic Geochemistry* **2011**, *42* (9), 1109-1146.
- (127) Henry, R. C. History and fundamentals of multivariate air quality receptor models. *Chemometrics and Intelligent Laboratory Systems* **1997**, *37* 37-42.
- (128) Hopke, P. K. *Receptor modeling for air quality management*, Elsevier: Amsterdam, **1991**.
- (129) Kenski, D. M.; Wadden, R. A.; Scheff, P. A.; Lonneman, W. A. Receptor Modeling Approach to Voc Emission Inventory Validation. *Journal of Environmental Engineering-Asce* **1995**, *121* (7), 483-491.
- (130) Bzdusek, P. A.; Christensen, E. R.; Lee, C. M.; Pakdeesusuk, U.; Freedman, D. L. PCB congeners and dechlorination in sediments of Lake Hartwell, South Carolina, determined from cores collected in 1987 and 1998 RID A-4615-2008. *Environmental science & technology* **2006**, *40* (1), 109-119.
- (131) Zuo, Q.; Duan, Y. H.; Yang, Y.; Wang, X. J.; Tao, S. Source apportionment of polycyclic aromatic hydrocarbons in surface soil in Tianjin, China. *Environmental Pollution* **2007**, *147* (2), 303-310.
- (132) Soonthornnonda, P.; Christensen, E. R. Source apportionment of pollutants and flows of combined sewer wastewater. *Water research* **2008**, *42* (8-9), 1989-1998.

- (133) Soonthornnonda, P.; Zou, Y.; Christensen, E. R.; Li, A. PCBs in Great Lakes sediments, determined by positive matrix factorization RID A-3395-2008. *Journal of Great Lakes Research* **2011**, 37 (1), 54-63.
- (134) Du, S.; Rodenburg, L. A. Source identification of atmospheric PCBs in Philadelphia/Camden using positive matrix factorization followed by the potential source contribution function. *Atmospheric Environment* **2007**, 41 (38), 8596-8608.
- (135) Paatero, P. Least squares formulation of robust non-negative factor analysis. *Chemometrics and Intelligent Laboratory Systems* **1997**, 37 (1), 23-35.
- (136) Paatero, P.; Tapper, U. Positive matrix factorization: A non-negative factor model with optimal utilization of error estimates of data values. *Environmetrics* **1994**, 5 (2), 111-126.
- (137) Paterson, K. G.; Sagady, J. L.; Hooper, D. L.; Bertman, S. B.; Carroll, M. A.; Shepson, P. B. Analysis of air quality data using positive matrix factorization. *Environmental science & technology* **1999**, 33 (4), 635-641.
- (138) Kim, E.; Hopke, P. K.; Edgerton, E. S. Source identification of Atlanta aerosol by positive matrix factorization. *Journal of the Air & Waste Management Association* **2003**, 53 (6), 731-739.
- (139) Wang, D.; Tian, F.; Yang, M.; Liu, C.; Li, Y.-F. Application of positive matrix factorization to identify potential sources of PAHs in soil of Dalian, China. *Environmental Pollution* **2009**, 157 (5), 1559-1564.
- (140) Zou, Y.; Christensen, E. R.; Li, A. Characteristic pattern analysis of polybromodiphenyl ethers in Great Lakes sediments: a combination of eigenspace projection and positive matrix factorization analysis. *Environmetrics* **2013**, 24 41-50.
- (141) Rodenburg, L. A.; Yu Meng, Q. Source Apportionment of Polychlorinated Biphenyls in Chicago Air from 1996-2007. *Environmental science & technology* **2013**.
- (142) Larsen Iii, R. K.; Baker, J. E. Source apportionment of polycyclic aromatic hydrocarbons in the urban atmosphere: a comparison of three methods. *Environmental science & technology* **2003**, 37 (9), 1873-1881.

- (143) Callén, M. S.; López, J. M.; Iturmendi, a.; Mastral, a. M. Nature and sources of particle associated polycyclic aromatic hydrocarbons (PAH) in the atmospheric environment of an urban area. *Environmental pollution (Barking, Essex : 1987)* **2012**, 1-9.
- (144) Sofowote, U. M.; McCarry, B. E.; Marvin, C. H. Source apportionment of PAH in Hamilton Harbour suspended sediments: comparison of two factor analysis methods. *Environmental science & technology* **2008**, 42 (16), 6007-6014.
- (145) Bzdusek, P. A. PCB or PAH Sources and Degradation in Aquatic Sediments Determined by Positive Matrix Factorization. University of Wisconsin-Milwaukee, **2005**.
- (146) USEPA. EPA Positive Matrix Factorization (PMF) 3.0 Fundamentals & User Guide. US Environmental Protection Agency, Office of Research and Development, Washington, D.C., 2008.
- (147) Lee, E.; Chan, C. K.; Paatero, P. Application of positive matrix factorization in source apportionment of particulate pollutants in Hong Kong. *Atmospheric Environment* **1999**, 33 (19), 3201-3212.
- (148) Paatero, P. User's Guide for Positive Matrix Factorization Programs PMF2 and PMF3. Part 1: Tutorial. University of Helsinki, Helsinki, Finland, 2003.
- (149) Bzdusek, P. A.; Christensen, E. R. Comparison of a new variant of PMF with other receptor modeling methods using artificial and real sediment PCB data sets. *Environmetrics* **2006**, 17 (4), 387-403.
- (150) Paatero, P.; Hopke, P. K.; Song, X.-H.; Ramadan, Z. Understanding and controlling rotations in factor analytic models. *Chemometrics and Intelligent Laboratory Systems* **2002**, 60 (1), 253-264.
- (151) Paatero, P.; Tapper, U. Analysis of different modes of factor analysis as least squares fit problems. *Chemometrics and Intelligent Laboratory Systems* **1993**, 18 (2), 183-194.
- (152) Shor, L. M.; Kosson, D. S.; Rockne, K. J.; Young, L. Y.; Taghon, G. L. Combined effects of contaminant desorption and toxicity on risk from PAH contaminated sediments. *Risk analysis* **2004**, 24 (5), 1109-1120.

- (153) Herrick, R. F.; McClean, M. D.; Meeker, J. D.; Baxter, L. K.; Weymouth, G. A. An unrecognized source of PCB contamination in schools and other buildings. *Environmental health perspectives* **2004**, *112* (10), 1051.
- (154) Rodenburg, L. A.; Guo, J.; Du, S.; Cavallo, G. J. Evidence for unique and ubiquitous environmental sources of 3, 3'-dichlorobiphenyl (PCB 11). *Environmental science & technology* **2009**, *44* (8), 2816-2821.
- (155) Hu, D. F.; Hornbuckle, K. C. Inadvertent Polychlorinated Biphenyls in Commercial Paint Pigments. *Environmental science & technology* **2010**, *44* (8), 2822-2827.
- (156) Hu, X.; Adamcakova-Dodd, A.; Lehmler, H.-J.; Hu, D.; Hornbuckle, K.; Thorne, P. S. Subchronic inhalation exposure study of an airborne polychlorinated biphenyl mixture resembling the Chicago ambient air congener profile. *Environmental science & technology* **2012**, *46* 9653-62.
- (157) Sun, P.; Blanchard, P.; Brice, K. A.; Hites, R. A. Trends in polycyclic aromatic hydrocarbon concentrations in the Great Lakes atmosphere. *Environmental science & technology* **2006a**, *40* (20), 6221-6227.
- (158) Sun, P.; Basu, I.; Hites, R. A. Temporal trends of polychlorinated biphenyls in precipitation and air at Chicago. *Environmental science & technology* **2006b**, *40* (4), 1178-1183.
- (159) Basu, I.; Hafner, W. D.; Mills, W. J.; Hites, R. a. Differences in Atmospheric Persistent Organic Pollutant Concentrations at Two Locations in Chicago. *Journal of Great Lakes Research* **2004**, *30* 310-315.
- (160) Great Lakes Commission. An Overview of U.S. Great Lakes Areas of Concern; **2002**.
- (161) Martinez, A.; Hornbuckle, K. C. Record of PCB congeners, sorbents and potential toxicity in core samples in Indiana Harbor and Ship Canal. *Chemosphere* **2011**, *85* (3), 542-547.
- (162) USACE. *Indiana Harbor and Canal Dredging and Disposal Project Ambient Air Monitoring Plan Volume 1*. US Army Corps of Engineers - Chicago District; 2003.
- (163) USEPA. *Quality Assurance Handbook for Air Pollution Measurement Systems Volume IV : Meteorological Measurements*; US Environmental Protection Agency; Research Triangle Park, NC, 2008.

- (164) Antweiler, R. C.; Taylor, H. E. Evaluation of statistical treatments of left-censored environmental data using coincident uncensored data sets: I. Summary statistics. *Environmental science & technology* **2008**, *42* (10), 3732-3738.
- (165) Totten, L. a.; Panangadan, M.; Eisenreich, S. J.; Cavallo, G. J.; Fikslin, T. J. Direct and indirect atmospheric deposition of PCBs to the Delaware River watershed. *Environmental science & technology* **2006**, *40* 2171-6.
- (166) Carlson, D. L.; Hites, R. A. Temperature dependence of atmospheric PCB concentrations. *Environmental science & technology* **2005**, *39* (3), 740-747.
- (167) Gigliotti, C. L.; Dachs, J.; Nelson, E. D.; Brunciak, P. A.; Eisenreich, S. J. Polycyclic aromatic hydrocarbons in the New Jersey coastal atmosphere. *Environmental science & technology* **2000**, *34* (17), 3547-3554.
- (168) Sun, P.; Ilora; Basu; Blanchard, P.; Brice, K. A.; Hites, R. A. Temporal and spatial trends of atmospheric polychlorinated biphenyl concentrations near the Great Lakes. *Environmental science & technology* **2007**, *41* (4), 1131-1136.
- (169) Sofuoglu, A.; Odabasi, M.; Tasdemir, Y.; Khalili, N. R.; Holsen, T. M. Temperature dependence of gas-phase polycyclic aromatic hydrocarbon and organochlorine pesticide concentrations in Chicago air. **2001**, *35* 6503-6510.
- (170) Simcik, M. F.; Basu, I.; Sweet, C. W.; Hites, R. A. Temperature dependence and temporal trends of polychlorinated biphenyl congeners in the Great Lakes atmosphere. *Environmental science & technology* **1999**, *33* (12), 1991-1995.
- (171) Venier, M.; Hung, H.; Tych, W.; Hites, R. a. Temporal trends of persistent organic pollutants: a comparison of different time series models. *Environmental science & technology* **2012**, *46* 3928-34.
- (172) Cortes, D. R.; Basu, I.; Sweet, C. W.; Hites, R. A. Temporal trends in and influence of wind on PAH concentrations measured near the Great Lakes. *Environmental science & technology* **2000**, *34* (3), 356-360.
- (173) Tasdemir, Y.; Vardar, N.; Odabasi, M.; Holsen, T. M. Concentrations and gas/particle partitioning of PCBs in Chicago. *Environmental pollution* **2004**, *131* 35-44.

- (174) Vardar, N.; Tasdemir, Y.; Odabasi, M.; Noll, K. E. Characterization of atmospheric concentrations and partitioning of PAHs in the Chicago atmosphere. *The Science of the total environment* **2004**, 327 163-74.
- (175) Green, M. L.; Depinto, J. V.; Sweet, C.; Hornbuckle, K. C. Regional spatial and temporal interpolation of atmospheric PCBs: Interpretation of Lake Michigan mass balance data. *Environmental science & technology* **2000**, 34 (9), 1833-1841.
- (176) Hafner, W. D.; Hites, R. A. Effects of wind and air trajectory directions on atmospheric concentrations of persistent organic pollutants near the great lakes. *Environmental science & technology* **2005**, 39 (20), 7817-7825.
- (177) Venier, M.; Hites, R. A. Regression Model of Partial Pressures of PCBs, PAHs, and Organochlorine Pesticides in the Great Lakes' Atmosphere. *Environmental science & technology* **2010**, 44 (2), 618-623.
- (178) Hillery, B. R.; Basu, I.; Sweet, C. W.; Hites, R. A. Temporal and spatial trends in a long-term study of gas phase PCB concentrations near the Great Lakes. *Environmental science & technology* **1997**, 31 (6), 1811-1816.
- (179) Buckley, D. R.; Rockne, K. J.; Li, A.; Mills, W. J. Soot deposition in the Great Lakes: Implications for semi-volatile hydrophobic organic pollutant deposition. *Environmental science & technology* **2004**, 38 (6), 1732-1739.
- (180) Li, A.; Rockne, K. J.; Sturchio, N.; Song, W.; Ford, J. C.; Buckley, D. R.; Mills, W. J. Polybrominated diphenyl ethers in the sediments of the Great Lakes. 4. Influencing factors, trends, and implications. *Environmental science & technology* **2006**, 40 (24), 7528-7534.
- (181) Zhao, X.; Drumm, L.; Yin, k.; Rockne, K. J. Segregation of PAH Contaminated Sediments during Hydraulic Dredging and Disposal. *ASCE J. Environ. Eng.* **2009**, 135 291-298.
- (182) Li, A.; Rockne, K. J.; Sturchio, N.; Song, W.; Ford, J. C.; Wei, H. PCBs in sediments of the Great Lakes--distribution and trends, homolog and chlorine patterns, and in situ degradation. *Environ Pollut* **2009**, 157 (1), 141-7.
- (183) Buehler, S. S.; Hites, R. A. Peer Reviewed: The Great Lakes' Integrated Atmospheric Deposition Network. *Environmental science & technology* **2002**, 36 (17), 354-359.

- (184) Miller, S. M.; Green, M. L.; Depinto, J. V.; Hornbuckle, K. C. Results from the Lake Michigan mass balance study: Concentrations and fluxes of atmospheric polychlorinated biphenyls and trans-nonachlor. *Environmental science & technology* **2001**, *35* (2), 278-285.
- (185) Hafner, W. D.; Carlson, D. L.; Hites, R. A. Influence of local human population on atmospheric polycyclic aromatic hydrocarbon concentrations. *Environmental science & technology* **2005**, *39* (19), 7374-7379.
- (186) Great Lakes Commission. An Overview of U.S. Great Lakes Areas of Concern. 2002.
- (187) Simcik, M. F.; Eisenreich, S. J.; Golden, K. A.; Liu, S.-P.; Lipiatou, E.; Swackhamer, D. L.; Long, D. T. Atmospheric loading of polycyclic aromatic hydrocarbons to Lake Michigan as recorded in the sediments. *Environmental science & technology* **1996**, *30* (10), 3039-3046.
- (188) Zhu, X. Ambient concentrations and personal exposure to polycyclic aromatic hydrocarbons (PAH) in an urban community with mixed sources of air pollution. *Journal of Exposure Science and Environmental Epidemiology* **2011**, *21* (5), 437-449.
- (189) Zhang, H.; Eisenreich, S. J.; Franz, T. R.; Baker, J. E.; Offenberg, J. H. Evidence for increased gaseous PCB fluxes to Lake Michigan from Chicago. *Environmental science & technology* **1999**, *33* (13), 2129-2137.
- (190) Granberg, K. J. Air monitoring for the Indiana Harbor and Canal Confined Disposal Facility project: Pre-dredging trends in PAHs and PCBs. *Multimedia Source Apportionment of Semivolatile Organic Contaminants in the Chicago Area of Influence*. 2013, Chapter 3.
- (191) Weschler, C. J.; Nazaroff, W. W. SVOC partitioning between the gas phase and settled dust indoors. *Atmospheric Environment* **2010**, *44* 3609-3620.
- (192) Hopke, P. K. Recent developments in receptor modeling. *Journal of chemometrics* **2003**, *17* (5), 255-265.
- (193) Hopke, P. K.; Ito, K.; Mar, T.; Christensen, W. F.; Eatough, D. J.; Henry, R. C.; Kim, E.; Laden, F.; Lall, R.; Larson, T. V.; Liu, H.; Neas, L.; Pinto, J.; Stölzel, M.; Suh, H.; Paatero, P.; Thurston, G. D. PM source apportionment and health effects: 1. Intercomparison of source apportionment results. *Journal of exposure science & environmental epidemiology* **2006**, *16* 275-86.

- (194) Kim, E.; Hopke, P. K.; Kenski, D. M.; Koerber, M. Sources of fine particles in a rural Midwestern US area RID C-6020-2008. *Environmental science & technology* **2005**, 39 (13), 4953-4960.
- (195) Reff, A.; Eberly, S. I.; Bhawe, P. V. Receptor modeling of ambient particulate matter data using positive matrix factorization: review of existing methods. *Journal of the Air & Waste Management Association (1995)* **2007**, 57 146-54.
- (196) Galarneau, E. Source specificity and atmospheric processing of airborne PAHs: Implications for source apportionment. *Atmospheric Environment* **2008**, 42 (35), 8139-8149.
- (197) USEPA. 2008 National Emissions Inventory, v. 2 Technical Support Document; US Environmental Protection Agency. Research Triangle Park, NC; 2012.
- (198) Henry, R. C. Multivariate receptor modeling by N-dimensional edge detection. *Chemometrics and Intelligent Laboratory Systems* **2003**, 65 (2), 179-189.
- (199) USEPA. Locating and Estimating Air Emissions from Sources of Polycyclic Organic Matter. US Environmental Protection Agency. Research Triangle Park, NC. 1998.
- (200) Demissie, M.; Xia, R.; Keefer, L.; Bhowmik, N. *The sediment budget of the Illinois River*, Illinois State Water Survey Champaign, IL: 2004.
- (201) Machesky, M. L.; Slowikowski, J. A.; Cahill, R. A.; Bogner, W. C.; Marlin, J. C.; Holm, T. R.; Darmody, R. G. Sediment quality and quantity issues related to the restoration of backwater lakes along the Illinois River waterway. *Aquatic Ecosystem Health & Management* 2005, 8 (1), 33-40.
- (202) Cahill, R. A.; Salmon, G. L.; Slowikowski, J. A.; Salmon, G. L. Lakes along the Illinois River. Illinois Sustainable Technology Center, Champaign, IL. 2008.
- (203) Slowikowski, J. A.; Larson, B. D.; Russell, A. M. Database Development to Support Sediment Characterization of the Middle Illinois River. Illinois State Water Survey, Champaign, IL. 2008.
- (204) Tiered Approach to Corrective Action Objectives. In *35 IL Adm. Code Part 742*, 2007.
- (205) Christensen, E. R.; Bzdusek, P. A. PAHs in sediments of the Black River and the Ashtabula River, Ohio: source apportionment by factor analysis. *Water research* **2005**, 39 (4), 511-524.

- (206) Li, K.; Christensen, E. R.; Van Camp, R. P.; Imamoglu, I. PAHs in dated sediments of Ashtabula River, Ohio, USA. *Environmental science & technology* **2001**, 35 (14), 2896-2902.
- (207) Christensen, E. R.; Li, A.; AbRazak, I. A.; Rachdawong, P.; Karls, J. F. Sources of polycyclic aromatic hydrocarbons in sediments of the Kinnickinnic River, Wisconsin RID A-3395-2008. *Journal of Great Lakes Research* **1997**, 23 (1), 61-73.
- (208) Stout, S. a.; Emsbo-Mattingly, S. D. Concentration and character of PAHs and other hydrocarbons in coals of varying rank – Implications for environmental studies of soils and sediments containing particulate coal. *Organic Geochemistry* **2008**, 39 801-819.
- (209) NIST. Certificate of Analysis, Standard Reference Material 1975. Diesel Particulate Extract. National Institute of Standards and Technology, Gaithersburg, MD, 2008; pp 1-9.
- (210) Demissie, M.; Bhowmik, N. *Peoria Lake sediment investigation*, Illinois State Water Survey, Surface Water Section at the University of Illinois, Champaign, IL: 1986.

APPENDICES

Appendix A. Map of PAH and PCB sources near the Confined Disposal Facility.

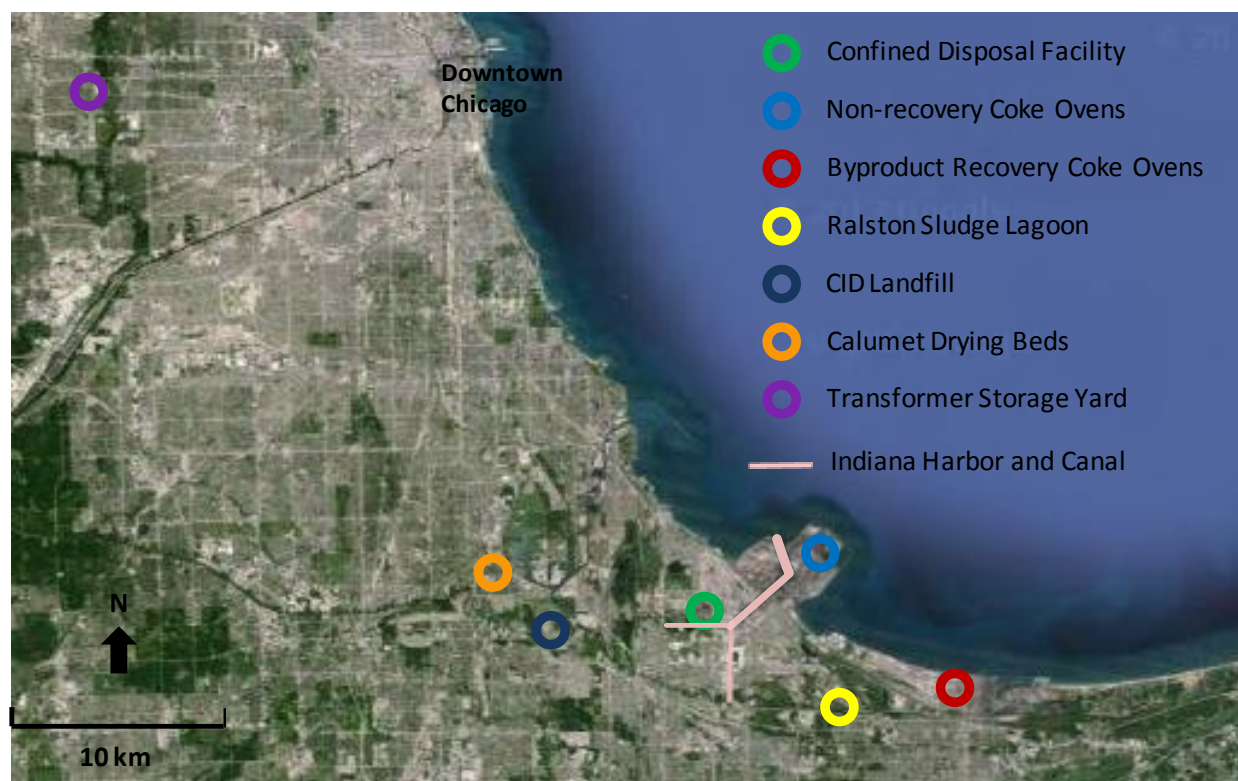


Figure A1. Location of the Indiana Harbor and Canal (IHC) Confined Disposal Facility (CDF) and various investigated atmospheric PAH and PCB sources. Note Figure 3.1 shows the CDF monitor stations and IHC area in greater detail. Aerial photograph ©Google Inc. 2013.

Appendix B. Establishment of an Invasive Plant Species (*Conium maculatum*) in Contaminated Roadside Soil in Cook County, Illinois.

This chapter is reproduced with permission from Gulezian, P.Z., J.L. Ison, K.J. Granberg, and *The American Midland Naturalist* (© 2012). It is a paper I co-authored with Paul Z. Gulezian and Jennifer L. Ison from the Biological Sciences Department at University of Illinois at Chicago. The research was part of my LEAP Integrative Graduate Education Research and Training (IGERT) fellowship. I was responsible for field sampling, soil dosing for the greenhouse experiments, all physical and chemical analyses of the soils, as well as multivariate statistical analysis. I also co-wrote the text. The paper was published in the journal *The American Midland Naturalist* with the following citation: Gulezian, P.Z., J.L. Ison, and K.J. Granberg (2012) Establishment of an Invasive Plant Species (*Conium maculatum*) in Contaminated Roadside Soil in Cook County, Illinois. *The American Midland Naturalist*. 168(2):375-395.

Establishment of an Invasive Plant Species (*Conium maculatum*) in Contaminated Roadside Soil in Cook County, Illinois

Paul Z. Gulezian¹, Jennifer L. Ison^{1,2,3} and Kelly J. Granberg⁴

Interactions between environmental variables in anthropogenically disturbed environments and physiological traits of invasive species may help explain reasons for invasive species' establishment in new areas. Here we analyze how soil contamination along roadsides may influence the establishment of *Conium maculatum* (poison hemlock) in Cook County, IL, USA. We combine analyses that: 1) characterize the soil and measure concentrations of heavy metals and polycyclic aromatic hydrocarbons (PAHs) where *Conium* is growing; 2) assess the genetic diversity and structure of individuals among nine known populations; and 3) test for tolerance to heavy metals and evidence for local soil growth advantage with greenhouse establishment experiments. We found elevated levels of metals and PAHs in the soil where *Conium* was growing. Specifically, arsenic (As), cadmium (Cd), and lead (Pb) were found at elevated levels

¹ Department of Biological Sciences, University of Illinois at Chicago, 845 W. Taylor St. M/C 066, Chicago, IL, 60607 USA

² Chicago Botanic Garden, 1000 Lake Cook Road, Glencoe, IL 60022 USA

³ Present address: Department of Ecology and Evolutionary Biology, University of Toronto, 25 Willcocks St., Toronto, ON M5S 3B2 Canada

⁴ Department of Civil and Materials Engineering, University of Illinois at Chicago, 842 W. Taylor St. M/C 246, Chicago, IL 60607 USA

Corresponding author's E-mail: paul.gulezian@gmail.com.

relative to US EPA ecological contamination thresholds. In a greenhouse study we found that *Conium* is more tolerant of soils containing heavy metals (As, Cd, Pb) than two native species. For the genetic analysis a total of 217 individuals (approximately 20-30 per population) were scored with 5 ISSR primers, yielding 114 variable loci. We found high levels of genetic diversity in all populations but little genetic structure or differentiation among populations. Although *Conium* shows a general tolerance to contamination, we found few significant associations between genetic diversity metrics and a suite of measured environmental and spatial parameters. Soil contamination is not driving the peculiar spatial distribution of *Conium* in Cook County, but these findings indicate that *Conium* is likely establishing in the Chicago region partially due to its ability to tolerate high levels of metal contamination.

Key words: invasive species, soil contamination, genetic diversity, *Conium maculatum*, ISSR, urban ecology, heavy metals, biological invasion.

Introduction

Invasive species can create a multitude of ecological problems. They can drastically alter resource use in ecosystems (Elton 1958; Vitousek et al. 1996), introduce new diseases and pathogens that can negatively affect native species and human health (Mack et al. 2000; Juliano and Lounibos 2005), and change species interactions and ecosystem processes in ways that result in lower levels of biodiversity in the ecosystems they invade (Sakai et al. 2001; Batten et al. 2006). When humans disturb the environment (through construction, damming rivers, plowing for agriculture, etc.), invasive species often exploit these disturbances by colonizing new areas and dramatically increasing in abundance (Hierro 2006; Kneitel and Perrault 2006). Interactions between environmental variables in anthropogenically disturbed environments and physiological traits of invasive species may explain invasive species' range expansions and colonization of new areas. This may be particularly true in urban areas since urban ecosystems and landscapes are highly altered by human activity (Sanderson et al. 2002). Here we investigate how soil contamination along roadsides may influence the establishment of *Conium maculatum* (poison hemlock) a plant considered invasive elsewhere and recently detected only along roadsides in Cook County, Illinois, USA.

Studies of soil contamination and plant invasion have explored relationships between concentrations of contaminants such as heavy metals in both soils and in plant tissues of different species growing near mine sites (Bech et al. 1997; Liu et al. 2005), considered how plants may adapt to contaminated substrates to form monospecific patches that may be associated with biological invasions (Henriques and Fernandes 1991; Urbansky et al. 2000), and examined how contaminants move through urban soils and/or how plants uptake these compounds for potential use as bioindicators of pollution (Mihaljevič et al. 2010; Keane et al. 2001). Genetic studies

have reconstructed invasion histories from an analysis of the genetic structure of multiple invasive populations (Dray Jr. et al. 2009; Henry et al. 2009; Prentis et al. 2009), and evaluated gene flow and/or population differentiation and genetic diversity of multiple invasive populations to predict the potential for future expansion and to inform ecological management (Mandák et al. 2009; Chun et al. 2010).

However, there are few published studies that examine how the establishment or spread of an invasive plant may be associated with soil contamination. Two studies have investigated the interaction of physical soil parameters and either genotype diversity or phenotypic plasticity of an invasive plant species (Morrison and Molofsky 1998; Pan et al. 2006), but neither addressed anthropogenic soil contamination with naturally establishing populations in the field. Despite a growing interest in genome-environment interactions in ecology, there is a dearth of information on such interactions for invasive species upon establishment in a new region. An assessment of levels of genetic variation at contaminated sites and patterns of genetic structure among these sites coupled with a quantification of specific soil contaminants may provide important insights into the processes associated with biological invasions.

This study was prompted by initial field investigations related to the presence of *Conium maculatum* (hereafter, *Conium*) in Cook County. *Conium*, widespread in the United States and Canada (USDA PLANTS database: <http://plants.usda.gov/>), was first observed in Cook County along the Bishop Ford Freeway (I-94) in 2006 (Gulezian and Nyberg 2008). The establishment of *Conium* in Cook County appeared to be a recent phenomenon, as there are no herbarium records of the species in Cook County (<http://www.vplants.org>). Subsequent surveys in 2007 and 2008 were conducted in which the roadsides of all major interstate highways in southern Cook County and any natural areas within 1 km of the roadway were searched for the plant. In total we

found nine populations, all along roadsides and/or near land owned by the Metropolitan Water Reclamation District of Greater Chicago (MWRD-GC). The MWRD-GC lands contained wastewater treatment plants (WWTPs), including the largest in the world at Stickney, and biosolids processing and drying facilities where biosolids are spread on large open concrete beds. Biosolids are likely to contain metals and persistent organic pollutants that are removed from the wastewater stream. The *Conium* populations' spatial connection to these facilities suggested soil contamination may be an important factor in *Conium*'s presence in Cook County.

Urban soils are often contaminated by a suite of diverse compounds, but we focused on two major classes of contaminants, heavy metals and polycyclic aromatic hydrocarbons (PAHs), given the populations' locations along interstate highways and biosolids drying beds. Vehicle and road wear, combustion byproducts, and pollutant-enriched biosolid material are likely to deposit in nearby soil and thus enrich its heavy metal and PAH content (Van Bohemen and Janssen van de Laak 2003; Oliver et al. 2005; Harrison et al. 2006). Chemical analysis demonstrated that soil where *Conium* was growing approached or exceeded contamination thresholds according to EPA ecological soil screening criteria (US EPA 2005a). Given this result, we examined *Conium*'s tolerance to specific soil contaminants and investigated whether genetic diversity within populations or genetic structure among populations was associated with measured contaminant concentrations.

The primary questions posed by this research are:

1. What is the overall genetic diversity of *Conium* populations in Cook County and what is the level of genetic differentiation among populations?
2. Using collections of seeds and soils, is there any evidence for local soil growth advantage for seeds growing in home soil versus other sites' soil in the greenhouse?

3. Are *Conium* seedlings more tolerant of heavy metals than two native species, *Desmodium canadense* (showy tick trefoil) and *Echinacea purpurea* (purple coneflower; hereafter *Desmodium* and *Echinacea*)?

4. Is there any discernible correlation between concentrations of soil contaminants and/or spatial variables and the genetic diversity (within) and genetic structure (among) the field populations?

Addressing these questions to gain insight into environment/genome interactions is important in understanding the spread of invasive plants in anthropogenically disturbed landscapes.

Methods

This research was divided into four principal research methodologies. The first section consisted of two seasons of **field surveys** to detect *Conium* populations along roadways and in natural areas in southern Cook County. The second was a **soil characterization analysis** that quantified various contaminants and physical/chemical parameters of the soil in which each *Conium* population grew. The third was a **genetic analysis** that quantified the levels and patterns of genetic variation in *Conium* plants among the nine populations. The fourth section was the **greenhouse establishment experiments** that tested for 1) local advantage (defined as seeds germinating and seedlings growing better in their original soil compared to soil from other populations), and 2) tolerance to heavy metals (defined as the growth of individuals from nine *Conium* populations relative to *Desmodium* and *Echinacea* seedlings in the presence of known levels of arsenic (As), cadmium (Cd), and lead (Pb)).

Study species. Many invasive plants have life history traits (fast growth rates, tolerance to pollution, generalist resource use) that can be advantageous in disturbed habitats (Thuiller et al. 2006). *Conium maculatum* (poison hemlock) is a non-native plant in the carrot family

(Umbelliferae) that is often considered an invasive species throughout the United States²¹²⁻²¹⁴. It is biennial and self-incompatible and a single plant produces thousands of seeds (Baskin and Baskin 1990). Its seeds do not disperse easily by gravity over long distances, so the plant is often carried by water, in the hair of mammals, and by human activity to colonize new areas²¹⁵. The species is native to Europe, North Africa, and Asia, and has been documented in every American state and Canadian province except for Mississippi, Florida, Alaska, Hawaii, Manitoba, Yukon, and the Northwest Territories. *Conium* is commonly found in most of Illinois except for the northeastern counties (Cook, McHenry, Lake; USDA PLANTS database: <http://plants.usda.gov/>).

Field surveys. The first population of *Conium* in Cook County (Calumet) was documented in 2006. Detailed systematic surveys were conducted during May and June of 2007 and 2008 and nine populations were detected. Since *Conium* is a biennial, two consecutive years of surveys allowed for better detection of populations since only second year plants are conspicuous. The nine *Conium* populations were located in two distinct ‘hotspots’ in southern Cook County (Fig. 1). Four populations (Stickney, Harlem, I-55-1, I-55-2) were located near interstate I-55 and the Stickney WWTP near McCook, IL and five populations (Calumet, CalDryBed, BFN-1, BFN-2, 130th/Doty) were located near interstate I-90/94 close to 130th St. and the Calumet WWTP in southeastern Chicago. Given the widespread nature of the species in other places across the continent, it seemed unlikely that it would be regularly associated with a particular habitat in Cook County. This peculiar, localized distribution inspired our investigation.

We conducted surveys by car (with one driver and a second observer), by bicycle, and on foot during *Conium*’s flowering time in May and June. Second year plants are 2 m or more in height and produce many large umbels of bright, conspicuous white flowers, permitting easy detection

even from the window of a car traveling on an interstate highway. We recorded frequency of occurrence, the location of each population, and estimated densities by walking around the perimeter of each *Conium* patch with a GPS device (Garmin Colorado 400t) that calculated distances and areas. We surveyed all of the roadsides of the 5 major interstate highways (2-90, 2-94, 90/94, 57, and 55) in southern Cook County, accounting for 272 miles of roadway. In order to survey areas with different types of land use near the roadways, 12 miles were surveyed on foot, and 35 miles were surveyed by bicycle, respectively, on paths within and between natural areas for all of the natural areas adjacent to (a boundary within 1 km of) the surveyed interstate roadways. The surveyed natural areas included: Beaubien Woods (I-94), Bartell Grasslands (I-57), Chicago Portage (I-55), Bemis Woods South (I-294), Thatcher Woods (I-290). No *Conium* populations were detected in any natural area.

Soil sample collection. We sampled soil at each of the nine *Conium* populations in June of 2008 by extracting cores with a stainless steel probe inserted manually at grade. One, two, and three samples were extracted from each population based on its respective size (small; up to 2000 m², medium; 2000 to 6000 m², and large; over 6000 m²) for a total of fifteen cores within all populations. Soil cores measured 2 cm in diameter by 30 cm in length, except for one core in each medium and large population that was segmented and only the top 20 cm composited and analyzed (note that no significant differences were found between segments and full cores). In addition to within-population soil cores, soil cores offset 500 m from the boundary of each population were taken to permit comparison of roadside soil where *Conium* was both present and absent, for a total of twenty four soil cores collected for analysis in the sampling effort. The probe was rinsed with de-ionized water and wiped clean between each sample. Cores were sealed in labeled glass jars and refrigerated for storage within eight hours of sampling. Samples

were prepared for analysis by homogenization and removal of rocks, organic matter, and debris appearing larger than 1 cm in any two directions with a clean stainless steel spoon and spatula. In June 2009 we also collected nearly 10 liters of soil from each population by shovel and bucket at core locations to be used in the greenhouse establishment experiments.

Soil contamination analysis. Soil samples were analyzed for 20 metals and 20 PAHs by National Environmental Laboratory Accreditation Program (NELAP) certified analytical laboratory StatAnalysis, Inc., Chicago, IL. Metals were extracted from subsamples by the acid digestion procedure given in US EPA method 3050B (US EPA 1996a) and analyzed by inductively coupled plasma-mass spectrometry per EPA method 6020A (US EPA 2007): except for mercury, which was analyzed by cold vapor atomic absorption given in method 7471A (US EPA 1994). PAHs were extracted from soil subsamples according to EPA ultrasonic extraction method 3550B (US EPA 1996b), followed by analysis via gas chromatography/mass spectrometry in selective ion mode per method 8270C (US EPA 1996c).

Physical and chemical soil characterization. Soil samples were quantified for physical and chemical parameters including: wet bulk density, percent solids (the complement of percent moisture), organic matter, organic carbon, nitrogen, black carbon, pH, and salinity. Bulk density was determined by gravimetrically weighing the soil and measuring its volume in a 50 ml graduated conical tube after shaking and three taps on a hard surface to settle (if clayey soil, after mixing and compaction with pestle to air space similar to original cores). Solids were determined from gravimetric weighing of sub-samples pre- and post-oven drying (105 °C, 48 h), while organic matter was determined by gravimetric weighing of dried sub-samples pre and post muffle furnace combustion (375 °C, 24 h) as described in Buckley et al. (2004). Organic carbon, nitrogen, and black carbon measurements were taken from dried or combusted subsamples by

elemental analysis (Buckley et al. 2004). Salinity and pH were measured in a 1:1 soil to de-ionized water suspension by conductivity cell and combination electrode respectively, following vortex and manual shaking for one minute at ten minute intervals over an hour and settling over an hour (Janzen 1993; Hendershot et al. 1993).

Field sampling of plant tissue. During the 2008 flowering season we collected leaf samples from all the identified Cook County *Conium* populations. *Conium* plants do not grow clonally and individual flowering plants in the field are easily distinguished from each other. No two tissue samples within a population had the same genotype, confirming our identification of individuals. For five of the populations (130th/Doty, BFN-1, Calumet, Harlem, and Stickney) we assessed the spatial range of the population and estimated total flowering plants. We then systematically walked the population (most were elongated rectangles in shape, given the roadside locations) and sampled every third to tenth plant we came to, depending on population size, so that we would collect around 30 leaf samples upon reaching the end of the population. Two populations (BFN-2 and CalDryBed) had between 20-24 flowering plants so we collected samples from all flowering plants. Two distinct nearby (380 m) populations (I-55-1 and I-55-2) had very few flowering plants, so all of the plants from these populations were sampled, and the samples were combined for the genetic analysis (21 total samples). All tissue samples (217 total samples) were dried immediately in silica gel and stored at room temperature.

Genetic laboratory analysis. Dried tissue samples were homogenized to a fine powder using Talboys High Throughput Homogenizer (Henry Troemner LLC, Thorofare, NJ) and DNA was extracted using a Qiagen DNeasy Plant Mini Kit (Qiagen, Germantown, MD). We quantified the amount of DNA in each extraction using a NanoDrop ND-1000 (version 3.3). Thirty potential inter simple sequence repeat (ISSR) primers were screened for amplification, variability, and

consistency of results in *Conium*. ISSRs are highly variable dominant markers that use microsatellite regions in the genome as primers, and the presence or absence of bands on an agarose gel indicates differences in primer binding sites between individuals. We chose five inter-simple sequence repeats (ISSR) primers (table 2) for our study, which yielded 114 variable bands. A 25 μ l volume polymerase chain reaction (PCR) was carried out for each *Conium* sample for each ISSR primer. We used the following 25 μ L polymerase chain reaction mixture: 10 ng template DNA, 1.0 μ M ISSR primer, 12.5 μ L PCR MasterMix 2 \times (Promega:50 U/mL Taq DNA polymerase in a proprietary reaction buffer, pH 8.5, 400 μ M of each dNTP, and 3 mM $MgCl_2$), 12.5 μ g/ μ L of bovine serum albumin, and an additional 0.675 mM $MgCl_2$. The thermocycling conditions consisted of: a five minute denaturing step at 94 $^{\circ}C$, then 35 cycles of the following 45 second denaturing step (94 $^{\circ}C$), 45 second of annealing step (50 $^{\circ}C$), two minute elongation step (72 $^{\circ}C$), then a final five minute elongation step at 72 $^{\circ}C$. If a PCR reaction failed for any given *Conium* sample up to two additional reactions were conducted. Five samples required re-extraction of DNA.

PCR products were electrophoresed on high resolution 1.25% agarous gels (Sigma-Aldrich) containing ethidium bromide to visualize DNA. Every sixth well of the agarose gel had a 100-1000 base pair ladder. Gels were run for 200 minutes at 100 volts. Gels were then placed in GeneFlash imaging box equipped with an ultraviolet light and a camera (syngene bio imaging synoptics Ltd version 0.34). To ensure that we captured every band regardless of brightness we took four pictures per gel at four, eight, twelve, and sixteen second exposures. Gel images were printed and scored by eye independently by two researchers. Individual bands were scored for presence or absence. To ensure that banding pattern differences were unrelated to the PCR

reactions and agarose gel we mixed up individuals from populations in each PCR reaction and on agarose gels.

Genetic data analysis. Observed and expected heterozygosities were calculated using GenAlEx6.2²¹⁶. Population structure was evaluated using the Bayesian approach implemented in Hickory 1.1²¹⁷ and AFLPDAT [ENREF_219](#)²¹⁸. GenAlEx utilizes standard statistical methods and assumes the populations are in Hardy-Weinberg equilibrium. We used GenAlEx to get an estimate of population heterozygosities and Nei's unbiased pairwise genetic distance²¹⁹. We also used GenAlEx to perform an analysis of molecular variance (AMOVA) to determine how molecular variation was apportioned among and within populations, and a Mantel test to investigate the relationship between genetic distance and geographic distance for our molecular data. However, since our populations have recently established in the region, the populations may violate Hardy-Weinberg equilibrium. Therefore we also used a Bayesian statistic program, Hickory 1.1, which does not assume Hardy-Weinberg equilibrium, to get an overall estimate of population structure. We used AFLPDAT, which is a group of functions for R to get proportion polymorphic bands and intra-population genetic diversity for each population. We ran AFLPDAT in R 2.10.1²²⁰.

Greenhouse establishment experiments. The goals of this part of the study were to set up controlled experiments to test: 1) whether seeds from a given population grow better in their home soils, and 2) whether *Conium* grows better in soils spiked with As, Cd, and Pb than *Desmodium* and *Echinacea*. Seeds and soils were collected from the nine known *Conium* field populations. *Conium* seeds were collected from each field population from a minimum of 10 individuals evenly distributed throughout each population, and all seeds from a given population were pooled together en masse. *Desmodium* and *Echinacea* were selected as comparable species

because they have similar seed sizes to *Conium*, are often used in roadside plantings of native species by the Illinois Department of Transportation, and commonly occur in many of the natural ecosystems of the Chicago region.

A complete factorial design was implemented for the *Conium*-only local advantage test, with each combination of field population seed source and field population soil source replicated three times. Thirty seeds from a given population were placed on the top of soil from each population in a small greenhouse cup (volume = 388 mL per cup) for each replicate and watered once a day. Each combination of seed and soil (30 seeds per population per soil replicate) from both the *Conium*-only local advantage and the three-species metal tolerance experiments ($n = 408$) was randomly placed in one of fifteen greenhouse trays. Each tray was randomly rotated daily to control for the potential influence of position on the greenhouse bench.

For the metal tolerance experiment, a complete factorial design was used as well. Peat moss was spiked with Pb, Cd, and As to 1000 mg/kg, 100 mg/kg, and 100 mg/kg (dry weight basis) respectively, elevated concentrations within an order of magnitude of those measured in *Conium* field soil cores. Spiking salts lead(II) chloride, cadmium chloride, and sodium arsenate (dibasic heptahydrate) were chosen to maximize metal bioavailability in terms of water solubility and to minimize nutrient enrichment by presence of nitrogen or phosphorous (Janzen 1993). In addition to three individual metal treatments, a combination treatment of all three metals and a control treatment (without metal pollutants) were prepared for a total of five treatments.

Soil spiking was done by fully dissolving a known mass of each metal salt in beakers of de-ionized water and mixing thoroughly with a known mass of peat moss for each soil treatment: Pb, Cd, As, and Combo (Pb, Cd, and As). A Peat control was mixed with pure de-ionized water. Saturated soil treatments were allowed to dry and equilibrate for 48 hours under a fume hood

with regular mixing before being potted for seeding. Seeds from all nine *Conium* populations and from catalog-bought *Desmodium* and *Echinacea* sources (Prairie Moon Nursery, Winona, MN) were placed in each spiked treatment in triplicate to conduct the metal tolerance experiment. Prairie Moon Nursery is a nursery specializing in native plants, and the *Desmodium* and *Echinacea* seeds we used were not seeds from cultivars but rather from native plants that were collected from prairie remnant populations in the field. We did analysis of seedling growth at the population level and at the species level (with *Conium* populations pooled). Each seed population had 15 replicates among five treatments: Pb, As, Cd, Combo, and control (peat moss without addition of metals).

The seedlings were monitored daily for germination and growth rates over 45 days. Seedlings were counted as established at the appearance of the first true leaf. Heights were measured and seedlings were placed into two height classes: 0-5 cm and 5-10 cm. At the end of the growth phase (45 days), above ground biomass (AGB) was harvested, dried in an oven for 48 hours at 90 °C, and weighed. These data provide a metric for overall plant performance and are the primary results of the establishment experiment. We used final counts of germinated and ungerminated seeds and numbers of individuals in different size classes to characterize the relative growth among the 11 populations as well.

Quantitative and statistical analysis. Statistical analyses were done with SYSTAT software package (v. 12, Systat Software, Inc., Chicago, IL USA). The AGB measurements for each population of seeds in each spiked treatment (As, Cd, Pb, Combo) were standardized to the mean AGB of a given population of seeds in the Peat control to account for differences among species in germination times and growth rates.

To investigate the relationships between metrics of genetic diversity and soil and/or spatial variables measured in the field for each population, we used rank correlations. Significant negative correlations between genetic diversity and soil contaminant concentrations would be evidence for locally adapted *Conium* genotypes. Our correlations were at the population scale, with $n = 8$ since the I-55-1 and I-55-2 populations were combined for all genetic analyses. Correlation of ranks was calculated using the Spearman correlation coefficient, or rho (ρ), a nonparametric statistic, as recommended by Zar (1996). For all variables the lowest value was given the rank of 1 (if there was a single instance of that value) and large values had higher ranks. Positive correlations imply that low values of one variable are associated with low values of the other variable. We used three genetic metrics (mean heterozygosity (H_e), proportion of variable loci, and intra-population genetic diversity) and compared those variables to 20 soil or spatial variables measured for each field population. A t-distribution is usually used to determine the significance of the rank correlations, but is a poor approximation of the sample distribution of ρ when $n < 10$. In our analysis with $n = 8$ populations ($df = 6$), therefore, significant results at the 0.05 level are obtained when the absolute value of ρ is at least 0.62 and 0.72, for directional and non-directional tests, respectively (Zar 1996).

Results

Field populations and soil characterization. The relative locations of the nine *Conium* field populations, the MWRD-GC biosolids drying beds, and the associated roadways are shown in Figure 1. The nine *Conium* populations were located in two distinct ‘hotspots’ in southern Cook County. Four populations (Stickney, Harlem, I-55-1, I-55-2) were located near interstate I-55 close to McCook, IL and the Stickney WWTP, and five populations (Calumet, CalDryBed, BFN-

1, BFN-2, 130th/Doty) were located near interstate I-90/94 close to 130th St. and the Calumet WWTP in southeastern Chicago. Table 1 summarizes several of the key soil and spatial measurements for each population. The total area covered by each *Conium* population varied considerably from 50 to 60,000 m². The distances to the nearest population ranged from 100 to 1,450 m. The Calumet and Western Suburbs hotspots shown in Fig. 1 are about 20 km apart.

In general, soil parameter and contamination data seldom differentiated significantly between the populations, hotspots, or population interiors and exteriors. Arsenic, barium, cadmium, chromium, copper, iron, lead, manganese, mercury, nickel, potassium, vanadium, and zinc among metals; and anthracene, phenanthrene, pyrene, fluoranthene, chrysene, benz(a)anthracene, benzo(b)fluoranthene, benzo(a)pyrene, benzo(k)fluoranthene, indeno(1,2,3-cd)pyrene, benzo(g,h,i)perylene, and dibenz(a,h)anthracene among PAHs were frequently detected, while other metals and lightweight PAHs were less so. Table 1 shows single or mean soil population concentrations (recall the number of samples were relative to *Conium* population area) of As, Cd, and Pb ranging from 6.7 to 18.5, 1.3 to 24.5, and 78.0 to 356.7 mg/kg dry weight, respectively. Figure 2 depicts the soil concentrations of As, Cd, and Pb with solid lines indicating soil screening levels of concern for plants (US EPA 2005a), illustrating that at least one population nearly reaches or exceeds contamination thresholds for each of the metals. While the average concentration of total PAHs (11.1 mg/kg, not shown) and levels of individual PAHs may exceed human health risk standards, the risk to plant life is not as clear as for the metals (US EPA, 2005b). The relatively high As, Cd, and Pb concentrations shown and their known interactions with plants (Keane et al. 2001; Uveges et al. 2002; Liu et al. 2005) motivated our interest in a controlled test of metal tolerance for *Conium* in the greenhouse. All soil parameters, PAH, and metal data were used in correlation analyses with genetics metrics.

Genetic analysis. The primer nucleotide sequences, the number of individuals successfully amplified, and the total number of polymorphic bands found in all the individuals analyzed for each of the five ISSR markers are reported in Table 2. Table 3 describes the genetic diversity found in nine *Conium* populations ($n = 217$) using 114 loci from five ISSR markers. The observed number of bands ranged from 83 to 104, with very few bands being unique to a single population. Heterozygosities ranged from 0.143 to 0.232 and the proportion of variable loci (PVI) ranged from 0.523 to 0.798.

The analysis of molecular variance (AMOVA) demonstrated significant levels of variation ($p < 0.01$) among populations, with 16% of the total variation among populations while 84% was due to differences between individuals within populations. A neighbor-joining phenogram (Fig. 3) based on the pairwise values of Nei's unbiased genetic distance indicates that genetic distances among populations are small (< 0.04) compared to previous studies of non-invasive plants in their home range (Ma et al. 2008), but similar to studies of invasive plants like *Miconia calvescens*; Le Roux et al. 2008). The phenogram shows that CalDryBed, the most physically isolated population (Table 1), is clearly the most genetically distinct population, but there is no overall geographic pattern to the distribution of the populations in the figure. In several cases, genetic distances clearly do not reflect physical proximity (Fig. 1). An example is the close clustering of the Harlem and 130th/Doty populations, two populations in separate invasion 'hotspots', located over 30 km apart. Moreover, the results of the Mantel test ($r = 0.062$, $p = 0.01$) revealed no pattern of genetic differentiation by geographic distance.

Rank correlations between genetic metrics and soil/spatial field parameters. Rank correlations at the population scale ($n = 8$) between metrics of genetic diversity and variables measured in the field for soil and spatial attributes of each population are given in Table 4. There

are few significant correlations, and overall, it appears that the populations' genetic diversity does not correlate with most of the measured soil and spatial attributes. However, there are several significant associations of note. Mean heterozygosity and distance to nearest population are negatively correlated, as are intra-population genetic diversity and distance to nearest population. Mean heterozygosity and intra-population genetic diversity are both positively correlated to pH. Although concentrations of barium and potassium were the only metal measurements to correlate significantly (negatively) with genetic metrics, there is a general trend of negative correlations between many of the metal concentrations and metrics like mean heterozygosity, proportion of variable loci, and intra-population genetic diversity. Of the 24 correlations shown in Table 4 between metal concentrations (using the 8 metals with the highest mean concentrations across all samples) and genetic diversity metrics, 23 are negative correlations, so while we found few significant correlations, the trend is a consistent negative association between genetic diversity and levels of soil contamination.

Greenhouse establishment local advantage experiment. Figure 4 illustrates *Conium* growth expressed as mean weights of above ground biomass for seeds grown on local population soil and on soil from all other *Conium* populations. There is no clear local advantage for any of the seed and soil pairs.

Greenhouse metal tolerance experiment. Figure 5 shows the metal tolerance (As, Cd, Pb, Combo) among three species from the greenhouse experiment. We report mean AGB which has been divided by the mean weight from the peat control for each population of seeds. *Conium* grows significantly better in the As treatment than *Echinacea* (ANOVA $p = 0.002$, $F = 7.82$, $df = 2$, pairwise comparisons significant at the 0.05 level). *Conium* also grows significantly better in

Combo (As, Cd, Pb) treatment than both *Desmodium* and *Echinacea* (ANOVA $p < 0.0001$, $F = 13.19$, $df = 2$, pairwise comparisons significant at the 0.05 level).

Discussion

Given that *Conium* is widespread in much of North America (USDA) and is a known colonizer of wetland margins and riparian areas (Stephens 1980, Whitson et al. 1992), the historical absence of *Conium* in Cook County, Illinois suggests that *Conium* would not be expected to be exclusively associated with contaminated sites along the roadways of a major urban area. The interesting question, therefore, is why *Conium* is associated with such sites in Cook County. *Conium* clearly shows at least a general tolerance to anthropogenic soil contamination in both the field (Fig. 2) and the greenhouse (Fig. 5), but it is unclear that this tolerance to contaminated soils is driving its establishment in the Chicago region. Although we found high levels of genetic diversity in our populations, which is consistent with the expectation for successful, non-clonal, invasive plants in adverse environments (Lee 2002), we did not find significant positive correlations between genetic diversity and concentrations of soil contaminants (Table 4). Such a result would be expected for successfully colonizing populations under adverse conditions (high soil contaminants in our study). In fact, though not significant, the vast majority of the correlations between genetic diversity and soil contaminant concentrations reported in Table 4 were negative, suggesting that high diversity was more likely associated with low levels of contamination. Moreover, we found little population genetic differentiation and structure among all known populations (Fig. 3). We also found no significant evidence for a particular *Conium* population associated with high metal or PAH contamination (Table 4).

Considered alone, the genetic analysis serves as an interesting assessment of the genetics of an invasive species that has recently established populations in a new region. Ward et al. (2008) summarized the ecological genetics of invasive plants and found that invasive plant populations in the invaded range can have both high and low levels of genetic diversity. When genetic structure is measured, the results tend to reflect the reproductive biology of the species in question. Cross-breeding species like *Conium* tend to have high genetic diversity within populations and low genetic differentiation among populations. This is indeed what we found, which is not surprising. For example, all of the values for the genetic diversity metrics in our populations are generally high when compared to values from previous studies on other invasive species including: buffelgrass (*Pennisetum ciliare* L. Link; PVI ranged from 0.222 to 0.519; Gutierrez-Ozuna et al. 2009); alligator weed (*Alternanthera philoxeroides*; $H_e = 0.0056$, PVI was 0.0648; Geng et al. 2007); fountain grass (*Pennisetum setaceum*; no genetic variability detected with 18 ISSR primers; Poulin et al. 2005); and cat's claw creeper (*Macfadyena unguis-cati* L. Gentry; Prentis et al. 2009) and bladder campion (*Silene latifolia*; Taylor and Keller 2007). This is true even for the *Conium* populations with relatively low numbers of individuals. Table 3 shows that all populations had proportions of variable loci of at least 0.50, with several populations reporting values close to 0.80. This is a large amount of variability for relatively small, relatively isolated, and relatively young (from a colonization standpoint) populations. It seems very likely that *Conium* is not clonal even though it forms dense monospecific stands. Although we sampled plants in a stratified manner (i.e. did not sample two plants next to each other), we still found that no two individuals had exactly the same genotype, even in populations where we censused all plants. Consequently, all plants seem to be the result of sexual

reproduction by seed, consistent with evidence that *Conium* is self-incompatible (Baskin and Baskin 1990).

Also notable is the virtual lack of any genetic differentiation among *Conium* populations. Figure 3 shows a cluster tree of the structure of the eight populations, which is remarkable for the relatively short lengths of the branches between nodes given the numerical scale. CalDryBed is the most genetically unique population. Even relatively small populations like CalDryBed and I-55 (comprised of I-55-1 and I-55-2 for genetic analysis due to small population sizes) that do not show much differentiation from larger populations do not seem to suffer much loss of genetic diversity. Although small populations may not show reduced diversity, there may be evidence that more isolated populations do. Table 4 shows significant negative correlations between distance to nearest population and both mean heterozygosity and intra-population gene diversity. This apparent reduction in diversity with increasing spatial isolation is more consistent with expectations for colonizing populations, but the general lack of genetic differentiation and the relatively high genetic diversity are more unusual and an especially remarkable attribute for the invasive *Conium* populations in Cook County.

Although we did not find significant correlations between levels of genetic diversity and soil contaminant concentrations, it is likely that *Conium*'s general tolerance to contaminants like As, Cd, and Pb (as compared to other species; Fig. 5) may allow it to colonize and reproduce in roadside areas that harbor these pollutants. The results of our spiked metal treatments in the greenhouse seedling establishment experiment are consistent with the idea that *Conium*'s tolerance to soil contamination allows it to do well enough in disturbed soils and roadside locations that may serve as 'footholds' in a new region. Whether *Conium* will remain exclusively associated with these roadside habitats or whether it will expand to other kinds of habitats and

micro-environments is unclear. What is clear, however, is that our results showing populations with consistently high genetic diversity compared to previous studies of invasive plants (Poulin et al. 2005; Geng et al. 2007; Gutierrez-Ozuna et al. 2009) indicate that *Conium* is only able to successfully colonize areas along roadsides in Cook County that receive a large amount of seed from a diverse source, or multiple introductions of seed from several genetically distinct sources. This established high diversity (Table 3) and *Conium*'s general tolerance to particular heavy metals (Fig. 5) only increases the species' adaptability to new environmental conditions. Therefore we find no evidence that indicates *Conium* will remain limited to the particular roadside habitats where we detected it.

The principal goal of this study was to combine analysis of the genetic variation of populations of a recently established invasive species with an assessment of a specific kind of anthropogenic environmental contamination. The only other similar study to investigate how environmental contamination (copper, tributyltin) may be promoting biological invasion concerns marine sessile invertebrates in New South Wales, Australia, but that study did not incorporate a genetic assessment of the invading populations (Dafforn et al. 2009). Although we had good reason to believe that tolerance to soil contamination, and particularly contamination by heavy metals (Table 1, Figs. 1 and 2), may be aiding *Conium*'s establishment in Cook County, we did not find specific evidence to conclude that a tolerance to soil contamination is actively driving the invasion process for this species in this region.

However, an alternative hypothesis that we did not explicitly test is provided by research on fungal endophytes that impart habitat-specific stress tolerances to their plant hosts which can increase plant survival in high stress environments, such as contaminated soils. Kim et al. (2008) found that *Phytolacca americana* (pokeweed) plants from sites with contaminated soils in South

Korea contained a single dominant fungal endophyte that was missing from pokeweed plants that grew in uncontaminated sites. Moreover, the endophyte was measured in highest abundance in leaves where the highest concentrations of metals were found. It is possible that the *Conium* plants that grow in the contaminated roadside habitats we studied also harbor endophytes that promote their survival in such high-stress habitats. Other studies have demonstrated that fungal symbionts have the ability to grant metal tolerance to plants (Monnet et al. 2001, Wilhite et al. 2001, Al-Karaki et al. 2001), so this is a possibility worth investigating for the *Conium* populations in Cook County.

What is striking is the overall lack of relationship between the genetic diversity metrics and the levels of soil contamination, even in light of the peculiar spatial association with sites with demonstrated metal contamination. As indicated in Table 4, few measures of genetic diversity were correlated (positively or negatively) with levels of soil contamination. In fact, we only found two metals (barium and potassium) that were significantly negatively associated with any genetic diversity metric (mean heterozygosity, proportion of variable loci, or intra-population genetic diversity). Neither metal was found in very high concentrations in the field, nor is either regarded as particularly toxic, as compared to metals like arsenic, cadmium, lead, and mercury, although potassium is an essential plant nutrient. The general lack of significant relationships between soil and genetics variables may indicate that *Conium* is just particularly opportunistic, with some capacity to tolerate disturbed soils that harbor relatively high levels of contaminants. So while our soil and genetics characterizations generated a good baseline data set, they did not clarify specific reasons for why *Conium* may be occurring in these particular locations in the region. Our dataset may benefit from an analysis using roadside dispersal models (Floerl and

Inglis 2005; Drake and Lodge 2006; Pysek et al. 2008) if the distribution and genetics of *Conium* populations along roadsides in regions near the Chicago area was also known.

The greenhouse experiments did not provide any significant evidence of local advantage (Fig. 4), further supporting the idea that the *Conium* populations in Cook County are not specifically promoted by the soils in which they are growing. In fact, only two of the nine seed populations (I-55-1, BFN-1) grew better in their own local soil than they grew in all of the other eight field soils. Even CalDryBed, the population with the lowest mean heterozygosity (Table 3) and the basal root on the cluster tree (Fig. 3), did not show any difference in AGB growth between local and other soils. Hypothetically, if one expected to observe local adaptation to soil that was reflected in the genetic diversity of the individuals of a population, a reduction in genetic variation would be consistent with natural selection for a particular ecotype having higher fitness (seed set, etc) in a particular soil (Hufford and Mazer 2003; Lopez et al. 2009). Although we did not do range-wide sampling that would allow us to test for a contamination-resistant *Conium* ecotype, we did not even find evidence for the mere promotion of seedling growth by local soil for any of our populations. Thus, it would seem unlikely that we would detect a contamination-resistant *Conium* ecotype even if we had done the requisite range-wide sampling and analysis.

However, we did find evidence for *Conium*'s tolerance to soils spiked with known concentrations of As, Cd, and Pb, as compared to *Desmodium* and *Echinacea*. *Conium* seedlings were more tolerant of the As and combo (As, Cd, and Pb) treatments ($p < 0.05$, Fig. 5). These are important results because they demonstrate that *Conium* has a general tolerance to some of the contaminants that we found at elevated levels in the roadside soils where *Conium* has colonized the region. This general tolerance to metal contamination may serve to allow most *Conium* individuals to grow well enough in highly disturbed, contaminated areas to form self-sustaining

populations that export seed to colonize new areas in the region. Since this tolerance does not seem to be the exclusive attribute of a particular *Conium* population with low diversity, this may also allow *Conium* to maintain its observed relatively high genetic diversity, an attribute of an invasive species that is often viewed as an advantage when colonizing new areas with lots of habitat heterogeneity and environmental variability (Lee 2002).

This study sought to generate relevant information about *Conium*'s recent establishment in the Chicago region's urban landscapes through a characterization of the soil and the genetics of the known *Conium* populations. Our specific ideas about soil contamination promoting the invasion of this species were motivated by our field surveys showing *Conium* populations to be associated with contaminated soil characteristic of roadway and biosolid influence. We did find evidence that *Conium*'s general tolerance to metals like As, Cd, and Pb may allow it to colonize and thrive in highly disturbed areas with contaminated soil along roadways, but we did not find convincing evidence that genetic diversity and levels of soil contamination were positively correlated. We cannot claim, therefore, that metal contamination is driving the distribution of *Conium* in Cook County in any clear way. The peculiar spatial association with MWRD land and roadsides remains poorly understood. Even so, the results of our greenhouse seedling experiments may help clarify reasons for *Conium*'s initial success in colonizing the region. Other studies have shown that invasive plant species like *Solidago canadensis* (Canada goldenrod) can out-compete native species in lead-contaminated soil in greenhouse competition experiments (Zhang et al. 2008). In our study, *Conium*'s apparent relative advantage over *Desmodium* and *Echinacea* in soils contaminated with As and with a combination of As, Cd, and Pb may partially explain its success in colonizing roadside soils with relatively high levels of metal contamination.

Although we were not able to clearly explain the processes that generated the curious distribution patterns of *Conium* populations in Cook County, this interdisciplinary approach to explaining invasive plant establishment is likely to be successful if enough reasonably relevant possibilities (such as fungal endosymbionts) are investigated. We encourage others to modify our techniques and refine our central approach to suit their research questions while preserving the combination of a genetic analysis with assessments of environmental contamination or other kinds of anthropogenic alterations. Invasive species are clearly connected to human activities and the disruption of ‘natural’ ecosystem processes (Vitousek et al. 1996; Mack et al. 2000; Hierro et al. 2006), and specific investigations into genome and environment interactions are likely to help explain reasons for many invasive species’ success in colonizing and succeeding in new areas.

Acknowledgements. We thank Chicago Wilderness and the NSF IGERT LEAP (Landscape Ecological and Anthropogenic Processes, <http://www.uic.edu/depts/bios/leap/>) program at UIC for research funds and stipend support (grants CW-2008-04275 and NSF-0549245). The Illinois Native Plant Society (INPS) provided support for the initial field survey work. MWRD-GC provided access to their land and permission to collect plant and soil samples. H. Findlay assisted with greenhouse data collection and scoring ISSR bands. J. Hassan and D. Reitz assisted with genetic laboratory work. We thank M.V. Ashley, D. Nyberg, K. Rockne, and D. Zaya for valuable guidance throughout this project and for helpful feedback on earlier drafts of the manuscript.

Literature Cited

- Al-Karaki G.N., R. Hammad, and M. Rusan. 2001. Response of two tomato cultivars differing in salt tolerance to inoculation with mycorrhizal fungi under salt stress. *Mycorrhiza*, 11:43-47
- Baskin J.M. and C.C. Baskin. 1990. Seed germination ecology of poison hemlock, *Conium maculatum*. *Can J Botany*, 68:2018-2024
- Batten K.M., M. Scow, K. Davies, and S. Harrison. 2006. Two invasive plants alter soil microbial community composition in serpentine grasslands. *Biol Invasions*, 8:217-230
- Bech J., C. Poschenrieder, M. Llugany, J. Barcelo, P. Tume, F.J. Tobias, J.L. Barranzuela, and E. R. Vasquez. 1997. Arsenic and heavy metal contamination of soil and vegetation around a copper mine in Northern Peru. *Sci Total Environ*, 203:83-91
- Buckley D.R., K.J. Rockne, A. Li, and W.J. Mills. 2004. Soot Deposition in the Great Lakes: Implications for semi-volatile hydrophobic organic pollutant deposition. *Environ Sci Technol*, 38:1732-1739
- Christen D. and G. Matlack. 2006. The role of roadsides in plant invasions: a demographic approach. *Conserv Biol*, 20:385-391
- Chun Y.J., B. Fumanal, B. Laitung, and F. Bretagnolle. 2010. Gene flow and population admixture as the primary post-invasion processes in common ragweed (*Ambrosia artemisiifolia*) populations in France. *New Phytol*, 185:1100–1107
- Dafforn K.A., T.M. Glasby, and E.L. Johnston. 2009. Links between estuarine condition and spatial distributions of marine invaders. *Divers Distrib*, 15:807-821
- Drake J.M. and D.M. Lodge. 2006. Alle effects, propagule pressure and the probability of establishment: risk analysis for biological invasions. *Biol Invasions*, 8:365-375
- Dray Jr. F.A., R.E. Hale, P.T. Madeira, B.C. Bennett, and T.D. Center. 2009. Concordance between life history traits, invasion history, and allozyme diversity of the Everglades invader *Melaleuca quinquenervia*. *Aquat Bot*, 90:296–302
- Ehrich D. 2006. AFLPDAT: a collection of r functions for convenient handling of AFLP data. *Mol Ecol Notes*, 6:603-604
- Elton C.S. 1958. The ecology of invasions by animals and plants. University of Chicago Press, Chicago

- Esselman E.J., L. JianQiang, D. Crawford, J. Windus, and A. Wolfe. 1999. Clonal diversity in the rare *Calamagrostis porteri* ssp. *insperata* (Poaceae): comparative results for allozymes and random amplified polymorphic DNA (RAPD) and intersimple sequence repeat (ISSR) markers. *Mol Ecol*, 8:443-451
- Floerl O. and G.J. Inglis. 2005. Starting the invasion pathway: the interaction between source populations and human transport vectors. *Biol Invasions*, 7:589-606
- Geng Y.P., X.Y. Pan, C.Y. Xu, W.J. Zhang, B. Li, J.K. Chen, B.R. Lu, and Z.P. Song. 2007. Phenotypic plasticity rather than locally adapted ecotypes allows the invasive alligator weed to colonize a wide range of habitats. *Biol Invasions*, 9:245-256
- Gulezian P.Z. and D.W. Nyberg. 2008. Invasion in progress: dispersal limitation, human vehicle vectors, and the invasion of a problematic exotic species: *Conium maculatum*. A report to the Illinois Native Plant Society. *Erigenia*
- Gutierrez-Ozuna R., L.E. Eguiarte, and F. Molina-Freaner. 2009. Genotypic diversity among pasture and roadside populations of the invasive buffelgrass (*Pennisetum ciliare* L. Link) in north-western Mexico. *J Arid Environ*, 73:26-32
- Harrison E.Z., S.R. Oakes, M. Hysell, and A. Hay. 2006. Organic chemicals in sewage sludges. *Sci Total Environ*, 367:481-497
- Hendershot W.H., H. Lalonde, and M. Duquette. 1993. Soil reaction and exchangeable acidity. In: Carter M.R. (ed) Soil sampling and methods of analysis. Lewis Publishers, Boca Raton, Florida
- Henriques F.S. and J.C. Fernandes. 1991. Metal uptake and distribution in rush (*Juncus conglomeratus* L.) plants growing in pyrites mine tailings at Lousal, Portugal. *Sci Total Environ*, 102:253-260
- Henry P., G. Le Lay, J. Goudet, A. Guisan, S. Jahodová, and G. Besnard. 2009. Reduced genetic diversity, increased isolation and multiple introductions of invasive giant hogweed in the western Swiss Alps. *Mol Ecol*, 18:2819-2831
- Hierro J.L., D. Villarreal, Ö. Eren, J.M. Graham, and R.M. Callaway. 2006. Disturbance facilitates invasion: the effects are stronger abroad than at home. *Am Nat*, 168:144-156
- Holsinger K.E., P.O. Lewis, D.K. Dey. 2002. A Bayesian approach to inferring population structure from dominant markers. *Mol Ecol*, 11:1157-1164

- Holsinger K.E. and P.O. Lewis. 2003. HICKORY: a package for analysis of population genetic data. V. 8. University of Connecticut, Storrs
- Hufford K.M. and S.J. Mazer. 2003. Plant ecotypes: genetic differentiation in the age of ecological restoration. *Trends Ecol Evol*, 19:147-155
- Janzen H.H. 1993. Soluble salts. In: Carter M.R. (ed) Soil sampling and methods of analysis. Lewis Publishers, Boca Raton, Florida
- Juliano S.A. and L.P. Lounibos. 2005. Ecology of invasive mosquitoes: effects on resident species and human health. *Ecol Lett*, 8:588-574
- Keane B., M.H. Collier, J.R. Shann, and S.H. Rogstad. 2001. Metal content of dandelion (*Taraxacum officinale*) leaves in relation to soil contamination and airborne particulate matter. *Sci Total Environ*, 281:63-78
- Kim, Y.O., R.J. Rodriguez, E.J. Lee, and R.S. Redman. 2008. *Phytolacca americana* from contaminated and noncontaminated soils of South Korea: effects of elevated temperature, CO₂ and simulated acid rain on plant growth response. *J. Chem. Ecol*, 34:1501-1509
- Kneitel J.M. and D. Perrault. 2006. Disturbance-induced changes in community composition increase species invasion success. *Community Ecol*, 7: 245-252
- Lee C.E. 2002. Evolutionary genetics of invasive species. *Trends Ecol Evol*, 17:386-391
- Le Roux J.J., A.M. Wiecek, and J.Y. Meyer. 2008. Genetic diversity and structure of the invasive tree *Miconia calvescens* in Pacific islands. *Divers Distrib*, 14:935-948
- Liu H., A. Probst, and B. Liao. 2005. Metal contamination of soils and crops affected by the Chenzhou lead/zinc mine spill (Hunan, China). *Sci Total Environ*, 339:153-166
- Lopez S., F. Rousset, F.H. Shaw, R.G. Shaw, and O. Ronce. 2009. Joint effects of inbreeding and local adaptation on the evolution of genetic load after fragmentation. *Conserv Biol*, 23:1618-1627
- Ma X., X.Q. Zhang, Y.H. Zhou, S.Q. Bai, and W. Liu. 2008. Assessing genetic diversity of *Elymus sibiricus* (Poaceae: Triticeae) populations from Qinghai-Tibet Plateau by ISSR markers. *Biochem Syst Ecol*, 36:514-522
- Mack R.N., D. Simberloff, W.N. Lonsdale, H. Evans, M. Clout, and F.A. Bazzaz. 2000. Biotic invasions: causes, epidemiology, global consequences, and control. *Ecol Appl*, 10:689-710

- Mal T. and J. Lovett-Doust. 2005. Phenotypic plasticity in vegetative and reproductive traits in an invasive weed, *Lythrum salicaria* (Lythraceae), in response to soil moisture. *Am J Bot*, 92:819-825
- Mandák B., P. Zákavský, D. Kořínková, P. Dostál, and I. Plačková. 2009. Low population differentiation and high genetic diversity in the invasive species *Carduus acanthoides* L. (Asteraceae) within its native range in the Czech Republic. *Biol J Linn Soc*, 98:596–607
- Mihaljevič M., V. Ettler, O. Šebek, P. Drahota, L. Strnad, R. Procházka, J. Zeman, and O. Sracek. 2010. Alteration of arsenopyrite in soils under different vegetation covers. *Sci Total Environ*, 408:1286-1294
- Monnet, F., N. Vaillant, A. Hitmi, A. Coudret, and H. Sallanon. 2001. Endophytic *Neotyphodium lolii* induced tolerance to Zn stress in *Lolium perenne*. *Physiol. Plantarum*, 113:557-563
- Morrison S.L. and J. Molofsky. 1998. Effects of genotypes, soil moisture, and competition on the growth of an invasive grass, *Phalaris arundinacea* (reed canary grass). *Can J Bot*, 76:1939-1946
- Nei M. 1978. Estimation of average heterozygosity and genetic distance from a small number of individuals. *Genetics*, 89:538-590
- Oliver I.W., M.J. McLaughlin, and G. Merrington. 2005. Temporal trends of total and potentially available element concentrations in sewage biosolids: a comparison of biosolid surveys conducted 18 years apart. *Sci Total Environ*, 337:139-145
- Pan X., Y. Geng, W. Zhang, B.Li, and J. Chen. 2006. The influence of abiotic stress and phenotypic plasticity on the distribution of invasive *Alternanthera philoxeroides* along a riparian zone. *Acta Oecol*, 3:333-341
- Peakall R. and P.E. Smouse. 2006. GENALEX 6: genetic analysis in Excel. Population genetic software for teaching and research. *Mol Ecol Notes*, 6:288-295. Available via <http://www.anu.edu.au/BoZo/GenALEX>
- Poulin J., S.G. Weller, and A.K. Sakai. 2005. Genetic diversity does not affect the invasiveness of fountain grass (*Pennisetum setaceum*) in Arizona, California and Hawaii. *Divers Distrib*, 11:241-247
- Prentis P.J., D.P. Sigg, S. Raghu, K. Dhileepan, A. Pavasovic, and A.J. Lowe. 2009. Understanding invasion history: genetic structure and diversity of two globally invasive plants and implications for their management. *Divers Distrib*, 15:822–830

- Pysek P., V. Jarosik, J. Mullerova, J. Pergl, and J. Wild. 2008. Comparing the rate of invasion by *Heracleum mantegazzianum* at continental, regional, and local scales. *Divers Distrib*, 14:355-363
- R Development Core Team. 2009. R: a language and environment for statistical computing. Vienna: R Foundation for Statistical Computer. <http://www.r-project.org>
- Sakai A.K., F.W. Allendorf, J.S. Holt, D.M. Lodge, J. Molofsky, K.A. With, S. Baughman, R.J. Cabin, J.E. Cohen, N.C. Ellstrand, D.E. McCauley, P. O'Neil, I.M. Parker, J.N. Thompson, and S.G. Weller. 2001. The population biology of invasive species. *Ann Rev Ecol Syst*, 32:305-332
- Saltonstall K. 2002. Cryptic invasion by a non-native genotype of the common reed, *Phragmites australis*, into North America. *P Natl Acad Sci USA*, 99:2445–2449
- Sanderson E.W., J. Jaiteh, M.A. Levy, K.H. Redford, A.V. Wannebo, and G. Woolmer. 2002. The human footprint and the last of the wild. *Bioscience*, 52:891-904
- Stephens H.A. 1980. Poisonous plants of the central U.S. The Regents Press of Kansas, Lawrence, Kansas
- Swink F. and G. Wilhelm. 1994. Plants of the Chicago region. Indiana Academy of Science, Indianapolis
- Taylor D.R. and S.R. Keller. 2007. Historical range expansion determines the phylogenetic diversity introduced during contemporary species invasion. *Evolution*, 61:334-345
- Thuiller W., D.M. Richardson, M. Rouget, Ş. Proches, and J.R. Wilson. 2006. Interactions between environment, species traits, and human uses describe patterns of plant invasions. *Ecology*, 87:1755-1769
- Urbansky E.T., M.L. Magnuson, C.A. Kelty , and S.K. Brown. 2000. Perchlorate uptake by salt cedar (*Tamarix ramosissima*) in the Las Vegas Wash riparian ecosystem. *Sci Total Environ*, 256:227-232
- US EPA. 1994. (United States Environmental Protection Agency). Method 7471A, Revision 1 - Mercury in solid or semisolid waste (manual cold-vapor technique). In: SW-846 manual (Test methods for evaluating solid waste, physical/ chemical methods) 3rd ed. <http://www.epa.gov/epaoswer/hazwaste/testmethods/sw846/index.htm>.

- US EPA. 1996a. Method 3050B, Revision 3 - Acid digestion of sediments, sludges, and soil. In: SW-846 manual (Test methods for evaluating solid waste, physical/chemical methods) 3rd ed. <http://www.epa.gov/epaoswer/hazwaste/testmethods/sw846/index.htm>.
- US EPA. 1996b. Method 3550B, Revision 3 - Ultrasonic extraction. In: SW-846 manual (Test methods for evaluating solid waste, physical/ chemical methods) 3rd ed. <http://www.epa.gov/epaoswer/hazwaste/testmethods/sw846/index.htm>.
- US EPA. 1996c. Method 8270C, Revision 3 – Semivolatile organic compounds by gas chromatography/mass spectrometry (GC/MS). In: SW-846 manual (Test methods for evaluating solid waste, physical/ chemical methods) 3rd ed. <http://www.epa.gov/epaoswer/hazwaste/testmethods/sw846/index.htm>.
- US EPA. 2005a. Ecological Soil Screening Levels for As, Cd, Pb. Interim Final. OSWER Directive 9285.7-62 (As), -65 (Cd), -70 (Pb). USEPA. Office of Solid Waste and Emergency Response. Washington, DC. March <http://www.epa.gov/ecotox/ecossl/>
- US EPA. 2005b. Ecological Soil Screening Levels for Polycyclic Aromatic Hydrocarbons. Interim Final. OSWER Directive 9285.7-78. USEPA. Office of Solid Waste and Emergency Response. Washington, DC. March <http://www.epa.gov/ecotox/ecossl/>
- US EPA. 2007. Method 6020A, Revision 4- Inductively coupled plasma-mass spectrometry. In: SW-846 manual (Test methods for evaluating solid waste, physical/chemical methods) 3rd ed. <http://www.epa.gov/epaoswer/hazwaste/testmethods/sw846/index.htm>.
- Uveges J.L., A.L. Corbett, T.K. Mal. 2002. Effects of lead contamination on the growth of *Lythrum salicaria* (purple loosestrife). *Environ Pollut*, 120:319-323
- Van Bohemen H.D. and W.H. Janssen van de Laak. 2003. The influence of road infrastructure and traffic on soil, water, and air quality. *Environ Manage*, 31:50-68
- Vitousek P.M., C.M. D'Antonio, L.L. Loope, and R. Westbrooks. 1996. Biological invasions as global environmental change. *Am Sci*, 84:468-478
- von der Lippe M. and I. Kowarik. 2007. Long-distance dispersal of plants by vehicles as a driver of plant invasions. *Conserv Biol*, 21:986-996
- Ward S.M., J.F. Gaskin, and L.M. Wilson. 2008. Ecological genetics of plant invasion: What do we know? *Invas Plant Sci Manag*, 1:98-109
- Whitson T.D., L. Burrill, S. Dewey, D. Cudney, B. Nelson, R. Lee, and R. Parker. 1992. Weeds of the West. The Western Society of Weed Science , University of Wyoming, Laramie

- Wilhite, S.E., R.D. Lumsden, and D.C. Straney. 2001. Peptide synthetase gene in *Trichoderma virens*. *Appl. Environ. Microbiol*, 11:5055-5062
- Wolfe A.D., Q.Y. Xiang, and S.R. Kephart. 1998. Assessing hybridization in natural populations of *Penstemon* (Scrophulariaceae) using hypervariable intersimple sequence repeat (ISSR) bands. *Mol Ecol*, 7:1107-1125.
- Zar J.H. 1996. Biostatistical analysis. Prentice Hall, Upper Saddle River, New Jersey
- Zhang Q., R. Yang, J. Tang, and X. Chen. 2008. Competitive interaction between the invasive *Solidago canadensis* and native *Kummerowia striata* in lead contaminated soil. *Bot Stud*, 49:385-391

Table 1. Select field soil and spatial parameters for the 9 *Conium* populations found in Cook County. Pop. Area is the total area covered by all the *Conium* individuals in a population (defined as a contiguous area of at least 50% *Conium* cover) and Distance to Nearest Pop. is the distance measured to the nearest known *Conium* population. For the soil parameters, single values are reported for small populations (55-1, 55-2, CalDryBed, BFN-2, and 130th/Doty). Mean values for large and medium populations are accompanied by the standard deviation (Stickney, Calumet, n = 3) and the range (Harlem, BFN1, n = 2), respectively.

Soil Parameters							Spatial Parameters	
	(mg/kg dry soil)				(% dry wt.)	(g/ml wet wt.)	(m ²)	(m)
	As	Cd	Pb	pH	Organic matter	Bulk density	Pop. Area	Distance to Nearest Pop.
I-55-1	6.70	1.30	78.0	7.86	3.559	1.263	100	380
I-55-2	9.50	1.50	92.0	8.11	3.847	1.163	50	380
Stickney	11.43 ± 3.87	6.50 ± 1.25	107.0 ± 53.05	7.47 ± 0.19	5.641 ± 1.79	1.071 ± 0.14	6000	660
Harlem	6.65 ± 0.25	1.80 ± 0.60	152.5 ± 22.5	7.60 ± 0.13	6.474 ± 1.22	1.034 ± 0.03	3250	660
CalDryBed	18.0	16.0	240.0	6.63	15.079	0.801	200	1450
Calumet	18.50 ± 8.26	5.52 ± 2.51	356.7 ± 253.84	7.89 ± 0.21	3.733 ± 1.19	1.160 ± 0.17	60000	100
BFN-1	11.68 ± 7.33	24.53 ± 23.48	334.8 ± 255.25	7.70 ± 0.05	3.890 ± 1.29	1.109 ± 0.03	4000	100
BFN-2	13.0	2.60	280.0	7.78	8.307	1.049	150	100
130 th /Doty	9.60	1.30	140.0	7.39	2.057	1.447	2000	900

Table 2. ISSR marker information. All markers had an annealing temperature of 55 °C.

Primer	Sequence	Individuals Scored	Total Polymorphic Bands
811	[GA] ₈ C	172	25
816	[CA] ₈ T	209	22
818	[CA] ₈ G	209	33
825	[AC] ₈ T	210	18
830	[TG] ₈ G	183	16

Table 3. Summary of the genetic structure for the 9 *Conium* populations (n=217) using 114 loci from 5 ISSR markers. I-55-1 and I-55-2 populations were grouped into one I-55 population for all genetic analysis due to small numbers of individuals. Genetic analysis of the populations from GenAlEx program. No. Bands is the number of polymorphic bands for each population. No. Private Bands is the number of bands only found in a given population. Mean H_e is the mean heterozygosity of each population, and SE of Mean H_e is the standard error of the mean. Proportion of Variable Loci is the mean proportion of loci (for 5 ISSR markers) in a population that are polymorphic. Intra-Population Genetic Diversity is the mean proportion of loci (for 5 ISSR markers) that are different between two individuals in each population (average number of pairwise differences between individuals within the same population).

Population	No. of Individuals	No. of Bands	No. of Private Bands	Mean H_e	SE of Mean H_e	Proportion of Variable Loci	Intra-Population Genetic Diversity
I-55	20	94	0	0.232	0.018	0.722	0.251
Stickney	32	104	2	0.227	0.018	0.798	0.228
Harlem	30	97	0	0.202	0.017	0.730	0.196
CalDryBed	20	83	0	0.143	0.017	0.523	0.148
Calumet	24	94	0	0.215	0.019	0.690	0.213
BFN-1	23	100	0	0.228	0.018	0.791	0.223
BFN-2	34	93	0	0.220	0.018	0.706	0.231
130th/Doty	31	102	1	0.189	0.017	0.758	0.183

Table 4. Correlations at the population scale (n = 8) between metrics of genetic diversity and variables measured in the field for soil and spatial attributes of each population. With n = 8 (df = 6), significant results at the .05 level are given when the absolute value of ρ is at least 0.62 (marked with ^x) and 0.72 (marked with *), for directional and non-directional tests, respectively.

Variable	Mean H_e	Proportion of Variable Loci	Intra-Population Genetic Diversity
As	-0.21	-0.54	-0.17
Ba	-0.45	-0.64 ^x	-0.40
Cd	0.095	0	-0.095
Cu	-0.38	-0.57	-0.33
Pb	-0.19	-0.38	-0.24
Hg	-0.095	-0.29	-0.24
K	-0.71 ^x	-0.52	-0.76*
Zn	-0.26	-0.36	-0.36
Total Metals	-0.48	0.33	-0.43
Total PAHs	-0.048	0	-0.19
pH	0.71 ^x	-0.14	0.77*
Bulk Density	0.36	0.31	0.26
Liquid % Salinity	-0.36	-0.12	-0.21
% Solids	0.48	0.43	0.24
% Nitrogen	-0.30	-0.44	-0.084
% Organic Carbon	-0.071	-0.50	0.26
% Black Carbon	0.38	-0.048	0.67 ^x
% Organic Matter	-0.31	-0.36	-0.17
Population Area	0.007	0.33	-0.21
Dist. to Nearest Pop.	-0.65 ^x	-0.012	-0.65 ^x

Figure 1. Map of *Conium* field populations, MWRD-GC biosolids drying beds, and associated roadways. Upper left is the West Suburbs ‘hotspot’, upper right is the Calumet ‘hotspot’. Populations are symbolized with respect to size of *Conium* population area, as listed in Table 1. Map projection: Illinois SPCS East NAD83 feet. Data sources: USGS Orthoimagery (2008) and IL Dept of Transportation Highway Data (2009).

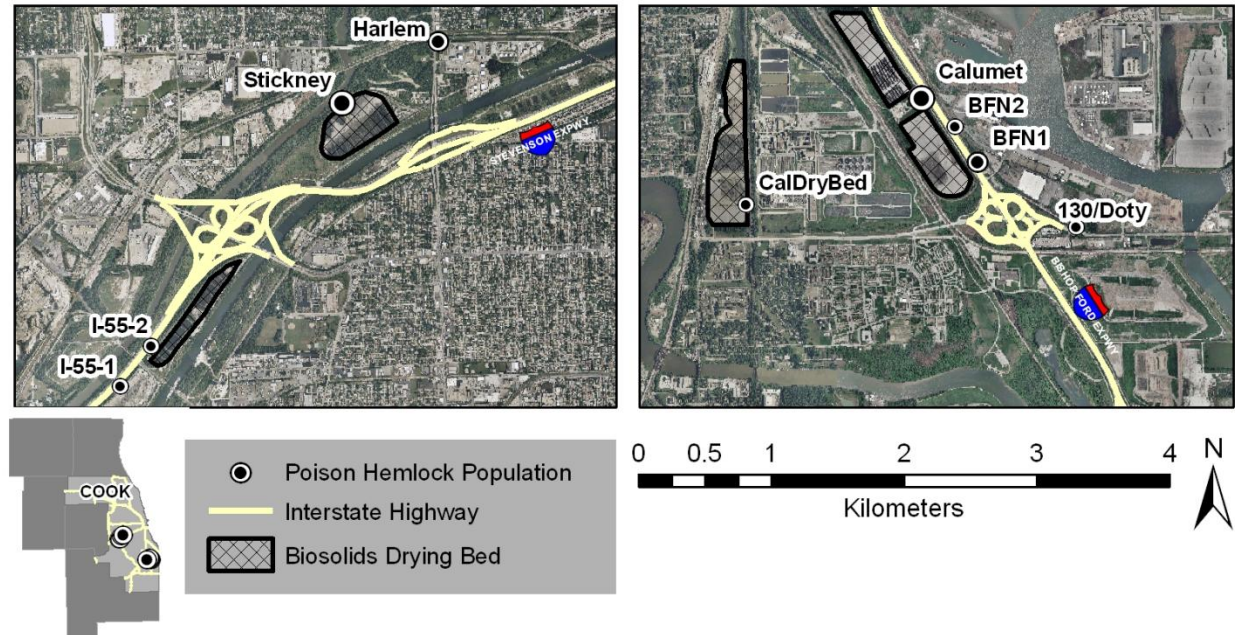


Figure 2. Soil concentrations of As, Cd, and Pb at each *Conium* population. Solid lines are contamination thresholds from the US EPA Ecological Soil Screening Levels for plants (US EPA 2005a). Note log scale.

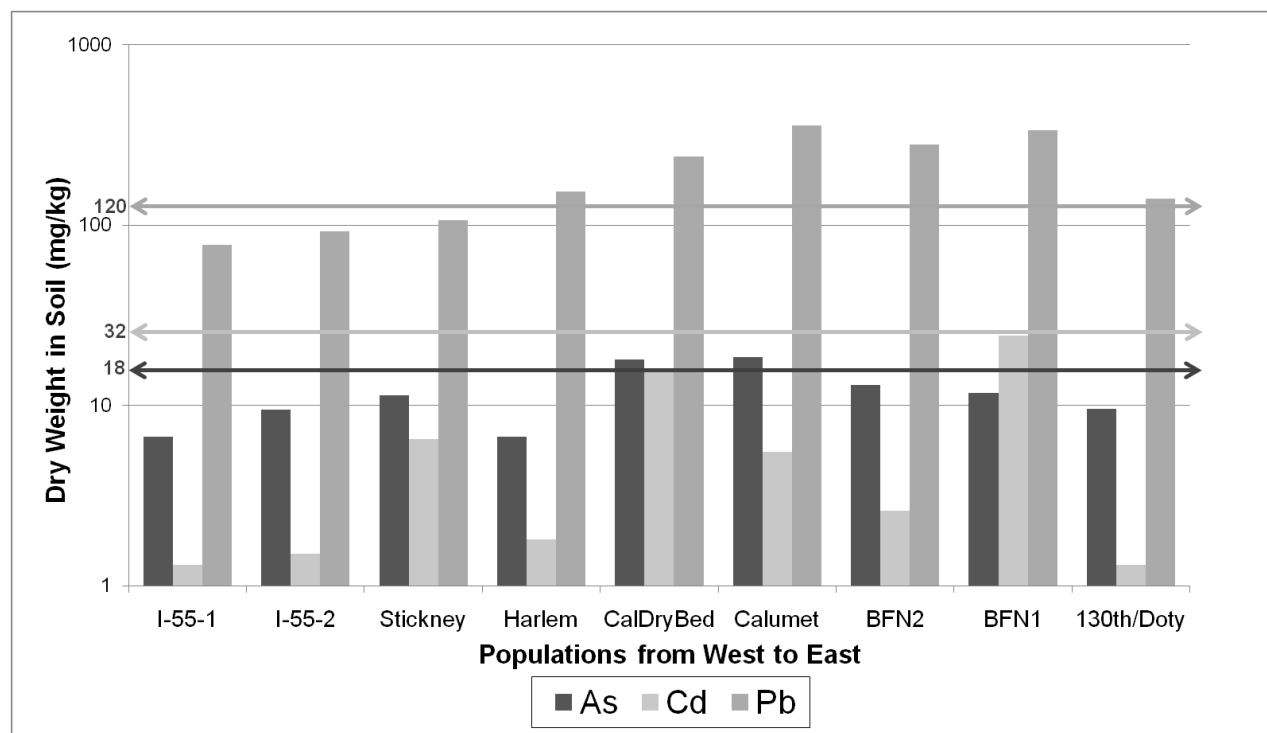


Figure 3. Phenogram of genetic differentiation between *Conium* populations measured by Nei's unbiased pairwise genetic distance.

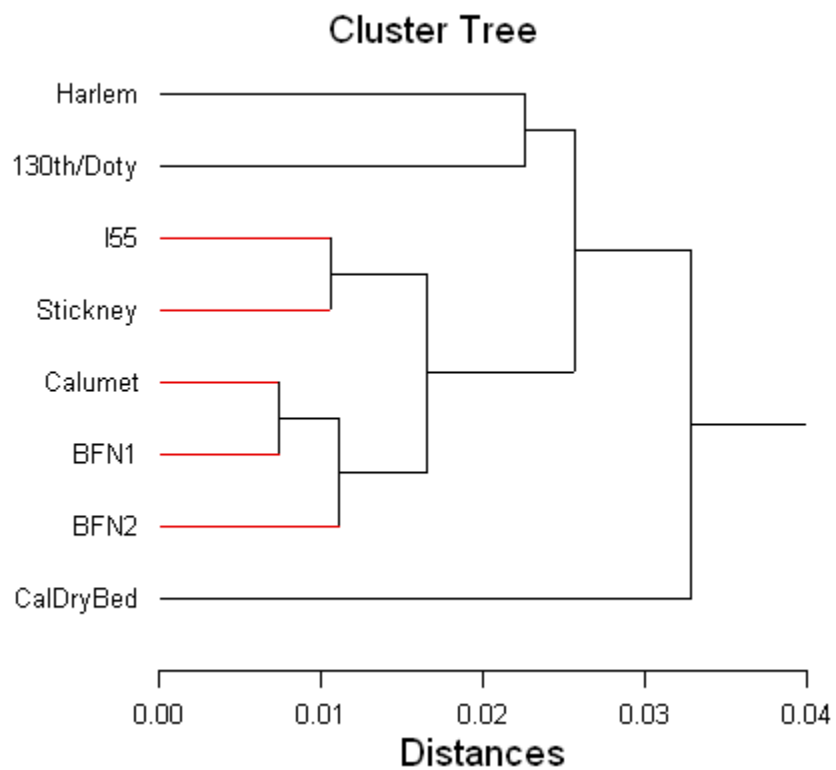


Figure 4. *Conium* growth expressed as mean weights of above ground biomass for seeds grown on home (local) and away (soil of all other *Conium* populations). Error bars are ± 1 standard error. $n = 3$ for home soils, $n = 24$ for away soils.

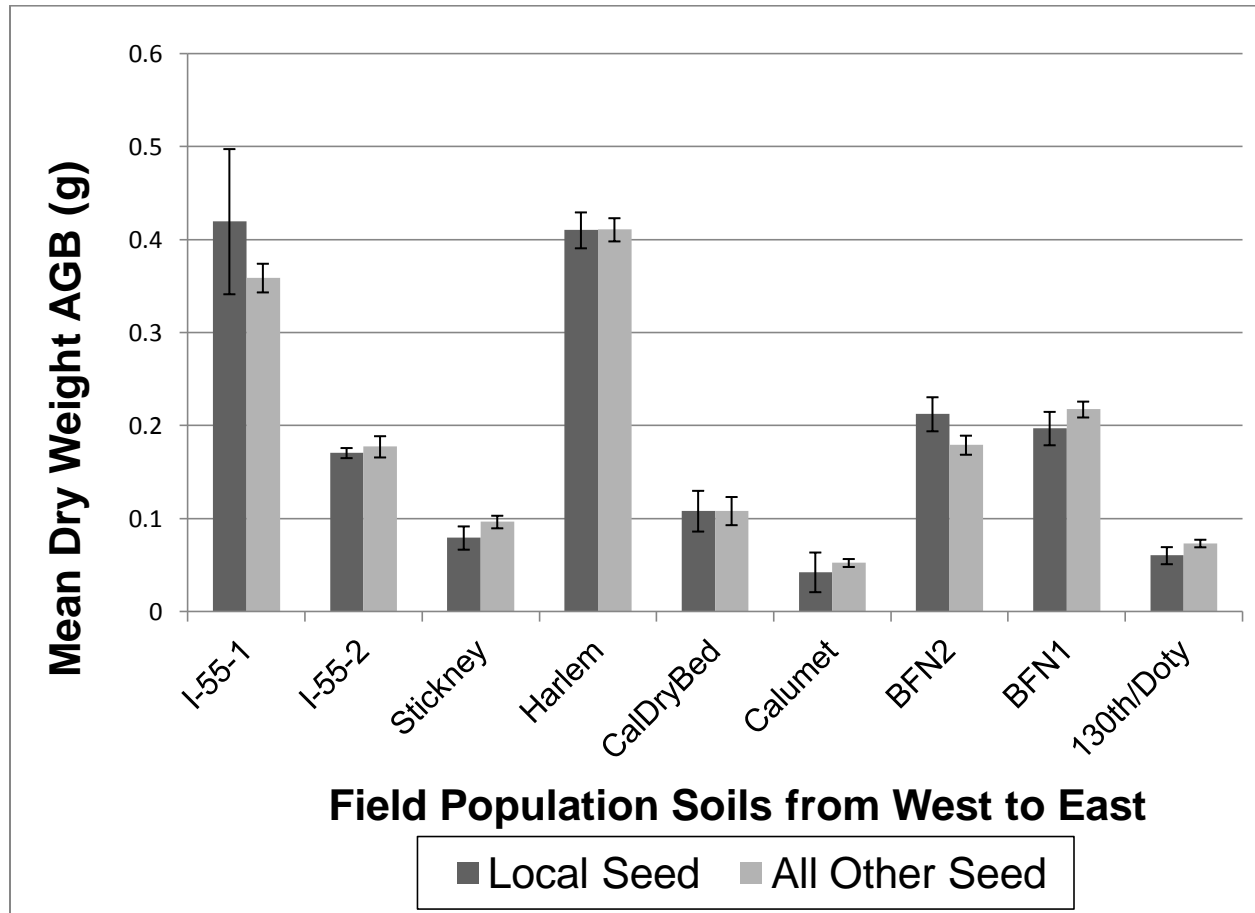
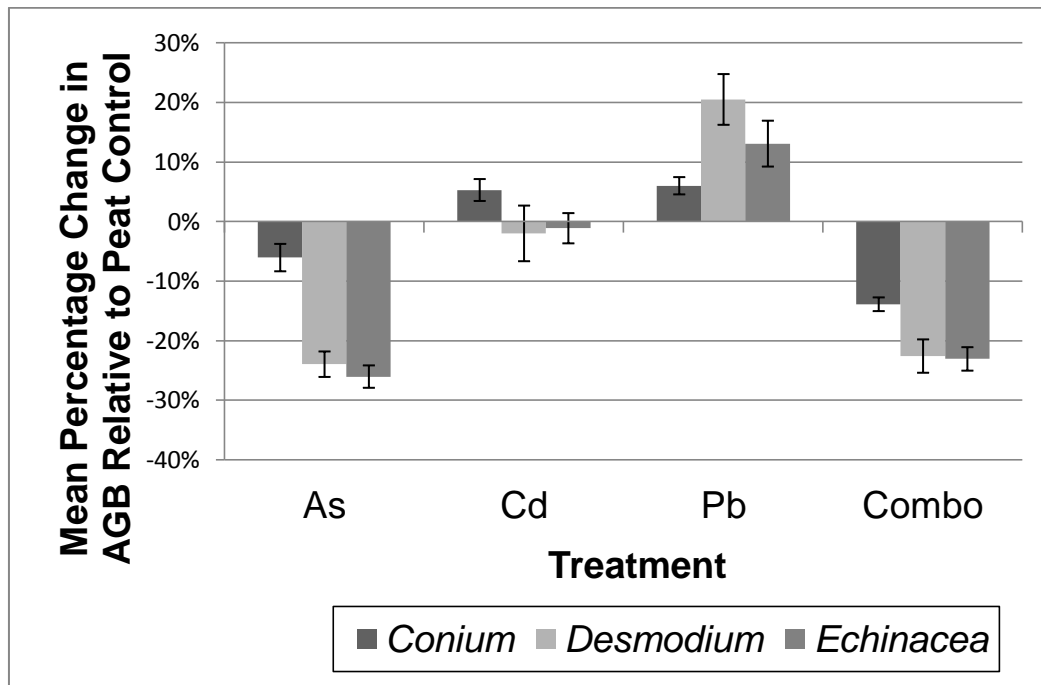


Figure 5. Metal tolerance (As, Cd, Pb, Combo) among three species from the greenhouse experiment. Depicted is the percentage change in above ground biomass (AGB) for a given metal treatment relative to the growth in the peat control without added metals. Error bars are ± 1 standard error. $n = 27$ for *Conium*, $n = 3$ for *Desmodium* and *Echinacea*.



Appendix C. Permissions and licenses for reuse of copyrighted material.

Title: IMMUNOCHEMICAL DETECTION OF POLYCYCLIC AROMATIC HYDROCARBONS (PAHs)

Author: Karsten A. Fährnich, Miloslav Pravda, George G. Guilbault

Publication: Analytical Letters

Publisher: Taylor & Francis

Date: May 8, 2002

Copyright © 2002 Taylor & Francis

Thesis/Dissertation Reuse Request

Taylor & Francis is pleased to offer reuses of its content for a thesis or dissertation free of charge contingent on resubmission of permission request if work is published.

ELSEVIER LICENSE TERMS AND CONDITIONS

Jul 08, 2013

This is a License Agreement between Kelly Granberg ("You") and Elsevier ("Elsevier") provided by Copyright Clearance Center ("CCC"). The license consists of your order details, the terms and conditions provided by Elsevier, and the payment terms and conditions.

All payments must be made in full to CCC. For payment instructions, please see information listed at the bottom of this form.

Supplier	Elsevier Limited The Boulevard,Langford Lane Kidlington,Oxford,OX5 1GB,UK
Registered Company Number	1982084
Customer name	Kelly Granberg
License number	3184430099323
License date	Jul 08, 2013
Licensed content publisher	Elsevier
Licensed content publication	Science of The Total Environment
Licensed content title	Polycyclic aromatic hydrocarbons (PAHs) in Chicago air
Licensed content author	Mustafa Odabasi,Nedim Vardar,Aysun Sofuoglu,Yucel Tasdemir,Thomas M Holsen
Licensed content date	16 February 1999
Licensed content volume number	227
Licensed content issue number	1
Number of pages	11
Start Page	57
End Page	67
Type of Use	reuse in a thesis/dissertation
Intended publisher of new work	other
Portion	figures/tables/illustrations
Number of figures/tables/illustrations	1
Format	electronic
Are you the author of this Elsevier article?	No
Will you be translating?	No
Title of your thesis/dissertation	Multimedia Source Apportionment of Semivolatile Organic Contaminants in the Chicago Area of Influence
Expected completion date	Aug 2013
Estimated size (number of pages)	266
Elsevier VAT number	GB 494 6272 12
Supplier	Elsevier Limited The Boulevard,Langford Lane Kidlington,Oxford,OX5 1GB,UK

Registered Company Number	1982084
Customer name	Kelly Granberg
License number	3184430470704
License date	Jul 08, 2013
Licensed content publisher	Elsevier
Licensed content publication	Atmospheric Environment
Licensed content title	Source apportionment and source/sink relationships of PAHs in the coastal atmosphere of Chicago and Lake Michigan
Licensed content author	Matt F. Simcik, Steven J. Eisenreich, Paul J. Lioy
Licensed content date	December 1999
Licensed content volume number	33
Licensed content issue number	30
Number of pages	9
Start Page	5071
End Page	5079
Type of Use	reuse in a thesis/dissertation
Intended publisher of new work	other
Portion	figures/tables/illustrations
Number of figures/tables/illustrations	1
Format	electronic
Are you the author of this Elsevier article?	No
Will you be translating?	No
Order reference number	
Title of your thesis/dissertation	Multimedia Source Apportionment of Semivolatile Organic Contaminants in the Chicago Area of Influence
Expected completion date	Aug 2013
Estimated size (number of pages)	266
Elsevier VAT number	GB 494 6272 12
Supplier	Elsevier Limited The Boulevard, Langford Lane Kidlington, Oxford, OX5 1GB, UK
Registered Company Number	1982084
Customer name	Kelly Granberg

License number	3184421150748
License date	Jul 08, 2013
Licensed content publisher	Elsevier
Licensed content publication	Water Research
Licensed content title	Source apportionment of PAHs in sediments using factor analysis by time records: Application to Lake Michigan, USA
Licensed content author	Erik R. Christensen,Sidharta Arora
Licensed content date	January 2007
Licensed content volume number	41
Licensed content issue number	1
Number of pages	9
Start Page	168
End Page	176
Type of Use	reuse in a thesis/dissertation
Portion	figures/tables/illustrations
Number of figures/tables/illustrations	1
Format	electronic
Are you the author of this Elsevier article?	No
Will you be translating?	No
Order reference number	
Title of your thesis/dissertation	Multimedia Source Apportionment of Semivolatile Organic Contaminants in the Chicago Area of Influence
Expected completion date	Aug 2013
Estimated size (number of pages)	266
Elsevier VAT number	GB 494 6272 12

Supplier	Elsevier Limited The Boulevard,Langford Lane Kidlington,Oxford,OX5 1GB,UK
Registered Company Number	1982084
Customer name	Kelly Granberg
License number	3184430285786

License date	Jul 08, 2013
Licensed content publisher	Elsevier
Licensed content publication	Science of The Total Environment
Licensed content title	Towards a global historical emission inventory for selected PCB congeners — A mass balance approach: 3. An update
Licensed content author	Knut Breivik, Andy Sweetman, Jozef M. Pacyna, Kevin C. Jones
Licensed content date	15 May 2007
Licensed content volume number	377
Licensed content issue number	2–3
Number of pages	12
Start Page	296
End Page	307
Type of Use	reuse in a thesis/dissertation
Intended publisher of new work	other
Portion	figures/tables/illustrations
Number of figures/tables/illustrations	1
Format	electronic
Are you the author of this Elsevier article?	No
Will you be translating?	No
Order reference number	
Title of your thesis/dissertation	Multimedia Source Apportionment of Semivolatile Organic Contaminants in the Chicago Area of Influence
Expected completion date	Aug 2013
Estimated size (number of pages)	266
Elsevier VAT number	GB 494 6272 12

Supplier	Elsevier Limited The Boulevard, Langford Lane Kidlington, Oxford, OX5 1GB, UK
Registered Company Number	1982084
Customer name	Kelly Granberg
License number	3184430660823
License date	Jul 08, 2013

Licensed content publisher	Elsevier
Licensed content publication	Atmospheric Environment
Licensed content title	Atmospheric PCB congeners across Chicago
Licensed content author	Dingfei Hu,Hans-Joachim Lehmler,Andres Martinez,Kai Wang,Keri C. Hornbuckle
Licensed content date	April 2010
Licensed content volume number	44
Licensed content issue number	12
Number of pages	8
Start Page	1550
End Page	1557
Type of Use	reuse in a thesis/dissertation
Intended publisher of new work	other
Portion	figures/tables/illustrations
Number of figures/tables/illustrations	1
Format	electronic
Are you the author of this Elsevier article?	No
Will you be translating?	No
Order reference number	
Title of your thesis/dissertation	Multimedia Source Apportionment of Semivolatile Organic Contaminants in the Chicago Area of Influence
Expected completion date	Aug 2013
Estimated size (number of pages)	266
Elsevier VAT number	GB 494 6272 12

Terms and Conditions

INTRODUCTION

1. The publisher for this copyrighted material is Elsevier. By clicking "accept" in connection with completing this licensing transaction, you agree that the following terms and conditions apply to this transaction (along with the Billing and Payment terms and conditions established by Copyright Clearance Center, Inc. ("CCC"), at the time that you opened your Rightslink account and that are available at any time at

<http://myaccount.copyright.com>).

GENERAL TERMS

2. Elsevier hereby grants you permission to reproduce the aforementioned material subject to the terms and conditions indicated.

3. Acknowledgement: If any part of the material to be used (for example, figures) has appeared in our publication with credit or acknowledgement to another source, permission must also be sought from that source. If such permission is not obtained then that material may not be included in your publication/copies. Suitable acknowledgement to the source must be made, either as a footnote or in a reference list at the end of your publication, as follows:

“Reprinted from Publication title, Vol /edition number, Author(s), Title of article / title of chapter, Pages No., Copyright (Year), with permission from Elsevier [OR APPLICABLE SOCIETY COPYRIGHT OWNER].” Also Lancet special credit - “Reprinted from The Lancet, Vol. number, Author(s), Title of article, Pages No., Copyright (Year), with permission from Elsevier.”

4. Reproduction of this material is confined to the purpose and/or media for which permission is hereby given.

5. Altering/Modifying Material: Not Permitted. However figures and illustrations may be altered/adapted minimally to serve your work. Any other abbreviations, additions, deletions and/or any other alterations shall be made only with prior written authorization of Elsevier Ltd. (Please contact Elsevier at permissions@elsevier.com)

6. If the permission fee for the requested use of our material is waived in this instance, please be advised that your future requests for Elsevier materials may attract a fee.

7. Reservation of Rights: Publisher reserves all rights not specifically granted in the combination of (i) the license details provided by you and accepted in the course of this licensing transaction, (ii) these terms and conditions and (iii) CCC's Billing and Payment terms and conditions.

8. License Contingent Upon Payment: While you may exercise the rights licensed immediately upon issuance of the license at the end of the licensing process for the transaction, provided that you have disclosed complete and accurate details of your proposed use, no license is finally effective unless and until full payment is received from you (either by publisher or by CCC) as provided in CCC's Billing and Payment terms and conditions. If full payment is not received on a timely basis, then any license preliminarily granted shall be deemed automatically revoked and shall be void as if never granted. Further, in the event that you breach any of these terms and conditions or any of CCC's Billing and Payment terms and conditions, the license is automatically revoked and shall be void as if never granted. Use of materials as described in a revoked license, as well as any

use of the materials beyond the scope of an unrevoked license, may constitute copyright infringement and publisher reserves the right to take any and all action to protect its copyright in the materials.

9. Warranties: Publisher makes no representations or warranties with respect to the licensed material.

10. Indemnity: You hereby indemnify and agree to hold harmless publisher and CCC, and their respective officers, directors, employees and agents, from and against any and all claims arising out of your use of the licensed material other than as specifically authorized pursuant to this license.

11. No Transfer of License: This license is personal to you and may not be sublicensed, assigned, or transferred by you to any other person without publisher's written permission.

12. No Amendment Except in Writing: This license may not be amended except in a writing signed by both parties (or, in the case of publisher, by CCC on publisher's behalf).

13. Objection to Contrary Terms: Publisher hereby objects to any terms contained in any purchase order, acknowledgment, check endorsement or other writing prepared by you, which terms are inconsistent with these terms and conditions or CCC's Billing and Payment terms and conditions. These terms and conditions, together with CCC's Billing and Payment terms and conditions (which are incorporated herein), comprise the entire agreement between you and publisher (and CCC) concerning this licensing transaction. In the event of any conflict between your obligations established by these terms and conditions and those established by CCC's Billing and Payment terms and conditions, these terms and conditions shall control.

14. Revocation: Elsevier or Copyright Clearance Center may deny the permissions described in this License at their sole discretion, for any reason or no reason, with a full refund payable to you. Notice of such denial will be made using the contact information provided by you. Failure to receive such notice will not alter or invalidate the denial. In no event will Elsevier or Copyright Clearance Center be responsible or liable for any costs, expenses or damage incurred by you as a result of a denial of your permission request, other than a refund of the amount(s) paid by you to Elsevier and/or Copyright Clearance Center for denied permissions.

LIMITED LICENSE

The following terms and conditions apply only to specific license types:

15. **Translation:** This permission is granted for non-exclusive world **English** rights only unless your license was granted for translation rights. If you licensed translation rights you may only translate this content into the languages you requested. A professional translator must perform all translations and reproduce the content word for word preserving the integrity of the article. If this license is to re-use 1 or 2 figures then permission is granted

for non-exclusive world rights in all languages.

16. Website: The following terms and conditions apply to electronic reserve and author websites:

Electronic reserve: If licensed material is to be posted to website, the web site is to be password-protected and made available only to bona fide students registered on a relevant course if: This license was made in connection with a course, This permission is granted for 1 year only. You may obtain a license for future website posting, All content posted to the web site must maintain the copyright information line on the bottom of each image, A hyper-text must be included to the Homepage of the journal from which you are licensing at <http://www.sciencedirect.com/science/journal/xxxxx> or the Elsevier homepage for books at <http://www.elsevier.com> , and Central Storage: This license does not include permission for a scanned version of the material to be stored in a central repository such as that provided by Heron/XanEdu.

17. Author website for journals with the following additional clauses:

All content posted to the web site must maintain the copyright information line on the bottom of each image, and the permission granted is limited to the personal version of your paper. You are not allowed to download and post the published electronic version of your article (whether PDF or HTML, proof or final version), nor may you scan the printed edition to create an electronic version. A hyper-text must be included to the Homepage of the journal from which you are licensing at <http://www.sciencedirect.com/science/journal/xxxxx> . As part of our normal production process, you will receive an e-mail notice when your article appears on Elsevier's online service ScienceDirect (www.sciencedirect.com). That e-mail will include the article's Digital Object Identifier (DOI). This number provides the electronic link to the published article and should be included in the posting of your personal version. We ask that you wait until you receive this e-mail and have the DOI to do any posting.

Central Storage: This license does not include permission for a scanned version of the material to be stored in a central repository such as that provided by Heron/XanEdu.

18. Author website for books with the following additional clauses: Authors are permitted to place a brief summary of their work online only. A hyper-text must be included to the Elsevier homepage at <http://www.elsevier.com> . All content posted to the web site must maintain the copyright information line on the bottom of each image. You are not allowed to download and post the published electronic version of your chapter, nor may you scan the printed edition to create an electronic version.

Central Storage: This license does not include permission for a scanned version of the material to be stored in a central repository such as that provided by Heron/XanEdu.

19. Website (regular and for author): A hyper-text must be included to the Homepage of the journal from which you are licensing at <http://www.sciencedirect.com/science/journal/xxxxx>. or for books to the Elsevier

homepage at <http://www.elsevier.com>

20. Thesis/Dissertation: If your license is for use in a thesis/dissertation your thesis may be submitted to your institution in either print or electronic form. Should your thesis be published commercially, please reapply for permission. These requirements include permission for the Library and Archives of Canada to supply single copies, on demand, of the complete thesis and include permission for UMI to supply single copies, on demand, of the complete thesis. Should your thesis be published commercially, please reapply for permission.

21. Other Conditions:

v1.6

If you would like to pay for this license now, please remit this license along with your payment made payable to "COPYRIGHT CLEARANCE CENTER" otherwise you will be invoiced within 48 hours of the license date. Payment should be in the form of a check or money order referencing your account number and this invoice number RLNK501061107. Once you receive your invoice for this order, you may pay your invoice by credit card. Please follow instructions provided at that time.

Make Payment To:
Copyright Clearance Center
Dept 001
P.O. Box 843006
Boston, MA 02284-3006

For suggestions or comments regarding this order, contact RightsLink Customer Support: customercare@copyright.com or +1-877-622-5543 (toll free in the US) or +1-978-646-2777.

Gratis licenses (referencing \$0 in the Total field) are free. Please retain this printable license for your reference. No payment is required.



The American Midland Naturalist

Department of Biological
University of Notre Dame
Notre Dame, Indiana
46556 U.S.A.

tel (574)631-7481
fax (574) 631-7413
e-mail: ammidnat@nd.edu
web: www.nd.edu/~ammidnat

The American Midland Naturalist Copyright Owned Request Form Granting Permission to use published work.

This form confirms *the American Midland Naturalist* ("AMN"), a publication of the University of Notre Dame, hereby grants Kelly Granberg, Ph.D. Candidate, Environmental Engineering, University of Illinois-Chicago, the non-exclusive right to use the article listed below for personal, educational and/or academic purposes during the full term of the copyright.

Name of article: Establishment of an Invasive Plant Species (*Conium maculatum*) in Contaminated Roadside Soil in Cook County, Illinois

Author: Gulezian, P.Z., J.L. Ison, and K.J. Granberg

Volume and date of first publication in AMN: 168(2): October 2012: p375-395

How article will be used: As an appendix to doctoral thesis

The right granted herein is non-exclusive, non-assignable and limited in scope to use of the Article in hard copy, other print format or pdf, e-book and languages worldwide. This does not include the right to use the Article solely for financial gain. The University of Notre Dame warrants that it is the sole copyright owner of the publication, that it has complete authority and capacity to grant the rights contained herein, and that no other releases or permissions are necessary.

By granting this non-exclusive right to limited use of the Article, neither the University of Notre Dame or AMN release or revoke their copyright ownership or other interest of any kind or nature whatsoever in the Article.

AMERICAN MIDLAND NATURALIST

By *Hope Helbach*

Date 7/23/13



UNIVERSITY OF ILLINOIS
AT CHICAGO

Department of Civil and Materials Engineering (MC 246)
College of Engineering
842 West Taylor Street
Chicago, Illinois 60607-7023

July 9, 2013

RE: Permission to use published research article in my thesis.

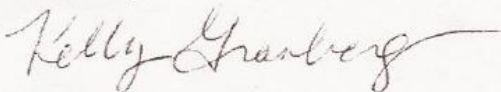
I am writing to request permission to use the following co-authored research article published in The American Midland Naturalist as an appendix to my doctoral thesis:

Gulezian, P.Z., J.L. Ison, and K.J. Granberg (2012) Establishment of an Invasive Plant Species (Conium maculatum) in Contaminated Roadside Soil in Cook County, Illinois. The American Midland Naturalist. 168(2):375-395

This material will appear as submitted for publication, and will use the conventional style of the Graduate College of the University of Illinois at Chicago as acknowledgment unless you request otherwise.

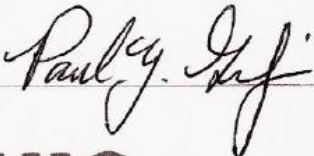
Thank you for your kind consideration of this request.

Sincerely,



Kelly Granberg
PhD Candidate
842 West Taylor St., M/C 246: University of Illinois-Chicago
Chicago, IL 60607 USA kgranb3@uic.edu

The above request is approved.

Approved by: Paul Gulezian  Date: 16 July 2013

UIC

Phone (312) 996-3428 • Fax (312) 996-2426

UNIVERSITY OF ILLINOIS
AT CHICAGO

Department of Civil and Materials Engineering (MC 246)
College of Engineering
842 West Taylor Street
Chicago, Illinois 60607-7023

July 9, 2013

RE: Permission to use published research article in my thesis.

I am writing to request permission to use the following co-authored research article published in The American Midland Naturalist as an appendix to my doctoral thesis:

Gulezian, P.Z., J.L. Ison, and K.J. Granberg (2012) Establishment of an Invasive Plant Species (*Conium maculatum*) in Contaminated Roadside Soil in Cook County, Illinois. The American Midland Naturalist. 168(2):375-395

This material will appear as submitted for publication, and will use the conventional style of the Graduate College of the University of Illinois at Chicago as acknowledgment unless you request otherwise.

Thank you for your kind consideration of this request.

Sincerely,



Kelly Granberg
PhD Candidate
842 West Taylor St., M/C 246; University of Illinois-Chicago
Chicago, IL 60607 USA kgranb3@uic.edu

The above request is approved.

Approved by:  Date: July 17, 2013

UIC

Phone (312) 996-3428 • Fax (312) 996-2426

VITA

Kelly J. Granberg
kgranb3@uic.edu

Education

PhD, Environmental Engineering, University of Illinois Chicago 2007 - 2013

- *Dissertation*: Multimedia source apportionment of semivolatile organic contaminants in the Chicago area of influence
- *Advisor*: Dr. Karl Rockne, P.E.
- *GPA*: 4.00 / 4.00

BS, Biological Systems Engineering, University of Wisconsin at Madison 1998 - 2003

- Natural Resources and Environment focus, Honors Graduate, GPA 3.72 / 4.00

Research Experience

Graduate Researcher, University of Illinois Chicago, Applied Environmental Laboratory 2007 - 2013

- *Contaminant Source Apportionment*: Sources of polycyclic aromatic hydrocarbons (PAHs), polychlorinated biphenyls (PCBs), heavy metals, and Polybrominated Diphenyl Ethers (PBDEs) in air, sediment, soil, and wastewater using multivariate receptor models (Positive Matrix Factorization, UNMIX, Principal Components Analysis) and environmental forensics techniques (diagnostic ratios)
- *Wastewater Treatment*: Fate of emerging and legacy hydrophobic organic contaminants (PBDEs, PAHs) in anaerobic digesters from industrial and domestic wastewater by environmental analysis (sludge and biosolids sampling, Soxhlet extraction, cleanup, instrumental analysis by EA and GCMS)
- *Great Lakes Sediment Monitoring*: Sediment coring and porewater analysis on a research vessel

Graduate Principal Investigator, University of Illinois Chicago, Integrated Ecology Laboratory 2008 - 2009

- *Interdisciplinary Conservation*: Soil contaminant effects on establishment of invasive plant Poison Hemlock (*Conium maculatum*) in Cook County Illinois by environmental engineering, landscape ecology, and molecular biology techniques
- Awarded to K. Granberg, P. Gulezian and J. Ison, Chicago Wilderness, \$13,460

Teaching Experience

Graduate Teaching Assistant, University of Illinois Chicago, Civil and Materials Engineering 2008 - 2011

- *Fluid Mechanics*: Lead fluid and hydraulic laboratories weekly, substitute lecture, conduct office hours, and evaluate laboratory reports, assignments, and examinations (50 students per semester)
- *Engineering Hydrology*: Assist with hydrologic model computer laboratories (HEC-RAS, HEC-HMS), conduct office hours, and evaluate assignments (40 students per semester)

Professional Experience

Engineering Intern, US Army Corps of Engineers, Chicago District, Environmental Division 2008

- Model air quality impacts from Confined Disposal Facility emissions (SCREEN3)
- Support community outreach and public meetings

Senior Site Development Engineer, Lake County, IL, Planning, Building and Development 2003 - 2007

- Manage 200 concurrent commercial site development permits and enforce county regulations
- Review engineering plans and storm-water management reports
- Inspect on-site grading, drainage, erosion control, wetland and floodplain impacts
- Meet with land owners, developers, consultants, regulators, elected officials, and public

Environmental Engineering Trainee, Budapest Power Plant Ltd. (BE Rt.) Budapest, Hungary 2002

- Perform Life Cycle Assessments of energy produced from coal and natural gas fired plants
- Co-write and edit annual Sustainability Report

Engineering Specialist, Wisconsin Department of Natural Resources, Madison, WI 2001 - 2002

- Register FEMA maps and locate engineering studies with ArcInfo and ArcView
- Conduct dam safety inspections
- Perform Global Positioning System hydraulic surveys

Undergraduate Research Assistant, University of Wisconsin at Madison 2000

- Manufacture loading system components and strain-measuring devices for post-frame building

Skills, Techniques

- Positive matrix factorization computational models (MATLAB, EPA), Statistical software (SYSTAT, Origin), Geographic Information Science (ArcGIS), Extensive field sampling, Soxhlet extraction, Silica gel cleanup, Instrumental analysis by GCMS and EA, Writing reports, proposals, and manuscripts, Interdisciplinary research.

Certifications, Memberships

- Engineer In Training (EIT), Society of Women Engineers (SWE), American Chemical Society (ACE), American Society of Civil Engineers (ASCE)

Fellowships, Awards, Honors, Funded Research Grants

- 1) **National Science Foundation (NSF) Integrated Graduate Education, Research, and Training (IGERT) Fellow**, Landscape Ecological & Anthropogenic Processes (LEAP) program, University of Illinois at Chicago, 2007 - 2011
- 2) **Institute for Environmental Science and Policy (IESP) Pre-doctoral Fellow**, University of Illinois at Chicago, 2011 - 2012
- 3) **Anchor QEA**, Scholarship recipient for water resource graduate study, 2012
- 4) **Source apportionment of polycyclic aromatic hydrocarbons in Illinois River sediments**, Awarded to K. Rockne and K. Granberg, 2010, Illinois Sustainable Technology Center, \$5,000
- 5) **National Academy of Engineers Grand Challenges Chicago Summit**, University of Illinois, College of Engineering student representative and poster competitor, 2010
- 6) **World Wide Workshop for Young Environmental Scientists**, Scholarship recipient from Universite Paris-Est Water Environment & Urban Systems Laboratory, Val-de-Marne County, and H₂O Paris foundation, 2010
- 7) **Women in Science and Engineering Travel Grant**, University of Illinois at Chicago, 2010
- 8) **Graduate Student Council Travel Award**, University of Illinois at Chicago, 2010, 2011, 2013
- 9) **Graduate College Student Presenter Award**, University of Illinois at Chicago, 2011, 2013
- 10) **Keeping the Chicago Region Free of Poison Hemlock: An Interdisciplinary Approach to Studying the Invasion Front of a Known Invasive Plant**, Awarded to Granberg, K., P. Gulezian and J. Ison, 2008 - 2009, Chicago Wilderness, \$13,460
- 11) **Vespucci Initiative Summer Institute**, Scholarship recipient from University of Buffalo, NSF IGERT, Geographic Information Science program, 2008

Journal Publications, Conference Proceedings, Technical Reports

- 1) Gulezian, P.Z., J.L. Ison, and **K.J. Granberg** (2012) Establishment of an Invasive Plant Species (*Conium maculatum*) in Contaminated Roadside Soil in Cook County, Illinois. *The American Midland Naturalist*. 168(2):375-395
- 2) **Granberg, K.J.**, K. Rockne, J.C. Marlin, E.R. Christensen (2011) Source Apportionment of Polycyclic Aromatic Hydrocarbons in Illinois River Sediment. Battelle 7th International Conference on Remediation of Contaminated Sediments, Feb.10
- 3) **Granberg, K.**, K. Rockne (2010) Sources of Heavy Metals and Polycyclic Aromatic Hydrocarbons to Transportation Corridor Swales in Chicago, USA. World Wide Workshop for Young Environmental Scientists, May 31
- 4) **Granberg, K.J.**, P.Z. Gulezian, and J.L. Ison (2009) Keeping the Chicago Region Free of Poison Hemlock: An Interdisciplinary Approach to Studying the Invasion Front of a Known Invasive Plant. Final project report to the Chicago Wilderness/Illinois Conservation Foundation, Dec. 31, 14 pp

Presentations

- 1) **Granberg, K.J.**, K.J. Rockne, L.T. Thai, J. Miller, and T. Willoughby (2013) Positive Matrix Factorization Source Apportionment of PAHs and PCBs in an Industrial Harbor Air-Shed. Talk: International Conference on Remediation of Contaminated Sediments, Feb.5
- 2) **Granberg, K.J.**, K.J. Rockne, L.T. Thai and J. Miller (2012) Sources of Polycyclic Aromatic Hydrocarbons (PAHs) and Polychlorinated Biphenyls (PCBs) in an Industrial Lake Michigan Harbor. Poster: University of Illinois at Chicago Water Research Forum, April 10
- 3) **Granberg, K.J.**, K.J. Rockne, L.T. Thai, J. Miller, T. Willoughby (2011) Receptor Modeling of PAHs and PCBs in a Contaminated Harbor Air-Shed. Talk: National Meeting of the American Chemical Society, Sep. 1
- 4) **Granberg, K.J.**, K. Rockne, J.C. Marlin, E.R. Christensen (2011) Source Apportionment of Polycyclic Aromatic Hydrocarbons in Illinois River Sediment. Talk: International Conference on Remediation of Contaminated Sediments, Feb.10
- 5) **Thai, L.T.**, J. Miller, L. Vanden Berg, D. Wethington, T. Willoughby, K.J. Rockne, **K.J. Granberg** (2011) Indiana Harbor and Canal Confined Disposal Facility Air Monitoring. Talk: International Conference on Remediation of Contaminated Sediments, Feb. 8
- 6) **Granberg, K.**, A. Aziz, and K. Rockne (2010) Brominated Flame Retardants: An Ongoing Threat to Urban Aquatic Systems. Poster: National Academy of Engineering Grand Challenges Chicago Summit, April 21
- 7) **Gulezian, P.Z.**, J.L. Ison and **K.J. Granberg** (2010) Causes and Consequences of Poison Hemlock's (*Conium maculatum*) Range Expansion into an Urban Area Associated with Heavy Metals and PAHs. Poster: University of Illinois at Chicago Student Research Forum, April 20
- 8) **Gulezian, P.**, **K. Granberg** and J. Ison (2009) Poison Hemlock's Recent Invasion: An Interdisciplinary Analysis. Talk: Association for Environment Studies and Sciences Conference, Oct. 9
- 9) **Granberg, K.**, **P. Gulezian** and **J. Ison** (2008) Keeping the Chicago Region Free of Poison Hemlock: An Interdisciplinary Approach to Studying the Invasion Front of a Known Invasive Plant. Invited Speaker: Chicago State University Biology Department Seminar, April 21
- 10) **Jayaraj, J.**, K. Yin, **K. Granberg** and K. Rockne (2008) Rapid and Extensive Debromination of Brominated Flame Retardants in Thermophilic Municipal Wastewater Digesters. Poster: University of Illinois at Chicago Research Forum, April 18
- 11) **Granberg, K.**, K. Rockne, J. Jayaraj and A. Li (2008) The Role of Black Carbon on Hydrophobic Compound Fate in Anaerobic Digesters. Invited Speaker: The 29th Annual Illinois Water Environment Association conference and exhibition, March 18
- 12) **Rockne, K.**, A. Li, J. Jayaraj and **K. Granberg** (2008) A Comparative Study of Brominated Flame Retardant Fate in Urban and Suburban Anaerobic Digesters. Invited Speaker: The 29th Annual Illinois Water Environment Association conference and exhibition, March 18